Nasrin Abbasi Gharibkandi

Nanoparticle radioconjugates of ^{103}Pd/^{103m}Rh and ^{109}Pd/^{109m}Ag *in- vivo* generators for Auger electron therapy

Supervisor: prof. Aleksander Bilewicz

Auxiliary supervisor: Agnieszka Majkowska-Pilip, PhD-DSc

Laboratory of Radiopharmaceutical Chemistry

Centre of Radiochemistry and Nuclear Chemistry

**Institute of Nuclear Chemistry and Technology**

Warsaw, 2025

1
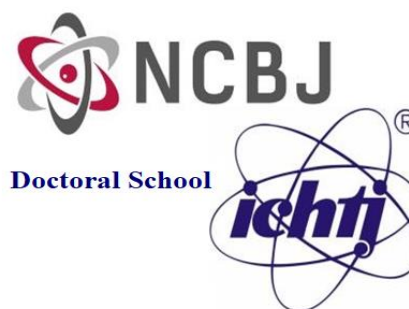
Mgr Nasrin Abbasi Gharibkandi

Oparte na nanocząstkach radiokonjugaty generatorów *in vivo* ^{103}Pd/^{103m}Rh i ^{109}Pd/^{109m}Ag dla terapii elektronami Auger

Promotor: prof. Aleksander Bilewicz

Promotor pomocniczy: Dr hab. inż. Agnieszka Majkowska-Pilip, prof. Instytutu

Pracownia Chemii Radiofarmaceutycznej

Centrum Radiochemii i Chemii Jądrowej

Instytut Chemii i Techniki Jądrowej
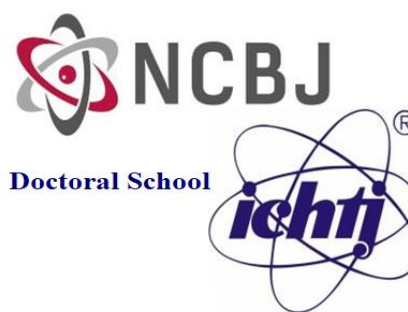
Warszawa, 2025

Acknowledgments

First and foremost, I would like to express my deepest gratitude to my supervisor, Professor Aleksander Bilewicz. His unwavering support, guidance, and understanding have been invaluable throughout my PhD journey. I cannot find the words to adequately thank him for his kindness and mentorship.

I am also profoundly grateful to Professor Agnieszka Majkowska, whose constant help and support meant so much to me during this journey.

I extend my heartfelt thanks to my parents, whose love and support have been unwavering throughout my whole life. Their sacrifices, encouragement, and constant presence in my life gave me the strength to continue, even on the toughest days. They provided me with the foundation I needed to pursue my dreams, and I am forever grateful for everything they have done for me.

I would also like to express my gratitude to my siblings and my nephews, Komeil and Amir Mohammad, for their unconditional love. Their encouragement, understanding, and the strong bond we share have been a source of comfort and strength for me. Knowing that I could count on them has been truly heartwarming.

To my fiancé, I am deeply thankful for your patience, understanding, and for standing by me through the ups and downs of this experience. Your love, care, and belief in me have made all the difference, and I truly could not have done this without you by my side. Thank you for being my rock, for all the sacrifices you've made, and for sharing this journey with me.

Finally, I am grateful to everyone who has contributed to this journey, whether through encouragement, advice, or support. Your support and kindness will never be forgotten.

This doctoral dissertation was prepared as a collection of thematically related scientific articles:

1. Nasrin Abbasi Gharibkandi, Joanna Gierałtowska, Kamil Wawrowicz, Aleksander Bilewicz. "Nanostructures as Radionuclide Carriers in Auger Electron Therapy" Materials 15, 2022, 1143. IF=3.4 (2022)

2. Nasrin Abbasi Gharibkandi, Kamil Wawrowicz, Agnieszka Majkowska-Pilip, Kinga Żelechowska-Matysiak, Mateusz Wierzbicki, Aleksander Bilewicz, Au@^{109}Pd core–shell nanoparticle conjugated to trastuzumab for the therapy of HER2+ cancers: studies on the applicability of ^{109}Pd/^{109m}Ag *in vivo* generator in combined β$^-$ Auger electron therapy. EJNMMI Radiopharmacy and Chemistry 8, 26 (2023) IF= 4.4 (2024)

3. Nasrin Abbasi Gharibkandi, Agnieszka Majkowska-Pilip, Rafał Walczak, Mateusz Wierzbicki, Aleksander Bilewicz, Au@^{109}Pd core-shell nanoparticle conjugated to panitumumab for the combined β$^-$ - Auger electron therapy of triple-negative breast cancer. International Journal of Molecular Sciences 25, 13555 (2024), IF=4.9 (2023)

4. Nasrin Abbasi Gharibkandi, Kamil Wawrowicz, Rafał Walczak, Agnieszka Majkowska-Pilip, Mateusz Wierzbicki, Aleksander Bilewicz, ^{109}Pd/^{109m}Ag *in vivo* generator in the form of nanoparticles for combined β$^-$ - Auger electron therapy of hepatocellular carcinoma. EJNMMI Radiopharmacy and Chemistry 9, 59 (2024), IF= 4.4 (2024)

Table of contents:

LIST OF SYMBOLS AND NOTATIONS USED

Short form	Description
HCC	Hepatocellular carcinoma
EPR	Enhanced permeability and retention effect
Au@Pt	Platinum gold core-shell nanoparticles
Pd-PEG nanoparticles	PEGylated palladium nanoparticles
Au@^{109}Pd nanoparticles	$^{(109)}$Palladium core-shell gold nanoparticles
Au@^{109}Pd-PEG- trastuzumab	$^{(109)}$Palladium core-shell gold nanoparticles conjugated with trastuzumab
Au@^{109}Pd-PEG- panitumumab	$^{(109)}$Palladium core-shell gold nanoparticles conjugated with panitumumab
Au@Pd-^{125}I-PEG-trastuzumab	^{125}I- labeled Palladium core-shell gold nanoparticles conjugated with trastuzumab
^{198}Au-trastuzumab	^{198}Au nanoparticles conjugated with trastuzumab
EC	Electron capture
IT	Internal transition
$T_{1/2}$	Half life
LET	Linear energy transfer
SSBs	Single-strand breaks
DSBs	Double-strand breaks
TEM	Transmission Electron Microscopy
DLS	Dynamic Light Scattering
iTLC	Instant Thin Layer Chromatography
LSC	Liquid Scintilation Counter
cpm	Counts per minute
nm	Nanometer
PBS buffer	Phosphate-Buffered Saline
HS	Human Serum
HER2	Human epidermal growth factor receptor 2
EGFR	Epidermal growth factor receptor
ROS	Reactive oxygen species
CD44	P-gly coprotein 1 ligands
GPC3	glypican-3

GC33	(codrituzumab), a humanized monoclonal antibody
PSMA	prostate-specific membrane antigen

ABSTRACT

Although not widely used, Auger electron emitter therapy shows promise as a selective strategy for cancer treatment. The low-energy Auger electrons are emitted by radioisotopes that decay through electron capture or internal conversion processes. Typically, 5 to more than 35 Auger electrons, with energies ranging from a few eV to approximately 1 keV, are emitted per decaying atom. The linear energy transfer (LET) of Auger electrons ranges from 4 to 26 keV/µm. This makes them capable of inducing double-stranded DNA breaks. The therapeutic efficacy of Auger electron targeted radiotherapy can be increased by the simultaneous combination of low- and high-LET radiation. Therefore, we introduce the concept of using ^{109}Pd ($T_{1/2}$= 13.7 h) in the form of a ^{109}Pd/^{109m}Ag *in vivo* generator. ^{109}Pd undergoes β^- decay to ^{109m}Ag (39.6 s), thereafter transitioning to stable ^{109}Ag, comprising the emission of 88-keV photons and the cascade release of conversion and Auger electrons. Hence, we can take the advantages of both β^- and Auger electrons, by inducing the cross-fire effect and DNA double-strand breaks, respectively.

Due to the unique properties of nanoparticles for cancer diagnosis and treatment, this study utilized palladium radionuclide in the form of ^{109}Pd nanoparticles (5 nm) and Au@^{109}Pd core-shell nanoparticles (15 nm). Core-shell Au@^{109}Pd nanoparticles were conjugated with the monoclonal antibodies trastuzumab and panitumumab to specifically target the Her2 and EGFR receptors, respectively, and small PEGylated Pd nanoparticles were investigated for the therapy of hepatocellular carcinoma (HCC). The most important part of the thesis consists of numerous studies carried out *in vitro* using adherent cell cultures and three-dimensional spheroids as tumor models with a defined microenvironment. The accumulation of ^{109}Pd-PEG nanoparticles and Au@^{109}Pd in the cell nuclei or cell nuclei membrane led to DNA double-strand breaks (DSBs) and cell viability reduction, even at low doses. Moreover, in order to conduct comparative studies, Pd, and Au@Pd nanoparticles were also labeled by chemisorption with radionuclides ^{125}I (Auger emitter) and ^{131}I (β^- and γ-emitter). Results showed that ^{109}Pd-labeled Pd nanoparticles were significantly more cytotoxic than those labeled with either ^{131}I or ^{125}I. Studies with Au@^{109}Pd-trastuzumab radiobioconjugates showed that despite the lack of nuclear localization, a cytotoxic effect was achieved by aggregation of Au@^{109}Pd-trastuzumab conjugates in the perinuclear area. In contrast, Au@^{109}Pd-panitumumab radiobioconjugates in MDA-MB-231 cells show similar internalization but significant transport into the cell nucleus (>10%).

The doctoral thesis consists of an introduction, an evaluation of the four attached publications, and a summary and conclusions. The thesis also includes an appendix in which I have included unpublished results related to the properties of *in vivo* generators in the form of a ^{103}Pd cyclam complex and Au@^{103}Pd core-shell nanoparticles.

ABSTRAKT

Mimo, braku szerokiego zastosowania terapia z wykorzystaniem emiterów elektronów Augera jest uważana za obiecującą strategię selektywnego leczenia raka, szczególnie jego przerzutów. Niskoenergetyczne elektrony Augera są emitowane przez radioizotopy, które rozpadają się poprzez wychwyt elektronów lub w wyniku konwersji wewnętrznej jądra. Liniowy transfer energii (LET) elektronów Augera jest wysoki i mieści się w zakresie od 4 do 26 keV/µm. Dzięki temu mogą one wywoływać podwójnoniciowe pęknięcia DNA. Ostatnio stwierdzono, że skuteczność terapeutyczna wewnętrznej radioterapii może zostać istotnie zwiększona poprzez jednoczesne stosowanie promieniowania o niskim i wysokim LET. Dlatego w mojej pracy zaproponowałam wykorzystanie radionuklidu ^{109}Pd ($t_{1/2}$=13,7 h) w postaci generatora *in vivo* ^{109}Pd/^{109m}Ag. ^{109}Pd ulega rozpadowi β$^-$ do ^{109m}Ag ($t_{1/2}$=39,6 s), a następnie przechodzi w stabilny ^{109}Ag, emitując kwant gamma 88 keV oraz elektrony konwersji i Augera. Pozwala to wykorzystanie zalet zarówno cząstek β$^-$ (efekt ognia krzyżowego) jak i elektronów Augera, indukując dwuniciowe pęknięcia DNA.

Ponieważ nanocząstki pozwalają na uzyskanie wysokich aktywności właściwych, w moich badaniach wykorzystałam radionuklid ^{109}Pd w postaci nanocząstek ^{109}Pd (5 nm) oraz nanocząstek typu „core shell" Au@^{109}Pd (15 nm). Aby specyficznie ukierunkować je odpowiednio na receptory Her2 i EGFR, nanocząstki Au@^{109}Pd zostały skoniugowane z przeciwciałami monoklonalnymi trastuzumabem i panitumumabem, a 5 nm nanocząstki stosowano w postaci koniugatu ^{109}Pd NPs z PEG. Najistotniejszą część rozprawy stanowią badania przeprowadzone w warunkach *in vitro* z wykorzystaniem hodowli komórek adherentnych oraz trójwymiarowych sferoidów, jako modeli guza o zdefiniowanym i ukształtowanym mikrośrodowisku. Akumulacja nanocząstek ^{109}Pd-PEG i Au@^{109}Pd w jądrach komórkowych lub na błonie jąder komórkowych doprowadziła do dwuniciowych pęknięć DNA i zmniejszenia żywotności komórek. W celu przeprowadzenia badań porównawczych, nanocząstki Pd i Au@Pd znakowano metodą chemisorpcji radionuklidami ^{125}I (emiter elektronów Augera) i ^{131}I (emiter β$^-$ i γ). Otrzymane wyniki wykazały, że nanocząstki Pd znakowane ^{109}Pd były znacznie bardziej cytotoksyczne niż znakowane ^{131}I lub ^{125}I. Badania z radiobiokonjugatami Au@^{109}Pd-trastuzumab wykazały, że pomimo braku lokalizacji jądrowej, efekt cytotoksyczny uzyskano poprzez agregację radiokoniugatów Au@^{109}Pd-trastuzumab i ich kumulację w obszarze okołojądrowym. Natomiast radiobiokoniugaty Au@^{109}Pd-panitumumab w komórkach MDA-MB-231 wykazywały obok wysokiej internalizacji, także znaczny transport do jądra komórkowego (>10%). Rozprawa doktorska składa się ze wstępu, omówienia czterech załączonych publikacji oraz podsumowania i wniosków. Praca zawiera również dodatkowy rozdział, w którym zamieściłam niepublikowane wyniki dotyczące właściwości generatorów *in vivo* opartych na również obiecującym emiterze elektronów Augera, ^{103}Pd.

INTRODUCTION
RADIONUCLIDE THERAPY

Nuclear medicine consists of the application of two main types of isotopes for treatment purposes: stable isotopes, which do not undergo radioactive decay over time, and unstable isotopes. Stable isotopes are mostly used as tracers in pharmacokinetic studies to investigate human biochemical pathways and play an important role in medical research of new drugs [1]. Unstable isotopes possess an excessive number of neutrons or protons, and the stability of radioisotope nuclei is typically obtained by the emission of an α and/or an electron or positron, along with the release of energy as gamma-rays (electromagnetic radiation), as well as conversion and Auger electrons.

Radionuclide therapy offers several advantages over external beam radiation therapy, wherein the radioactive source is placed nearby or inside the targeted tissue. These include fewer treatment sessions and lower morbidity to non-target tissues because of the proximity of the radioactive source to the target tissue [2]. The starting point of radionuclide therapy dates back to the early 1900s, by the discovery of radioactivity by Henri Becquerel and Marie Curie. In 1901, Becquerel experienced significant skin inflammation after keeping a radium tube in his pocket for a long time. This finding resulted in the initial application of radium in treatment, when Henri Alexandre Danlos and Eugene Bloch applied radium to a tuberculous skin lesion. In 1903, Alexander Graham Bell proposed the setup of radium sources in proximity to tumors, and in 1913, Frederick Proescher published the first research on the intravenous administration of radium for the treatment of different disorders [3]. The development of multifield external beam radiation therapy, along with the potential risks associated with using radium and very costly decontamination attempts, resulted in the decline in radium-based treatments [2]. This prompted research into novel radionuclides such as ^{60}Co, ^{137}Cs, and ^{192}Ir, as well as innovative delivery methods aimed at reducing toxicity to non-target tissues and protecting providers from radiation exposure during radioisotope administration [4]. The selection of an optimum radionuclide for therapy requires finding an ideal radioisotope with properties that meet the therapeutic requirements of both the provider and the patient. This issue is complex, considering the particular disease, the required treatment duration, treatment objectives, patient tolerance during treatment, and overall treatment efficiency compared to the disease pathophysiology. Evaluating each radionuclide or radiopharmaceutical for its suitability for clinical usage is important. The requirements for therapeutic radionuclides may be divided into two main categories, namely physical and biochemical characteristics [5]. Physical properties include the parameters such as the physical half-life, emission types, radiation energy, daughter radionuclides, production methods, and radionuclide purity [6, 7]. Biochemical factors include tissue targeting, tumor retention of radioactivity, *in vivo* stability, and cytotoxicity [8]. Moreover, the efficacy of radionuclide therapies may be improved by

fractionated dose radiotherapy protocols, combining radiopharmaceuticals with radiosensitizing agents, or employing pre-targeting radionuclide approaches (pRIT) [9].

Another factor that must be considered is the particular type of radioactivity. The radiation types currently used for solid tumors are mostly ß and sometimes ɣ radiation because of their long ranges and adjustable energy levels. The α particle, or helium nucleus, possesses considerable mass and energy, associated with a very short range. In most cases, the α particle is considered inappropriate for radiation therapy due to its limited range and the extensive tissue damage that it causes. Particularly, it is inappropriate for vertebral augmentation therapy since its short range in bone. However, recent researches have shown that α-emitters targeted to cancer cells via antibodies and protein vectors offer the potential to inhibit the growth of various surface tumors, tumor metastasis, and leukemias [10, 11]. Additionally, due to the high energy of α-particles, they do not face the same resistance the hypoxic tissue does, which is common with β and external beam radiations. Therefore, it is reasonable to assume that α particles will play a crucial role in future radionuclide therapies.

The selection of an optimum radionuclide for therapy requires finding an ideal radioisotope with properties that meet the therapeutic requirements of both the provider and the patient. This issue is complex, considering the particular disease, the required treatment duration, treatment objective, patient tolerance during treatment, and treatment overall efficiency compared to the disease pathophysiology.

As my work focuses on the radionuclide ^{109}Pd, which emits $β^-$ radiation along with conversion and Auger electrons, I will briefly describe the characteristics of these types of radiation in the following paragraphs.

BETA-EMITTERS IN RADIONUCLIDE THERAPY
Beta particles are high-energy, high-speed electrons or positrons emitted by the radioactive decay of an atomic nucleus. As beta particles pass through matter, they lose their kinetic energy and finally stop. Due to their relatively small mass, the recoil energy of the daughter nucleus is insignificant. Furthermore, the linear energy transfer (LET) of these negatively charged particles (-1) is minimal (~0.2 keV/μm) through their path, which can extend up to a centimeter, with the exception of the final few nanometers at the end of the range, where the main part of the energy is released. Thus, their treatment efficacy depends on the presence of extremely high radionuclide concentrations within the area of interest. The broad range of these generated electrons results in the so-called cross-fire effect, a condition that eliminates the necessity to target every single cell inside the tumor, so long as all cells are in the range of the decomposing atoms. The likelihood of the released beta particles penetrating the targeted cell nucleus is dependent on (i) the spatial position of the decomposing atom relative to the nucleus, specifically the DNA of the cancer cell; (ii) its proximity to the nucleus; and (iii) the radius of the nucleus. It is obvious

that intracellular localization of β^- emitting radiopharmaceuticals is highly beneficial and should always be sought [12].

Historically, investigations into radionuclide-based cancer therapy have mainly utilized β^- particle emitters. When cells are exposed to β^- particles, the resulting survival curves often exhibit a notable characteristic known as a distinct shoulder [13]. Despite the relatively low *in vitro* toxicity, these radionuclides are still pursued for targeted therapy, mostly because of their accessibility and advantageous physical properties (e.g., energy and range of emitted electrons resulting in cross-fire irradiation; physical half-lives that correlate with the biological half-lives of the carrier molecules). The primary advantage of cross-fire is that it eliminates the necessity for the radiotherapeutic agent to be present in every targeted tissue, hence counteracting an appropriate degree of heterogeneity. Due to the low ionization densities of energetic electrons, administering an effective therapeutic dose to the targeted tissue requires that (i) the distances among these foci do not exceed twice the maximum range of the emitted energetic β^- particles, and (ii) the concentration of the radiotherapeutic agent is sufficiently great to achieve a cumulative cross-fire dose of approximately 10.000 cGy to all the targeted cells. As the dosage is inversely proportional to the square of the distance, the concentration of the therapeutic compound required to achieve cytotoxic doses increases significantly with a rise in non-uniform radionuclide distribution.

Along with the commonly used ^{131}I in thyroid therapy and radiopharmaceuticals labeled with high-energy ^{90}Y and ^{188}Re, the most widely utilized radiopharmaceuticals for targeted therapy of small tumors and metastases are those labeled with the ^{177}Lu radionuclide. This radionuclide can be produced in very high activities, thanks to the high cross-section of the ^{176}Lu(n,γ)^{177}Lu nuclear reaction of as much as 2090 b [14], even in small research reactors. The specific activity of ^{177}Lu obtained in this method using a target material highly enriched in ^{176}Lu is 40 GBq/μmol, but there are still 3 carrier atoms for each ^{177}Lu atom. The by-product formed during the activation of ^{176}Lu in a nuclear reactor is ^{177m}Lu with a long half-life of 160 d, which cannot be separated from the ^{177}Lu radionuclide. The activity of ^{177m}Lu is quite low but imposes on hospitals the obligation to store radioactive waste, e.g., radioactive urine of patients, for a long time, which is very expensive.

These limitations mean that the production of carrier-free ^{177}Lu is necessary in the reaction ^{176}Yb(n,γ)^{177}Yb(β^-)^{177}Lu. It is difficult and takes a long time to separate two lanthanides that are very close to each other. This is especially true in the case of Yb and Lu, which have very similar chemical properties because they are so close together in the lanthanide series (the difference in ionic radii is only 0.7 pm). The use of extraction resins solved this problem. Currently, carrier-free ^{177}Lu is already widely used in medical practice.

Radionuclides with similar properties that could replace ^{177}Lu are ^{161}Tb and ^{47}Sc. The first isotope is also a lanthanide and is produced in a way similar to ^{177}Lu, using the neighboring Gd enriched in ^{160}Gd as a target material in the reaction ^{160}Gd(n,γ)^{161}Gd(β$^-$)^{161}Tb. Since ^{161}Tb also emits Auger electrons, I will describe the properties of this radionuclide and radiopharmaceuticals based on this radionuclide in the section on Auger electron emitters.

The advantage of ^{47}Sc over the aforementioned radioisotopes is that it can be obtained by irradiating targets composed of elements with significantly different chemical properties. In the indirect method, enriched titanium is used as a target material, from which ^{47}Sc is formed in the reaction ^{47}Ti(n,p)^{47}Sc or ^{48}Ti(p,2p)^{47}Sc, while in the indirect method, targets enriched in ^{46}Ca are irradiated, using the reaction ^{46}Ca(n,γ)^{47}Ca(β$^-$)^{47}Sc [15].

All three radionuclides have similar chemical properties; all occur in the 3+ oxidation state, and form kinetically stable complexes with DOTA. Their half-life is long enough to label mAbs, but they are also suitable for labeling peptides, as proven by the excellent clinical results of ^{177}Lu-DOTATATE or ^{177}Lu-PSMA therapy. The radionuclides ^{47}Sc and ^{161}Tb have advantages over ^{177}Lu by enabling the use of the β$^+$ emitters ^{44}Sc and ^{152}Tb, which create ideal theranostic pairs for accurate dosimetry assessment and personalized therapy.

AUGER ELECTRON EMITTERS IN TARGETED RADIOTHERAPY

In addition to β$^-$ and α particles, Conversion and Auger electrons can also be effective in targeted radionuclide therapy. During the decay of several radioactive atoms, a vacancy is created, mainly in the K shell, due to electron capture (EC) and/or internal conversion (IC) of nuclei (Fig. 1). Each vacancy is immediately filled by an electron transitioning from a higher shell. This procedure results in a cascade of atomic electron transitions that move the vacancy toward the outermost shell. Transitions of inner-shell electrons lead to the emission of distinctive X-ray photons or an Auger, Coster-Kronig, or super-Coster-Kronig monoenergetic electron (collectively referred to as Auger electrons). On average, between 5 to over 35 Auger electrons, with energy ranging from a few eV to approximately 1 keV, are emitted per one decaying atom [16]. The linear energy transfer (LET) of Auger electrons varies from 4 to 26 keV/µm [7], indicating that Auger electrons resemble α particles and induce significant cellular damage. Moreover, following the emission of Auger electrons, daughter nuclide is in form of an extremely reactive, highly positively charged cation, such as +35 in the case of ^{195}Pt after the decay of ^{195m}Pt.

The incredibly low energy of Auger electrons yields two primary consequences: (i) these light, negatively charged particles move along curved paths, with a range in water from a part of a nanometer to about 0.5

μm; (ii) multiple ionizations occur in the immediate vicinity (a few nanometers) of the decay site, similar to the alpha particles observed along the path [17].
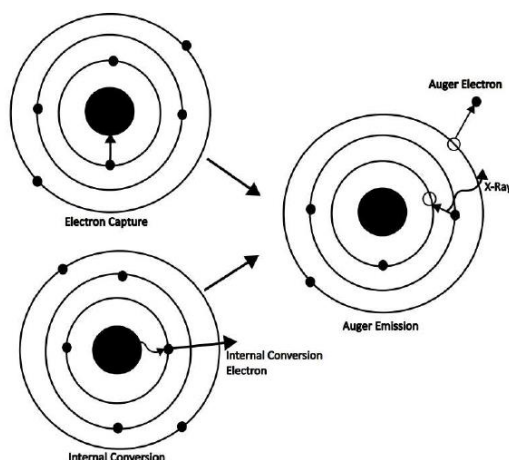

Fig. 1. Schematic of Auger electron emissions after EC and IC decays of radioisotopes [12, 18].

This means, that Auger emitters are interesting candidates for targeted radionuclide therapy. It is possible to inject approximately tenfold the radioactivity of Auger electron emitters compared to β⁻ particle emitters without toxic side effects, particularly affecting the bone marrow. Therefore, it can be assumed that radiopharmaceuticals labeled with Auger electron emitters will gain widespread application in radionuclide therapy in the near future. This assumption is grounded on the significant cytotoxicity and therapeutic efficacy reported, the availability of several low-energy electron-emitting radionuclides in non-carrier-added forms, characterized by variable physical half-lives and established chemical properties. Furthermore, minimal autoradiolysis levels (even at high specific activities) of radiopharmaceuticals labeled with Auger emitters are also a significant benefit [7].

CHARACTERISTICS OF COMMONLY USED AUGER ELECTRON EMITTERS

In contrast to α-particle emitters, of which only a few possess suitable properties for targeted therapy, the number of Auger electron emitters is much higher. The availability of α emitters is also limited compared to Auger electron emitters, which could potentially be generated on available cyclotrons with high activity. Moreover, the cost of α emitters is significantly high. For therapeutic applications, an Auger electron emitter must possess the following characteristics:

- The emission of a substantial quantity of electrons,
- The half-life must be sufficiently long to enable the drug to reach its target while simultaneously being short enough to prevent unnecessary exposure to ionizing radiation. The significance of this property is less essential for Auger electrons compared to either β or α particles,

- The disintegration of the parent nucleus must yield a very long-lived or stable nucleus, which is essential for any kind of internal radiation therapy,
- The radionuclide must be easily producible and separable from the target using a cost-effective process,
- It should be in a non-carrier added form or possess high specific activity,
- There should be straightforward methods for conjugating radionuclides with biomolecules.

The properties of the radiation released by the radionuclide are crucial from the point of therapeutic efficacy. It is believed that the Auger electron emitter should not be a source of other forms of radiation, such as β^-; however, in the case of the ^{161}Tb (β^- emitter), the emission of Auger electrons was considered advantageous for therapeutic applications [19]. The same applies for γ radiation emission, which may provide simultaneous monitoring of therapeutic success. The most commonly used Auger emitters (^{111}In, ^{125}I, ^{201}Tl, ^{67}Ga, ^{99m}Tc) generate gamma quanta with great efficiency and are extensively used in the diagnostic SPECT (Single Photon Emission Computer Tomography) techniques. On the other hand, this emission contributes to healthy organ toxicity, especially at high doses of radioactivity, which is often required for effective radionuclide therapy [20]. Therefore, the efficacy of Auger radionuclides in therapy is estimated based on their photon-to-electron energy yield (p/e) ratio [21]. Since photons deposit most of their energy in healthy tissues away from small targets, their dosage contribution is typically undesirable in Auger therapy. Therefore, a low p/e ratio is highly recommended for radiation patient exposure.

Bernhardt et al. [21] selected 5 radionuclides (^{103m}Rh, ^{58m}Co, ^{119}Sb, ^{161}Ho, ^{189m}Os) for Auger electron therapy to deliver a sufficiently high dose to the tumor while minimizing exposure to surrounding tissue, as the energy of the emitted electrons is below 40 keV. He also stated that due to p/e ratio of 0.04, and high availability, radionuclide ^{103m}Rh is one of the most promising radionuclides for Auger radiotherapy. ^{103m}Rh decays via isomeric transition to stable ^{103}Rh, resulting in the emission of Auger electrons. The decay of ^{103m}Rh is associated with a high Auger electron emission yield compared to its photon emissions (X-rays). ^{103m}Rh emits about 30 times more low energy (<40 keV) electrons than photons (2–40 keV) per decay. It is noteworthy that ^{103m}Rh is a daughter isotope of ^{103}Pd, which is one of the subjects of my doctoral thesis. Hence, it is worth concentrating on Auger electron emitters with low-γ radiation, such as ^{135}La, ^{189m,191}Os, and ^{103,109}Pd.

An essential factor regarding expected therapeutic outcomes is the number of released conversion electrons, which possess a higher range than Auger electrons. They can induce cell death by binding to the surface without requiring internalization and nucleus translocation. They can also generate a cross-fire effect by affecting surrounding cells in close proximity to the breakdown site. Table 1 shows the Auger electron emitters that are already used or can potentially be used in targeted radiotherapy [22-24].

Table 1. Advanced list of the candidates for Targeted Auger Therapy

Radionuclie	T$_{1/2}$ mother radionuclide	T$_{1/2}$ Daughter nuclide	Deacay mode	Production method
TI-201	3 d	Stable	EC	Accelerator
Hg-197	64 h			Accelerator, Reactor
Pt-195m	4.3 d	50 y	IT	Accelerator, Reactor
Pt-193m	4 d	Stable		Accelerator
Ir-193m	10 d			
Ir-189	13 d		EC	
Os-191	15 d		ß$^-$	Reactor + MS
Os-189m	6 h		IT	Generator
Ta-177	57 h		EC	
Lu-177	6.7 d		ß$^-$	Reactor
Yb-169	32 d		EC	Accelerator, Reactor
Tm-167	9.2 d			Accelerator
Er-165	10 h			
Ho-161	2.5 h			
Tb-161	6.9 d		ß$^-$	Reactor
Tb-155	5.3 d		EC	Accelerator
La-135	19 h		EC, ß$^+$	
Cs-131	9.7 d		EC	Reactor
I-125	60 d			
I-123	13 h			Accelerator
Te-125m	58 h		IT	Generator
Sb-119	38 h		EC	Accelerator
Sn-117m	14 d		IT	
In-111	2.8 d		EC	
Cd-107	6.5 h		EC, ß$^+$	
Tc-99m	6 h	211 100 y		
Ge-71	11 h	Stable	EC	Accelerator
Ga-67	78 h			
Co-58m	9.2 h	0.192 y	IT	Accelerator

Pd-103	16 d	56 m	EC	Accelerator, reactor
Rh-103m	56 m	stable	IT	Generator

Iodine ^{125}I is the most widely used Auger electron emitter in medicine. However, it was primarily used for diagnosing thyroid diseases through γ radiation emission and by labeling monoclonal antibodies in SPECT imaging and brachytherapy. ^{111}In, ^{67}Ga, and ^{201}Tl are also commercially available Auger emitters commonly used in SPECT diagnostics.^{111}In is often used in receptor diagnostics such as Octreoscan™ (^{111}In-pentetreotide); ^{67}Ga, commonly used in medical imaging, is administered as gallium citrate for the purpose of determining hypoxia, or oxygen deficiency, in tissues; and ^{201}Tl can be used in perfusion radiopharmaceuticals, such as ^{201}TlCl.

PRODUCTION OF AUGER ELECTRON EMITTER

Applying convenient nuclear reactions, Auger electron emitters can be generated by particle cyclotrons, reactors, and bremsstrahlung gamma rays. Moreover, the radionuclide generator system serves as a feasible production method [25]. It should be noted that although Auger emitters are potential therapeutic agents, they typically accumulate only a few tens of keV at the target site, which is much less than for alpha-emitting radionuclides. Hence, in relation to Auger emitters, the production of a substantial quantity of radioactive nuclei and subsequent radiopharmaceuticals with great molar-specific activity is significantly important to fully use the potential of Auger electron emitters. Several Auger emitters generate a low energy of penetrating gamma-rays [26]. This not only reduces the radiation burden associated with the cumulative radiation dose during production and delivery processes, but also allows for the consideration of potential radioisotope enrichment processes using electromagnetic mass separators and centrifuges.

The most important and commercially available isotopes ^{111}In, ^{67}Ga, and ^{201}Tl are obtained by cyclotron through the following reactions: ^{111}Cd(p,n)^{111}In with a yield of 72 MBq µA^{-1} h^{-1} for a proton energy of 15-0 MeV, ^{67}Zn (p, n)^{67}Ga shows a yield of 87 MBq µA^{-1} h^{-1}, and ^{203}Tl (p,3n) ^{201}Pb→^{201}Tl nuclear reaction offers a capacity of 78.5 MBq µA^{-1} h^{-1}. This enables the acquisition of activities beyond 20 GBq, sufficient for Auger electron therapy. The high activities of ^{125}I are obtained in the reactor by irradiating xenon gas in the reaction ^{124}Xe(n,γ)→^{125m}Xe (57s)→ ^{125}I.

BIOLOGICAL ACTION OF AUGER ELECTRONS

At the beginning of the 20th century, scientists showed minimal interest in investigating the radiobiological effects of low-energy electrons. However, in the early 1960s, Carlson and White [27] established that the decay of the Auger electron emitter ^{125}I results in the fragmentation of $CH_3^{125}I$ and $C_2H_5^{125}I$ molecules. By the late 1960s, numerous studies reported the radiobiological effects of ^{125}I and other Auger electron

emitters in prokaryotic and eukaryotic species. These studies proved a direct correlation between double-strand breaks (DSB) and phage survivability when exposed to DNA-incorporated ^{125}I decay [28]. These observations resulted in the belief that the same is true for mammalian cells, yielding 1 DSB per decaying atom.

The biological effect results from the ionization induced by the emitted low-energy electrons, which can directly damage DNA strands and other essential cellular structures, such as mitochondria and cell membrane. There is also an indirect effect resulting from the forming of reactive oxygen species during water radiolysis and the neutralization of the highly positive cation generated after the emission of Auger electrons. This process involves the withdrawal of electrons from the cytoplasm. As a result, more radicals will be formed and the cytotoxic effect will increase [29].

The first mechanism is the most effective and widely described in the literature, as the introduction of an Auger electron emitter into a DNA strand causes damage to the genetic material with a single radionuclide decay. The direct mechanism involves affecting DNA by incorporating into its structure, most often on the basis of affinity to one of the nitrogen bases. It was found that Auger electron emitters ^{123}I and ^{125}I, conjugated with iododeoxyuridine (IUdR) which is incorporated directly into DNA, significantly reduce the survival of mammalian cells [16]. The lethal radiation dose for [125]I- IUdR was 7 times lower than that of X-rays, indicating high cytotoxicity for Auger electrons emitted by ^{125}I incorporated into DNA. However, no significant cytotoxic effect was found for ^{125}I located in the cytoplasm, bound to the cell membrane, or outside the cell. Thus, the disintegration of the Auger emitter in close proximity to nuclear DNA is necessary to fully utilize the high LET value of these electrons [16]. This effect can also be obtained by using oligopeptides, aptamers, acridines, anthracyclines, transport peptides to the cell nucleus (NLS), or complexes intercalating into the nucleus, such as cis-platin, labeled with Auger emitters. The subsequent section provides a more detailed description of these radioconjugates.

Apart from the direct interaction of Auger electrons with DNA, single- and double-strand breaks can be caused also indirectly by the hydroxyl radicals (•OH) and other reactive oxide species (ROS) generated by the Auger electrons in water [30]. The emission of Auger electrons from the decaying atom results in the formation of a highly positively charged cation. This chemical form of atom is highly unstable, and for its neutralization, electrons from water in the cytoplasm or directly from DNA may be used. This extremely rapid process is called "Coulomb explosion" and contributes to the improvement of cytotoxicity as the secondary mechanism of free radical generation and DNA destabilization.

It was also found that the generation of large amounts of ROS in the cytoplasm near the cell nucleus can cause their diffusion into the cell nucleus and destruction of nuclear DNA and DNA located in mitochondria

(mtDNA) [31]. mtDNA defects caused by the action of Auger electrons cause damage to an important genetic element containing information about the amino acid sequence in the proteins and induce cell death.

Furthermore, it has been postulated that since the cell membrane has a critical role in cell survival, the effects of Auger electrons emitted by membrane-bound radiolabeled mAbs should be also considered [32]. Another mechanism was presented for ^{125}I-DCIBzL (iodinated analog of inhibitor of PSMA) exhibiting a high affinity for PSMA receptors. Confocal microscopy utilizing a fluorescent analog of DCIBzL revealed that this agent was mainly localized in the perinuclear area of PSMA-expressing cells, rather than in the cell nucleus [33]. During mitosis, especially in anaphase, when the condensed chromosomes are pulled towards spindle poles, the cellular genetic material is in the range of action of the Auger emitter localized outside the nucleus, in the perinuclear area. Since the close proximity of the spindle poles and chromosomes occurs only in actively dividing tumors, this mechanism can effectively spare the kidneys, which have a significant PSMA expression but possess a low mitotic index.

Another proposed mechanism contributing to the enhancement of cytotoxic activity is the "radiation-induced bystander effect" (RIBE) [34]. This effect refers to the irradiation of surrounding cells localized close to those exposed to ionizing radiation. Despite the absence of direct radiation interaction with these cells, significant changes in the cells are evident. This refers to DNA mutations and the instability of genetic material, leading to the activation of programmed death cell. The RIBE mechanism is frequently mentioned as a supplementary effect contributing to cytotoxicity, but the exact explanation for this phenomenon remains unknown. It is generally expected that RIBE is realized by information transmission from irradiated cells to the neighboring cells by stress signal factors. Reactive oxygen and nitrogen species, cytokines (*e.g.,* TGF-β), and micro RNA (miRNA) may play a significant role as RIBE activation triggers; however, the bystander effect may occur through different pathways based on the type of cancer cells affected. In summary, the greatest cytotoxic effect will be achieved when we introduce the Auger electron emitter into the nucleus near DNA, while other previously mentioned mechanisms of toxicity may also occur on a smaller scale.

RADIOBIOCONJUGATES LABELED WITH AUGER EMITTERS

The type of molecular target for the transport of the Auger emitter dictates the selection of vector molecule for the radiobioconjugate. If the molecular target is nuclear DNA strands, the radiopharmaceutical must contain components that facilitate its localization into the cell nucleus in proximity to the DNA, preferably with incorporating properties. To target the cell cytoplasm, the vector should be a peptide or monoclonal antibody that enables cellular internalization (receptor agonist). At last, if the molecular target is just the

cell membrane, the most suitable vectors will be those that bind to the receptor without undergoing internalization (receptor antagonists) [35].

Auger electron emitters, in the form of metal cations, can be attached to the vectors using multidental chelating compounds commonly used in radiopharmacy, such as DOTA (1,4,7,10-tetraazacyclododecane-1,4,7,10-tetraacetic acid), NOTA (1,4,7-triazacyclonane-1,4,7-triacetic acid), or DTPA (diethylenetriaminepentaacetic acid) (1,4,7,10-tetraazacyclododecane-1,4,7,10-tetraacetic acid). The attachment of halogen Auger electron emitters (^{77}Br or ^{123,124,125}I) to biomolecules arises by halogenation reactions, such as the electrophilic substitution of tyrosine in peptides and proteins. In contrast to chelation, the iodization approach is characterized by a significantly lower efficiency of only 40–60%. Moreover, the *in vivo* stability of these compounds is low due to the presence of a dehalogenase enzyme that cleaves radioactive bromine or iodine [16].

The last basic approach used in the synthesis of radiopharmaceuticals labeled with Auger electron emitters is the use of nanoparticles as carriers. This method is widely used because of the distinctive properties of nanoparticles, which, thanks to their small size, can penetrate the cells, resulting in increased drug delivery efficiency. The application of nanoparticles may involve the chemisorption of radionuclides on the surface or the attachment of complexed radionuclides to the surface of the nanoparticle via a polymer linker [36]. Since my doctoral thesis focuses on using nanostructures for the immobilization of ^{103,109}Pd radionuclides, my coworkers and I published a review paper, which is enclosed to the thesis as attachment publication number 1.

REVIEW OF RADIOBIOCONJUGATES LABELED WITH AUGER ELECTRON EMITTERS.

Research on novel radiopharmaceuticals for Auger electron-targeted radiotherapy has primarily concentrated on radiobioconjugates labeled with ^{111}In and ^{125}I. This was because of their high availability and the ease of attachment to biomolecules. Recently, however, an increasing number of works have been published on radioconjugates labeled with other Auger electron emitters, including ^{67}Ga, ^{201}Tl, ^{197m,197}Hg, ^{193m,195m}Pt, ^{58m}Co, ^{119}Sb, ^{161}Ho and ^{135}La. In last few years, much attention has been paid to radiobioconjugates based on ^{161}Tb, an emitter of both β$^-$ radiation and Auger electrons.

DNA-BINDING RADIOBIOCONJUGATES
NUCLEOSIDE ANALOGUES: DEOXYNUCLEOTIDE AND OLIGONUCLEOTIDES

Nucleoside analogues are a group of compounds that intercalate into DNA by substituting specific nitrogenous bases. The most widely studied compound is the thymine analogue, 5-iodo-2'-deoxyuridine (IdUR), usually labeled with $^{123/125}$I. The advantage of this ligand is its DNA incorporation ability by replacing thymine. In spite of the rapid elimination of ^{125}I-IdUR from the body and its relatively limited tumor uptake, the therapeutic efficacy in patients has been proven to be considerable. A number of studies

evaluated the effect of the radionuclide, comparing [77]Br and ^{131}I, along with various alterations to the basic structure, such as [^{123}I]5-iodo-4-thio-2'-deoxyuridine. Nucleoside analogues and other DNA intercalators have minimal selectivity for cancer cells, therefore adversely affecting healthy cells. Efforts to conjugate vector molecules, which direct nucleotides to receptors on cancer cells, yielded inadequate results, as the nucleotides with the attached vectors lost their incorporation properties. Furthermore, the limitation of this group of compounds is that their action is limited only to cells in the S phase of the cell cycle, resulting in a small number of cells being susceptible to the action of these substances. Despite their numerous advantages, the current interest in these vectors is relatively low due to their significant limitations [37]. Additionally, oligonucleotides can serve as vectors to directly target specific DNA sequences and affect mRNA. ^{111}In-labeled 2'-O-methyl RNA (2'OMeRNA) is an oligonucleotide that has been evaluated for application in Auger therapy. This compound revealed significant selectivity for telomerase-overexpressing cells and a direct effect on DNA, as determined by double-strand damage assays [38].

ACRIDINE

Acridines are well-known compounds that intercalate with DNA. They are heterocyclic, three-ring compounds that bind to DNA through interactions between base pairs, particularly guanine and cytosine. Its combination with ^{125}I demonstrated efficient intercalation. However, the efficiency of double-strand break (DSB) generation was approximately 25% lower than that of ^{125}I-labelled iododeoxyuridine. Since acridines are low molecular weight compounds, their efficacy is significant due to the attachment site of radioactive iodine, where a relatively large atom may inhibit intercalation. Therefore, it is crucial to conduct the synthesis reaction properly [39].

CIS-PLATINUM

Cis-Platinum is one of the most important cytostatic agents, consisting of the Pt^{2+} cation surrounded by two chlorine atoms and two amino groups. It interacts with the DNA strand through the guanine of one chain, with the guanines of adjacent chains, or other bases or proteins. Platinum has two radionuclides, [193m]Pt and [195m]Pt, that exhibit the best characteristics among all discovered Auger emitters, with the highest number of emitted Auger electron per decay, being 27 ([193m]Pt) and 37 ([195m]Pt). Therefore, cisplatin labeled with these radionuclides could be an ideal agent for both chemo and radiotherapy. Due to the intercalation of cisplatin into the DNA strand, very high cytotoxicity can be expected [40]. However, as recently shown by Wawrowicz et al. [41], the production of high levels of [193m]Pt or [195m]Pt activities that are required for therapy is currently not possible. To label cis-platinum with an Auger electron emitter, the chlorine atoms in the complex were replaced with radionuclide [125]I. However, the study indicated a relatively low tumor uptake, with high accumulation in the liver and spleen [42].

ANTHRACYCLINS

Doxorubicin and daunorubicin are the most commonly used anthracycline antibiotics in cancer therapy. Crystallographic studies have demonstrated that doxorubicin and daunorubicin induce intercalation complexes with DNA, particularly at the 5'-GC-3' and 5'-CG-3' sequences [43]. The potential of anthracyclines to intercalate DNA has inspired investigations into their application in Auger electron therapy, including the labeling of daunorubicin derivatives with [125]I. The radiobioconjugate exhibits considerable cytotoxicity; nevertheless, a significant limitation of this approach is the elevated side effects in comparison with unlabeled daunorubicin, even when the antibiotic dosage remains the same [44]. The presence of an Auger electron emitter in the drug structure may provide a reduction in the required antibiotic dosage and avoid other side effects [45]. All intercalating compounds labeled with Auger electron emitters, as previously stated, exhibit significant cytotoxicity; however, they lack selectivity for cancer cells.

RADIOBIOCONJUGATES NOT INTERCALATING INTO DNA

Pouget et al.[32] indicated that the intercalation of a bioconjugate labeled with an Auger electron emitter into DNA is not necessary for cellular damage**.** Subsequently, numerous studies concentrated on identifying a suitable vector that specifically binds to receptors on cancer cells, capable of internalizing and penetrating the cell nucleus. Radiobioconjugates of cellular receptor antagonists can also be beneficial for Auger electron therapy. These compounds accumulate in the cell membrane receptors, leading to cell destruction. Various small molecules, peptides, monoclonal antibodies, and their fragments possess these characteristics.

SMALL BIOLOGICALLY ACTIVE MOLECULES LABELED WITH AUGER EMITTERS
MIBG (Meta-iodo-benzylguanidine)

MIBG is a vector applied for pheochromocytomas, neuroblastomas (extracranial solid tumors), and carcinoid tumors. High selectivity of uptake by tumors is achieved by the action of norepinephrine transporters, with relatively low accumulation in the healthy cells. MIBG labeled with a β^- emitter such as ^{131}I, is commonly used in the treatment of neuroblastoma; however, due to the use of the β^- emitter, its efficacy in addressing micrometastases is limited, which inspired extensive research into MIBG labeled with Auger electron emitters such as [123/125]I [46].

PSMA (Prostate Specific Membrane Antigen)

To date, only three PSMA receptor-targeting ligands radiolabeled with Auger electron emitters have been evolved in preclinical studies. In a study conducted in 2015, Kiess et al. [33] developed a ^{125}I-labeled 2-[3-[1-carboxy-5-(4-125I-iodo-benzoylamino)-pentyl] -ureido] pentanedioic acid (^{125}I-DCIBzL) for PSMA-specific targeting. *In vitro* studies showed high specific cellular accumulation and toxicity. This radiobioconjugate effectively induced DNA damage and resulted in delayed tumor growth in PC3-xenografts bearing mice. The study also confirmed the high cellular internalization of ^{125}I-DCIBzL and the

interaction of Auger electrons during cell mitosis. Recent studies by Müller et al. [19] demonstrated the potential of the ^{161}Tb radionuclide, which emits both β$^-$ and Auger electrons. They investigated it with a small urea derivative, a peptidomimetic conjugated with a DOTA chelator (PSMA-617). They showed that ^{161}Tb could be 3-fold more therapeutically efficient than ^{177}Lu, which emits only β$^-$ particles. Moreover, *in vivo* studies have demonstrated that ^{161}Tb-PSMA-617 has higher specific antitumor efficacy on single cancer cells and small cancer metastases. A ^{135}La radiobioconjugate with PSMA was also synthesized using a new bifunctional chelator, Py-Macrodipa. However, disintegration of the complex was observed in studies on a mouse model [47].

STEROIDS

Steroids have different molecular targets, including estrogen (ER), progesterone (PR), androgen (AR), and glucocorticoid (GR) receptors. For instance, estrogen receptors are overexpressed in breast cancer. The influence of androgen receptors seems to be particularly interesting in the case of triple-negative breast cancer. Clinical trials indicate that the presence of AR results in a reduced number of relapses, distant metastases, and reduced mortality rates [48]. The therapeutic efficacy of ^{123}I-labeled steroids, especially estrogen, has been evaluated, and the generation of DNA single- and double-stranded breaks has been confirmed [49].

PEPTIDES
SOMATOSTATIN ANALOGS

The majority of neuroendocrine tumors (NETs) express somatostatin receptors (SSTRs), making them ideal candidates for treatment with somatostatin analogue (SST analogue)-derived radiopeptides. Somatostatin analogues, such as octreotide and lanreotide, are synthetic peptides that mimic the biological functions of the natural peptide somatostatin, but have a significantly longer half-life (90 min vs 2 min), being resistant to plasma degradation [50].

The high affinity of these peptides for SSTRs and high internalization level of the peptide-conjugates can result in an increase in the tumor retention of the radiopeptide and efficient targeting. Furthermore, the small size of these peptides enables their quick clearance from the bloodstream, optimizing their therapeutic potential [51].

The potential application of these vectors in Auger electron therapy is related to the significant binding affinity of these peptides for tumor cells, leading to their subsequent internalization to the interior of the cell after binding to the receptor and partial translocation of the radiobioconjugate to the cell nucleus. The effectiveness of therapy using the radiopharmaceutical ^{111}In-DTPA-Octreotide (Oktreoscan™), frequently used in the diagnosis of neuroendocrine tumor, was evaluated. The results indicated a strong correlation

between the cytotoxic effects and receptor expression levels, as well as the inhibition of micrometastase formation in a rat liver tumor model. These findings not only highlight its efficacy but also indicate a significant increase in survival times [52]. In a study, Thisgaard et al. evaluated the efficacy of cobalt-labeled octreotide analogs for Auger electron targeted therapy. Receptor-specific binding and high cellular internalization levels ($\geq 88\%$) have been obtained in the case of all three cobalt-conjugated peptides (DOTATATE, DOTATOC, and DOTANOC). Cell survival studies showed a dose-dependent reduction. ^{58m}Co-DOTATATE indicated greater efficacy in cellular mortality per cumulated decay compared to ^{111}In- and ^{177}Lu-DOTATATE. Moreover, *in vivo* pharmacokinetic studies showed significant receptor-specific tumor accumulation [53].

EXENDIN

Exendin, a peptide that binds to the glucagon-like peptide receptor 1 (GLP-1), is utilized in the treatment of neuroendocrine tumors. ^{111}In-labeled Exendin was evaluated as a potential therapeutic compound; however, administration of high doses led to considerable kidney damage due to the biodistribution mechanism of exendin, which exhibits substantial renal accumulation. This is a significant problem, indicating that exendin derivatives are currently no of practical use [54].

BOMBESIN

It is a 14-amino acid peptide. It was originally extracted from the fire toad (Bombina bombina), a member of the fire toad family. Its strong affinity for gastrin-releasing receptors (GRP- r), overexpressed in prostate cancer and lymph node metastases, was identified. Bombesin is a non-internalizing antagonist of the GRP-r receptor. To facilitate its internalization, bombesin was modified by Tat (49–57), a peptide derived from a transactivator of the HIV-1 transcription protein, possessing a membrane translocation domain and an area responsible for nucleus localization. Cellular investigations have demonstrated that ^{99m}Tc-N_2S_2-Tat-(49–57)-Lys3-bombezine was significantly internalized into the nucleus of breast and prostate cancer cells [55]. Research continued by incorporating TAT-modified bombesin and the HYNIC-^{99m}Tc complex onto gold nanoparticles. A multimodal radiopharmaceutical was developed, utilizing Auger electron emission and hyperthermia after laser irradiation [56].

MONOCLONAL ANTIBODIES AND THEIR FRAGMENTS

- The overexpression of specific receptors on the cell membrane characterizes several malignancies and is associated with a more aggressive disease progression. Below are some of the most commonly overexpressed receptors: The Epidermal Growth Factor Receptor (EGFR) family is a subclass of receptor tyrosine kinase (RTK) proteins, comprising four members: EGFR (ErbB1, HER1), ErbB2 (HER2, neu in rodents), ErbB3 (HER3), and ErbB4 (HER4).
- Vascular endothelial growth factor receptor (VEGFR), involved in angiogenesis.

- Insulin-like growth factor 1 receptor (IGFR1), a transmembrane receptor that belongs to the extensive group of tyrosine kinase receptors, is activated by the hormone insulin-like growth factor 1 (IGF-1).

Numerous monoclonal antibodies have been developed that selectively bind to the aforementioned receptors. Reilly et al. conducted studies comparing ^{111}In-labeled human epidermal growth factor (hEGF), a 53-amino acid peptide, with the monoclonal antibody (MAb) 528 (IgG2a) for imaging EGFR-positive breast cancer. The ^{111}In-labeled anti-EGFR 528 monoclonal antibody exhibited tenfold higher tumor accumulation compared to the ^{111}In-DTPA-hEGF polypeptide (21.6% vs. 2.2% ID/g). The greater tumor uptake of the ^{111}In-mAb 528 antibody in comparison with ^{111}In-DTPA-hEGF indicates that radioimmunotherapy using monoclonal antibodies for cancers expressing EGFR receptors may be more effective than targeted radiotherapy employing peptide vectors [20].

The second member of the EGFR family, human EGF receptor 2 (HER2), has also been investigated as a radiotheranostic target. HER2 receptor overexpression is reported in about one-quarter of breast and ovarian cancer patients. The overexpression of these receptors is associated with more aggressive breast and ovarian cancer proliferation and a worse prognosis for those with lymph node metastases. On the other hand, the presence of the receptor facilitated targeted therapy with monoclonal antibodies, including trastuzumab and pertuzumab, as well as an antibody-drug combination (ADC) such as Kadcyla (trastuzumab - emtansine conjugate) [57]. Trastuzumab has been found to increase the internalization of the HER2 receptor, which is one of the proposed mechanisms of the drug's action [58]. Unfortunately, within a year, almost all patients with HER2+ metastatic breast cancer exhibited drug resistance; hence, it is anticipated that radioimmunotherapy may serve as one of the several approaches for improving the efficacy of trastuzumab treatment and overcoming drug resistance. Alongside several *in vitro* and *in vivo* studies, comprising clinical trials using trastuzumab labeled with β$^-$ and α-emitters, research was also done to explore the potential application of Auger electron emitters for the treatment of small metastatic tumors in breast and ovarian cancer.

THP-trastuzumab and DOTA-trastuzumab were synthesized and then radiolabeled with ^{67}Ga and ^{111}In Auger electron emitters, respectively [59]. The radiopharmaceuticals were assessed for HER2-specific binding and internalization. Additionally, their effects on the viability and clonogenicity of HER2-positive HCC1954 and HER2-negative MDA-MB-231 cell lines were evaluated. Studies have demonstrated that the viability and clonogenicity of HER2-positive cells decreased when radionuclides were incorporated into the cells through conjugation with trastuzumab. However, this reduction was not observed when the same level of radioactivity was administered without antibody conjugation. This clearly indicates that for therapeutic effects, ^{67}Ga and ^{111}In must be internalized into the cells.

To enhance the nuclear localization of the radiolabeled trastuzumab, researchers combined it with a Nuclear Localization Sequence (NLS) peptide, enabling it to cross the nuclear envelope. Reilly's group has extensively utilized this mechanism along with the Auger electron emitter, [111]In [60, 61]. They demonstrated that ^{111}In-trastuzumab significantly induced DNA double-strand breaks (DSBs) and markedly reduced clonogenic survival.

Another study demonstrated the efficacy of [^{125}I]I-zolbetuximab, a radiopharmaceutical targeting the Claudin 18.2 (CLDN 18.2) receptor in gastric cancer. The compound showed a molar activity of 1.75×10^2 GBq/μmol, together with a labeling efficiency of more than 99%. The prolonged tumor retention and rapid metabolic elimination at other tissues of [^{125}I] I-zolbetuximab were observed in both small-animal SPECT-CT imaging and biodistribution studies. Due to the excellent targeting capability of zolbetuximab for CLDN18.2, [^{125}I]I-zolbetuximab exhibits remarkable specific binding and retention in tumors with CLDN18.2 overexpression [62].

Numerous studies have focused on the use of nanostructures to bind Auger emitters. This approach offers the advantage of achieving high specific activities for radiobioconjugates, which is especially important in Auger electron therapy. Researchers synthesized radiobioconjugates using trastuzumab and panitumumab conjugated with gold, platinum, and palladium nanoparticles, and a polymer block labeled with isotopes such as ^{111}In, ^{125}I, and [103,109]Pd. These radiobioconjugates are widely discussed in review publication no. 1, as well as publications 2 and 3 attached to the doctoral dissertation.

RADIOBIOCONJUGATES BASED ON β⁻ + AUGER ELECTRON EMITTER - [161]Tb

There are four different radionuclides of Tb which are being used in SPECT ([155]Tb) and PET ([152]Tb) imaging studies as well as therapeutic applications ([149]Tb and [161]Tb), making Tb family ideal for theranostic applications. The radiolanthanide [161]Tb ($t_{1/2}$=6.89 d) has recently been introduced for therapeutic applications due to its emission of β⁻ particles (E $_{β-av}$= 154 keV) and γ-radiation (E$_γ$ = 49 keV, I = 17.0% and E$_γ$ = 75 keV, I = 10.0%), which are appropriate for therapeutic applications and single-photon emission computed tomography (SPECT), respectively [63]. In addition to emitting one beta particle per decay, an average of 2.24 Auger and conversion electrons are also released. These electrons have energies ranging from 3 to 50 keV, contributing to 27% of the total energy from beta decay. However, they produce a significantly higher local dose density due to their shorter range in tissue, which is between 0.5 and 30 μm. With this yield of conversion and Auger electrons, [161]Tb is similar to radionuclides such as ^{67}Ga and [111]In [64].[161]Tb has radiochemical features comparable to those of ^{177}Lu; however, the γ-radiation released by [161]Tb has lower energy [65]. Uygur et al. [65] evaluated the therapeutic efficacy of [161]Tb-radiolabeled PSMA-617. [161]Tb-PSMA-617 showed hydrophilic characteristics and high stability with a radiochemical yield of 95% for up to 72 hours. According to *in vitro* studies, [161]Tb-PSMA-617 exhibited high cytotoxicity

to LNCaP cells; however, it did not affect PC-3 cells. Moreover, *in vivo* scintigraphy imaging demonstrated the accumulation of [161]Tb-PSMA-617 in the prostate, kidneys, and bladder.

The enhanced therapeutic efficacy of [161]Tb has been shown in many *in vitro* and *in vivo* studies. [161]Tb-DOTA-cm09 showed more efficacy in reducing the viability of cancer cells compared to ^{177}Lu-DOTA-cm09 in folate receptor-positive KB and IGROV-1 cells. Furthermore, [161]Tb-DOTA-cm09 significantly inhibited tumor proliferation and improved the survival of tumor-bearing mice with greater efficiency [66]. In contrast to previous beliefs suggesting that internalization is essential for the efficiency of short-ranged IC and Auger electrons, the non-internalizing somatostatin antagonist [161]Tb-TbDOTA-LM3 has been demonstrated to be 100 times more effective than its ^{177}Lu-based equivalent in reducing the viability of tumor cells. In contrast, compared to [177]Lu- DOTATOC (the internalizing somatostatin agonist), [161]Tb-DOTATOC showed only 5-times higher efficacy in reducing the viability of tumor cells. The *in vivo* results confirmed that the cell membrane-localizing [161]Tb-DOTA-LM3 was much more effective in inhibiting tumor development compared to ^{177}Lu-DOTA-LM3 and [161]Tb-DOTATOC. These results clearly confirmed that the cell membrane is a better therapeutic target for Auger electrons than the cytoplasm [67, 68].

IN VIVO GENERATORS FOR AUGER ELECTRON EMITTERS

A cancer patient may have substantial non-resectable metastases with inadequate penetration and potential heterogeneity in target expression, as well as dispersed single cells and micro-metastases, which serve as targets for both β^- particles and Auger electrons. Based on the results obtained for [161]Tb-labeled bioconjugates, an optimal therapy should consist of a combination of therapeutic radionuclides, including β^- and Auger emitters, conjugated to the same carrier molecules. A potential approach might include using an *in vivo* generator, in which the parent and daughter radionuclides show distinct decay patterns [69]. If the targeted molecule, radiolabeled with the parent radionuclide, is internalized into the tumor cells, it is quite likely that the daughter radionuclide will decay within the same cell, if its half-life is suitably short. This is a reasonable assumption for radioactive metals, which get trapped within cells. An instance of this generator system is [114m]In/[114]In, as proposed by Tolmachev et al. [70] for therapeutic purposes. Upon translocation into the tumor cell nucleus, the breakdown of metastable [114m]In ($t_{1/2} = 49.5$ d) would generate lethal Auger electrons, while the daughter radionuclide [114]In ($t_{1/2} = 72$ s) releases high-energy β^- particles, which are effective in treating larger tumors and metastases.

Lubberink et al. [71] proposed the application of the Auger electron and positron-emitting generator [134]Ce/[134]La ($t_{1/2} = 3.16$ d and 6.45 min) for radionuclide therapy. It combines β^+ with Auger electrons. Beta$^+$ particles possess energy comparable to those released by [90]Y. Bioconjugates labeled with [134]Ce/[134]La *in vivo* generator may be useful in the therapy of numerous cancer patients exhibiting both substantial tumors,

optimally managed with high-energy β^+ particles, and isolated disseminated tumor cells or micrometastases, which are more effectively treated with low-energy Auger and conversion electrons. Additionally, the positron-emitting ^{134}La can be applied to investigate kinetics and dosimetry using PET technique. The PET resolution, recovery, and quantitative accuracy were slightly lower for ^{134}La in comparison to ^{18}F. The absorbed dosages to single cells from ^{134}Ce/^{134}La were greater than those from ^{90}Y and ^{111}In, and the absorbed dosages to spheres simulating bulk tumors were nearly equivalent to those for ^{90}Y and tenfold greater than those for ^{111}In. Unfortunately, the whole-body absorbed dosages from the somatostatin analog octreotide were greater for ^{134}Ce/^{134}La compared to ^{90}Y, due to the annihilation of photons from ^{134}La. Finally, this preliminary examination of the medicinal potential of ^{134}Ce/^{134}La is promising [71].

Other *in vivo* generators that produce Auger electron emitters include the ^{103}Pd/^{103m}Rh and ^{109}Pd/^{109m}Ag generators, which have been thoroughly described in the attached publications 2, 3, and 4.

RECOIL EFFECTS IN *IN VIVO* GENERATORS

The most important consideration while using an *in vivo* generator is the chemical outcome of the parent degradation. In several instances, the change of atomic number results in a substantial difference between the chemistry of the parent and daughter radionuclides (e.g., the transition from alkali rubidium to noble krypton). Nevertheless, even if both parent and daughter radionuclides exhibit almost identical chemical behavior, such as in transitions amongst lanthanides, there is a potential for chemical alteration because of the atomic effects of nuclear disintegration. Molecular alterations resulting from nuclear reactions are known as Szilard-Chalmers reactions, initially defined by Szilard and Chalmers in 1934 as a method for separating iodine isotopes following the chemical disturbances induced by neutron capture [72]. Subsequently, several Szilard-Chalmers-type reactions have been documented for medical isotope production [73], particularly in generator reactions.

Medical radionuclides are often employed as labels on chemically specific "targeting" molecules, including peptides, antibodies, or receptor-specific small molecules. In the application of an *in vivo* generator in these targeted systems, there are two possibilities for the daughter radionuclide to dissociate from the parent: either due to the elemental disparities between the parent and daughter or as a result of the physical and chemical disturbances induced by the nuclear decay process. The dislocation of the daughter radionuclide from the targeted molecule can be either advantageous or disadvantageous, depending on the intended application of the generator. Thus, it is crucial to understand when dislocation is anticipated and to recognize its consequences.

Zeevart et al. explained the physical issues related to the expected chemical rearrangement in publications [74, 75]. Their initial strategy involved examining if the recoil of the daughter nucleus following β^- decay, considering both the released neutrino and electron, might generate enough energy

needed to separate the daughter from strong polydentate chelates. In many cases, the binding energy of the chelate is excessively high to be surpassed by the minimal energy involved in nuclear recoil. For instance, in the case of the ^{90}Sr/^{90}Y complexed with 1,4,7,10 tetraazacyclododecane-1,4,7,10 tetra-acetic acid (DOTA), about 1% of all β$^-$ decays resulted in the removal of the daughter radionuclide ^{90}Y [76]. Internal transition (IT) decays also align with the retention of stable chelation under low energy recoil, as seen by the transition of ^{44m}Sc to ^{44g}Sc, which results in no detectable dislocation of the daughter atom from stable chelate complexes with DOTA [77]. In contrast, for alternative decay mechanisms, the physical recoil energy may significantly surpass the binding energy. This refers to the ^{213}Bi $\xrightarrow{\beta-(45\,m)}$ ^{213}Po $\xrightarrow{\alpha(4.2\mu s)}$ ^{209}Pb decay, wherein the average β$^-$ and α recoil energy is approximately 100 keV, in contrast to the binding energy of the daughter Pb^{2+} with the prevalent chelators DOTA or its amide derivative, which has an energy of several electronvolts.

Electron capture (EC) decays are effective in liberating daughter radionuclides from strong chelates, as demonstrated with ^{140}Nd and ^{134}Ce. In these cases, the Auger electron cascade resulting from nuclear absorption of an inner shell electron induces atomic rearrangements that avoid chelation. In comparable Auger processes, including the decay of ^{165}Er, it is estimated that the autoionization subsequent to the transition to ^{165}Ho leaves the daughter in an unstable and extremely oxidized state, with an average loss of 7.6 electrons per decay [78]. Studies of the electron capture decay of radiolanthanides indicate that the daughter radionuclides do not preserve the chemical state of the parents following the significant loss of electrons [79]. A similar result applies to the analogous process of internal conversion (IC). In the decay of DOTA-bound ^{166}Dy, 72% of all decays result in an IC-induced Auger cascade, and consistently, 72% of daughter ^{166}Ho atoms are observed free of DOTA, indicating that the delocalization is a Szilard-Chalmers reaction.

Another explanation was proposed by Wang et al. [80]. They investigated the ^{166}Dy/^{166}Ho *in vivo* generator and suggested that the loss of daughter radionuclides is due to their de-excitation through internal transformation, which emits Auger electrons. This process occurs instead of loss being caused by the recoil energy associated with the emission of beta particles and neutrinos. As a consequence, the de-excited daughter radionuclides become highly charged, leading to the capture of electrons from the surrounding donor atoms of the chelator. Additionally, when electrons are transferred to these highly charged atoms, the donor atoms of the chelators become positively charged. This positive charge results in the breaking of metal-ligand bonds due to the Coulomb repulsive force between the positively charged atoms, causing the daughter radionuclides to be released as free cations.

According to Zeevaart et al. [76] and Nath et al.[81] one method for counteracting the daughter atoms' Auger-induced displacement is to conjugate the metal ions through a ligand with a comprehensive

delocalized π-electron system, such as heme. These ligands show the ability to quench the phenomenon known as the "Coulomb explosion" by transporting delocalized electrons to the metal core within time scales equivalent to the Auger cascade.

As a general rule, when both the daughter and parent radionuclides can form stable complexes with the bioconjugate-chelate moiety, the parent EC, IC, and alpha decays will result in the dislocation of the daughter, while beta and isomeric transitions typically maintain the daughter in the parent's chemical state. The recoil effects in ^{103}Pd/^{103m}Rh and ^{109}Pd/^{109m}Ag *in vivo* generators studied in the dissertation have been extensively discussed in the attached publications 2, 3, and 4.

PALLADIUM RADIONUCLIDES IN NUCLEAR MEDICINE

In nuclear medicine, ^{103}Pd-metal was introduced in 1987 as implanted seeds for brachytherapy. In this form, ^{103}Pd is widely used today. Besides brachytherapy, three palladium radionuclides, ^{103}Pd, ^{109}Pd, and ^{112}Pd, possess properties suitable for use in nuclear medicine; however, they have not been studied extensively.

^{103}Pd has a half-life of 17 days and decays by electron capture and Auger electron emissions to the ^{103m}Rh-daughter ($t_{1/2}$=56 min), which decays to stable ^{103}Rh, emitting a cascade of Auger electrons. ^{103}Pd is obtained through a cyclotron as a high-specific, no-carrier-added product and can be easily produced by neutron irradiation of an enriched ^{102}Pd target. The second radionuclide of palladium, ^{109}Pd, decays by β$^-$ particle emission (E$_{β(max)}$=1.12 MeV, 100% yield) to the daughter nuclide, ^{109m}Ag ($t_{1/2}$=39.6 s), which in turn emits a photon (88 keV, 3.6% yield) accompanied by a cascade of conversion and Auger electron emissions leading to the stable Ag. ^{109}Pd can be simply produced from an isotopically enriched ^{108}Pd target in a nuclear reactor. The third radionuclide, ^{112}Pd, emits β$^-$ radiation and decays to ^{112}Ag, which also emits β$^-$ radiation ($t_{1/2}$=3.13 h). Despite its favorable half-life of 21 h, it has not yet found any medical applications.

^{109}Pd-based compounds have been examined to manage homograft rejection, and ^{103}Pd-metal was launched in 1987 as implanted seeds for brachytherapy [82]. In spite of the initial applications, subsequent advancements have been quite limited. Palladium radioisotopes have been rarely utilized in radiopharmaceutical investigations, and only a limited number of ligands, including DTPA and porphyrins, were investigated [83, 84]. The most plausible explanation is that the palladium coordination chemistry does not align with the chelators considered to be gold standards in nuclear medicine, specifically derivatives of DOTA (1,4,7,10-tetraazacyclododecane-1,4,7,10-tetraacetic acid) and NOTA (1,4,7-triazacyclononane-1,4,7-triacetic acid).

As mentioned, ^{103}Pd is one of the radionuclides commonly used in clinical low-dose brachytherapy. Laprise-Pelletier synthesized core-shell nanoparticles (<50 nm) with a ^{103}Pd core coated with a gold shell ([^{103}Pd] Pd@Au nanoparticles-PEG). Moreover, analogous nanoparticles were radiolabeled with the high-

energy β⁻ emitter gold-198 ([^{103}Pd] Pd@[^{198}Au] Au nanoparticles-PEG). Four weeks after injection of 60 MBq of both types of nanoparticles in PC3 tumor-bearing mice, the tumor volume diminished by 56% and 75% in the groups that received [^{103}Pd] Pd@Au-PEG and [^{103}Pd] Pd@[^{198}Au] Au-PEG nanoparticles, respectively [85]. Moeendarbari et al. [86] developed ^{103}Pd-coated gold nanoseeds, with a 100 nm inner gold core and an exterior ^{103}Pd shell. The [^{103}Pd] Pd@Au nanoseeds considerably inhibit prostate tumor growth and lower tumor metabolic activity five weeks after treatment.

Pineau et al. conducted a study on the coordination of natural Pd^{2+} and $^{109}Pd^{2+}$ with bifunctional cyclam derivatives: TE1PA, TE1Bn (benzyl cyclam), and TE1Py (pyridylmethyl cyclam). The goal of their research was to explore the coordination of both ^{64}Cu and ^{109}Pd, which may facilitate the development of innovative radiopharmaceuticals utilizing the ^{64}Cu/^{103}Pd or ^{64}Cu/^{109}Pd theranostic pairs. This study demonstrated that ligand functionalization resulted in a reduction in the thermodynamic stability of the complexes, which nonetheless exhibited high stability constants (log K_{ML} = 38.4 for [Pd(TE1PA)]$^{+}$). Radiolabeling studies have shown that the incorporation of the picolinate pendant on the cyclam backbone enhanced both the ^{109}Pd-radiolabeling efficiency under moderate conditions and the stability against transchelation. This facilitates the attractive application of bifunctional TE1PA derivatives for therapeutic applications via Pd radioisotopes, and for theranostic applications when paired with ^{64}Cu for PET imaging [87].

Porphyrin analogs labeled with an appropriate therapeutic radionuclide may serve as potential agents for targeted cancer radiation therapy. T. Das et al. [88] radiolabeled a porphyrin derivative 5,10,15,20-tetrakis[3,4-bis(carboethoxymethyleneoxy)phenyl]-porphyrin with ^{109}Pd. ^{109}Pd was produced with a specific activity of about 1.85 GBq/mg and radionuclidic purity of 100% by the thermal neutron irradiation of an enriched (98% in ^{108}Pd) metallic palladium target at a flux of 3×10^{13} n/cm² s for 3 days. The ^{109}Pd-porphyrin complexes were generated with high radiochemical purity (>98%) and demonstrated stability for up to 24 hours at room temperature. Moreover, biodistribution studies on mice with fibrosarcoma tumors showed significant tumor uptake [(5.28±1.46) % injected activity (IA)/g] 30 min after injection. The complex demonstrated advantageous tumor/blood and tumor/muscle ratios [1.69±0.23 and 5.00±1.54, respectively, at 3 hours p.i.]; nevertheless, there was significant liver uptake over the research period (> 20% IA).

In a recently published study, Hindié et al. [89] employed the Monte Carlo algorithm CELLDOSE to evaluate absorbed doses from ^{103}Pd/^{103m}Rh in relation to ^{177}Lu and ^{161}Tb in individual cells and cell clusters, considering diverse radionuclide distributions. Tumor heterogeneity and the prospective advantages of dual-targeting were investigated as well. The results indicated that, throughout a single cell, the nuclear

absorbed dose and membrane absorbed dose of ^{103}Pd were 7 to 10 times and 9 to 25 times greater than that of ^{177}Lu, respectively. In the 19-cell clusters, the absorbed doses of ^{103}Pd were also significantly higher than those of ^{177}Lu. In all cases, ^{161}Tb was placed between ^{103}Pd and ^{177}Lu. Non-uniform targeting of four unlabeled cells within the cluster led to moderate to severe dosage heterogeneity. For instance, with intranuclear ^{103}Pd, unlabeled cells absorbed just 14% of the anticipated nuclear dosage. The utilization of two ^{103}Pd-labeled radiopharmaceuticals reduced dosage heterogeneity. As a result, ^{103}Pd, an advanced Auger emitter, may provide significantly greater absorbed doses than ^{177}Lu to individual tumor cells and cell aggregates. This might expand the use of TRT in adjuvant or neoadjuvant contexts or for addressing minimum residual disease.

AIM OF THE THESIS
The main considerations in the selection of a radionuclide for targeted radionuclide therapy are the energy of the emitted particles and the range of these particles in tissues. For larger tumors, the best therapeutic effects are achieved using radiopharmaceuticals based on β$^-$ particle emitters. One challenge of using β-emitting targeted radionuclide therapy is the harm caused to normal, healthy cells. This damage happens because β$^-$ particles can travel longer distances in tissue, leading to unwanted radiation effects. The effective tissue range of β$^-$ particles is not optimal for the treatment of tumors consisting of small cell clusters or single cells and micrometastases, as a significant portion of the decay energy is deposited outside the boundary of the tumor. Targeted radiotherapy based on α particles is a promising alternative to β$^-$ particles, because the α particles deposit their whole energy within a few cell diameters (50–100 μm). Unfortunately, the availability of alpha emitters is limited, and they have not found widespread applications yet. Besides α emitters, radionuclides that decay with the emission of very low energy Auger electrons are well suited for the treatment of small tumors, micrometastases, or residual tumors after the surgical resection of a primary lesion. Because the path length of Auger electrons is short, compared to the size of a cell, they are minimally toxic to surrounding non-targeted cells; therefore, it is possible to inject about 10-fold greater radioactivity of Auger emitters than β$^-$ particle emitters without toxic side effects.

In order to enhance therapeutic efficacy, an interesting alternative is to ensure simultaneous implementation of low- and high-LET radiation. The principle of this strategy is primary damage of massive tumors *via* β$^-$ radiation with subsequent treatment enhancement due to the tumor subpopulations (such as cancer stem cells), metastatic sites, or single tumors targeting with Auger electrons or α emitters. The mentioned approach is frequently used in the tandem treatment of metastatic prostate cancer, where ^{177}Lu-labeled PSMA-617 is followed by ^{225}Ac-PSMA-617 therapy [90]. Published in the last decade, breakthrough findings from Mueller et al. [66] revealed that the application of ^{161}Tb (T$_{1/2}$=6.95 d) can induce a considerably greater therapeutic effect than observed in comparable studies with ^{177}Lu (6.64 d). As

mentioned, ^{161}Tb has decay properties similar to those of ^{177}Lu but, additionally, emits a substantial number of conversion and Auger electrons. This phenomenon was also confirmed by dosimetric calculations, which clearly proved the superiority of ^{161}Tb over ^{177}Lu in the therapeutic management of minor neoplastic lesions (<200 μm) [91].

Our group possessed the idea of using another radionuclide, ^{109}Pd (with a half-life of 13.7 hours), in the form of a ^{109}Pd/^{109m}Ag *in vivo* generator, as an alternative to the previously proposed ^{161}Tb. Our approach aims to utilize β$^-$ and Auger electron emitters through this *in vivo* generator, thereby aligning with the latest trends in the design of radiopharmaceuticals that emphasize innovative pathways for tissue deposition of emitted radiation. ^{109}Pd decays through a β$^-$ transition (β$_{max}$ = 1.12 MeV, 100% yield) to ^{109m}Ag (39.6 s), which subsequently decays to stable ^{109}Ag, emitting 88-keV photons (3.6%), followed by a cascade of conversion and Auger electrons. Therefore, the combination of ^{109m}Ag and ^{109}Pd leads to the formation of an *in vivo* generator, which is beneficial against ^{161}Tb with a greater number of Auger/conversion electrons and higher β$^-$ particle energy [92]. Furthermore, in contrast to ^{161}Tb, ^{109}Pd can be simply produced by thermal neutron irradiation. Activating the enriched metallic Pd target for 3 days, results in a specific activity of 25 GBq/mg.

Consequently, the objective of my doctoral thesis was to experimentally verify the effectiveness of radioconjugates of ^{109}Pd/^{109m}Ag in an *in vivo* generator for combined β$^-$ and Auger electron therapy.

For efficient Auger electron therapy, the application of radiopharmaceuticals with very high specific activity is necessary. Therefore, we decided to label bioconjugates using nanotechnology by synthesizing monoclonal antibodies conjugated to gold nanoparticles (15 nm) coated with a monolayer of ^{109}Pd. In this case, the ^{109}Pd atoms will stay on the surface of the nanoparticle, and the ^{109m}Ag atoms formed in the decay process will be able to emit Auger electrons freely. We have estimated that it is possible to deposit over 11,000 palladium atoms (assuming an atomic radius of 140 pm) onto the surface of a single gold nanoparticle. This could lead to a significant (300-fold) increase in specific activity compared to the ^{111}In chelation by DOTA. Therefore, our proposed application of ^{109}Pd-coated AuNPs (Au@^{109}Pd) is expected to yield a high specific activity of a potential radiopharmaceutical with valuable radiochemical properties for combined β$^-$ and Auger electron therapy.

An additional important goal of my doctoral thesis was to verify whether ^{109m}Ag can diffuse from the nanoparticle surface after the decay of ^{109}Pd, potentially causing toxic effects on surrounding healthy cells. In addition, as part of my work, I conducted initial studies on the behavior of a promising *in vivo* ^{103}Pd/^{103m}Rh generator, which only emits an Auger electron cascade and low-energy γ quanta.

OVERVIEW OF ATTACHED PUBLICATIONS
PUBLICATION NO. 1

Nasrin Abbasi Gharibkandi, Joanna Gierałtowska, Kamil Wawrowicz, Aleksander Bilewicz. "Nanostructures as Radionuclide Carriers in Auger Electron Therapy" Materials 15, 2022, 1143. IF=3.4 (2022)

The common subject among the four attached publications is our approach to combining palladium radionuclides with biological vectors using nanostructures. This method enables the synthesis of radiobioconjugates with exceptionally high specific activity, making it possible to utilize even radionuclides produced with carrier-added form.

Publication no. 1 is a review paper in which my colleagues and I collected previously published results on using various nanostructures for immobilizing Auger emitters and linking them with biomolecules.

Commonly used Auger emitters such as ^{111}In and ^{125}I can be attached to biomolecules through halogenation ([123,124,125]I) or by chelating agents such as DTPA and DOTA. However, the specific activity achieved while labeling monoclonal antibodies is often insufficient for practical therapeutic use. For instance, the specific activity of ^{111}In-labeled trastuzumab does not exceed 0.24 MBq/µg, meaning that only 1 in 50 antibody molecules is radiolabeled [93]. As a result, the cytotoxicity is limited due to an insufficient number of radiolabeled molecules binding to cell receptors.

Additionally, simply increasing the number of chelators conjugated to the antibodies may not improve specific activity, as it could decrease their immunoreactivity. A promising alternative is to use nanoparticle-based delivery systems, which can achieve higher specific activity by attaching multiple chelators to their larger surface area. As I discussed in my review paper and subsequent publications, it is also feasible to synthesize metallic nanoparticles containing radioactive atoms (such as [103,109]Pd), utilizing chemisorption iodine radionuclides onto the surfaces of gold (Au) or platinum (Pt) nanoparticles, and applying core shell nanoparticles (Au@[103,109]Pd). Nanoparticles can be modified with different vectors, including antibodies, peptides, or small biologically active molecules showing high affinity to the tumor cell receptors, improving the delivery of radioactivity and therapeutic efficacy. Nanoparticles facilitate multimodal approaches by combining imaging, radiotherapy, and chemotherapy. Unique properties such as magnetization or photosensitization further enhance delivery, allowing the use of external stimuli such as magnetic fields, near-infrared radiation, or hyperthermia to boost therapeutic outcomes. These advancements in nanomedicine present significant opportunities for optimizing Auger electron therapy in cancer treatment. Fig.2 presents various nanostructures applied as a carrier and reviewed in our publication.
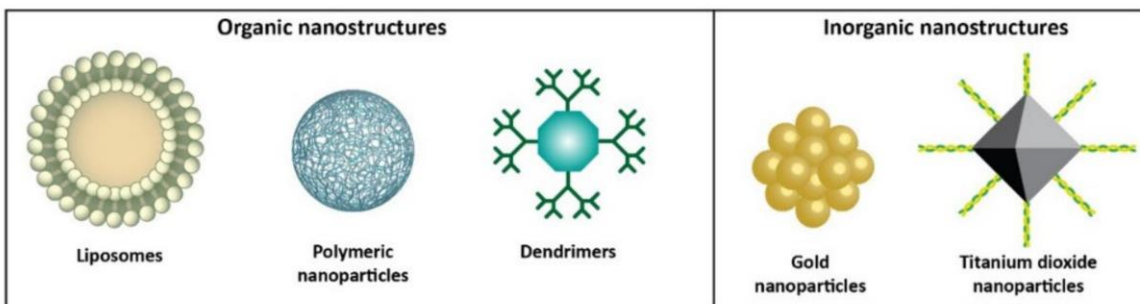
Fig. 2. Organic and inorganic nanomaterials discussed in this review.

Among organic nanostructures, metal-chelating polymers with attached multiple chelating groups have been studied to increase the specific activity of the radioimmunoconjugates [94]. Block copolymer micelles (BCM), which are amphiphilic copolymer nanostructures consisting of a hydrophobic core that can enclose chemotherapeutics, while the surrounding hydrophilic corona can be labeled with radionuclides, have also been used. The researchers synthesized 30 nm BCM labeled with ^{111}In using the chelator DTPA and loaded with the radiosensitizer methotrexate, nuclear localization signal (NLS) peptides, and trastuzumab fab vectors. BCM enables the simultaneous delivery of Auger emitters to the cell nucleus and the radiosensitizer, resulting in a synergistic therapeutic effect [95].

Other solutions include the use of dendrimers with attached chelators and the commonly used liposomes in chemotherapy. As shown in Fig. 3, liposomes can contain a chemotherapeutic agent, such as doxorubicin, a radionuclide, and surface-attached vectors guiding them to cancer cells.
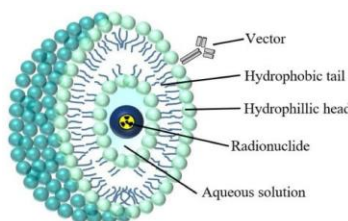

Fig. 3. Structure of a liposome containing a radionuclide.

Liposomes were labeled with [123,125]I [96] and [111]In [97]. However, compared to liposomes containing chemotherapeutics, the use of liposomes for radionuclide delivery is limited.

In contrast to organic nanostructures, the use of metallic nanoparticles as radionuclide carriers is much greater. In particular, the properties of gold nanoparticles facilitate the attachment of targeting vectors and radionuclide-binding chelators to their surface by means of a strong gold-thiol bond. Iodine radionuclides can also be easily attached to the surface of Au nanoparticles by chemisorption. In the research conducted by the Reilly group [31, 98, 99] it has been found that the application of Au nanoparticles as a carrier of

[111]In greatly increases the effectiveness of Auger therapy without reducing its specificity. For instance, ^{111}In-AuNP-trastuzumab conjugates were selectively bound, internalized, and deposited near the nucleus in HER2-positive SK-BR-3 and MDA-MB-361 human breast cancer cells. Strong tumor growth inhibition properties of ^{111}In-AuNP-trastuzumab were also reported. The authors concluded that increasing the specific activity by the multiplication of ^{111}In-DTPA chelate on Au nanoparticles significantly enhances the cytotoxic potential against HER2-overexpressed breast cancer cells and extends their cytotoxicity to cells with intermediate HER2 expression.

In addition to Au nanoparticles, titanium dioxide (TiO_2) nanoparticles are also being utilized as carriers for [125]I [100]. Due to their high surface activity and non-toxic nature, TiO_2 nanoparticles are increasingly employed in medical applications, including cancer therapy and antibacterial treatments. A study was conducted to investigate the therapeutic effects of ^{125}I-TiO_2 in tumor-grafted mice. The results showed that tumor growth was inhibited in the group treated with ^{125}I-TiO_2 compared to the group that received free [125]I. The observed effect is attributed to the higher retention of ^{125}I-TiO_2 in the tumor, in contrast to the inadequate retention and subsequent diffusion of free ^{125}I to other organs.

In the review article, I also included a chapter on using high-Z nanoparticles to increase the absorbed radiation dose deposited in tumors from external X-ray radiation. The radiosensitization effect arises from the strong interaction between photons and high-Z (high atomic number) atoms. This interaction leads to an increase in local dose deposition and the emission of conversion and Auger electrons. This phenomenon is highly relevant to radiation oncologists because it enhances the generation of secondary electrons when nanoparticles with high-Z elements are introduced into cancer cells and then exposed to X-rays. Numerous research groups are actively developing new radiosensitization agents using high-Z elements, including gold (Z=79), hafnium (Z=72), gadolinium (Z=64), iodine (Z=53), platinum (Z=78), and bismuth (Z=83). This approach has significant potential for cancer therapy.

In summary, the use of nanoparticles as carriers for radionuclides, especially Auger electron emitters, remains limited despite the advantages offered by the high specific activity of radiobioconjugates. This is due to the difficulty of systemic administration, which causes the accumulation of nanoparticle conjugates by the liver, lungs, and spleen, resulting in rapid blood clearance and minimal accumulation by the tumor. Therapeutic efficacy may only be achieved by the direct administration of radioactive nanobioconjugates to the tumor or the postoperative cavity after tumor resection. This therapy approach, termed targeted nanobrachytherapy, has been proposed for the local treatment of advanced breast and prostate cancer. *In vivo* studies indicate that radioactively labeled nanoparticle bioconjugates, when delivered directly into the tumor, display almost perfect retention within the tumor, with minimal uptake in the liver and spleen.

High-Z element nanoparticles also hold significant potential; they are commonly studied as sensitizers for external X-ray radiation and have been discussed in numerous articles. These studies are currently in the clinical trial phase.

PUBLICATION NO. 2

The studies presented in publication no. 2 aimed to synthesis and characterize radiobioconjugates prepared from core-shell nanoparticles, whereby gold nanoparticles were coated with a thin layer of the radioactive isotope ^{109}Pd. I chose ^{109}Pd due to its interesting properties as a radionuclide. It emits both β⁻ radiation and conversion and Auger electrons, making it particularly effective for radionuclide therapy. The significant number of recent publications focused on ^{161}Tb—another radionuclide that emits β⁻ and Auger electrons—supports our decision.

The proposed isotope, ^{109}Pd, undergoes a β⁻ decay transition (with a maximum energy of 1.12 MeV and a yield of 100%) to form ^{109m}Ag, which has a half-life of 39.6 seconds. This decay process is accompanied by the emission of an 88 keV photon (3.6%), followed by the cascade emission of conversion and Auger electrons. As a result, the combination of ^{109m}Ag and ^{109}Pd forms an *in vivo* generator. This system is advantageous compared to ^{161}Tb, as it produces a higher number of Auger and conversion electrons and has β⁻ particles with higher energy. Additionally, unlike ^{161}Tb, ^{109}Pd can be easily produced through thermal neutron irradiation, achieving a specific activity of up to 50 GBq/mg.

Several key issues must be addressed to effectively utilize the ^{109}Pd/^{109m}Ag *in vivo* generator in radionuclide therapy. First, it is essential to select an appropriate bifunctional chelator; then, a radiobioconjugate with high specific activity needs to be synthesized, and finally, the problem of releasing the ^{109m}Ag daughter radionuclide after decay must be resolved. At present, there is no commercially available bifunctional chelator that can effectively complex palladium cations. Even when using proposed ligands based on the macrocyclic cyclam [87], the specific activity of the resulting antibody radioconjugates remains unsatisfactory. Moreover, as I demonstrated in the attached publication (no. 4), the ^{109}Pd-cyclam complexes completely release the daughter ^{109m}Ag radionuclides.

As we proposed, the most effective solution to meet these requirements is the use of nanoparticles to bind [109]Pd and conjugate them with biological vectors. In the studies outlined in the attached publications 2 and 3, gold nanoparticles were coated with a layer of [109]Pd. In publication 4, we used palladium nanoparticles with a diameter of 5 nm. In both cases, the [109]Pd atoms were located on or next to the surface of the nanoparticles, so facilitating the easy emission of short-range Auger electrons. The specific activity of these conjugates was high, and importantly, my studies found that the daughter radionuclide [109m]Ag did not escape from the nanoparticle's surface. Measurements of aliquots taken immediately after centrifugation of the nanoparticles showed no presence of free daughter [109m]Ag in the solution.

I found this surprising because, typically, following β^- decay, a daughter atom with entirely different properties is formed, and the daughter radionuclide is released from the complex. However, the situation changes significantly when the parent radionuclide is immobilized on a metallic surface rather than in a chelate complex. The use of a metallic surface, such as a gold nanoparticle, as a carrier for the parent radionuclides facilitates the availability of delocalized electrons in the metal. Following nuclear decay and the emission of Auger electrons, the strongly positively charged daughter radionuclide neutralizes its charge by taking electrons from neighboring Au and Pd atoms. Consequently, this positive charge is quickly transferred to the entire nanoparticle, resulting in a slight change in the surface charge. The release of [109m]Ag from the nanoparticle surface is therefore unfeasible. This effect was also observed in the *in vivo* [166]Dy/[166]Ho generator deposited on the surface of gold nanoparticles [80]. This phenomenon is beneficial from the perspective of potential therapeutic applications. Since [109m]Ag remains in the nanoparticle structure, there is a negligible risk of Auger electrons damaging surrounding healthy tissue.

The radiobioconjugate of core-shell Au@[109]Pd nanoparticles with monoclonal antibodies was obtained through a four-step procedure. First, the synthesis of gold nanoparticles was performed in an aqueous solution, based on the methods described by Turkevich et al. [101], with slight modifications made by me. The synthesis of the core-shell nanoparticles followed the method outlined by Wawrowicz et al. [102] for the synthesis of Au@Pt nanoparticles. Next, conjugation with the monoclonal antibody trastuzumab was carried out by the method described by Cai et al. [31], and finally, an excess of HS-PEG-COOH (5 kDa) was added to enhance the dispersion of the bioconjugates. The resulting product was purified by centrifugation, was dispersed in deionized water, and was characterized using transmission electron microscopy (TEM), dynamic light scattering (DLS), and the determination of the number of trastuzumab molecules attached to the Au@[109]Pd nanoparticle.

In biological studies, we demonstrated that the synthesized Au@[109]Pd-PEG-trastuzumab radiobioconjugate successfully recognizes and specifically binds to transmembrane HER2 receptors. Furthermore, it

penetrates the cell membrane and localizes inside target cells in 96%. Because Auger electrons have a limited range, the internalization of radiobioconjugates is crucial for achieving optimal therapeutic effects.
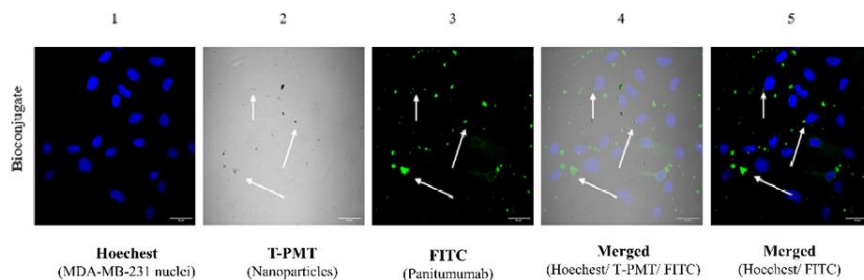

Fig. 4. Internalization of Au@Pd-trastuzumab by SKOV-3 cells determined by confocal microscopy.

The confocal images (Fig. 4) confirm that only trastuzumab-conjugated nanoparticles can enter HER2-positive ovarian cancer cells. The dark spots on the bright background in panel 2 represent Au@Pd particles. In panel 3, the green fluorescence indicates the secondary antibody attached to trastuzumab, which is an important part of the bioconjugate and the merged signals in panels 4 and 5 show that the bioconjugate particles successfully entered the SKOV-3 cells, clustered together, and localized near the nuclear envelope. This accumulation close to the cell's most sensitive organelle suggests that the radioactive bioconjugates can cause high cytotoxicity.

As shown in Fig. 5, cytotoxicity studies confirm this assumption.
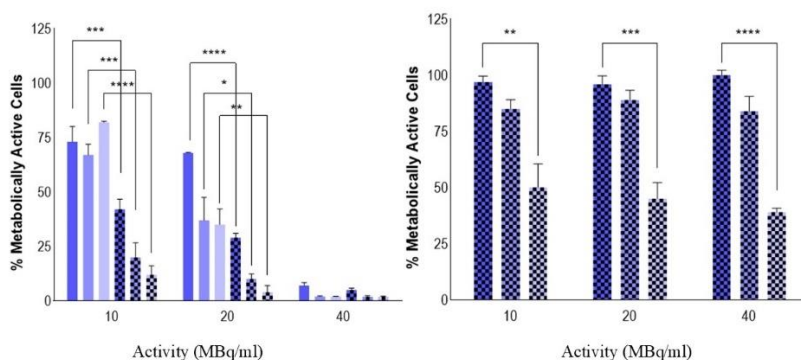

Fig. 5. Metabolic viability of HER2+ SKOV-3 (left) and HER2- MDA-MB-231 (right) cells after treatment with different radioactivity of Au@^{109}Pd-trastuzumab conjugates (right) after 24 h, 48 h, and 72 h of treatment.

The results indicate that the use of the Au@^{109}Pd-trastuzumab radioconjugate leads to a high reduction in the metabolic activity of SKOV-3 cells in a dose-dependent manner. These observed changes also progress over time. Triple-negative MDA-MB-231 cells, used for comparative analysis, demonstrate a cytotoxic effect despite the lack of targeting and internalization, although this effect is much less pronounced than in SKOV-3 cells. This cytotoxicity is entirely attributed to the effects of long-range β^- radiation, which does not require targeting or internalization to be effective.

In vitro studies have highlighted the important role of the trastuzumab vector, which facilitates the cellular internalization and cytoplasmic localization of the Au@^{109}Pd-trastuzumab conjugate in SKOV-3 cells. Confocal images (Fig. 4) show that the conjugate accumulates in the perinuclear region surrounding the cell nucleus. With β^- radiation, cellular internalization is not necessary due to the fact that the range of β^- radiation emitted by ^{109}Pd is several millimeters in comparison to the nanometer range of Auger electrons. As a result, β^- particles can target DNA without the internalization of ^{109}Pd, showing a crossfire effect.

However, the interaction of Auger electrons with essential cellular components is necessary to induce cytotoxic effects, which are correlated with the Auger electron emissions from ^{109m}Ag, the daughter radionuclide. Cellular DNA is often regarded as the most sensitive target for Auger electron emitters, given that the double-stranded DNA helix has a diameter of 2 nm. During typical Auger emissions, the greatest energy is released within spheres of 1-2 nm around the decay site. Additionally, as suggested in various publications, the cell membrane plays a crucial role in cell viability, and the influence of Auger electrons generated by radioactively labeled monoclonal antibodies bound to the cell membrane should not be overlooked. However, the nuclear membrane has not yet been considered a therapeutic target for Auger electrons [67]. Nonetheless, the significant accumulation of agglomerated nanoparticles on the nuclear membrane, as shown in confocal microscopy images (Fig. 4), may lead to Auger electron-induced damage to the nuclear envelope, hence contributing to cell death. I consider this hypothesis as a major achievement of the presented studies.

To verify the therapeutic enhancement for simultaneous emission of β^- particles and conversion/Auger electrons, I decided to perform a comparable analysis with ^{125}I (Auger) and ^{198}Au (β^-) radionuclides. Both were directly implemented into the nanoparticle structure by the chemisorption of iodine in ^{125}I-labeled Au@Pd-trastuzumab or by using radioactive ^{198}Au-trastuzumab radiobioconjugates, as previously described [103].

Table 2. Comparison of cytotoxicity of radiobioconjugates labeled with Auger electron emitter (^{125}I), β-emitter (^{198}Au) and Auger and β-electron emitter (^{109}Pd/^{109m}Ag   *in vivo* generator). Activity concentration: 20 MBq/ml, incubation time: 48 h.

Radiobioconjugate	$T_{1/2}$ (days)	Decay mode	Decay number in 48 h	Radiation emitted	% of metabolic activity in MTS test
Au@Pd^{125}I-trastuzumab	59.49	EC	3.42×10^{12}	Auger, low energy gamma	60
^{198}Au-trastuzumab	2.69	β^-	2.70×10^{12}	β^-_{avg} (315 keV)	53
Au@^{109}Pd-trastuzumab	0.57	β^-, IT	1.30×10^{12}	β^-_{avg} (436 keV) + Auger/conversion	10

The comparison provided in Table 2 is undoubtedly an approximation rather than clear evidence leading to an unambiguous conclusion. This comparison does not consider several parameters, including the radionuclide's half-life, radiation intensity, and energy. My intention was to compare the obtained data with currently existing alternative pathways. The acquired results, however, clearly reveal that the cytotoxicity of the ^{109}Pd/^{109m}Ag in $vivo$ generator-based conjugate (β^- and Auger electron emitter) is significantly higher than that of the conjugates radiolabeled with the same activities of β^- or Auger electron emitters. This effect will be much greater when considering the significantly shorter half-life of ^{109}Pd. Due to the both components decay (β^- and conversion/Auger electrons), the ^{109}Pd/^{109m}Ag in $vivo$ generator, similarly to ^{161}Tb, presents a unique potential in this field. Despite the lack of nuclear localization, which is highly required for efficient Auger electron therapy, an adequate cytotoxic effect was attained. As mentioned, we assume that the toxic effect could have been induced by Auger/conversion electrons emitted from the nanoparticles in the perinuclear area, efficiently damaging the nuclear envelope. Therefore, radiobioconjugates labeled with the ^{109}Pd/^{109m}Ag radionuclide generator might show the advantages of both β^- emitters and Auger electrons (high LET, double-stranded DNA breaks). Therefore, it can be expected that ^{109}Pd/^{109m}Ag-labeled vectors may have a more substantial antitumor performance when used either for the treatment of small tumor clusters or for targeting medium-sized tumors.

PUBLICATION NO. 3

Nasrin Abbasi Gharibkandi, Agnieszka Majkowska-Pilip, Rafał Walczak, Mateusz Wierzbicki, Aleksander Bilewicz, Au@^{109}Pd core-shell nanoparticle conjugated to panitumumab for the combined β^- - Auger electron therapy of triple-negative breast cancer. International Journal of Molecular Sciences 25, 13555 (2024), IF=4.9 (2023)

The promising results described in publication no. 2 motivated me to investigate additional radiobioconjugates based on the ^{109}Pd/^{109m}Ag generator. In publication no. 3, my colleagues and I presented

the results of our studies on radiobioconjugates, whereby, similar to the findings in publication no. 2, palladium radionuclides were immobilized on the surface of Au@Pd core-shell nanoparticles. The earlier results with the Au@^{109}Pd-trastuzumab radiobioconjugate demonstrated a high cytotoxic effect, despite the lack of nuclear localization, which is crucial for effective Auger electron therapy. These encouraging properties of the ^{109}Pd@^{109m}Ag-trastuzumab radiobioconjugate for treating HER2+ tumors led us to expand our studies to another aggressive form of breast cancer: triple-negative breast cancer (TNBC). By substituting trastuzumab with panitumumab in the radioconjugate, we aimed to achieve improved cytotoxicity results. Our optimism stemmed from panitumumab's ability to partially localize (>10%) into the nucleus of MDA-MB-231 cells, allowing it to be closer to the DNA strand. Additionally, it localizes in the cell membrane, making it a good target for Auger electron therapy [104]. This contrasts with the trastuzumab conjugate, which primarily localizes in the cytoplasm.

The synthesis of the Au@^{109}Pd-panitumumab radiobioconjugate was performed similarly to the previously described Au@^{109}Pd-trastuzumab. However, for the synthesis of Au@^{109}Pd-panitumumab, we used ^{109}Pd with a significantly higher specific activity achieved through extended neutron irradiation. This required the implementation of a specialized procedure to isolate the resulting impurity, ^{111}Ag. The isolation process involved the co-precipitation of ^{111}Ag with AgCl. The Au@^{109}Pd-panitumumab exhibited physicochemical properties similar to those of Au@^{109}Pd-trastuzumab. Basic data are presented in Table 1.

Table 1

Comparison of the properties of Au@^{109}Pd-panitumumab and Au@^{109}Pd-trastuzumab

	Au@^{109}Pd-panitumumab	Au@^{109}Pd-trastuzumab
Hydrodynamic diameter (nm)	82.79 ± 0.43	90.88 ± 0.66
Zeta potential (mV)	−25.0 ± 1.8	-25.1 ± 1.6
Number of antibody molecules per one nanoparticle	19	9.5

However, significant differences were observed in biological studies. Both Au@Pd-PEG-panitumumab and Au@Pd-PEG-trastzumab internalize into the cytoplasm with efficiency of >90%; however, only panitumumab can enter the cell nucleus. While passage through the cell membrane is a rapid process, penetration of the cell nucleus is slow and reaches 6% after 72 h of incubation. As shown in Fig.6 internalization of Au@Pd-PEG-panitumumab has a particular impact on the cytotoxicity of non-radioactive bioconjugates.
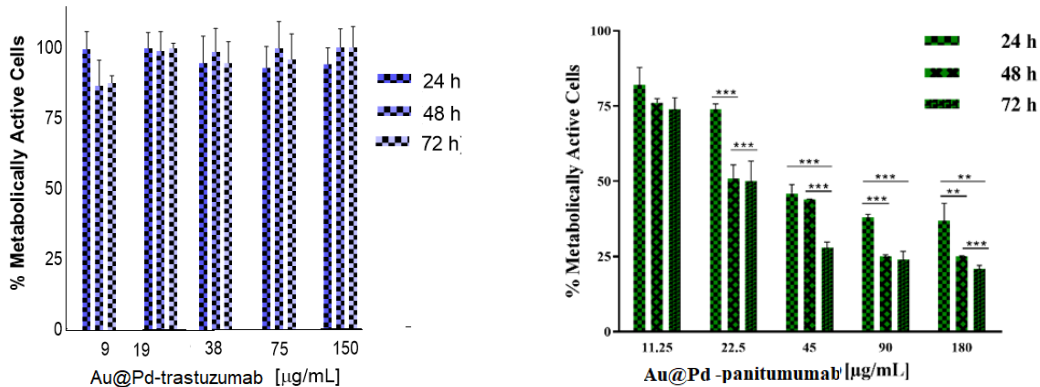
Fig. 6. Metabolic viability of SKOV-3 and MDA-MB-231 cells after treatment with different concentrations of Au@Pd-PEG-trastuzumab (left) and Au@Pd-PEG-panitumumab non-radioactive conjugates respectively (right).

The significant impact of Au@Pd-PEG-panitumumab on MDA-MB-231 cell viability is observed for concentrations above 22.5 μg/mL. A similar cytotoxic effect of Au-PEG-panitumumab NP conjugates on TNBC was also observed by Yook et al. [105]. The authors proposed that the cytotoxic effects of panitumumab nanoparticle conjugates on MDA-MB-231 cells may result from the immunotoxic effects of the panitumumab antibody linked to the nanoparticles, as indicated by various clinical studies. They suggested that the internalization of Au-PEG-panitumumab nanoparticles into the cell nucleus could potentially cause nuclear damage to the cells. Furthermore, since the cytotoxicity of Pd nanoparticles is significantly greater than that of Au nanoparticles, Au@Pd-PEG-panitumumab exhibits enhanced cytotoxicity. This finding aligns with our previous studies on the Au@Pd-PEG-trastuzumab conjugates in SKOV-3 cells (Fig. 6, left). In those studies, we did not observe nuclear localization of the conjugate within the cell nuclei, indicating that the nanoparticles did not cause any nuclear damage to the cells.

Unexpectedly, the situation differs significantly for radioactive bioconjugates. As illustrated in Fig. 7, the cytotoxicity of Au@^{109}Pd-PEG-panitumab is lower than that of Au@^{109}Pd-PEG-trastuzumab, despite the fact that panitumumab partially introduces ^{109}Pd into the cell nucleus. This internalization should enhance the cytotoxicity of the Auger emitter-labeled radioconjugate.
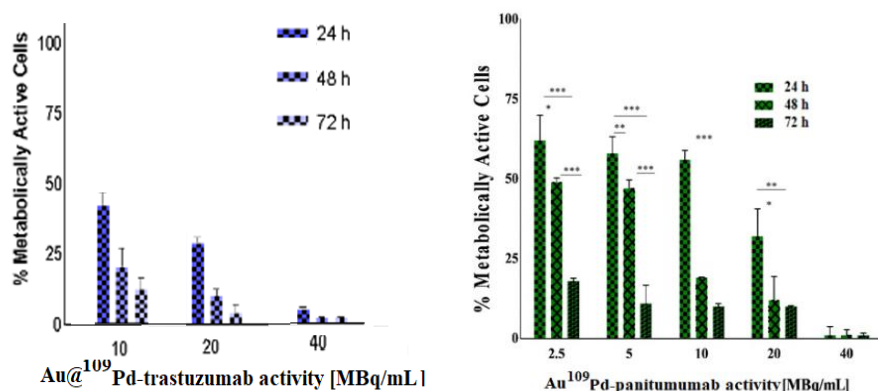
Fig. 7. Metabolic viability of SKOV-3 and MDA-MB-231 cells after treatment with different radioactivity of Au@^{109}Pd-PEG-trastuzumab (left) and Au@^{109}Pd-PEG-panitumumab radioconjugates (right).

This phenomenon can be explained as follows: As I wrote in the case of the Au@^{109}Pd-trastuzumab conjugate, in the cytoplasm we observe more significant agglomeration of bioconjugate and its localization at the cell membrane, which can cause its destruction and cell death (Fig. 4). The phenomena is much diminished for Au@^{109}Pd-panitumumab (Fig. 8)
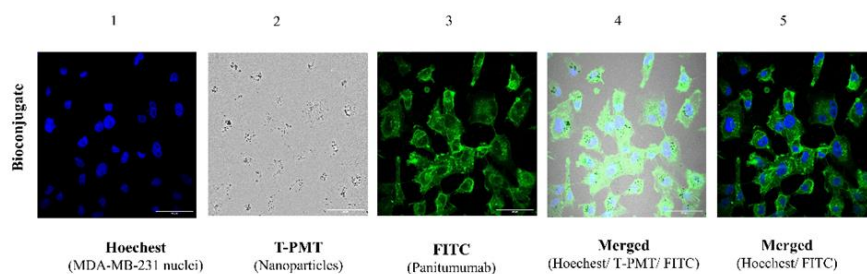

Fig. 8. Internalization of Au@Pd-panitumumab by MDA-MB-231 cells determined by confocal microscopy.

We must also consider that the few millimeters range of β$^-$ particles emitted by ^{109}Pd and there is no need for internalization of β$^-$ emitters into the nucleus. The additional important factor that may contribute to the lower cytotoxicity of radioactive Au@^{109}Pd-panitumumab to MDA-MB-231 cells, compared to Au@^{109}Pd-trastuzumab on SKOV-3 cells, is the greater radiosensitivity of SKOV-3 cells. In contrast, triple-negative cancer cells, such as MDA-MB-231, are known for their high radioresistance [106].

The cytotoxic effects of radiation emitted by the ^{109}Pd/^{109m}Ag *in vivo* generator are confirmed by the presence of double-strand breaks (DSBs) in confocal images of MA-MB-231 cells treated with Au@^{109}Pd-PEG-panitumumab (Fig. 9).
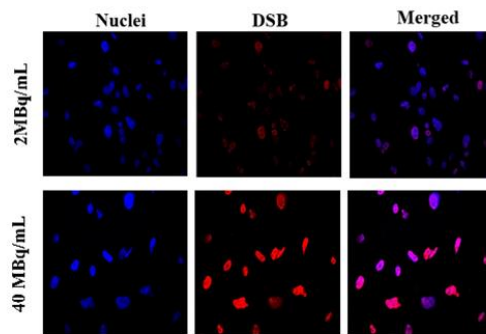
Fig. 9. Confocal immunofluorescence microscopy exhibiting γH2A.X foci (red) in the nucleus (counterstained blue with DAPI) of MDA-MB-231 breast cancer cells treated with 2 and 40 MBg/mL radioactivity of Au@^{109}Pd-PEG-panitumumab recorded after 24 h of incubation.

In contrast to the 40 MBq/mL, the low radioactivity level of 2 MBq/mL shows a negligible occurrence of double-strand breaks (DSBs). This suggests that DSBs are mainly caused by radiation itself, rather than being significantly affected by the immunotoxic effects of panitumumab or by the reactive oxygen species produced on the surface of Au@Pd nanoparticles.

Similarly, as observed in the HepG2 cells treated with ^{109}Pd-PEG nanoparticles (see attached publication no. 4), the high linear energy transfer Auger and conversion electrons emitted by the ^{109}Pd/^{109m}Ag *in vivo* generator lead to the formation of a significant number of DSBs. However, comparing our results with those of ^{109}Pd-PEG nanoparticles on HepG2 cells, a significantly higher number of γH2A.X foci is observed for the Au@^{109}Pd-PEG-panitumumab radiobioconjugate. This effect is due to the greater internalization into the nucleus caused by the presence of the vector, panitumumab.

In publication no. 3, we demonstrate, similar to previous studies (publication no. 2), that, unlike most chelator-based generators, we observed complete retention of the daughter isotope on the nanoparticles. This finding has significant implications for targeted therapy, as it prevents the displacement of radioactivity outside the targeted area. The Au@^{109}Pd-PEG-panitumumab nanoparticle conjugates show multiple toxic interactions with cancer cells. They are radiotoxic, emitting both β⁻ and Auger electrons, and display immunotoxicity due to the presence of the panitumumab antibody. However, the radiotoxic effects of Auger electrons become predominant because of the relatively high internalization of the radiobioconjugate into the cell nucleus, facilitated by the panitumumab vector. This emission of high linear energy transfer radiation is crucial for treating highly resistant triple-negative breast cancer cells.

PUBLICATION NO. 4

Nasrin Abbasi Gharibkandi, Kamil Wawrowicz, Rafał Walczak, Agnieszka Majkowska-Pilip, Mateusz Wierzbicki, Aleksander Bilewicz, ^{109}Pd/^{109m}Ag *in vivo* generator in the form of nanoparticles for combined β$^-$ - Auger electron therapy of hepatocellular carcinoma. EJNMMI Radiopharmacy and Chemistry 9, 59 (2024), IF= 4.4 (2024)

In the attached publication no. 4, we investigated the possibility of using radioactive palladium nanoparticles for the treatment of hepatocellular carcinoma (HCC). The inspiration for these studies was recently published in Angewandte Chemie, a "highly significant paper" concerning the selective toxicity of small platinum nanoparticles towards HCC cells [107]. The authors explained the strong and selective cytotoxic effect of small nanoparticles by the intracellular oxidation Pt^o to Pt^{2+} and the release of Pt^{2+} ions from Pt nanoparticles, which inhibit cell division by binding to DNA and causing DNA damage.

It was found that a few types of cancer cells, including hepatocellular carcinoma cells (HepG2), have a higher oxidative state owing to high concentration of H_2O_2 [107]. On the other hand, low H_2O_2 levels were found in non-cancerous liver cells, where the toxicity of Pt nanoparticles was not observed. This facilitates selective HCC treatment.

Previous project in my lab involved the use of 2 nm radioactive nanoparticles containing $^{193m/195m}$Pt radionuclides. These nanoparticles, effective emitters of Auger electrons, were expected to dissolve and release $^{193m/195m}$Pt^{2+} cations capable of binding to DNA strands, leading to irreparable double-strand breaks. This system fulfills the requirements for effective Auger electron therapy. Unfortunately, the project was unsuccessful. After reviewing the literature and conducting experimental studies, we concluded that obtaining sufficient activities of ^{193m}Pt or ^{195m}Pt for *in vitro* studies, let alone for therapeutic use, is not feasible [41].

Therefore, during my doctoral studies, I attempted to implement this idea using other more available radionuclides, ^{103}Pd and ^{109}Pd. I aimed to explore whether the effect of dissolving platinum nanoparticles is also applicable for palladium nanoparticles. The similar d^8 electron configurations and considerable chemical similarity of Pd^{2+} and Pt^{2+} cations make palladium radionuclides interesting candidates for Auger electron therapy. Additionally, numerous publications have confirmed the anti-cancer properties of Pd^{2+} cations, their complexes, and nanoparticles. Consequently, the two palladium radionuclides, ^{103}Pd and ^{109}Pd, could act as excellent alternatives for ^{195m}Pt.

HCC is the fifth most common cancer and remains one of the top three deadliest cancers globally. In advanced-stage HCC, systemic chemotherapy is used to restrict drug exposure to the liver; but its success is hindered by adverse effects such as nausea, fatigue, and toxicity to healthy liver cells. Other treatment methods including transarterial chemoembolization and radioembolization, wherein chemotherapeutic

drugs or radioactive microspheres are injected into the artery supplying blood to the liver tumor. These methods are considered palliative treatments for liver cancer.

Nanotechnology is a promising alternative to improve the effectiveness and specificity of cancer treatments. Nanoparticles typically accumulate in the liver following systemic administration, although this accumulation is affected by their properties, including size and charge. Specificity for the liver cancer cells can be attained through passive targeting using the enhanced permeability and retention (EPR) effect. This effect allows small-sized nanoparticle drugs to accumulate more effectively in tumors compared to healthy tissues.

In the previous publications no 2 and 3, we demonstrated promising results using radiobioconjugates of gold nanoparticles coated with a ^{109}Pd layer attached to trastuzumab. The successful results encouraged us to continue our studies focused on HCC therapy using small 5 nm PEGylated ^{109}Pd nanoparticles. Because of the anticipated dissolution of nanoparticles in HepG2 cells having higher H_2O_2 levels, we expected a substantial toxic effect.

My preliminary results carried out in H_2O_2 solutions indicate that, contrary to my predictions, 5 nm diameter ^{109}Pd nanoparticles do not dissolve at all in strongly oxidizing H_2O_2 environments. Therefore, we aimed to evaluate their ability to penetrate the nuclear membrane. Using radioactive ^{109}Pd nanoparticles, we observed a time-dependent cellular accumulation, with uptake reaching approximately 15% after 24 hours (Fig. 10). In addition, after cell isolation, we showed that by increasing the time, the percentage of the internalized ^{109}Pd in the nucleus increased to 50% after 72 h.
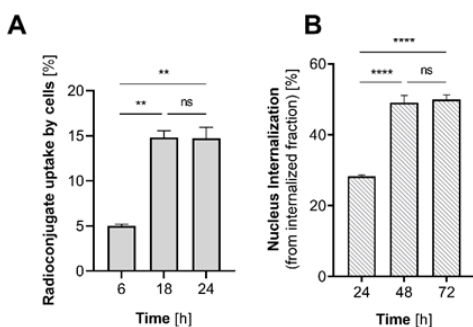

Fig. 10. ^{109}Pd nanoparticles specifically bound to HepG2 cells (A) and intranuclear uptake of ^{109}Pd nanoparticles (B).

High internalization of ^{109}Pd-PEG nanoparticles into the cytoplasm and nucleus of the cell caused significant cytotoxicity. To evaluate the therapeutic mechanism, I conducted experiments using Pd-PEG-nanoparticles labeled through chemisorption with ^{125}I (Auger electron and γ emitters) and ^{131}I (β$^-$ and γ emitters).
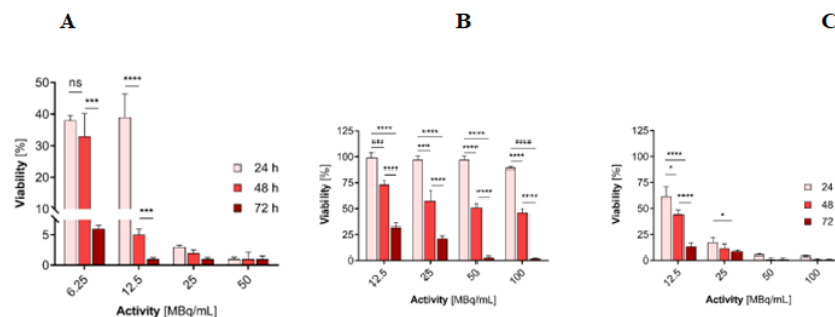
Fig. 11. Metabolic viability of HepG2 cells after treatment with different radioactive doses of ^{109}Pd-nanoparticles (A), ^{125}I-Pd-PEG- (B) and ^{131}I-Pd-PEG nanoparticles after 24 h, 48 h, and 72 h treatment.

Results presented in Fig.11 showed that ^{109}Pd-labeled nanoparticles exhibited significantly higher cytotoxicity than those labeled with either ^{131}I or ^{125}I. This effect has been also observed repeatedly when comparing bioconjugates labeled with ^{161}Tb and ^{177}Lu [108]. As explained, the higher efficacy of ^{161}Tb compared to ^{177}Lu and other β⁻ radioisotopes is mainly due to the more significant amount of Auger and low-energy conversion electrons, whose doses are deposited over relatively short distances. The authors of the study demonstrated that in a 100-µm metastasis, CE and Auger electrons were responsible for 71% of the radiation dose deposited by ^{161}Tb. For tumours with a 5 mm diameter, the absorbed dose was similar across all three radionuclides. Consequently, ^{109}Pd- nanoparticles, similar to ^{161}Tb radioconjugates, should be used for small metastatic cancers, where the Auger electron radiation becomes essential. This conclusion is well supported by studies on HepG2 cell spheroids, which are three-dimensional (3D) cell cultures that better mimic tissue physiology.

In my study, I compared the formation of double-strand breaks following exposure to non-radioactive Pd-PEG nanoparticle, β⁻ radiation from ^{131}I-Pd-PEG nanoparticles, and the simultaneous β⁻ and Auger electrons emitted by ^{109}Pd nanoparticles (Fig. 12). The cytotoxicity results of non-radioactive Pd-PEG nanoparticles, ^{109}Pd, and ^{131}I-Pd-PEG nanoparticles exhibit a strong correlation with the occurrence of DSBs in the HepG2 cells, as visualized by γH2A.X foci. The high LET Auger and conversion electrons emitted by the ^{109}Pd/^{109m}Ag *in vivo* generator are responsible for the high number of DSBs formation. The number of DSBs is significantly reduced following β⁻ particle irradiation, attributable to the extended interaction range and lower LET of β⁻ particles. The significance of DSBs in radionuclide therapy was demonstrated in many studies, which indicate that cell death may occur in the form of apoptosis if there are more than 150,000 SSBs and only 500 DSBs. This information is essential for understanding the effects of radiation on cells during radionuclide therapy, which aims to selectively target and destroy cancer cells while minimizing damage to healthy tissues.
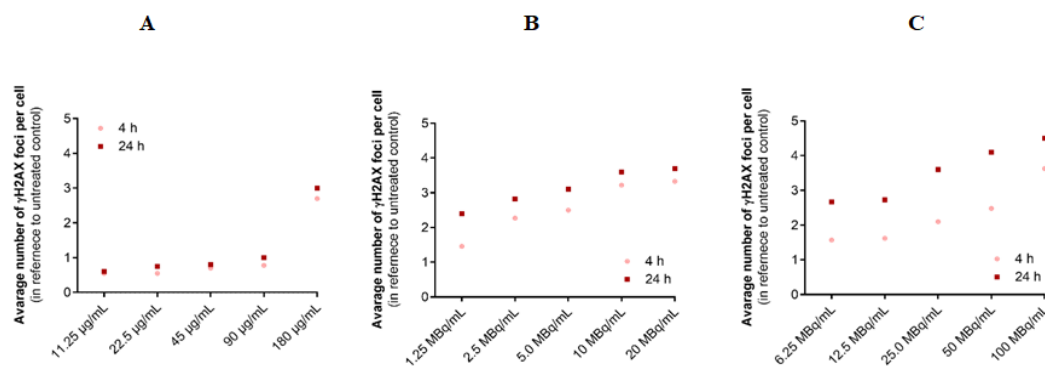
Fig. 12. γH2A.X foci formation in HepG2 cells after treatment with non-radioactive Pd-PEG nanoparticles (A); ^{109}Pd-nanoparticles (B) and ^{131}I-Pd nanoparticles (C).

In conclusion, my studies demonstrated that, contrary to our expectations, Pd-PEG nanoparticles are not soluble in solutions of hydrogen peroxide, the concentration of which is elevated in HepG2 cells. However, Pd-PEG nanoparticles exhibit significant toxicity due to their extensive internalization into the cytoplasm of HepG2 cells, with over 50% uptake occurring in the nucleus. As a result, ^{109}Pd nanoparticles present a potential approach for the treatment of hepatocellular carcinoma (HCC), outperforming typical therapies such as sorafenib and radioembolization.

The proposed solution offers an additional advantage: the accumulation of inorganic nanoparticles in the liver following intravenous administration. Accumulation of inorganic nanoparticles in the liver and spleen is usually the main disadvantage of nanoparticle conjugates, limiting their therapeutic use in medicine. However, in the case of HCC tumors, this accumulation may be beneficial. It allows the ^{109}Pd-PEG nanoparticles to concentrate in the target organ, where, due to the leaky blood vessels associated with HCC tumors (a phenomenon known as the Enhanced Permeability and Retention effect), we can expect increased accumulation in cancer cells.

APPENDIX
UNPUBLISHED RESULTS ON ^{103}Pd/^{103m}Rh *IN VIVO* GENERATORS
The results presented in my dissertation focus on *in vitro* studies of radioconjugates derived from the ^{109}Pd/^{109m}Ag *in vivo* generator. Initially, I aimed to explore also the ^{103}Pd/^{103m}Rh generator during my study. As mentioned in the introduction, ^{103}Pd has significant potential for use in Auger electron therapy, particularly for treating small tumor metastases, due to its minimal ratio of emitted photons to electrons [24]. Currently, there are no reports on the use of ^{103}Pd in targeted radionuclide therapy. This isotope is primarily employed in brachytherapy, which requires a much lower specific activity. It can be produced

through two methods: in a reactor via the $^{102}Pd(n,)^{103}Pd$ reaction or in a cyclotron through the $^{103}Rh(p,n)^{103}Pd$ reaction. To obtain sufficient activity for my planned studies using the reactor method, a high neutron flux of greater than 10^{15} n s^{-1} cm^{-2} is necessary.

Conversely, using the cyclotron method presents significant difficulties in dissolving the inert rhodium target post-proton irradiation, even with aqua regia. The only feasible approach is anodic dissolution. Unfortunately, I do not have access to the necessary electrochemical equipment for working with radioactive materials. As a result, I have limited my studies to the radionuclide ^{109}Pd. However, In the PRISMAP project, after the 2023 competition, our team successfully obtained an initial portion of 1.5 GBq of ^{103}Pd produced from the high-flux reactor at the ILL in Grenoble. We utilized this material to conduct fundamental research on $^{103}Pd/^{103m}Rh$ *in vivo* generators, focusing specifically on ^{103}Pd cyclam complexes and Au@^{103}Pd core-shell nanoparticles.

The longer half-life of ^{103m}Rh ($t_{\frac{1}{2}}$=56.11 min) compared to ^{109m}Ag ($t_{1/2}$=39 s) makes the release of Auger electron-emitting ^{103m}Rh from ^{103}Pd conjugates, or the absence of this release, significantly more important than that of ^{109m}Ag from ^{109}Pd. Initially I investigated the very stable ^{103}Pd-cyclam complex. To investigate the release of ^{103m}Rh from the ^{103}Pd-cyclam complex, I applied magnesium oxide, known for its strong affinity for adsorbing uncomplexed Rh^{3+} ions [109]. The presence of free $^{103m}Rh^{3+}$ cation in the solution indicates its release from the ^{103}Pd-cyclam complex after the radioactive decay of ^{103}Pd.

The complex of 1,4,8,11-tetraazacyclotetradecane-6-carboxylic acid (C-carboxylic acid-cyclam) with ^{103}Pd was prepared by mixing $^{103}PdCl_2$ with a 0.001 M solution of the ligand. After this, 50 mg of magnesium oxide (MgO) powder was added into 1 mL of the complex solution. The mixture was thoroughly mixed for about 10 minutes and then centrifuged. The magnesium oxide fraction was combined with a liquid scintillator and analyzed using a liquid scintillation counter (LSC).

The results shown in Fig. 13 indicate a decline in activity over the 240-minute measurement period, which suggests the presence of free ^{103m}Rh in the solution. The linear relationship between ln A and time allows the calculation of the decay constant (k) for the radionuclide. I can then use the formula $t_{1/2} = \ln (2)/k$ to determine the half-life ($t_{1/2}$). Based on my measurements, the calculated half-life is 60.8 minutes, while the literature value for ^{103m}Rh is 56.12 minutes.
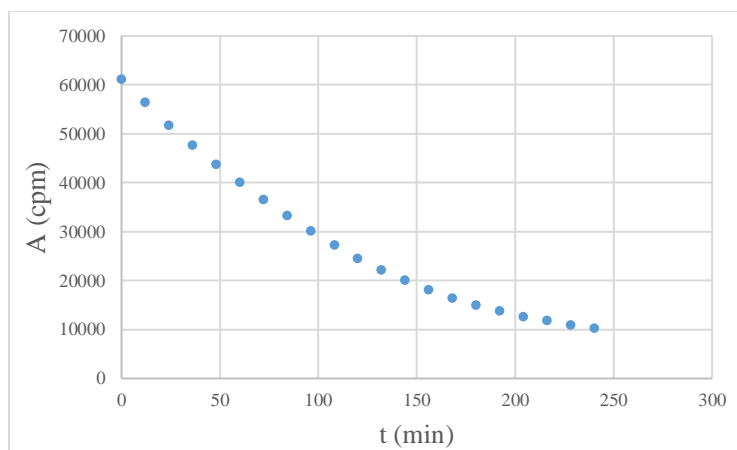
Fig. 13. Radioactivity of MgO after equilibration with [103]Pd-C-carboxylic acid solution. The measurement started 5 min after the separation. The radioactivity was measured successively at 12-min intervals. Activity in count per minute (cpm).

The results presented in Fig. 13 clearly show that after the decay of [103]Pd, the resulting radionuclide [103m]Rh dissociates from the complex. A similar effect was observed by Jensen et al. [110] when studying the macrocyclic sulfur complex [[103]Pd]16aneS$_4$4-diol. This study demonstrated that approximately 93% of [103m]Rh remains in the macrocyclic [[103]Pd]16aneS4-O-octyl complex. This phenomenon can be explained by Zeevaart and coworkers [74, 111], who conducted comprehensive estimates of the recoil energy associated with Auger electrons, photons, and neutrinos emission. They reported that the generated total energy is lower than the energy of chemical bonds in palladium-macrocyclic complexes, making it inadequate for the release of [103m]Rh from the complex. Additionally, Rh^{3+} forms stable complexes with 16aneS4, allowing it to remain bound within the complex [112]. The observed partial release of [103m]Rh is probably due to the formation of the highly charged [103m]Rh^{n+} cation after the nuclear reaction $^{103}Pd \xrightarrow{EC(branching\ ratio\ 99.97\%)} {}^{103m}Rh$. As explained in publication no. 2 regarding the [109]Pd/[109m]Ag generator, the highly charged [103m]Rh^{n+} ion extracts electrons from the surrounding donor atoms of the chelators, resulting in the formation of a Rh^{3+} cation [80]. Additionally, as a result of electron transfer to these highly charged atoms, the donor atoms of the chelators acquire a positive charge. This induced charge leads to a repulsive force between the positively charged atoms, causing the metal-ligand bonds to break and allowing the release of [103m]Rh as free cations.

The situation changes when the parent radionuclide is immobilized on the Au@Pd metallic surface instead of in the chelate complex. The studies on the release of [103m]Rh from Au@[103]Pd nanoparticles were conducted as described below:

51

The Au@^{103}Pd nanoparticles were equilibrated for 24 hours with 1 mL of PBS buffer and then centrifuged for 10 minutes. An aliquot of 0.5 mL was combined with a liquid scintillator and measured using LSC at intervals of 1.5 minutes. The obtained results are shown in Fig. 14.
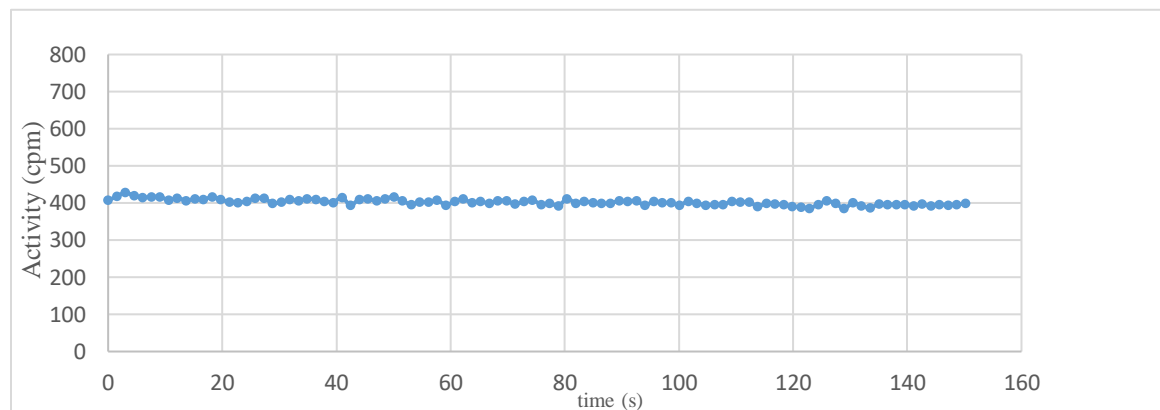

Fig. 14. Radioactivity of aliquot (PBS buffer) after equilibration with Au@^{103}Pd nanoparticles. The measurement started 5 min after the separation. The radioactivity was measured successively at 1.5-min. intervals. Activity in count per minute (cpm).

The data in Fig. 14 clearly indicates that ^{103m}Rh is not released from Au@^{103m}Rh nanoparticles. If free ^{103m}Rh was present in the solution, a reduction in activity would be observed during the measurements. The application of a metallic surface as the carrier for the mother radionuclides facilitates the availability of several delocalized metallic electrons. Following the nuclear decay of ^{103}Pd, highly positively charged ^{103m}Rh^{n+} takes electrons from neighboring Au or Pd atoms on the nanoparticle surface. As a result, the positive charge is rapidly transferred to the entire nanoparticle, causing only a marginal change in the surface charge. Therefore, the release of ^{103m}Rh from the nanoparticles surface is not observed.

The results clearly demonstrate that using metallic nanoparticles as carriers for Auger electron emitters effectively prevents the release of decay products. This approach enhances the effectiveness of Auger electron therapy and reduces side effects.

SUMMARY AND CONCLUSIONS

My doctoral thesis aimed to synthesize and evaluate the specificity and toxicity of radioactive nanoparticle bioconjugates based on the ^{109}Pd/^{109m}Ag *in vivo* generator for the treatment of breast, ovarian, and hepatocellular carcinoma. My studies initially focused also on another palladium *in vivo* generator: ^{103}Pd/^{103m}Rh. However, during my experiments, I obtained only a single portion of ^{103}Pd, which allowed me to conduct preliminary studies; the results of these studies are included in the appendix. Looking ahead, the

planned delivery of ^{103}Pd in the PRISMAP project will allow other group members to continue this research as part of the NCN (National Science Center) project.

In this dissertation, I focused on the synthesis of nanoparticle carriers, their functionalization with PEG molecules and monoclonal antibodies, and the studies of the biological properties of the obtained non-radioactive and radioactive bioconjugates. A significant part of my research was dedicated to the study of the behavior of ^{109}Pd/^{109m}Ag and ^{103}Pd/^{103m}Rh *in vivo* generators, both as macrocyclic complexes and when deposited on gold nanoparticles.

In principle, I achieved my research goals. However, despite conducting numerous chemical and biological studies, some conclusions still require additional confirmation. I was unable to directly and unequivocally explain the high cytotoxicity of the Au@^{109}Pd-trastuzumab radiobioconjugate. This high cytotoxicity was observed even in the absence of localization of the conjugate within the cell nucleus. The mechanism proposed in my doctoral thesis suggests that the presence of agglomerated nanoparticles in the perinuclear area is responsible for this high cytotoxicity. This finding is significant, as it indicates that, in addition to DNA strands and cell membranes, the nuclear membrane may potentially serve as a target for Auger emitters. Nonetheless, this concept requires further investigation.

The most important conclusions derived from the conducted research are as follows:

a) By depositing palladium atoms onto the surface of gold nanoparticles, it is possible to obtain homogeneous core-shell nanoparticles.

b) Furthermore, functionalizing the nanoparticle surface by attaching monoclonal antibodies ensures efficient and selective bioconjugate-receptor interactions, promoting internalization into the cytoplasm and localization in the perinuclear area. In the case of the Au@Pt-panitumumab conjugate, there is also partial localization into the cell nucleus.

c) The ^{109}Pd/^{109m}Ag *in vivo* generator in the form trastuzumab conjugated to core-shell Au@^{109}Pd nanoparticles generated significantly better *in vitro* cytotoxicity compared to the radioconjugate of trastuzumab Au@Pd nanoparticles labeled with either ^{125}I (an Auger emitter) or trastuzumab conjugate of ^{198}Au (a β^- emitter). The decay of both components (β^- and conversion/Auger electrons) causes the ^{109}Pd/^{109m}Ag *in vivo* generator to exhibit characteristics similar to ^{161}Tb. .

d) The Au@^{109}Pd-PEG-trastuzumab and Au@^{109}Pd-PEG-panitumumab nanoparticle conjugates have been found to exhibit multiple toxic interactions with cancer cells. It is radiotoxic, emitting β^- and Auger electrons, and exhibits immunotoxicity due to the presence of the antibody. Additionally, bioconjugates demonstrate chemotoxicity due to the catalytic generation of ROS on Pd nanoparticles. However, the radiotoxic effects of Auger electrons become dominant due to the relatively high internalization of the radiobioconjugate into the cell nucleus, which is caused by the presence of the

panitumumab vector. The high toxicity of Au^{109}Pd-trastuzumab is probably related to the localization in the perinuclear area and the radiation-induced destruction of the nuclear membrane.

e) Unfortunately, the anticipated dissolution of 5 nm palladium nanoparticles in the oxidizing environment of HepG2 cells and hydrogen peroxide solutions was not confirmed. However, it was observed that small palladium nanoparticles with a diameter of 5 nm exhibit significant intranuclear localization.

f) The studies of 5 nm ^{109}Pd-PEG on HepG2 cells revealed that these nanoparticles, similarly to Au@^{109}Pd trastuzumab conjugates, were significantly more effective *in vitro* than Pd-PEG nanoparticles labeled with either ^{125}I (Auger emitter) or ^{131}I (β$^-$ emitter). This is due to the unique potential presented by the ^{109}Pd/^{109m}Ag *in vivo* generator, which emits both β$^-$ and conversion/Auger electrons.

g) In contrast to the *in vivo* generators based on chelate complexes of ^{109}Pd/^{109m}Ag and ^{103}Pd/^{103m}Rh, the *in vivo* generators utilizing core-shell Au@^{103,109}Pd nanoparticles did not release detectable levels of the daughter radionuclides ^{109m}Ag and ^{103m}Rh in water or PBS buffer after equilibration with the nanoparticles. It showed that complete retention of ^{109m}Ag was accomplished following the nuclear decay of the immobilized ^{109}Pd on the AuNPs surface. We have explained this effect by easy neutralization of exited highly charged daughter nuclide several delocalized metallic electrons. Following nuclear decay, the highly positively charged daughter radionuclide takes electrons from neighboring Au atoms on the surface. As a result, the positive charge is rapidly distributed throughout nanoparticle, causing only a marginal change in the surface charge. This conclusion is important because it indicates that the presence of free electrons in the environment prevents the release of the daughter radionuclide. This finding has significant implications for the development of radiopharmaceuticals using *in vivo* generators.

However, it is necessary to be aware of the limitations of the proposed nanoparticle-based bioconjugates. Accumulation of radioactively labeled nanobioconjugates in the liver, lungs, and spleen may expose these organs to radiation and reduce the accumulation of these radiobioconjugates in tumors. As a result, the intravenous administration of Au@^{109}Pd-PEG-panitumumab and Au@^{109}Pd-PEG-trastuzumab is not feasible. Many studies suggest that in the case of this type of radiobioconjugates, local administration directly to the tumor or to the resection cavity is more effective. In the case of hepatocellular carcinoma, labeled nanoparticles can be administered through the hepatic vein, as proposed in publication no. 4. Despite these limitations, the concept of using a ^{109}Pd/^{109m}Ag *in vivo* generator and the promising results encourage further exploration of this treatment strategy. I believe that additional studies with the ^{103}Pd/^{103m}Rh *in vivo* generator will yield even better results. This is due to the longer half-life of ^{103}Pd and its significantly greater Auger electron emission. Additionally, the absence of β$^-$ radiation should allow the use of higher activity levels.

REFERENCES:

1. Nitipir, C., et al., *Update on radionuclide therapy in oncology.* Oncol Lett, 2017. **14**(6): p. 7011-7015.

2. Delclos, L. *Are Interstitial Radium Applications Passe? ¹.* in *Renaissance of Interstitial Brachytherapy: 12th Annual San Francisco Cancer Symposium, San Francisco, Calif., March 1977*. 1978. Karger Medical and Scientific Publishers.

3. Jacox, H.W., *X Rays and Radium in the Treatment of Diseases of the Skin*. 1967, The Radiological Society of North America.

4. Schaeflein, J.W., et al., *Some observations on iridium 192.* Front. Radiat. Ther. Oncol., 1978. **12**: p. 13-20.

5. Hoefnagel, C.A., *Eur. J. Nucl. Med.*, 1991. **18**: p. 408-431.

6. Troutner, D.E., *Chemical and physical properties of radionuclides.* Int. J. Rad. Appl. Instrum. B. 1987. **14**(3): p. 171-176.

7. Volkert, W., et al., *Therapeutic radionuclides: production and decay property considerations.* J. Nucl. Med., 1991. **32**(1): p. 174-185.

8. Kassis, A.I. and S.J. Adelstein, *Radiobiologic principles in radionuclide therapy.* J. Nucl. Med., 2005. **46**(1 suppl): p. 4S-12S.

9. Cutler, C.S. et al. Nanoparticles and phage display selected peptides for imaging and therapy of cancer. In: Baum, R., Rösch, F. (eds) Theranostics, Gallium-68, and other Radionuclides. Recent Results in Cancer Research, vol 194. Springer, Berlin 2013.

10. Parker, C., et al., *Targeted alpha therapy, an emerging class of cancer agents: a review.* JAMA Oncology, 2018. **4**(12): p. 1765-1772.

11. Allen, B.J., *Clinical trials of targeted alpha therapy for cancer.* Reviews on Recent Clinical Trials, 2008. **3**(3): p. 185.

12. Kassis, A.I. *Therapeutic radionuclides: biophysical and radiobiologic principles*. Semin Nucl Med . 2008,38(5): p. 358-66.

13. Burki, H., C. Koch, and S. Wolff, *Molecular suicide studies of 125I and 3H disintegration in the DNA of Chinese hamster cells.* Current Topics in Radiation Research Quarterly, 1978. **12**(1-4): p. 408-425.

14. Firestone, R., et al., *The 8th edition of the Table of Isotopes.* 1997.

15. Mikolajczak, R., et al., *Production of scandium radionuclides for theranostic applications: towards standardization of quality requirements.* EJNMMI Radiopharmacy and Chemistry, 2021. **6**(1): p. 19.

16. Ku, A., et al., *Auger electrons for cancer therapy–a review.* EJNMMI Radiopharmacy and Chemistry, 2019. **4**: p. 1-36.

17. Cole, A., *Absorption of 20-eV to 50,000-eV electron beams in air and plastic.* Radiat. Res., 1969. **38**(1): p. 7-33.

18. Buchanan, C.M., et al., *Modelling Potential Candidates for Targeted Auger Therapy.* Biophysica, 2024. **4**(4): p. 711-723.

19. Müller, C., et al., *Terbium-161 for PSMA-targeted radionuclide therapy of prostate cancer.* EJNMMI, 2019. **46**: p. 1919-1930.

20. Aghevlian, S., A.J. Boyle, and R.M. Reilly, *Radioimmunotherapy of cancer with high linear energy transfer (LET) radiation delivered by radionuclides emitting α-particles or Auger electrons.* Adv. Drug Deliv. Rev., 2017. **109**: p. 102-118.

21. Bernhardt, P., et al., *Low-energy electron emitters for targeted radiotherapy of small tumours.* Acta Oncol., 2001. **40**(5): p. 602-608.

22. Qaim, S.M., *Nuclear data for medical radionuclides.* J. Radioanal. Nucl. Chem. 2015. **305**: p. 233-245.

23. Fonslet, J., et al., *135La as an Auger-electron emitter for targeted internal radiotherapy.* Phys. Med. Biol., 2017. **63**(1): p. 015026.

24. Filosofov, D., et al., *Potent candidates for Targeted Auger Therapy: Production and radiochemical considerations.* Nucl. Med.Biol. 2021. **94**: p. 1-19.

25. Pillai, M., A. Dash, and F. Knapp Jr, *Radiopharmaceuticals applications: Insights and future' Edited by R. Santos-Oliveira. Lambert Academic Publishing, 2016, pp 63-118.* 26.   Eckerman, K.F. and A. Endo, *MIRD: radionuclide data and decay schemes*. SNMMI, 2007.

27. Carlson, T.A. and R.M. White, *Formation of fragment ions from CH3Te125 and C2H5Te125 following the nuclear decays of CH3I125 and C2H5I125.* J. Chem. Phys., 1963. **38**(12): p. 2930-2934.

28. Schmidt, A. and G. Hotz, *The occurrence of double-strand breaks in coliphage T1-DNA by iodine-125 decay.* Int. J. Radiat. Biol., 1973. **24**(3): p. 307-313.

29. Larson, S.M., et al., *Radioimmunotherapy of human tumours.* Nat. Rev. Cancer, 2015. **15**(6): p. 347-360.

30. Kassis, A.I., R.S. Harapanhalli, and S.J. Adelstein, *Strand breaks in plasmid DNA after positional changes of Auger electron-emitting iodine-125: direct compared to indirect effects.* Radiat.Res. 1999. **152**(5): p. 530-538.

31. Cai, Z., et al., *111In-labeled trastuzumab-modified gold nanoparticles are cytotoxic in vitro to HER2-positive breast cancer cells and arrest tumor growth in vivo in athymic mice after intratumoral injection.* Nucl. Med. Biol., 2016. **43**(12): p. 818-826.

32. Pouget, J.-P., et al., *Cell membrane is a more sensitive target than cytoplasm to dense ionization produced by Auger electrons.* Radiat. Res., 2008. **170**(2): p. 192-200.

33. Kiess, A.P., et al., *Auger radiopharmaceutical therapy targeting prostate-specific membrane antigen.* J. Nucl. Med., 2015. **56**(9): p. 1401-1407.

34. Najafi, M., et al., *The mechanisms of radiation-induced bystander effect.* J. Biomed. Phys. Eng. 2014. **4**(4): p. 163.

35. Sobolev, A., *The Delivery of biologically active agents into the nuclei of target cells for the purposes of translational medicine.* Acta Naturae (english version), 2020. **12**(4 (47)): p. 47-56.

36. Gharibkandi, N.A., et al., *Nanostructures as radionuclide carriers in Auger electron therapy.* Materials, 2022. **15**(3): p. 1143.

37. Thisgaard, H., et al., *Highly effective Auger-electron therapy in an orthotopic glioblastoma xenograft model using convection-enhanced delivery.* Theranostics, 2016. **6**(12): p. 2278.

38. Jackson, M.R., et al., *Radiolabeled oligonucleotides targeting the RNA subunit of telomerase inhibit telomerase and induce DNA damage in telomerase-positive cancer cells.* Cancer Res., 2019. **79**(18): p. 4627-4637.

39. Onizuka, K., et al., *Reactive OFF-ON type alkylating agents for higher-ordered structures of nucleic acids.* Nucleic Acids Res., 2019. **47**(13): p. 6578-6589.

40. Howell, R.W., et al., *Radiotoxicity of platinum-195m-labeled trans-platinum (II) in mammalian cells.* Radiation Res., 1994. **140**(1): p. 55-62.

41. Wawrowicz, K. and A. Bilewicz, *Challenging production of Auger electron emitter platinum-195m via double-neutron capture activation of an iridium-193 target.* Bio-Algorithms Med-Syst., 2023. **19**(1): p. 35-39.

42. Garnuszek, P. and I. Licińska, *Preliminary radiochemical and biological studies on the liposome encapsulated platinum-[125 I] iodohistamine complex.* Nucl. Med. Rev., 2002. **5**(2): p. 145-149.

43. Chaires, J.B., J.E. Herrera, and M.J. Waring, *Preferential binding of daunomycin to 5'TACG and 5'TAGC sequences revealed by footprinting titration experiments.* Biochemistry, 1990. **29**(26): p. 6145-6153.

44. Ickenstein, L.M., et al., *A novel 125I-labeled daunorubicin derivative for radionuclide-based cancer therapy.* Nucl. Med. Biol., 2006. **33**(6): p. 773-783.

45. Fondell, A., et al., *Nuclisome: a novel concept for radionuclide therapy using targeting liposomes.* EJNMMI, 2010. **37**: p. 114-123.

46. Shinohara, A., et al., *Rational evaluation of the therapeutic effect and dosimetry of auger electrons for radionuclide therapy in a cell culture model.* Annals , 2018. **32**: p. 114-122.

47. Hu, A., et al., *Construction of the Bioconjugate Py-Macrodipa-PSMA and Its In Vivo Investigations with Large 132/135La3+ and Small 47Sc3+ Radiometal Ions.* Eur. J. Inorg. Chem. 2023. **26**(35): p. e202300457.

48. Louie, M.C. and M.B. Sevigny, *Steroid hormone receptors as prognostic markers in breast cancer.* Am. J. Cancer Res., 2017. **7**(8): p. 1617.

49. Cornelissen, B., K. A Vallis, *Targeting the nucleus: an overview of Auger-electron radionuclide therapy.* Curr. Drug Discov. Technol.,2010. **7**(4): p. 263-279.

50. Kwekkeboom, D.J., et al., *Treatment of patients with gastro-entero-pancreatic (GEP) tumours with the novel radiolabelled somatostatin analogue [177 Lu-DOTA 0, Tyr 3] octreotate.* EJNMMI, 2003. **30**: p. 417-422.

51. Reubi, J.C., *Somatostatin and other peptide receptors as tools for tumor diagnosis and treatment.* Neuroendocrinol., 2004. **80**(Suppl. 1): p. 51-56.

52. Giovanella, L., *Nuclear medicine therapy: side effects and complications*. 2019: Springer.

53. Thisgaard, H., et al., *Evaluation of Cobalt-Labeled Octreotide Analogs for Molecular Imaging and Auger Electron–Based Radionuclide Therapy*. J. Nucl. Med., 2014. **55**(8): p. 1311-1316.

54. Jansen, T.J., et al., *Exendin-4 analogs in insulinoma theranostics.* J. Label. Compd. Radiopharm., 2019. **62**(10): p. 656-672.

55. Santos-Cuevas, C.L., et al., *Design, preparation, in vitro and in vivo evaluation of 99mTc-N2S2-Tat (49–57)-bombesin: a target-specific hybrid radiopharmaceutical.* Int. J. Pharm., 2009. **375**(1-2): p. 75-83.

56. Jiménez-Mancilla, N., et al., *Multifunctional targeted therapy system based on 99mTc/177Lu-labeled gold nanoparticles-Tat (49–57)-Lys3-bombesin internalized in nuclei of prostate cancer cells.* J. Label. Compd. Radiopharm., 2013. **56**(13): p. 663-671.

57. Arteaga, C.L., et al., *Treatment of HER2-positive breast cancer: current status and future perspectives.* Nat. Rev. Clin. Oncol., 2012. **9**(1): p. 16-32.

58. Baselga, J., J. Albanell, *Mechanism of action of anti-HER2 monoclonal antibodies.* Ann. Oncol. 2001. **12**: p. S35-S41.

59. bin Othman, M.F., et al., *In vitro cytotoxicity of Auger electron-emitting [67Ga] Ga-trastuzumab.* Nucl. Med.Biol., 2020. **80**: p. 57-64.

60. Costantini, D.L., et al., *Trastuzumab-resistant breast cancer cells remain sensitive to the Auger electron–emitting radiotherapeutic agent 111In-NLS-trastuzumab and are radiosensitized by methotrexate.* J. Nucl. Med., 2008. **49**(9): p. 1498-1505.

61. Costantini, D.L., et al., *111In-labeled trastuzumab (Herceptin) modified with nuclear localization sequences (NLS): an Auger electron-emitting radiotherapeutic agent for HER2/neu-amplified breast cancer.* J. Nucl. Med., 2007. **48**(8): p. 1357-1368.

62. Wang, Y., et al., *Preparation of Radiolabeled Zolbetuximab Targeting CLDN18. 2 and Its Preliminary Evaluation for Potential Clinical Applications.* Mol. Pharmaceutics, 2024. **21**(8): p. 3838-3847.

63. Müller, C., et al., *Preclinical investigations and first-in-human application of 152Tb-PSMA-617 for PET/CT imaging of prostate cancer.* EJNMMI Research, 2019. **9**: p. 1-10.

64. Lehenberger, S., et al., *The low-energy β− and electron emitter 161Tb as an alternative to 177Lu for targeted radionuclide therapy.* Nucl. Med. Biol., 2011. **38**(6): p. 917-924.

65. Uygur, E., et al., *The radiolabeling of [161Tb] Tb-PSMA-617 by a novel radiolabeling method and preclinical evaluation by in vitro/in vivo methods. J Radioanal Nucl Chem* 2024, 333, 6403–6413
66. Müller, C., et al., *Direct in vitro and in vivo comparison of 161 Tb and 177 Lu using a tumour-targeting folate conjugate.* EJNMMI, 2014. **41**: p. 476-485.

67. Paillas, S., et al., *Localized irradiation of cell membrane by Auger electrons is cytotoxic through oxidative stress-mediated nontargeted effects.* Antioxid. Redox Signal. 2016. **25**(8): p. 467-484.

68. Van Laere, C., et al., *Terbium radionuclides for theranostic applications in nuclear medicine: from atom to bedside.* Theranostics, 2024. **14**(4): p. 1720.

69. Zweit, J., *Radionuclides and carrier molecules for therapy.* Phys. Med. Biol., 1996. **41**(10): p. 1905.

70. Tolmachev, V., et al., *114mIn, a candidate for radionuclide therapy: low-energy cyclotron production and labeling of DTPA-D-phe-octreotide.* Nucl. Med. Biol., 2000. **27**(2): p. 183-188.

71. Lubberink, M., H. Lundqvist, and V. Tolmachev, *Production, PET performance and dosimetric considerations of 134Ce/134La, an Auger electron and positron-emitting generator for radionuclide therapy.* Phys. Med. Biol., 2002. **47**(4): p. 615.

72. Szilard, L. and T. Chalmers, *Chemical separation of the radioactive element from its bombarded isotope in the Fermi effect.* Nature, 1934. **134**(3386): p. 462-462.

73. Zhernosekov, K.P., *Radiochemical aspects of production and processing of radiometals for preparation of metalloradiopharmaceuticals*. PhD Dissertation , Mainz, Univ., Diss., 2006.

74. Szucs, Z., J. van Rooyen, and J.R. Zeevaart, *Recoil effect on β-decaying in vivo generators, interpreted for 103Pd/103mRh.* Appl. Radiat. Isotop., 2009. **67**(7-8): p. 1401-1404.

75. Zeevaart, J., et al., *Recoil and conversion electron considerations of the 166Dy/166Ho in vivo generator.* Radiochimica Acta, vol. 2012, 100(2), pp. 109-113. .

76. Zeevaart, J.R., et al., *Recoil and conversion electron implications to be taken into account in the design of therapeutic radiopharmaceuticals utilising in vivo generators.* J. Label. Compd. Radiopharm. 2012. **55**(3): p. 115-119.

77. Huclier-Markai, S., et al., *Optimization of reaction conditions for the radiolabeling of DOTA and DOTA-peptide with 44m/44Sc and experimental evidence of the feasibility of an in vivo PET generator.* Nucl. Med. Biol., 2014. **41**: p. e36-e43.

78. Rao, D.V., et al., *Radiations emitted in the decay of 165Er: a promising medical radionuclide.* Med. Phys., 1977. **4**(3): p. 177-186.

79. Zhernosekov, K., et al., *A 140Nd/140Pr radionuclide generator based on physico-chemical transitions in 140Pr complexes after electron capture decay of 140Nd-DOTA.* Radiochim. Acta, 2007. **95**(6): p. 319-327.

80. Wang, R., et al., *Core–shell structured gold nanoparticles as carrier for 166Dy/166Ho in vivo generator.* EJNMMI Radiopharmacy and Chemistry, 2022. **7**(1): p. 16.

81. Nath, A., M. Prushan, and J. Gilbert, *Can super-excited molecules survive fragmentation?* J. Radioanal. Nucl. Chem., 2001. **247**(3): p. 589-591.

82. Lawrance, G.A., et al., *Palladium (II) as a versatile template for the formation of tetraaza macrocycles via Mannich-type reactions.* Inorg. Chim. Acta., 2005. **358**(11): p. 3227-3235.

83.   Wiesner, J. and E. Lingafelter, *The Crystal Structure of Bis (ethylenediamine) palladium (II) Chloride.* Inorg. Chem., 1966. **5**(10): p. 1770-1775.

84.   Chakraborty, S., et al., *Preparation and preliminary biological evaluation of a novel^ sup 109^ Pd labeled porphyrin derivative for possible use in targeted tumor therapy.* Q. J. Nucl. Med. Mol. Imaging, 2007. **51**(1): p. 16.

85.   Laprise-Pelletier, M., et al., *Low-dose prostate cancer brachytherapy with radioactive palladium–gold nanoparticles.* Adv. Healthc. Mater., 2017. **6**(4): p. 1601120.

86.   Moeendarbari, S., et al., *Theranostic nanoseeds for efficacious internal radiation therapy of unresectable solid tumors.* Sci. Rep., 2016. **6**(1): p. 20614.

87.   Pineau, J., et al., *Relevance of palladium to radiopharmaceutical development considering enhanced coordination properties of TE1PA.* Chem. Eur. J.2022. **28**(41): p. e202200942.

88.   Das, T., et al., *A novel [109Pd] palladium labeled porphyrin for possible use in targeted radiotherapy.* Radiochim. Acta, 2008. **96**(7): p. 427-433.

89.   Hindié, E., et al., *Palladium-103 (103Pd/103mRh), a promising Auger-electron emitter for targeted radionuclide therapy of disseminated tumor cells-absorbed doses in single cells and clusters, with comparison to 177Lu and 161Tb.* Theranostics, 2024. **14**(11): p. 4318.

90.   Khreish, F., et al., *225 Ac-PSMA-617/177 Lu-PSMA-617 tandem therapy of metastatic castration-resistant prostate cancer: pilot experience.* EJNMMI, 2020. **47**: p. 721-728.

91.   Uusijärvi, H., et al., *Electron-and positron-emitting radiolanthanides for therapy: aspects of dosimetry and production.* J. Nucl. Med., 2006. **47**(5): p. 807-814.

92.   Gharibkandi, N.A., et al., *Au@ 109Pd core–shell nanoparticle conjugated to trastuzumab for the therapy of HER2+ cancers: studies on the applicability of 109Pd/109mAg in vivo generator in combined β– auger electron therapy.* EJNMMI Radiopharmacy and Chemistry, 2023. **8**(1): p. 26.

93.   Chan, C., Z. Cai, and R.M. Reilly, *Trastuzumab labeled to high specific activity with 111 In by conjugation to G4 PAMAM dendrimers derivatized with multiple DTPA chelators exhibits increased cytotoxic potency on HER2-positive breast cancer cells.* Pharm. Res. 2013. **30**: p. 1999-2009.

94.   Torchilin, V. and A. Klibanov, *The antibody-linked chelating polymers for nuclear therapy and diagnostics.* Crit Rev Ther Drug Carrier Syst. , 1991. **7**(4): p. 275-308.

95.   Allen, C., D. Maysinger, and A. Eisenberg, *Nano-engineering block copolymer aggregates for drug delivery.* Colloids Surf. B Biointerfaces, 1999. **16**(1-4): p. 3-27.

96.   Emfietzoglou, D., et al., *Liposome-mediated radiotherapeutics within avascular tumor spheroids: comparative dosimetry study for various radionuclides, liposome systems, and a targeting antibody.* J. Nucl. Med., 2005. **46**(1): p. 89-97.

97.   Owen, J., et al., *Indium-111 labelling of liposomal HEGF for radionuclide delivery via ultrasound-induced cavitation.* J. Control. Rel., 2020. **319**: p. 222-233.

98.   Sung, W., S. Jung, and S.-J. Ye, *Evaluation of the microscopic dose enhancement for nanoparticle-enhanced Auger therapy.* Physics in Medicine & Biology, 2016. **61**(21): p. 7522.

99.   Chattopadhyay, N., et al., *Role of antibody-mediated tumor targeting and route of administration in nanoparticle tumor accumulation in vivo.* Mol. Pharm., 2012. **9**(8): p. 2168-2179.

100.   Su, W., et al., *Auger electrons constructed active sites on nanocatalysts for catalytic internal radiotherapy.* Adv. Sci., 2020. **7**(10): p. 1903585.

101.   Turkevich, J., P.C. Stevenson, and J. Hillier, *A study of the nucleation and growth processes in the synthesis of colloidal gold.* Discuss. Faraday Soc. 1951. **11**: p. 55-75.

102.   Wawrowicz, K., et al., *Au@ Pt core-shell nanoparticle bioconjugates for the therapy of HER2+ breast cancer and hepatocellular carcinoma. Model studies on the applicability of 193mPt and 195mPt radionuclides in Auger electron therapy.* Molecules, 2021. **26**(7): p. 2051.

103. Żelechowska-Matysiak, K., et al., *Doxorubicin-and Trastuzumab-Modified Gold Nanoparticles as Potential Multimodal Agents for Targeted Therapy of HER2+ Cancers.* Molecules, 2023. **28**(6): p. 2451.

104. Facca, V.J., et al., *Panitumumab-DOTA-111In: An epidermal growth factor receptor targeted theranostic for SPECT/CT imaging and Meitner–Auger electron radioimmunotherapy of triple-negative breast cancer.* Mol. Pharm., 2022. **19**(10): p. 3652-3663.

105. Yook, S., et al., *Radiation nanomedicine for EGFR-positive breast cancer: panitumumab-modified gold nanoparticles complexed to the β-particle-emitter, 177Lu.* Mol. Pharm., 2015. **12**(11): p. 3963-3972.

106. Kumar, H., et al., *A review of biological targets and therapeutic approaches in the management of triple-negative breast cancer.* J. Adv. Res., 2023. **54**: p. 271-292.

107. Shoshan, M.S., et al., *Peptide-coated platinum nanoparticles with selective toxicity against liver cancer cells.* Angew. Chem., Int. Ed. Engl., 2019. **58**(15): p. 4901-4905.

108. Champion, C., et al., *Comparison between three promising ß-emitting radionuclides, 67Cu, 47Sc and 161Tb, with emphasis on doses delivered to minimal residual disease.* Theranostics, 2016. **6**(10): p. 1611.

109. Lo, J., et al., *Radiochemical purity evaluation of rhodium-105 complexes by magnesium oxide.* International Journal of Radiation Applications and Instrumentation. Part A. Appl. Radiat. Isot., 1990. **41**(1): p. 103-105.

110. Jensen, A.I., et al., *A solid support generator of the Auger electron emitter rhodium-103m from [103Pd] palladium.* Appl. Radiat. Isot., 2020. **156**: p. 108985.

111. van Rooyen, J., Z. Szucs, and J.R. Zeevaart, *A possible in vivo generator 103Pd/103mRh—recoil considerations.* Appl. Radiat. Isot., 2008. **66**(10): p. 1346-1349.

112. Nilsson, J., et al. *Rh-103m-labelled somatostatin analogues: candidates for targeted radiation therapy of small neuroendocrine tumours*. EJNMMI 2006, 33 (Supplement2): p. S149-S149

PUBLICATION NO. 1

Nasrin Abbasi Gharibkandi, Joanna Gierałtowska, Kamil Wawrowicz, Aleksander Bilewicz

Review

Nanostructures as Radionuclide Carriers in Auger Electron Therapy

Nasrin Abbasi Gharibkandi, Joanna Gierałtowska, Kamil Wawrowicz * and **Aleksander Bilewicz ***

Institute of Nuclear Chemistry and Technology, 03-195 Warsaw, Poland; n.abbasi@ichtj.waw.pl (N.A.G.); j.gieraltowska@ichtj.waw.pl (J.G.)
* Correspondence: k.wawrowicz@ichtj.waw.pl (K.W.); a.bilewicz@ichtj.waw.pl (A.B.)

Abstract: The concept of nanoparticle-mediated radionuclide delivery in the cancer treatment has been widely discussed in the past decade. In particular, the use of inorganic and organic nanostructures in the development of radiopharmaceuticals enables the delivery of medically important radioisotopes for radionuclide therapy. In this review, we present the development of nanostructures for cancer therapy with Auger electron radionuclides. Following that, different types of nanoconstructs that can be used as carriers for Auger electron emitters, design principles, nanoparticle materials, and target vectors that overcame the main difficulties are described. In addition, systems in which high-Z element nanoparticles are used as radionuclide carriers, causing the emission of photoelectrons from the nanoparticle surface, are presented. Finally, future research opportunities in the field are discussed as well as issues that must be addressed before nanoparticle-based Auger electron radionuclide therapy can be transferred to clinical use.

Keywords: Auger electron therapy; nanostructures; radionuclides; organic nanocarriers; inorganic nanocarriers

1. Introduction

Cancer has been one of the main causes of death worldwide during the past decade. Surgery, external radiation therapy, and chemotherapy are still the major and first-line treatments in oncology used for malignant tumors. In the case of aggressive and proliferative cancers, in which metastatic sites are frequently spread throughout the whole body, chemotherapy is usually the main and only applicable therapy. Its efficacy may be limited by the tumor type, administered dose, overall health, and severe side effects. Unfortunately, the low tumor specificity of cytotoxic drugs also causes damage to surrounding healthy cells. Moreover, different types of cancer cells exhibit acquired or innate resistance to administered drugs. Therefore, it is necessary to search for new, less toxic, and more effective drug therapies designed to kill tumor cells specifically. Current studies are focused on the development of new approaches to treat cancer cells selectively, without affecting the healthy tissues. These methods also include targeted radionuclide therapy (TRT) in which cancer cells are killed by corpuscular radiation (electrons or α particles) emitted by radionuclides conjugated to biological vectors, such as peptides, monoclonal antibodies, their fragments, or other small biologically active molecules. Effective targeting with biological vectors can be achieved due to their ability of recognition and subsequent binding to transmembrane proteins, which are expressed (or overexpressed) in cancer cells and frequently play a crucial role in tumor physiology and pathomorphology. Typically, α or β particles emitting isotopes are used in TRT. In the case of solid tumors, targeting agents labeled with radionuclides are concentrated within the tumor, while a small dose of radiation is deposited into surrounding normal tissues.

It is widely accepted that metastasis is one of the leading reasons for recurrence and consequent cancer mortality [1]. It may contain a small number of cells and be spread throughout the organism, even over long distances by lymphatic or blood vessel penetration.

Unfortunately, the tissue range of β⁻ particles is about several hundred cells in length and thus, it is not the most suitable for the treatment of single cells or even small clusters of cells. Furthermore, non-specific irradiation of hematopoietic stem cells in the bone marrow limits the dose of radioactivity that can be safely administered to the patients, influencing the low effectiveness of TRT and consequently precluding the use of β⁻ emitters in this case. Treatment of small tumors, clusters of cells, or micrometastases can be more effective with α particles. The potential use of α-emitting radionuclides offers several significant advantages. The tissue range of α particles is only several cells in diameter (40–100 μm), which in combination with their high linear energy transfer (LET = 100 keV/μm), results in very high radiocytotoxicity. Their high radiobiological effectiveness is due to causing lethal double DNA (deoxyribonucleic acid) strand breaks. In contrast to β⁻ radiation, α particles possess high cytotoxic effectiveness even in hypoxic regions within a tumor [2]. Despite achieving notable therapeutic effects such as prostate cancer metastases treatment with ^{225}Ac-PSMA-617 (prostate specific membrane antigen) radiobioconjugate [3], this method cannot be used more widely due to the low availability of α-emitters. Current supplies of the most popular in nuclear medicine α-emitter (^{225}Ac) remain limited to isolated by-products from nuclear weapons processing and power plant development within the USA and Russia. The actual production level of ^{225}Ac (~1.7 Ci per year) is only adequate for preclinical studies and for a limited number of clinical trials [4]. Recent intensive work on cyclotron production of ^{225}Ac in the spallation reaction of ^{232}Th and by proton irradiation of ^{226}Ra target did not yield the expected results, mainly due to the contamination of ^{225}Ac by long-lived ^{227}Ac ($t_{1/2}$ = 20 y).

Auger emitters can overcome all of the current issues related to α emitters while still providing a similarly high LET component for therapeutic application. It was found that the Auger electron emitters located in the DNA strand were more radiotoxic than α particle emitter ^{210}Po [5]. Due to their very short range, the Auger electrons have properties similar to particles exhibiting high LET. As a result, they can induce several double-stranded DNA breaks over the distance of several nucleotides [6]. Furthermore, in contrast to α and β⁻ radiation, the Auger radiation emitters maintain low toxicity when transported in the blood or bone marrow, but become extremely efficient when incorporated into the DNA of the target cells. This type of targeted radionuclide therapy with Auger-electron emitters is known as Auger therapy.

The sources of Auger electrons are radionuclides, which decay through the electron capture or internal conversion processes, leaving vacancies in electron shells that are rapidly filled by electrons from external orbitals. These electron transitions are accompanied by the characteristic X-rays or cascades of Auger electrons. The mechanism of this phenomenon is shown in Figure 1.

Typically, an average of 5 to more than 35 Auger electrons—with energies between a few eV to around 1 keV—are emitted per one decaying atom. Linear energy transfer of Auger electrons ranges from 4 to 26 keV/μm [7,8], and therefore, Auger electrons are similar to α particles and induce significant damaging effects in cells. Since the path length of Auger electrons is relatively short (compared to the size of the cell), minimal toxicity to surrounding non-targeted cells is observed. Moreover, after emission of Auger electrons, the daughter nuclide is in the form of an extremely reactive, highly positively charged cation, such as +35 in the case of ^{195}Pt^{35+} after the decay of ^{195m}Pt. Neutralization of this cation is achieved by the electrons from water in the cytosol. Subsequently, secondary radicals are formed, and the enhancement of therapeutic efficacy can be observed. Auger emitters are therefore promising candidates for targeted radionuclide therapy. Indeed, it is possible to inject about 10-fold greater radioactivity of Auger emitters than β⁻ particle emitters without toxic side effects. As a result, radiopharmaceuticals labeled with Auger emitters are expected to become widely used in radionuclide therapy in the near future. The basis for this assumption includes their high cytotoxicity and therapeutic efficacies. Another advantage is the reported sufficient availability of many low-energy electron-emitting radionuclides in a non-carrier-added form, with variable physical half-lives and known

chemical properties. Furthermore, radiopharmaceuticals labeled with Auger emitters have very low autoradiolysis levels (even at high specific activity), which is a substantial benefit [8].
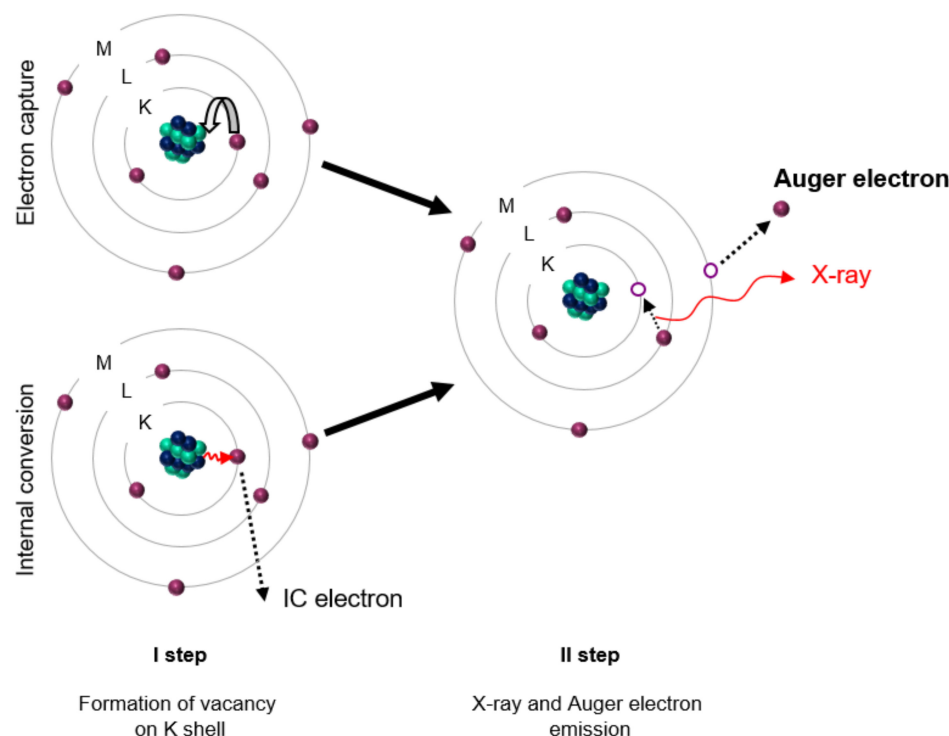

Figure 1. Emission of Auger and conversion electrons during electron capture and internal conversion. In the first step, the vacancy formation on the K shell by internal conversion or electron capture processes leads to atom excitation. In the following step, the atomic relaxation to the ground state occurs via radiative (X-ray) and nonradiative processes (i.e., Auger electron emission). Adapted from [7].

Although the potential for cancer therapy with Auger electrons has been widely established, there have been many barriers to the successful introduction of this therapy. Because most of the energy released by Auger electrons is deposited closely to the decay site [9], the successful use of Auger electron emitters in the therapy requires their precise delivery not only into the desired target cell but even more specifically to the sensitive organelles inside the cells. DNA in the cell nucleus is usually considered to be the most sensitive target for the delivery of Auger electron emitters. The double-strand DNA helix has a diameter of 2 nm and in a typical Auger radiation decay, the highest energy deposition occurs within spheres of 1–2 nm [10]. Hence, the calculated local energy deposition of an Auger emitter incorporated into DNA would hit both strands with an energy of 1.6 MGy or higher. For ^{125}I decays associated with DNA, this translates into "one decay = one double-strand break" [11]. Similar to the α radiation path through the cell nucleus, genetic information is lost in these double-strand breaks due to the destruction of several nucleotides in both DNA strands [12]. As mentioned, it is crucial that Auger radiation, which has high α-like cytotoxicity when located close to DNA, has low toxicity outside the cell nucleus [13].

Several radionuclides emitting Auger electrons are available for the radiolabeling of biological vectors (Table 1). The energy of emitted electrons, the half-life of the radionuclide, the ratio of emitted photons (penetrating forms of radiation) to electrons (non-penetrating), the possibility of easy binding to the biomolecule and the ease of producing high activity of the radionuclide in the non-carrier added form are the parameters that should be considered when selecting the appropriate radionuclide for Auger electron therapy.

Table 1. Characteristics of radionuclides with possible applications in Auger electron targeted therapy. The most promising radionuclides are marked in bold.

Radionuclide	Physical Half-Life	Electron Yield per Decay	Decay Mode	γ-Photon Energy (keV)	Method of Production
^{51}Cr	27.7 d	4.68	EC	320	reactor
^{67}Ga	**78.3 h**	**7.03**	**EC**	**93,185,300**	**cyclotron**
^{77}Br	57.0 d	4.96	EC	239	cyclotron
^{94}Tc	4.88 h	6.42	EC	511	cyclotron
^{99m}Tc	6.01 h	4.67	IT	141	cyclotron
^{111}In	**2.82 d**	**6.05**	**EC**	**171, 245**	**cyclotron**
^{114m}In	49.51d	7.74	EC	558	reactor
^{115m}In	4.49 h	5.04	IT	336	reactor
^{123}I	13.2 h	12.6	EC	159	cyclotron
^{124}I	4.18 d	8.6	EC	511	cyclotron
^{125}I	**59.4 d**	**21.0**	**EC**	**36**	**cyclotron**
^{135}La	19.5 h	10.9	EC	485.5	cyclotron
^{167}Tm	9.25 d	11.4	EC	207.8	cyclotron
^{193m}Pt	**4.33 d**	**27.0**	**IT**	**-**	**reactor/cyclotron**
^{195m}Pt	**4.03 d**	**37.0**	**IT**	**98.9**	**reactor/cyclotron**
^{197}Hg	**64.1 h**	**23.2**	**EC**	**134**	**cyclotron**
^{197m}Hg	**23.8 h**	**19.4**	**IT/EC**	**77**	**cyclotron**
^{201}Tl	73.0 h	36.9	EC	68–80	cyclotron
^{203}Pb	51.9 h	23.3	EC	279.2	cyclotron

The listed radionuclides can be easily attached to biomolecules by halogenation reactions (^{77}Br, ^{123,124,125}I) or by chelation with DTPA (diethylenetriaminepentaacetic acid), DOTA (2,2′,2″,2‴-(1,4,7,10-Tetraazacyclododecane-1,4,7,10-tetrayl)tetraacetic acid), NOTA (2,2′,2″-(1,4,7-triazacyclononane-1,4,7-triyl)triacetic acid), or sulfur ligands. However, in the case of labelled monoclonal antibodies, the obtained specific activity is too low for therapeutic application. For example, the specific activity of ^{111}In-labeled trastuzumab does not exceed 0.24 MBq/μg, resulting in only 1 of 50 molecules being radiolabeled [14]. As a result, a high proportion of HER-2 (human epidermal growth factor receptor 2) receptors were bound by non-radiolabeled immunoconjugates, limiting the cytotoxic efficacy. On the other hand, increasing the number of chelators conjugated with trastuzumab to increase specific activity may not be beneficial due to a possible decrease in antibody immunoreactivity [15]. Another approach to increase specific activity and optimize the efficacy of Auger electron targeted radionuclide therapy is to develop nanostructure-based delivery systems with many chelators attached to polymers, dendrimers, or inorganic nanoparticles working as carrier molecules.

Nanomedicine is one of the fastest growing scientific fields in the design of new diagnostic and therapeutic methods. Anticancer drug delivery systems represent a widely investigated research area in the context of nanoparticles medical application. The surface of nanoparticles can be modified with proper vectors (such as antibodies, peptides, or small biologically active molecules) which have high affinity to the receptors on tumor cells, and the number of these targeting ligands bound to one nanoparticle can be much more than one [16]. Specific binding to transmembrane receptors improves the delivery of radioactivity to the targeted tissue, which leads to improved therapeutic efficacy. In such drug delivery systems based on nanoparticles, high radiolabeling yield can be achieved due to the high surface area-to-volume ratio of nanoparticles. The large surface area of nanoparticles makes them suitable for modification by adding polymers (e.g., polyethylene glycol) and changing their surface properties to improve the stability and pharmacokinetics in vivo.

It also offers an opportunity to combine imaging, radiotherapeutic, or chemotherapeutic moieties for multimodal tumor imaging and therapy. The unique chemical and physical properties of some nanoparticles, such as magnetization and photosensitizing,

provide additional capabilities for the delivery enhancement of the radioisotopes in the presence of an external magnetic field. The improvement in the therapeutic efficacy can be achieved through the use of near-infrared radiation (Au nanoparticle) or alternating magnetic field-induced hyperthermia [17].

Another advantage of using nanoparticles in Auger electron therapy is their ability to passively accumulate in tumors following systemic intravenous injection via the enhanced permeability and retention (EPR) effect [18]. Because of the rapid vascularization required to serve rapidly growing tumors, most malignancies have leaky vasculature and defective vascular architecture. This fact, in combination with poor lymphatic drainage, allows for increased permeation and retention effects. Because of higher porosity and permeability, the leaky vasculature serves as a natural high-affinity target to various nanoparticles. Unfortunately, local drug deposition is unfeasible for larger tumors with poor vascularization and floating cancer cells such as lymphoma and leukemia. Target specificity is then achieved through the hybrid nanoparticles produced by conjugating them with tumor-specific biomolecules, including mAbs, aptamers, peptides, or various receptor-specific substrates.

Additionally, nanoparticles can avoid uptake by the reticuloendothelial and mononuclear phagocytic systems. The small size of nanoparticles also facilitates their circulation for prolonged retention (especially when polymer-stabilized conjugates are used), compared to compounds with low molecular weight. The ability of some nanoparticles to permanently bind radionuclides, such as gold nanoparticles, which bind heavy halogens such as the ^{125}I radionuclide [19,20], is a significant advantage.

In recent years, the concept of delivering radionuclides through nanoparticles for cancer treatment has been highly debated. A number of reviews summarizing studies with the therapeutic application of nanostructures as platforms for β^- and α radiation emitters have been published in more than 20 publications [21–25]. To the best of our knowledge, only one review article, a small part of which was devoted to the use of nanomaterials as carriers for Auger electron emitters, has been published so far [26].

In this review, the development of nanostructures for Auger electron cancer radiotherapy is analyzed (Figure 2). The current limitations of Auger radiation therapy, such as the requirement to deliver a therapeutic dose directly to the tumor cells, are also discussed. Another purpose of this article is to identify how different types of nanostructures can be used to overcome these limitations. Finally, potential future research opportunities and current questions that must be answered before nanoparticle-based Auger electron radiotherapy can be moved to clinical applications are listed.
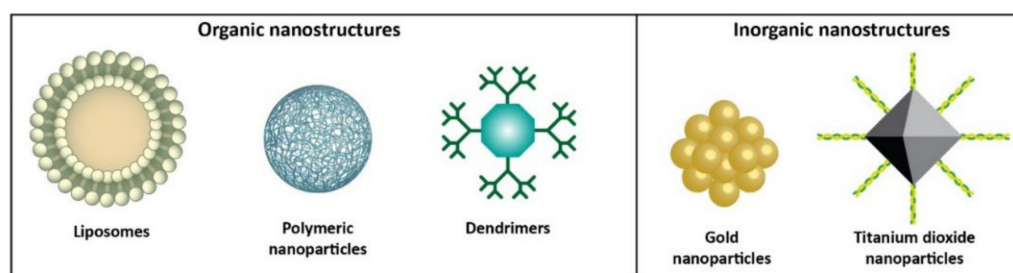

Figure 2. Organic and inorganic nanomaterials discussed in this review.

In Auger electron therapy, nanoparticles are primarily used as sensitizers for external beam radiation (the interaction of photons with high-Z nanoparticles, resulting in the emission of low-energy and short-range conversion and Auger electrons, which in turn increase the dose deposited in tissues) or as carriers for the delivery of Auger radiation emitters. Since the use of high-Z element nanostructures as sensitizers has been described in many review articles [27–31], we have limited our review only to radiobioconjugates where nanostructures are used as carriers for Auger electron emitters or as radionuclide carriers that induce the emission of photoelectrons from the nanoparticle surface.

2. Organic Nanocarriers

Recently, monoclonal antibodies (such as trastuzumab) targeting the human epidermal growth factor receptor (HER2) have become increasingly important in the treatment of HER2+ breast cancer. Unfortunately, such treatment is ineffective in many cases, including tumors that were sensitive during primary treatment and acquired resistance over time. Trastuzumab–chemotherapeutic conjugates were developed to overcome these limitations. In these conjugates, the chemotherapeutic agent is targeted and internalized by receptor-mediated endocytosis after trastuzumab binding to the cancer cell [32]. One of them is emtansine (DM1) (trastuzumab covalently bonded to the cytotoxic agent DM1), which is commonly used for the treatment of HER2+ metastatic breast cancer (BC) resistant to trastuzumab. Enhancement of therapeutic efficacy is related to the fact that, apart from inhibition of HER2, after prior release of emtansine in the lysosome, the depolymerization of tubulins leads to the prevention of microtubule formation [33]. Another approach for this purpose could be the application of trastuzumab labeled with corpuscular radiation emitters such as α, β, or Auger electron emitters.

An essential challenge in the production of radiopharmaceuticals based on Auger and conversion electron emitters is to increase their specific activity. Attaching numerous chelators to bigger particles, such as polymers, is a popular approach employed by many researchers. The use of metal-chelating polymers (MCP) with multiple chelating groups to increase the specific activity of the radioimmunoconjugates was first suggested by Torchilin [34], who attached multiple DTPA radionuclide-chelating groups to the amine pendant groups of polylysine. Subsequently, it was found that the maximum specific activity increased linearly with the number of metal chelators attached to the polymer backbone in a series of polyacrylamide-based MCPs with various numbers of attached DTPA and various degrees of polymerization [35].

The application of block copolymer micelles (BCM) for the multiplication of ^{111}In transport to cells is described in another publication of this research group [36]. BCMs are nanostructures of amphiphilic copolymers containing a hydrophobic core surrounded by a hydrophilic corona. Therapeutic agents can be encapsulated in the core of the micelles, while the hydrophilic blocks within the corona can be labeled with radionuclides for imaging or radiotherapy [37]. The researchers synthesized a radiobioconjugate containing a 30 nm BCM labeled with Auger electron emitter ^{111}In through the DTPA chelator and loaded with (1) radiosensitizer methotrexate, (2) trastuzumab fab vectors for active targeting of HER2+ cells, and (3) nuclear localization signal (NLS; CGYGPKKKRKVGG) peptides for nuclear translocation. The radiosensitizer (methotrexate) was encapsulated within the hydrophobic core of the micelles, while DTPA and NLS-trastuzumab were attached to the fab surface. Cellular accumulation, subcellular localization, and cytotoxicity of the radiobioconjugate were evaluated with MDA-MB-361 and SK-BR-3 human breast cancer cell lines overexpressing HER2 receptors, as well as with MDA-MB-231, which has HER2-negative status. The conjugation of NLS-trastuzumab fab to the surface of BCMs was found to have no effect on the immunoreactivity of the antibody toward HER2+ breast cancer, and it allows uptake of radiobioconjugates into the cell nucleus. The BCM also allows the co-delivery of low concentrations of methotrexate as a radiosensitizing agent. A synergistic cytotoxicity effect through the combining of ^{111}In-NLS-trastuzumab fab-BCMs and methotrexate was observed. As a result, it has been demonstrated that the use of BCMs allows for the simultaneous delivery of the Auger electron emitters and the sensitizer molecules to the cell nucleus, significantly enhancing the therapeutic effect.

Next, Reilly et al. [38,39] proposed the use of an MCP containing multiple DTPA molecules in order to increase the amount of delivered Auger emitters. They synthesized three different types of well-defined polyglutamide-based MCPs with hydrazide end groups. DTPA was used as a chelator in each of the pendant groups. In addition to the DTPA ligands, one MCP series contained about four NLS peptides. These polymers were site-specifically conjugated to aldehyde groups generated by NaIO$_4$ oxidation of the pendant glycan in the Fc domain of trastuzumab. The obtained immunoconjugates were

radiolabeled with [111]In. Receptor affinity studies demonstrated that neither the MCPs nor the presence of the NLS peptides interfered with specific antigen recognition on SK-BR-3 cells, although nonspecific binding was increased by polymer conjugation. The dissociation constant (K_D) values were in the low nanomolar range for each polymer. However, this work did not investigate the internalization of these immunoconjugates by SK-BR-3 HER2 receptors or the effect of the attachment of NLS peptides around the cell nucleus.

In previous works of this research group, trastuzumab was modified with DTPA for complexing Auger electron emitter ^{111}In and with NLS peptide to direct the delivery of radioimmunoconjugate to the nucleus of HER2-positive BC cells [40]. In in vitro experiments, ^{111}In-DTPA-NLS-trastuzumab radiobioconjugate was six times more cytotoxic than non-labeled trastuzumab towards HER2-overexpressing SK-BR-3 human BC cells. Despite these promising results for ^{111}In-DTPA-NLS-trastuzumab, a significant limitation was the low specific activity (0.24 MBq/μg) of the radiobioconjugate. As mentioned by the authors, only 1 in 50 molecules of trastuzumab were radiolabeled at such specific activity, resulting in the large numbers of HER2 receptors with unlabeled immunoconjugates, limiting the cytotoxic effect. To significantly increase the specific activity of the radiobioconjugate, the authors decided to label the trastuzumab vector with ^{111}In via a metal chelating polymer (MCP) containing multiple molecules of DTPA ligand [39]. The MCP contained a polyglutamide backbone with 29 pendant DTPA (17.4 kDa) or 24 pendant DTPA (23.6 kDa) attached, as well as three NLS peptides (CGYGPKKRKVGG). The MCPs were site-specifically linked to sodium metaperiodate-oxidized glycans on the Fc-domain of trastuzumab to minimize any steric inhibition of the MCP on binding to HER2 receptors. The obtained specific activity of ^{111}In labeled MCP-trastuzumab (8.9 MBq/μg) was 90 times greater than that of ^{111}In labeled trastuzumab modified with only two DTPA groups. Indium-111 labeled MCP-trastuzumab was bound, internalized, and transported into the nucleus of SK-BR-3 cells, but the process was slower than in the case of ^{111}In labeled trastuzumab. The nuclear uptake was more significant for the polymer radioimmunoconjugates, but NLS peptide modification did not improve the transport to the cell nucleus. As HER2 receptor internalization is lower than other members of the EGFR family, only 10–20% of ^{111}In labeled MCP-trastuzumab incubated with breast cancer cells was internalized (which was 30–50% of the radiobioconjugate bound to the cells), and most of the radiobioconjugates remained on the cell membrane. However, membrane-located Auger electron emitters have been shown to cause cytotoxicity in cancer cells [41]. The authors concluded that increasing the specific activity by conjugation of MCPs to trastuzumab greatly amplified the cytotoxic potency against HER2-overexpressed breast cancer cells and extended its cytotoxicity to cells with intermediate HER2 expression but without gene amplification, as well as to cells that are HER2 overexpressed but trastuzumab-resistant.

The influence of the type and construction of the polymer on biodistribution and cellular uptake of MCP-mAb conjugates is an essential issue in the design of MCP-mAb conjugates for clinical applications. The pendant groups can also play an important role. Boyle et al. [42] synthesized a series of polymers having a biotin end group to simplify the construction of MCP conjugates. In parallel, they derivatized a fragment of trastuzumab with streptavidin using a poly(ethylene glycol) linker. Streptavidin is a 66 kDa protein with a strong biotin affinity. Taking into account the dissociation constant (10^{-14} mol/L), the non-covalent bond between streptavidin and biotin is considered one of the strongest found in nature. This one-of-a-kind characteristic is the main reason why it is an ideal candidate for several medical applications, including drug delivery systems. Moreover, this allows for the simple functionalization of streptavidin with biologically active biotinylated molecules. It was shown that the attachment of the MCP to the trastuzumab-streptavidin conjugates had no significant effect on the rate of binding to the extracellular domain of HER2 or the dissociation rate (the interaction was characterized by a low nanomolar binding constant). The biodistribution and micro SPECT/CT (single-photon emission computed tomography/computed tomography) imaging studies on Balb/C mice showed that the tissue distribution of the trastuzumab Fab-streptavidin-MCP conjugates was dependent on

both the chemical structure of the polymer backbone and the nature of the pendant group to which the DTPA units were attached [43]. Rapid elimination from the blood and high liver uptake have been found to be related to the polyanionic character of the MCP. In the absence of In^{3+} saturation, there were several negative charges on each pendant group. When the polymer was saturated with In^{3+}, the $DTPA^{4-}$-In^{3+} complex had a charge of -1. As a result, the indium-saturated trastuzumab Fab-streptavidin-biotin-MCP conjugate was an anionic polyelectrolyte, as well. However, the ethylenediamine diamide was used as a linker between MCP and DTPA instead of the diethylenetriamine diamide, which contains a secondary amine protonated at neutral pH. Polymers with diethylenetriamine diamide-DTPA pendant groups are zwitterionic when saturated with trivalent metal ions. In this space at neutral pH, the negative charge of the $DTPA^{4-}$-In^{3+} complex is balanced by the positive charge associated with the protonated secondary amine of the diethylenetriamine diamide. It is known that the incorporation of zwitterionic polymers into micelles and other colloidal particles can reduce protein adsorption to surfaces and enhance blood circulation time. The authors concluded that the MCPs with a neutral net charge are the most suitable for the construction of radioimmunoconjugates. Unfortunately, due to the immunoreactivity of streptavidin and enhancement of streptavidin uptake by the kidneys, these conjugates are not acceptable for clinical use. Nevertheless, they are effective preclinically as a rapid method of examining site-directed MCPs.

Despite this, studies on streptavidin-modified nanoparticles were continued by the Hnatowich group [44]. They synthesized streptavidin-based nanoparticles, which were functionalized with two or three biotinylated components. In this concept, they functionalized streptavidin-based nanoparticles with three components: trastuzumab for effective HER2 receptor targeting, tat-peptide (containing NLS sequence) for the enhancement of cell membrane and nuclear envelope penetration, and antisense morpholino oligomer (MORF) for further targeting of RNA or DNA in the nucleus. Morpholinos are oligomers containing a methylenemorpholine ring as a framework, bound to each other with phosphorodiamidate groups. In general, MORF consists of about 25 of these sequences, each of them containing one of the DNA bases, enabling them to interact with ssDNA and mRNA. MORF and other oligomers can be designed as sense and antisense structures. The sense transcript is arranged from non-coding (antisense) DNA, while the antisense transcript is complimentary to coding (sense) DNA. Obviously, during transcription, when RNA is formed from a DNA matrix, thymine is replaced by uracil.

The biological function of MORF is to regulate gene expression, for example, by sterically blocking RNA access to molecules that could interact with RNA. According to this, MORF was considered a promising targeting agent. For this purpose, Liu et al. [45] investigated the possibility of MORF radiolabeling with ^{90}Y and ^{188}Re (β^-), ^{111}In (Auger), and ^{99m}Tc (γ) using DOTA (Macrocyclics, Dallas, TX, USA) or NHS-MAG$_3$ chelators and then performed stability and biodistribution studies in normal mice. Radiolabeling of MORF-DOTA with ^{111}In was performed with a 60% yield. After P4 purification, specific activity ranged from 60 to 90 µCi/µg, with a final purity of >93%. Stability studies in saline and human serum (HS) confirmed 48 h stability of ^{111}In-MORF in contrast to ^{90}Y-MORF, which showed a decrease in stability due to radiolysis and ^{90}Y-DOTA release. During biodistribution studies in normal mice, any unexpected accumulation in organs was noticed. Only the renal clearance mechanism revealed higher percentages of 9.31% and 8.38% ID/g in the kidneys after 1 and 3 h, respectively.

The higher accumulation of MORF in healthy tissues compared to cancerous tissues is a significant disadvantage of MORF systemic application in cancer treatment. When added to this also limited internalization, using them with radioactive isotopes becomes a challenge. To overcome these limitations and improve the pharmacokinetics, the same group [46] proposed MORF conjugates with protein nanoparticles. The general concept was to use streptavidin as a carrier molecule, conjugated with biotinylated (1) MORF, (2) monoclonal antibody, and (3) tat-peptide. They initially demonstrated that biotinylation had no effect on the biological functions of the used components. During primary stud-

ies, ^{111}In was used due to its accessibility and prior successful ^{111}In-MORF radiolabeling. Subsequently, evaluation of the cell and nucleus penetration ability against mRNA and verification of the cytotoxic potential of Auger emitter ^{111}In were evaluated. In some of the studies, ^{99m}Tc-antisense/tat/trastuzumab and ^{99m}Tc-sense/tat/trastuzumab radiobioconjugates were used for subcellular and in vivo biodistribution calculations. The percentage uptakes of ^{99m}Tc-antisense/tat/trastuzumab in the cells and nucleus were 8.20 ± 0.38% and 7.62 ± 0.42%, respectively. In comparison, the cell and nucleus fractions of ^{99m}Tc-sense/tat/trastuzumab were 7.20 ± 0.30% and 6.54 ± 0.34%, respectively. Cytotoxicity studies confirmed ^{111}In-related cell survival decrease for both antisense/sense fragments at a dose of 2.04 MBq/well. The membrane integrity assay yielded some interesting results, with the authors discovering that unlabeled nanoparticles combined with ^{111}In-DTPA were more efficient than radiolabeled nanoparticles bioconjugates. This was explained as a consequence of the synergistic interaction of the antibody and extracellularly located Auger emitter with the cell membrane. Dose escalation studies showed that as radioactivity increased, the surviving fraction decreased, with negligible non-specific toxicity. The cell survival fraction assay differentiated antisense and sense conjugates, with antisense nanoparticles showing a greater reduction with increasing radioactivity than sense nanoparticles. This was probably related to the enhanced nuclear uptake of antisense oligomers. Animal studies using ^{99m}Tc-antisense/tat/trastuzumab revealed the typical and extensively reported problems associated with nanoparticles. In addition to the tumor site (10.45% ID/g), high uptakes were also noticed in the liver (10.4% ID/g), kidneys (19.7% ID/g), and spleen (5.09% ID/g). Immunohistochemistry observations showed a lack of accumulation of tested bioconjugates in the nucleus of normal tissue after the intravenous application. In general, in vitro studies proved the high potency of streptavidin-based antisense/tat/trastuzumab nanoparticles, including cytotoxicity, and confirmed specific and rapid intranuclear location in cancerous cells, especially for antisense conjugates. The in vitro results proved that the antibody, despite its size, can also penetrate the nuclear envelope when the NLS peptide is used. The authors also concluded that both ^{111}In and MORF were responsible for the cytotoxic effect. However, in vivo biodistribution remains a crucial limiting parameter.

The same radiobioconjugates were evaluated using ^{125}I instead of ^{111}In in subsequent experiments, as described in another publication by Hnatowich [47]. In comparison to [111]In ($t_{1/2}$ = 2.8 d), which emits eight Auger electrons per decay, ^{125}I emits 21 Auger electrons per decay and has a much longer half-life ($t_{1/2}$ = 60 d). The lack of gamma emission and potential instability due to dehalogenation, common in halogenated chemicals in biological systems, are both disadvantages of ^{125}I, as reported by the authors. Tyrosine residues were used for ^{125}I incorporation into the MORF. A direct comparison of the results presented in both publications [46,47] is challenging due to the fact that the SK-BR-3 cell line was utilized for the ^{111}In evaluation, and the BT474 cell line was used for the ^{125}I evaluation. This is doubtful, especially since BT474 cells are thought to be more radiosensitive. Additionally, as previously stated, the half-lives of both radionuclides are significantly different. However, the minimum dose inducing cytotoxicity for ^{125}I was three times lower than for [111]In (10 µCi/well vs. 30 µCi/well). The authors hypothesized that a significant nucleus-to-cytoplasm ratio might be the result of non-covalent MORF binding to streptavidin and related to this improved release of, e.g., MORF. Even when the K_D parameter for streptavidin-biotin bound is set to a high value, it is still weaker than the covalent bound.

To verify this concept, they performed analogous studies as reported in the publication [48]. In these studies, the effects of two compounds were compared. Streptavidin-based "non-covalent" compounds consisted of Cy3-MORF/tat/trastuzumab. "Covalent" compounds included Cy5.5-DNA-trastuzumab (for fluorescent imaging) and ^{111}In-DTPA-trastuzumab-antisense DNA (for radiometric assays). Flow cytometry analysis confirmed high accumulation of the tested bioconjugates only in the case of HER2+ SK-BR-3 cells, at a similar level as native trastuzumab. Fluorescent imaging proved that both non-covalent

and covalent conjugates were localized in the cytosol. However, non-covalent conjugates were also found in the cell nucleus after 3 h of incubation. Radiometric subcellular distribution assays once again confirmed specific binding to HER2 receptors and the lack of internalization in HER2- MDA-MB-231 cells. The authors concluded that the presence of a covalent bond was responsible for the reduced release.

In a recently published work, Qin et al. [49] developed a curcumin-loaded nanomicelle composed of a photosensitizer chlorin e6 (Ce6) and amphiphilic poly(ethylene glycol) (poly(maleic anhydride-alt-1-octadecene)-poly(ethylene glycol) (C18-PMH-PEG)) to deliver ^{125}I to the nucleus, followed by 660 nm laser irradiation. These nanomicelles were designed for image-guided internal Auger and conversion electron therapy of cancer. The nuclear uptake of ^{125}I-labeled curcumin containing a phenolic hydroxyl group was observed under confocal microscopy and was consistent with previously published work [50]. The tumor was detected by fluorescence and SPECT imaging two hours after intravenous injection of ^{125}I-labeled Ce6-C18-PEG/Cur nanomicelles. The tumor was then irradiated with a 660 nm laser under bimodal imaging. The photodynamic reaction to the chlorin e6 photosensitizer enhanced the effect of EPR by destroying tumor blood vessels, increasing the cellular uptake of ^{125}I-labeled Ce6-C18-PEG/Cur and promoting lysosome escape of the nanoparticle. The released ^{125}I-labeled Cur was subsequently transported into the nucleus, where it caused DNA double-strand break damage in both in vitro and in vivo conditions. The presented studies demonstrated a novel strategy for the effective treatment of cancer that involves the delivery of Auger electron emitters into the cell nucleus under the local laser irradiation.

In another study, nanoparticles prepared from the widely used chitosan biopolymer were applied for nanoparticle-mediated radionuclide-gene therapy of liver cancer [51]. The alpha-fetoprotein (AFP) with the antisense oligonucleotide was labeled with Auger emitter ^{125}I and encapsulated with chitosan nanoparticles. The nanoparticles were then transfected into liver cancer cells (HepG2 cells) to disrupt the expression of their AFP gene. The damages of DNA and proteins in cells were determined by using the nanoscale confocal Raman scattering microscope (LabRam INV, Kyoto, Japan). The expression of the AFP gene and protein were also observed. All the biological effects were measured as the functions of the radiation intensity, the time of the transfection, and the size of the nanoparticle. The Auger electron generated by ^{125}I was discovered to damage the helical conformation and structure of DNA and depress the AFP gene expression. The DNA damage increased with the radiation intensity. The authors found that antisense oligonucleotide is an effective specific carrier of the Auger emitter ^{125}I into the target DNA, with chitosan nanoparticles inducing two times more damage than the pure ^{125}I-AFP-antisense oligonucleotide.

Other essential radionuclide nanocarriers, particularly Auger electron emitters, are dendrimers [52]. They have been widely studied as carriers of β$^-$ and α particle emitters, and two papers on their application as Auger electron emitters transporters have been published [14,53]. Dendrimers are unique among nanomaterials because of their stepwise synthesis, which enables the formation of well-defined and monodisperse structures with tunable size and number of terminal units. They consist of three main structural elements: the inner core from which dendritic branches grow, branch layers that define the generation of dendrimers, and a multivalent outer shell. The number of peripheral groups in dendrimers increases exponentially with the generation number [46]. This allows for the attachment of a large number of chelating molecules that can be labeled by cations for MRI, fluorescence, CT, and radionuclide-based imaging and therapy. The regulated structure of dendrimers also enables the simultaneous attachment of chemotherapeutic molecules and targeting moieties. The most popular is the PAMAM (poly(amidoamine)) dendrimer, which is constructed of repetitively branched amide and amine functional subunits. PAMAM dendrimers have been used to attach several chelators and targeting vectors because of their vast surface amine groups. Due to the polycationic surface, the electrostatic interaction with negatively charged residues on the cell surface is believed to trigger the endocytosis process. Mamede et al. [54] synthesized PAMAM dendrimer with avidin radiolabeled through DTPA chelator with a very high specific activity of Auger and conversion electron

emitter [111]In. They evaluated its internalization, biodistribution, and therapeutic effect in mice with intraperitoneal disseminated tumors. Avidin is a basic glycoprotein with a molecular mass of 67 kDa, which possesses a high-affinity biotin-binding site. Since the degree of complexation of chelating sites can affect the behavior of the radiolabeled compound, the DTPA chelating sites on bioconjugate were saturated with either radioactive or non-radioactive In^{3+}. The final product contained 52 DTPA chelator molecules linked to a single G4 molecule. It should be possible to achieve extremely high specific activity (theoretically, 37 GBq/μg). The radiolabeled dendrimer was internalized to SHIN-3 cells at 37 °C, and 77.6% of the radioconjugate was internalized after 24 h of incubation. The results clearly show the ability of this compound to internalize into cancer cells specifically, although its intracellular localization has yet to be discovered. The biodistribution in mice bearing an intraperitoneal disseminated tumor demonstrated a high dendrimer concentration in disseminated tumors with high tumor to background ratios.

In a more recent study, generation 1 and 4 PAMAM dendrimers were conjugated with a bifunctional pyridine-N-oxide DOTA analog and radiolabeled with Auger electron emitter [111]In [55]. The conjugate displayed satisfactory kinetic stability for at least 48 h after preparation. In the presence of EDTA/DTPA ligand competitors, the stability of the conjugates slightly decreased over the same time period. Biodistribution and elimination in rats were more favorable for the generation 1 ^{111}In conjugate than for generation 4. While the generation 1 ^{111}In conjugate was rapidly eliminated from the body, mainly through the urine, generation 4 ^{111}In showed high and long-term radioactivity accumulation in the liver and kidney, and this limits the use of this dendrimer in nuclear medicine.

Liposomes (Figure 3) are a class of nanoparticles that are well suited to cancer therapy due to their ease of production and ability to encapsulate a large payload of active therapeutics within the aqueous core of their spherical lipid bilayer. Hydrophilic substances dissolved in the core are unable to pass through the bilayer membrane easily [56]. Additionally, liposomes can be surface-modified with polyethylene glycol to protect them from the reticuloendothelial system (RES) and attach a targeting vector.
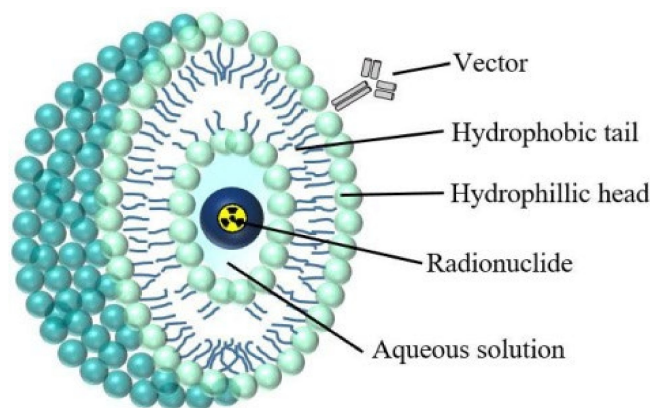

Figure 3. Structure of a liposome containing a radionuclide [25].

Liposome drug delivery systems have shown significant success in cancer therapy, with various products approved for use. Doxil®, a pegylated liposome containing doxorubicin, was the first FDA-approved nanodrug in 1995. Doxil® liposomes have been found to accumulate preferentially in mouse model tumors [57] as well as in patients with primary and metastatic disease [58].

Fondell et al. developed a two-step targeting strategy to meet the above criteria for effective targeted radiotherapy using Auger electron emitting radionuclides [59]. This concept was based on the use of liposomes loaded with significant amounts of ^{125}I-labeled amino-benzyl derivative of daunorubicin, which facilitates the localization of the internalized radionuclides in close vicinity to DNA in the cell nucleus [60]. The liposomes were also functionalized with anti-HER2 single-chain fragment F5 as a targeting agent. HER2+

tumor cells from both ovarian and breast cancer cell lines demonstrated rapid uptake of ^{125}I-labeled daunorubicin when delivered by F5-targeting liposomes. Biodistribution studies suggested that the developed bioconjugate (^{125}I labeled daunorubicin inside the functionalized liposome) accumulated highly in cancer cells compared to non-targeting liposomes. Hence, HER2-targeting liposomes loaded with the [125]I- amino benzyl by-product of daunorubicin are cell-toxic and also possess suitable therapeutic potential. Unfortunately, there have been no in vivo toxicity investigations.

In another research paper, tumor targeting and diffusion efficiency of the most clinically used liposomes, multilamellar vesicles (MLVs), small unilamellar vesicles (SUVs), and anti-PSMA monoclonal antibody (mAb) J591 studied on prostate cancer cell spheroids have been described [61].The most heterogeneous distribution of the absorbed dose was achieved with Auger or conversion electron emitters (^{123}I, ^{125}I); the absorbed dose ratios at the center of the spheroid (D_{core}) to the maximum absorbed dose (D_{max}) were 0.40 and 0.38 at 28 and 26 μm depth for the SUV-DMPC-chol liposome, respectively, and 0.42–0.52 for the antibody. At the center of the spheroid, the absorbed dose was increased by 2 to 10 times on average (Dcore). However, Auger emitters delivered more than 40% D_{max} to the (3β-[N-(N′,N′)-dimethylaminoethane)carbamoyl]cholesterol [DC-chol])—liposomes with high binding capacity, compared to β⁻ emitters. According to this study, it is possible to design radiolabeled liposomes capable of delivering a homogenous absorbed dose to the core of micrometastatic tumors.

Recently, Owen et al. [62] proposed the application of ultrasound-induced cavitation to release ^{111}In-labeled bioconjugates from liposomes. The liposome was loaded with a peptide, human epidermal growth factor (hEGF), coupled to a chelator for subsequent radiolabeling with indium-111. The obtained liposomes were efficiently radiolabeled with a 57% yield within 1 h. In the in vitro studies, the exposure of liposomes to ultrasound-activated cavitation for 20 s resulted in the release of ~12% of the ^{111}In labeled peptide. In biodistribution studies, it has also been demonstrated that the majority of ^{111}In-hEGF was accumulated in the kidneys and liver, whereas for liposomes loaded with ^{111}In-HEGF, renal clearance was reduced by 50%. Surprisingly, there was no significant accumulation of the loaded liposome in the liver. This study presented a novel approach to the targeted delivery of radiopharmaceuticals by combining acoustic cavitation-sensitive liposomes with radionuclides. In the conducted studies, the emission of γ quanta by ^{111}In was used to test biodistribution; however, the therapeutic properties of the radiopharmaceutical related to the emission of Auger electrons were not investigated.

3. Inorganic Nanocarriers

Inorganic nanoparticles, due to their size, chemical, and physical properties, are particularly attractive as therapeutic probes in cancer treatment. Radionuclides with specific emission properties can be incorporated into nanoparticles or attached to their surface and used for radionuclide therapy and radio imaging. Among the large number of synthesized inorganic nanoparticles, only gold nanoparticles (AuNPs) have been widely used as radionuclide carriers in Auger electron therapy, and in single studies, platinum and titanium oxide nanoparticles were also evaluated.

The unique properties of AuNPs, including surface properties, allow their use in a number of therapeutic methods where direct or indirect attachment of radionuclides is required. Additionally, AuNPs offer the possibility of surface functionalization with targeting biomolecules for specific accumulation and interaction with receptors overexpressed in tumor cells. Moreover, various synthesis methods are now available to manipulate the size and shape of gold nanoparticles. The following gold nanostructures have been synthesized and studied for different medical applications: nanospheres, nanorods, nanocages, nanostars, clusters, and core shell nanoparticles (Figure 4).
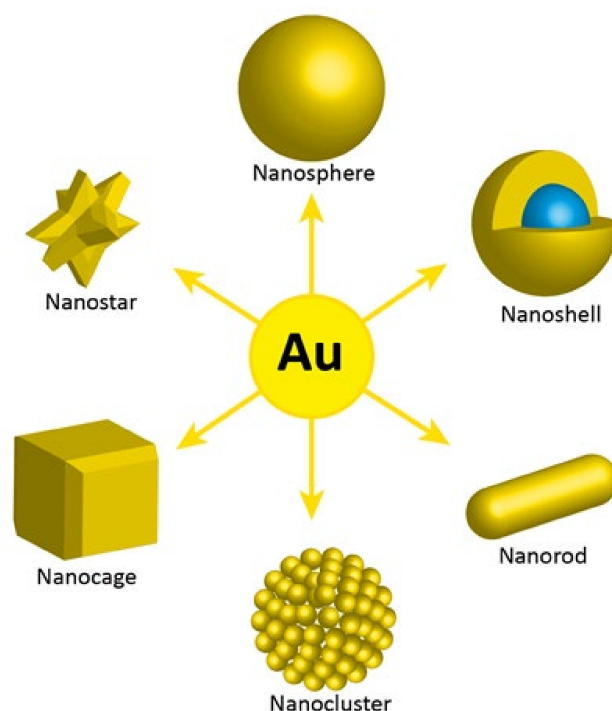
Figure 4. Different types of AuNPs, according to their shape and morphology.

Several studies have shown [63–65] that gold nanoparticles can be very effective in promoting the cytotoxic effect towards cancerous cells such as melanoma or head and neck tumors very effectively during irradiation with 150–250 kV X-rays. The results of these studies are noteworthy, as the administration of AuNPs followed by X-ray treatment reduced the size of the tumors and, in some cases, destroyed tumors significantly. Because AuNPs can be visualized through CT and planar X-rays, these nanoparticles, if systematically targeted, could serve as dual imaging (diagnostic) and therapeutic probes in the detection and therapy of cancer (theranostics) [66]. The potential of AuNPs in theranostics was also described by Chanda et al. [67]. The radioactive decay properties of ^{198}Au ($t_{1/2}$ = 2.7 d, β_{max} = 0.96 MeV) and ^{199}Au ($t_{1/2}$ = 3.14 d, β_{max} = 0.46 MeV) make them promising candidates for therapeutic applications. In addition, they both emit gamma quanta for dosimetry and pharmacokinetic studies. In studies related to Auger electron therapy, AuNPs are used as carriers for Auger electron emitters such as ^{125}I, which can be attached directly to the gold surface, or ^{111}In, which is complexed via DOTA or DTPA chelators. The nanoparticles were also surface-modified with monoclonal antibodies or peptide ligands to bind to tumor-associated antigens or receptors for active tumor targeting.

Radiobioconjugate biodistribution studies were initially conducted for future use in X-ray-induced radiotherapy. Reilly et al. synthesized radiobioconjugates by the modification of gold nanoparticles (30 nm) with polyethylene glycol chains linked to trastuzumab to target HER2-positive breast cancer (BC) cells and DTPA chelator to complex ^{111}In [68,69]. These trastuzumab-AuNP-^{111}In conjugates were further surface-coated with PEG to stabilize the particles against aggregation and minimize liver and spleen uptake. Despite long-chain PEG modification, tumor uptake in athymic mice with HER2-overexpressing MDA-MB-361 human BC xenografts was limited (1.2% ID/g) at 48 h post-intravenous injection. The uptake of trastuzumab-AuNP-^{111}In in the liver was low in contrast to uptake in the spleen (3% ID/g and 20% ID/g, respectively). Sequestration of AuNP by the liver and spleen, resulting in rapid clearance from the circulation and limited tumor uptake, is thus a major restriction of the intravenous administration of AuNP. The authors investigated local intratumoral injection of the bioconjugate to avoid liver and spleen uptake and maximize tumor localization of trastuzumab-AuNP. This route of administration yielded a 25-fold increase in trastuzumab-AuNP-^{111}In concentration in the tumor after 48 h p.i.

(30% ID/g) and a 10-fold decrease in the spleen uptake (2% ID/g). Therefore, intratumoral injection was used for further studies on the therapeutic effects of the trastuzumab-AuNP bioconjugates. This method should have clinical application as a form of neoadjuvant brachytherapy in which nanometer-sized seeds are bound and internalized into tumor cells, increasing the effectiveness of the therapy. Although trastuzumab-AuNP enhanced the effectiveness of X-radiation treatment of MDA-MB-361 tumors, the radiosensitizing properties were moderate [70].

As highlighted in Table 1, ^{111}In ($t_{1/2}$ = 2.8 d) emits an average of 6.9 low-energy Auger electrons as well as γ quanta (Eγ = 171 keV (90%) and 245 keV (94%)). Therefore, it is one of the most promising Auger electron emitters. Previously, Reilly's team [40] reported on ^{111}In-labeled trastuzumab containing a nuclear translocation sequence (NLS) peptide. Effective HER2-targeting SKBR-3 cells and subsequent—due to NLS presence—intranuclear location caused multiple DNA double-strand breaks, resulting in a 90% reduction in the survival of SKBR-3 breast cancer cells. As mentioned before, the obtained specific activity of labeled trastuzumab (0.24 MBq/μg) is insufficient for successful Auger therapy [14]. Therefore, as in the case of the previously described application of the chelating block copolymer to multiply ^{111}In transport to cells [36], the authors decided to use AuNPs to multiply ^{111}In transport to cells. The in vitro cytotoxicity of trastuzumab-AuNP-^{111}In on HER2+ breast cancer cells and their in vivo studies on tumor growth inhibitory properties and tissue toxicity after intratumoral injection in athymic mice with s.c. (injected subcutaneously) HER2-overexpressing MDA-MB-361 human BC xenografts have been described by Cai et al. [71]. The researchers showed that trastuzumab-AuNP-^{111}In was bound to and internalized by HER2+ human breast cancer cells (SK-BR-3 and MDA-MB-361). Unfortunately, the determined K_D for binding trastuzumab-AuNP-^{111}In to the HER2 receptor on SK-BR-3 cells was 46 times lower than previously reported for ^{111}In-labeled trastuzumab. The reduced binding affinity of trastuzumab-AuNP-^{111}In can be caused by a steric hindrance of AuNPs to HER2 receptors and a large number of trastuzumab and PEG molecules attached to each AuNP, which may further contribute to steric inhibition of receptor binding.

However, a greater number of trastuzumab molecules on AuNP provides stronger multivalent binding of trastuzumab-AuNP-^{111}In bioconjugate to breast cancer cells in comparison to ^{111}In-trastuzumab alone. The authors stated that a lower K_D value for trastuzumab-AuNP-^{111}In can most likely be achieved by reducing the number of trastuzumab and PEG molecules attached to AuNP, reducing steric hindrance in HER2.

Cellular studies have also shown that internalization was more efficient for trastuzumab-AuNP-^{111}In than with AuNP-^{111}In. As it is well known [72], trastuzumab binding promotes HER2 internalization. Widefield microscopy in fluorescence and dark-field modes revealed that trastuzumab-AuNP-^{111}In was internalized and deposited near the nucleus in the perinuclear area of SK-BR-3 and MDA-MB-361 cells. In contrast, the internalization of ^{111}In-labeled AuNPs was not visible. As trastuzumab locates in breast cancer cells in liposomes close to the nucleus, this affects the ability of the emitted Auger electrons to cause lethal DNA double-strand breaks. Since lysosome uptake of trastuzumab degrades HER2 receptors, resulting in cell death, the authors hypothesized that trastuzumab-AuNP-^{111}In might be toxic to breast cancer cells in two ways, by reducing HER2 and by causing DNA damage in breast cancer cells, owing to Auger electron emission.

In vivo studies were performed by local intratumoral injection of trastuzumab-AuNP-^{111}In in CD1 (cluster of differentiation 1) athymic mice with s.c. MDA-MB-361 xenografts that stopped tumor growth over 70 days. It was found that the injection of trastuzumab-AuNP-^{111}In had no effects on body weight, liver damage, renal toxicity, or hematopoietic toxicity compared to normal saline-treated control mice at 70 days. Irradiation of hematopoietic bone marrow was minimal due to intratumoral injection and the short range of Auger electrons.

In another study, Song et al. [73] described the cytotoxicity of ^{111}In-labeled AuNP on BC cells. In this study, AuNPs (14 nm) were conjugated to ^{111}In-DTPA-EGF to bind epi-

dermal growth factor receptors (EGFR) on breast cancer cells. EGF-AuNPs were prepared via direct interaction between gold and the disulfide bonds of EGF and then radiolabeled with ^{111}In, wherein it was shown that direct attachment of EGF to AuNPs does not perturb EGF-EGFR binding. The obtained results suggested that the disulfide groups of EGF can be exploited for binding to AuNPs. The synthesized ^{111}In-DTPA-EGF-AuNP conjugate was bound and internalized by EGFR-overexpressing MDA-MB-468 human breast cancer cells, reducing their surviving fraction to 4.4% after 4 h exposure. Assessment of double-stranded DNA breaks caused by Auger electrons has not been performed in this work.

Another study was conducted to evaluate the possibility of using AuNPs as a carrier for the Auger electron emitter [125]I [20]. The authors used the high affinity of gold atoms to heavy halogens for the immobilization of [125]I [74]. This is due to their nearly identical electronegativities, which are 2.4 for gold and 2.5 for iodine. The aim of this study was to use a citrate reduction technique (Turkevich method) for one-step synthesis of AuNPs labeled by [125]I. Appropriate synthesis conditions were selected to avoid the aggregation of nanoparticles. Synthesized nanoparticles were found to be extremely stable without any observable leakage of radioactivity into solution.

Apart from gold, TiO_2 nanoparticles were also applied as carriers for [125]I [75]. Because of their high surface activity and lack of toxicity, TiO_2 nanoparticles are widely used in medicine, including cancer therapy, antibacterial treatment, and biomolecule detection. Excess electrons (e.g., photoinduced electrons) are recognized to play an important role in the surface chemical activity of TiO_2 nanocatalysts. Due to the restricted penetration of light in tissue, the in vivo generation of excess electrons by light is difficult or impossible. Hence, this approach is only suitable for superficial tumors. In original studies, Su et al. [75] used ^{125}I to inject Auger electrons into TiO_2 nanoparticles to create in vivo active sites and investigated its use in cancer treatment. In the synthesized ^{125}I-TiO_2 NPs, Ti^{3+} ions were formed by the reaction between Ti^{4+} and Auger electrons emitted from [125]I. Consequently, Ti^{3+} stretched the O-H bond of the absorbed H_2O to decrease its bond energy, facilitating H_2O radiolysis. Finally, upon irradiation of γ-rays emitted by ^{125}I, the radiolysis of activated H_2O will occur more efficiently, leading to an enhanced generation of ●OH radicals. As a result, the therapeutic effect of Auger electrons emitted by ^{125}I is combined with the toxic effect of ●OH radicals generated on TiO_2 NPs' surface in the proposed system. The in vitro and in vivo studies showed high effectiveness of the proposed therapy. The therapeutic effect of ^{125}I-TiO_2 in vivo was examined in tumor xenograft mice. One group of mice received intratumorally free ^{125}I and the second group received intratumorally ^{125}I-TiO_2. In the group that received ^{125}I-TiO_2, inhibition of tumor growth was observed compared to the free ^{125}I group. Correspondingly, the survival rate in the ^{125}I-TiO_2 group was significantly improved over a 60-day follow-up period, during which all mice in the ^{125}I group died. However, this effect could be related to poor ^{125}I retention in the tumor and its diffusion to other organs, while the tumor retention of ^{125}I-TiO_2 was high.

4. Auger Electron Generation on High Atomic (Z) Number Nanocarriers

Recently, more and more attention has been paid to the use of nanoparticles with a high-Z number to increase the radiation-absorbed dose deposited in tumors from external X-ray radiation. The radiosensitization effect is based on the strong interaction of photons with high-Z atoms, resulting in an increase in the local dose deposition and emission of conversion and Auger electrons. This phenomenon is of great interest to radiation oncologists as it facilitates the generation of secondary electrons when nanoparticles are placed in cancer cells and exposed to X-rays. Several groups have worked on the development of new radiosensitization agents using high-Z elements such as Au (Z = 79), Hf (Z = 72), Gd (Z = 64), I (Z = 53), Pt (Z = 78), and Bi (Z = 83) [30]. As mentioned before, high-Z element nanostructures as sensitizers of external X-radiation have been described in many review articles, and therefore, we limited our review to the systems in which high-Z nanoparticles are used as radionuclide carriers that emit photoelectrons from their surface.

In a pioneering publication, another type of nanoparticle-enhanced radiation therapy was suggested by Pronschinske et al. [76]. They synthesized one-atom-thick layers of the radionuclide ^{125}I on gold and reported large amplification of low-energy electron emission. By scanning microscopy, supported by electronic structure simulations, they observed the nuclear transmutation of individual ^{125}I atoms into ^{125}Te and explained the surprising stability of the 2D film as it underwent radioactive decay. The metal interface geometry induced a 600% amplification of low-energy electron emission compared with atomic ^{125}I. This enhancement of biologically active low-energy electrons could indicate a new direction for highly targeted nanoparticle therapies.

Another radionuclide, ^{169}Yb, has been proposed to generate photo and Auger electrons on AuNPs. The ^{169}Yb ($t_{1/2}$ = 32.0 d) is an ideal radioisotope for this purpose because it emits photons with an average energy of 93 keV (just above the K edge of gold). Due to the absence of a commercially available ^{169}Yb source providing a sufficiently high dose rate necessary for in vitro and in vivo studies, the authors developed a surrogate external beam ^{169}Yb using erbium (Er) as a filter material and a standard copper (Cu)-filtered 250 kVp beam. They investigated the role of the energy range of photons present in the γ-ray spectrum of ^{169}Yb for gold-mediated radiosensitization through in vitro and in vivo studies. Human prostate cancer cells were pre-treated with gold nanoparticles using goserelin-conjugated gold nanorods and non-targeted gold nanoparticles.

Then, in vivo experiments were performed by irradiating tumor-bearing mice (human prostate cancer xenograft) pre-treated with actively targeted and non-targeted nanoparticles. The results revealed that the treatment with goserelin-conjugated gold nanorods in combination with X-ray irradiation (mimic ^{169}Yb radiation) is considerably more effective than radiation treatment alone.

Chao et al. [77] applied the ^{99m}Tc, a low-energy γ emitter, to generate conversion and Auger electrons by reaction with Hf atoms. Technetium-99m is one of the most widely used radioisotopes in diagnostic imaging, mainly for single-photon emission computed tomography (SPECT). Although ^{99m}Tc is the most commonly used radionuclide for imaging, it is only occasionally used for therapy. In a one-pot reaction, the authors prepared a PEG-modified coordination polymer, consisting of Hf^{4+} cations and tetrakis (4-carboxyphenyl) porphyrin, used as a chelating agent. Such a modified coordination polymer was labeled with ^{99m}Tc in high yield. The inherent biodegradability of coordination polymer nanoparticles due to weak coordination interactions between metal ions and organic linkers is an advantage compared to the typical inorganic nanoparticles. The in vivo therapeutic efficacy of ^{99m}Tc-labeled coordination polymer was evaluated following intravenous systemic administration and intratumoral local injection in mice bearing 4T1 tumors. In vivo SPECT imaging studies indicate that ^{99m}Tc-labeled coordination polymer shows prolonged tumor retention after local intratumoral injection as well as tumor accumulation by the EPR effect after intravenous injection. As a result, a significant therapeutic effect has been achieved, substantially delaying tumor growth by a single injection or eliminating tumors by multiple repeated treatments.

5. Conclusions

Radionuclide delivery systems using nanoparticles have notable potential in the field of nuclear medicine. In the case of Auger electron therapy, nanoparticles of high-Z elements are commonly studied as sensitizers of external X-ray radiation and have been described in many articles. These studies have now moved to the stage of clinical trials. However, the use of nanostructures as carriers for Auger electron emitters is still limited. This is undoubtedly related to the difficulty of systemic administration, which causes the sequestration of nanostructure conjugates by the liver and spleen, resulting in rapid blood clearance and minimal tumor absorption. Nevertheless, recently proposed novel targeted nanobrachytherapy approaches for the treatment of locally advanced breast and prostate cancers should broaden the application of nanoparticles in Auger electron therapy. The organ distribution studies reveal that intratumorally delivered radiolabeled nanoparticle

bioconjugates are almost completely retained in the tumor, having minimal uptake in the liver and spleen. In comparison with classical labeled biomolecules, nanostructures with attached Auger electron emitters have a significant advantage of delivering significantly higher radioactivity to the cancer tissue. This is particularly important in Auger electron therapy, where substantially higher radionuclide activity is required to achieve a therapeutic effect compared to α and β- emitters.

References

1. Steeg, P.S. Targeting metastasis. *Nat. Rev. Cancer* **2016**, *16*, 201–218. [CrossRef] [PubMed]
2. Langmuir, V.; Sutherland, R. Radiobiology of radioimmunotherapy: Current status. *Antib. Immunoconj. Radiopharm.* **1988**, *1*, 195–211. [CrossRef]
3. Kratochwil, C.; Bruchertseifer, F.; Giesel, F.L.; Weis, M.; Verburg, F.A.; Mottaghy, F.; Kopka, K.; Apostolidis, C.; Haberkorn, U.; Morgenstern, A. 225Ac-PSMA-617 for PSMA-Targeted α-Radiation Therapy of Metastatic Castration-Resistant Prostate Cancer. *J. Nucl. Med.* **2016**, *57*, 1941–1944. [CrossRef] [PubMed]
4. Morgenstern, A.; Bruchertseifer, F.; Apostolidis, C. Bismuth-213 and actinium-225generator performance and evolving therapeutic applications of two generator-derived alpha-emitting radioisotopes. *Curr. Radiopharm.* **2012**, *5*, 221–227. [CrossRef] [PubMed]
5. Howell, R.; Narra, V.; Rao, D.; Sastry, K.S. Radiobiological effects of intracellular sup 210 Po alpha emissions: A comparison with Auger emitters. *Radiat. Prot. Dosim.* **1990**, *31*, 325–328. [CrossRef]
6. Kassis, A.I.; Fayad, F.; Kinsey, B.M.; Sastry, K.S.; Taube, R.A.; Adelstein, S.J. Radiotoxicity of 125I in mammalian cells. *Radiat. Res.* **1987**, *111*, 305–318. [CrossRef]
7. Kassis, A.I. The amazing world of auger electrons. *Int. J. Radiat. Biol.* **2004**, *80*, 789–803. [CrossRef]
8. Aghevlian, S.; Boyle, A.J.; Reilly, R.M. Radioimmunotherapy of cancer with high linear energy transfer (LET) radiation delivered by radionuclides emitting α-particles or Auger electrons. *Adv. Drug Deliv. Rev.* **2017**, *109*, 102–118. [CrossRef]
9. Kassis, A.I. Molecular and cellular radiobiological effects of Auger emitting radionuclides. *Radiat. Prot. Dosim.* **2011**, *143*, 241–247. [CrossRef] [PubMed]
10. Buchegger, F.; Perillo-Adamer, F.; Dupertuis, Y.M.; Delaloye, A.B. Auger radiation targeted into DNA: A therapy perspective. *Eur. J. Nucl. Med. Mol. Imaging* **2006**, *33*, 1352–1363. [CrossRef]
11. Elmroth, K.; Stenerlöw, B. DNA-incorporated 125I induces more than one double-strand break per decay in mammalian cells. *Radiat. Res.* **2005**, *163*, 369–373. [CrossRef] [PubMed]
12. Lobachevsky, P.N.; Martin, R.F. Iodine-125 decay in a synthetic oligodeoxynucleotide. I. Fragment size distribution and evaluation of breakage probability. *Radiat. Res.* **2000**, *153*, 263–270. [CrossRef]
13. Rosenkranz, A.A.; Slastnikova, T.A.; Georgiev, G.P.; Zalutsky, M.R.; Sobolev, A.S. Delivery systems exploiting natural cell transport processes of macromolecules for intracellular targeting of Auger electron emitters. *Nucl. Med. Biol.* **2020**, *80–81*, 45–56. [CrossRef] [PubMed]
14. Chan, C.; Cai, Z.; Reilly, R.M. Trastuzumab labeled to high specific activity with ^{111}In by conjugation to G4 PAMAM dendrimers derivatized with multiple DTPA chelators exhibits increased cytotoxic potency on HER2-positive breast cancer cells. *Pharm. Res.* **2013**, *30*, 1999–2009. [CrossRef] [PubMed]
15. Reilly, R.M. The radiochemistry of monoclonal antibodies and peptides. In *Monoclonal Antibody and Peptide-Targeted Radiotherapy of Cancer*; John Wiley & Sons, Inc.: Hoboken, NJ, USA, 2010; pp. 39–100. [CrossRef]
16. Wawrowicz, K.; Majkowska-Pilip, A.; Gaweł, D.; Chajduk, E.; Pieńkowski, T.; Bilewicz, A. Au@Pt Core-Shell Nanoparticle Bioconjugates for the Therapy of HER2+ Breast Cancer and Hepatocellular Carcinoma. Model Studies on the Applicability of (193m)Pt and (195m)Pt Radionuclides in Auger Electron Therapy. *Molecules* **2021**, *26*, 2051. [CrossRef] [PubMed]
17. Zhang, Z.; Wang, J.; Chen, C. Near-infrared light-mediated nanoplatforms for cancer thermo-chemotherapy and optical imaging. *Adv. Mater.* **2013**, *25*, 3869–3880. [CrossRef]

18. England, C.G.; Gobin, A.M.; Frieboes, H.B. Evaluation of uptake and distribution of gold nanoparticles in solid tumors. *Eur. Phys. J. Plus* **2015**, *130*, 231–258. [CrossRef]

19. Ostrowski, S.; Majkowska-Pilip, A.; Bilewicz, A.; Dobrowolski, J.C. On Au n At clusters as potential astatine carriers. *RSC Adv.* **2017**, *7*, 35854–35857. [CrossRef]

20. Clanton, R.; Gonzalez, A.; Shankar, S.; Akabani, G. Rapid synthesis of (125)I integrated gold nanoparticles for use in combined neoplasm imaging and targeted radionuclide therapy. *Appl. Radiat. Isot.* **2018**, *131*, 49–57. [CrossRef]

21. Malapure, S.S.; Bhushan, S.; Kumar, R.; Bharati, S. Radiolabelled nanoparticles in cancer management: Current status and developments. *Chem. Biol. Lett.* **2018**, *5*, 25–34.

22. Pellico, J.; Gawne, P.J.; de Rosasles, T.M.R. Radiolabelling of nanomaterials for medical imaging and therapy. *Chem. Soc. Rev.* **2021**, *50*, 3355–3423. [CrossRef]

23. Pallares, R.M.; Abergel, R.J. Nanoparticles for targeted cancer radiotherapy. *Nano Res.* **2020**, *13*, 2887–2897. [CrossRef]

24. Aranda-Lara, L.; Morales-Avila, E.; Luna-Gutiérrez, M.A.; Olivé-Alvarez, E.; Isaac-Olivé, K. Radiolabeled liposomes and lipoproteins as lipidic nanoparticles for imaging and therapy. *Chem. Phys. Lipids* **2020**, *230*, 104934–104984. [CrossRef] [PubMed]

25. Majkowska-Pilip, A.; Gawęda, W.; Żelechowska-Matysiak, K.; Wawrowicz, K.; Bilewicz, A. Nanoparticles in targeted alpha therapy. *Nanomaterials* **2020**, *10*, 1366. [CrossRef] [PubMed]

26. Ku, A.; Facca, V.J.; Cai, Z.; Reilly, R.M. Auger electrons for cancer therapy—A review. *EJNMMI Radiopharm. Chem.* **2019**, *4*, 27–43. [CrossRef] [PubMed]

27. Kobayashi, K.; Usami, N.; Porcel, E.; Lacombe, S.; Le Sech, C. Enhancement of radiation effect by heavy elements. *Mutat. Res.* **2010**, *704*, 123–131. [CrossRef]

28. Abdollahi, B.B.; Malekzadeh, R.; Azar, F.P.; Salehnia, F.; Naseri, A.R.; Ghorbani, M.; Hamishehkar, H.; Farajollahi, A.R. Main Approaches to Enhance Radiosensitization in Cancer Cells by Nanoparticles: A Systematic Review. *Adv. Pharm. Bull.* **2021**, *11*, 212–223. [CrossRef]

29. Choi, J.; Kim, G.; Cho, S.B.; Im, H.J. Radiosensitizing high-Z metal nanoparticles for enhanced radiotherapy of glioblastoma multiforme. *J. Nanobiotechnol.* **2020**, *18*, 122–145. [CrossRef]

30. Laprise-Pelletier, M.; Simão, T.; Fortin, M.A. Gold Nanoparticles in Radiotherapy and Recent Progress in Nanobrachytherapy. *Adv. Healthc. Mater.* **2018**, *7*, 1701460–1701487. [CrossRef]

31. Yokoya, A.; Ito, T. Photon-induced Auger effect in biological systems: A review. *Int. J. Radiat. Biol.* **2017**, *93*, 743–756. [CrossRef]

32. Steinhauser, I.; Spänkuch, B.; Strebhardt, K.; Langer, K. Trastuzumab-modified nanoparticles: Optimisation of preparation and uptake in cancer cells. *Biomaterials* **2006**, *27*, 4975–4983. [CrossRef] [PubMed]

33. Loganzo, F.; Sung, M.; Gerber, H.P. Mechanisms of Resistance to Antibody-Drug Conjugates. *Mol. Cancer Ther.* **2016**, *15*, 2825–2834. [CrossRef] [PubMed]

34. Torchilin, V.P.; Klibanov, A.L. The antibody-linked chelating polymers for nuclear therapy and diagnostics. *Crit. Rev. Ther. Drug Carr. Syst.* **1991**, *7*, 275–308.

35. Liu, P.; Boyle, A.J.; Lu, Y.; Reilly, R.M.; Winnik, M.A. Biotinylated polyacrylamide-based metal-chelating polymers and their influence on antigen recognition following conjugation to a trastuzumab Fab fragment. *Biomacromolecules* **2012**, *13*, 2831–2842. [CrossRef]

36. Hoang, B.; Reilly, R.M.; Allen, C. Block copolymer micelles target Auger electron radiotherapy to the nucleus of HER2-positive breast cancer cells. *Biomacromolecules* **2012**, *13*, 455–465. [CrossRef]

37. Allen, C.; Maysinger, D.; Eisenberg, A. Nano-engineering block copolymer aggregates for drug delivery. *Colloids Surf. B Biointerfaces* **1999**, *16*, 3–27. [CrossRef]

38. Lu, Y.; Mbong, G.N.N.; Liu, P.; Chan, C.; Cai, Z.; Weinrich, D.; Boyle, A.J.; Reilly, R.M.; Winnik, M.A. Synthesis of polyglutamide-based metal-chelating polymers and their site-specific conjugation to trastuzumab for auger electron radioimmunotherapy. *Biomacromolecules* **2014**, *15*, 2027–2037. [CrossRef]

39. Mbong, G.N.N.; Lu, Y.; Chan, C.; Cai, Z.; Liu, P.; Boyle, A.J.; Winnik, M.A.; Reilly, R.M. Trastuzumab Labeled to High Specific Activity with (111)In by Site-Specific Conjugation to a Metal-Chelating Polymer Exhibits Amplified Auger Electron-Mediated Cytotoxicity on HER2-Positive Breast Cancer Cells. *Mol. Pharm.* **2015**, *12*, 1951–1960. [CrossRef]

40. Costantini, D.L.; Chan, C.; Cai, Z.; Vallis, K.A.; Reilly, R.M. (111)In-labeled trastuzumab (Herceptin) modified with nuclear localization sequences (NLS): An Auger electron-emitting radiotherapeutic agent for HER2/neu-amplified breast cancer. *J. Nucl. Med.* **2007**, *48*, 1357–1368. [CrossRef]

41. Pouget, J.-P.; Santoro, L.; Raymond, L.; Chouin, N.; Bardiès, M.; Bascoul-Mollevi, C.; Huguet, H.; Azria, D.; Kotzki, P.-O.; Pèlegrin, M.; et al. Cell membrane is a more sensitive target than cytoplasm to dense ionization produced by auger electrons. *Radiat. Res.* **2008**, *170*, 192–200. [CrossRef]

42. Boyle, A.J.; Liu, P.; Lu, Y.; Weinrich, D.; Scollard, D.A.; Mbong, G.N.N.; Winnik, M.A.; Reilly, R.M. The effect of metal-chelating polymers (MCPs) for ^{111}In complexed via the streptavidin-biotin system to trastuzumab Fab fragments on tumor and normal tissue distribution in mice. *Pharm. Res.* **2013**, *30*, 104–116. [CrossRef] [PubMed]

43. Liu, P.; Boyle, A.; Lu, Y.; Adams, J.; Chi, Y.; Reilly, R.M.; Winnik, M.A. Metal-Chelating Polymers (MCPs) with Zwitterionic Pendant Groups Complexed to Trastuzumab Exhibit Decreased Liver Accumulation Compared to Polyanionic MCP Immunoconjugates. *Biomacromolecules* **2015**, *16*, 3613–3623. [CrossRef] [PubMed]

44. Wang, Y.; Liu, X.; Chen, L.; Cheng, D.; Rusckowski, M.; Hnatowich, D.J. Tumor delivery of antisense oligomer using trastuzumab within a streptavidin nanoparticle. *Eur. J. Nucl. Med. Mol. Imaging* **2009**, *36*, 1977–1986. [CrossRef]

45. Liu, C.-B.; Liu, G.-Z.; Liu, N.; Zhang, Y.-M.; He, J.; Rusckowski, M.; Hnatowich, D.J. Radiolabeling morpholinos with 90Y, 111In, 188Re and 99mTc. *Nucl. Med. Biol.* **2003**, *30*, 207–214. [CrossRef]

46. Liu, X.; Wang, Y.; Nakamura, K.; Kawauchi, S.; Akalin, A.; Cheng, D.; Chen, L.; Rusckowski, M.; Hnatowich, D.J. Auger radiation-induced, antisense-mediated cytotoxicity of tumor cells using a 3-component streptavidin-delivery nanoparticle with 111In. *J. Nucl. Med.* **2009**, *50*, 582–590. [CrossRef]

47. Liu, X.; Nakamura, K.; Wang, Y.; Cheng, D.; Liang, M.; Xiao, N.; Chen, L.; Rusckowski, M.; Hnatowich, D.J. Auger-mediated cytotoxicity of cancer cells in culture by an 125I-antisense oligomer delivered as a three-component streptavidin nanoparticle. *J. Biomed. Nanotechnol.* **2010**, *6*, 153–157. [CrossRef]

48. Liu, Y.; Cheng, D.; Liu, X.; Liu, G.; Dou, S.; Xiao, N.; Chen, L.; Rusckowski, M.; Hnatowich, D.J. Comparing the intracellular fate of components within a noncovalent streptavidin nanoparticle with covalent conjugation. *Nucl. Med. Biol.* **2012**, *39*, 101–117. [CrossRef]

49. Qin, Y.; Shen, M.; Liu, X.; Gu, J.; Zhu, M.; Yi, X. Photo-Driven Delivery of (125)I-Labeled Nanomicelles for Nucleus-Targeted Internal Conversion Electron-Based Cancer Therapy. *ACS Appl. Mater. Interfaces* **2021**, *13*, 49671–49681. [CrossRef]

50. Zheng, P.; Ding, B.; Shi, R.; Jiang, Z.; Xu, W.; Li, G.; Ding, J.; Chen, X. A Multichannel Ca^{2+} Nanomodulator for Multilevel Mitochondrial Destruction-Mediated Cancer Therapy. *Adv. Mater.* **2021**, *33*, 2007426–2007437. [CrossRef]

51. Cheng, M.X.; Huang, Y.X.; Zhou, H.-J.; Liu, Z.; Li, J.-F. Biomedical effect of 125I-AFPasON in HCC evaluated with Raman spectra. *Soc. Nucl. Med.* **2010**, *51* (Suppl. 2), 1004.

52. Liko, F.; Hindré, F.; Fernandez-Megia, E. Dendrimers as Innovative Radiopharmaceuticals in Cancer Radionanotherapy. *Biomacromolecules* **2016**, *17*, 3103–3114. [CrossRef]

53. Kobayashi, H.; Kawamoto, S.; Saga, T.; Sato, N.; Ishimori, T.; Konishi, J.; Ono, K.; Togashi, K.; Brechbiel, M.W. Synthesis and pharmacokinetics of a novel tumor-targeting and internalizing therapeutic agent, Avidin-dendrimer-1B4M (X), to deliver radiometals emitting Auger electrons into the cell. *Bioconjug. Chem.* **2001**, *12*, 587–593. [CrossRef] [PubMed]

54. Mamede, M.; Saga, T.; Kobayashi, H.; Ishimori, T.; Higashi, T.; Sato, N.; Brechbiel, M.W.; Konishi, J. Radiolabeling of avidin with very high specific activity for internal radiation therapy of intraperitoneally disseminated tumors. *Clin. Cancer Res.* **2003**, *9*, 3756–3762. [PubMed]

55. Biricová, V.; Láznicková, A.; Lázníček, M.; Polášek, M.; Hermann, P. Radiolabeling of PAMAM dendrimers conjugated to a pyridine-N-oxide DOTA analog with 111In: Optimization of reaction conditions and biodistribution. *J. Pharm. Biomed. Anal.* **2011**, *56*, 505–512. [CrossRef] [PubMed]

56. Torchilin, V.P. Multifunctional nanocarriers. *Adv. Drug Deliv. Rev.* **2006**, *58*, 1532–1555. [CrossRef]

57. Proffitt, R.T.; Williams, L.E.; Presant, C.A.; Tin, G.W.; Uliana, J.A.; Gamble, R.C. Tumor-imaging potential of liposomes loaded with In-111-NTA: Biodistribution in mice. *J. Nucl. Med.* **1983**, *24*, 45–51.

58. Presant, C.A.; Proffitt, R.T.; Turner, A.F.; Williams, L.E.; Winsor, D.; Werner, J.L.; Kennedy, P.; Wiseman, C.; Gala, K.; McKenna, R.J.; et al. Successful imaging of human cancer with indium-111-labeled phospholipid vesicles. *Cancer* **1988**, *62*, 905–911. [CrossRef]

59. Fondell, A.; Edwards, K.; Unga, J.; Kullberg, E.; Park, J.W.; Gedda, L. In vitro evaluation and biodistribution of HER2-targeted liposomes loaded with an (125)I-labelled DNA-intercalator. *J. Drug Target.* **2011**, *19*, 846–855. [CrossRef]

60. Ickenstein, L.M.; Edwards, K.; Sjöberg, S.; Carlsson, J.; Gedda, L. A novel 125I-labeled daunorubicin derivative for radionuclide-based cancer therapy. *Nucl. Med. Biol.* **2006**, *33*, 773–783. [CrossRef]

61. Emfietzoglou, D.; Kostarelos, K.; Papakostas, A.; Yang, W.H.; Ballangrud, A.; Song, H. Liposome-mediated radiotherapeutics within avascular tumor spheroids: Comparative dosimetry study for various radionuclides, liposome systems, and a targeting antibody. *J. Nucl. Med.* **2005**, *46*, 89–97.

62. Owen, J.; Thomas, E.; Menon, J.; Gray, M.; Skaripa-Koukelli, I.; Gill, M.R.; Wallington, S.; Miller, R.L.; Vallis, K.A.; Carlisle, R. Indium-111 labelling of liposomal HEGF for radionuclide delivery via ultrasound-induced cavitation. *J. Control. Release* **2020**, *319*, 222–233. [CrossRef] [PubMed]

63. Hainfeld, J.F.; Slatkin, D.N.; Smilowitz, H.M. The use of gold nanoparticles to enhance radiotherapy in mice. *Phys. Med. Biol.* **2004**, *49*, N309–N315. [CrossRef]

64. Kim, S.R.; Kim, E.H. Feasibility study on the use of gold nanoparticles in fractionated kilovoltage X-ray treatment of melanoma. *Int. J. Radiat. Biol.* **2018**, *94*, 8–16. [CrossRef]

65. Teraoka, S.; Kakei, Y.; Akashi, M.; Iwata, E.; Hasegawa, T.; Miyawaki, D. Gold nanoparticles enhance X-ray irradiation-induced apoptosis in head and neck squamous cell carcinoma in vitro. *Biomed. Rep.* **2018**, *9*, 415–420. [CrossRef] [PubMed]

66. Mahan, M.M.; Doiron, A.L. Gold nanoparticles as X-ray, CT, and multimodal imaging contrast agents: Formulation, targeting, and methodology. *J. Nanomater.* **2018**, *2018*, 1–16. [CrossRef]

67. Chanda, N.; Kan, P.; Watkinson, L.D.; Shukla, R.; Zambre, A.; Carmack, T.L.; Engelbrecht, H.; Lever, J.R.; Katti, K.; Fent, G.M.; et al. Radioactive gold nanoparticles in cancer therapy: Therapeutic efficacy studies of GA-198AuNP nanoconstruct in prostate tumor-bearing mice. *Nanomedicine* **2010**, *6*, 201–209. [CrossRef]

68. Chattopadhyay, N.; Cai, Z.; Pignol, J.-P.; Keller, B.; Lechtman, E.; Bendayan, R.; Reilly, R.M. Design and characterization of HER-2-targeted gold nanoparticles for enhanced X-radiation treatment of locally advanced breast cancer. *Mol. Pharm.* **2010**, *7*, 2194–2206. [CrossRef]

69. Chattopadhyay, N.; Fonge, H.; Cai, Z.; Scollard, D.; Lechtman, E.; Done, S.J.; Pignol, J.-P.; Reilly, R.M. Role of Antibody-Mediated Tumor Targeting and Route of Administration in Nanoparticle Tumor Accumulation In Vivo. *Mol. Pharm.* **2012**, *9*, 2168–2179. [CrossRef]

70. Chattopadhyay, N.; Cai, Z.; Kwon, Y.L.; Lechtman, E.; Pignol, J.P.; Reilly, R.M. Molecularly targeted gold nanoparticles enhance the radiation response of breast cancer cells and tumor xenografts to X-radiation. *Breast Cancer Res. Treat.* **2013**, *137*, 81–91. [CrossRef]

71. Cai, Z.; Chattopadhyay, N.; Yang, K.; Kwon, Y.L.; Yook, S.; Pignol, J.-P.; Reilly, R.M. (111)In-labeled trastuzumab-modified gold nanoparticles are cytotoxic in vitro to HER2-positive breast cancer cells and arrest tumor growth in vivo in athymic mice after intratumoral injection. *Nucl. Med. Biol.* **2016**, *43*, 818–826. [CrossRef]

72. Valabrega, G.; Montemurro, F.; Aglietta, M. Trastuzumab: Mechanism of action, resistance and future perspectives in HER2-overexpressing breast cancer. *Ann. Oncol.* **2007**, *18*, 977–984. [CrossRef] [PubMed]

73. Song, L.; Falzone, N.; Vallis, K.A. EGF-coated gold nanoparticles provide an efficient nano-scale delivery system for the molecular radiotherapy of EGFR-positive cancer. *Int. J. Radiat. Biol.* **2016**, *92*, 716–723. [CrossRef]

74. Pyykkö, P. Theoretical chemistry of gold. II. *Inorg. Chim. Acta* **2005**, *358*, 4113–4130. [CrossRef]

75. Su, W.; Wang, H.; Wang, T.; Li, X.; Tang, Z.; Zhao, S.; Zhang, M.; Li, D.; Jiang, X.; Gong, T.; et al. Auger Electrons Constructed Active Sites on Nanocatalysts for Catalytic Internal Radiotherapy. *Adv. Sci.* **2020**, *7*, 1903585–1903593. [CrossRef] [PubMed]

76. Pronschinske, A.; Pedevilla, P.; Murphy, C.; Lewis, E.A.; Lucci, F.R.; Brown, G.; Pappas, G.; Michaelides, A.; Sykes, E.C.H. Enhancement of low-energy electron emission in 2D radioactive films. *Nat. Mater.* **2015**, *14*, 904–907. [CrossRef]

77. Chao, Y.; Liang, C.; Yang, Y.; Wang, G.; Maiti, D.; Tian, L.; Wang, F.; Pan, W.; Wu, S.; Yang, K.; et al. Highly Effective Radioisotope Cancer Therapy with a Non-Therapeutic Isotope Delivered and Sensitized by Nanoscale Coordination Polymers. *ACS Nano* **2018**, *12*, 7519–7528. [CrossRef]

PUBLICATION NO. 2

Nasrin Abbasi Gharibkandi, Kamil Wawrowicz, Agnieszka Majkowska-Pilip, Kinga Żelechowska-Matysiak, Mateusz Wierzbicki, Aleksander Bilewicz

RESEARCH ARTICLE

Au@^{109}Pd core–shell nanoparticle conjugated to trastuzumab for the therapy of HER2+ cancers: studies on the applicability of ^{109}Pd/^{109m}Ag in vivo generator in combined β$^−$ auger electron therapy

Nasrin Abbasi Gharibkandi[1], Kamil Wawrowicz[1,2], Agnieszka Majkowska-Pilip[1,4], Kinga Żelechowska-Matysiak[1], Mateusz Wierzbicki[3] and Aleksander Bilewicz[1*]

*Correspondence:
a.bilewicz@ichtj.waw.pl

[1] Centre of Radiochemistry
and Nuclear Chemistry,
Institute of Nuclear Chemistry
and Technology, Dorodna 16 St.,
03-195 Warsaw, Poland
[2] Center for Theranostics,
Jagiellonian University, Kopernika
40 St., 31-501 Cracow, Poland
[3] Institute of Biology,
Warsaw University of Life
Sciences, Ciszewskiego 8 St.,
02-786 Warsaw, Poland
[4] Department of Nuclear
Medicine, Central Clinical
Hospital of the Ministry
of the Interior
and Administration, Wołoska 137
St., Warsaw 02-507, Poland

Abstract

Background: In radionuclide therapy, to enhance therapeutic efficacy, an intriguing alternative is to ensure the simultaneous implementation of low- and high-LET radiation emitted from a one radionuclide. In the present study, we introduce the concept of utilizing ^{109}Pd ($T_{1/2}$ = 13.7 h) in the form of a ^{109}Pd/^{109m}Ag in vivo generator. In this system, ^{109}Pd emits beta particles of medium energy, while ^{109m}Ag releases a cascade of conversion and Auger electrons. ^{109}Pd was utilized in the form of 15 nm gold nanoparticles, which were coated with a monolayer of ^{109}Pd. In this system, the ^{109}Pd atoms are on the surface of the nanoparticle, while the ^{109m}Ag atoms generated in the decay reaction possess the capability for unhindered emission of Auger electrons.

Results: ^{109}Pd, obtained through neutron irradiation of natural palladium, was deposited onto 15-nm gold nanoparticles, exceeding a efficiency rate of 95%. In contrast to previously published data on in vivo generators based on chelators, where the daughter radionuclide diffuses away from the molecules, daughter radionuclide ^{109m}Ag remains on the surface of gold nanoparticles after the decay of ^{109}Pd. To obtain a radiobioconjugate with an affinity for HER2 receptors, polyethylene glycol chains and the monoclonal antibody trastuzumab were attached to the Au@Pd nanoparticles. The synthesized bioconjugate contained an average of 9.5 trastuzumab molecules per one nanoparticle. In vitro cell studies indicated specific binding of the Au@^{109}Pd-PEG-trastuzumab radiobioconjugate to the HER2 receptor on SKOV-3 cells, resulting in 90% internalization. Confocal images illustrated the accumulation of Au@^{109}Pd-PEG-trastuzumab in the perinuclear area surrounding the cell nucleus. Despite the lack of nuclear localization, which is necessary to achieve an effective cytotoxic effect of Auger electrons, a substantial cytotoxic effect, significantly greater than that of pure β$^−$ and pure Auger electron emitters was observed. We hypothesize that in the studied system, the cytotoxic effect of the Auger electrons could have also occurred through the damage to the cell's nuclear membrane by Auger electrons emitted from nanoparticles accumulated in the perinuclear area.

Conclusion: The obtained results show that trastuzumab-functionalized [109]Pd-labeled nanoparticles can be suitable for the application in combined β⁻—Auger electron targeted radionuclide therapy. Due to both components decay (β⁻ and conversion/Auger electrons), the [109]Pd/[109m]Ag in vivo generator presents unique potential in this field. Despite the lack of nuclear localization, which is highly required for efficient Auger electron therapy, an adequate cytotoxic effect was attained.

Keywords: [109]Pd/[109m]Ag in vivo generator, Radioimmunotherapy, Auger electron therapy, Nanotechnology

Background

Currently used therapeutic radiopharmaceuticals implemented into the clinical practice usually consist of β⁻ or α emitters (Stokke et al. 2022). Both types of these radionuclides exhibit dissimilar properties, predisposing them to realize the treatment of different-sized lesions. Relative long tissue penetration of β⁻ particles, reaching 0.5–12 mm with LET 0.2 keV/μm, makes them favorable for large tumors treatment (Sgouros). Conversely, high-LET (50–230 keV/μm) α particles with significantly shorter tissue range (40–100 μm) are much more effective against smaller cancer sites. A wide range of β⁻ emitters applications stem primarily from their high availability. On the other hand, α emitters show great potency for individual or combined treatments, but the limited accessibility of these radionuclides hampers their application in clinical practice. Thus, there is a constant need to look for innovative therapeutic strategies that are able to deal with larger and smaller tumors simultaneously by combining different types of radiation.

In order to enhance therapeutic efficacy, an interesting alternative is to ensure simultaneous implementation of low- and high-LET radiation. The principle of this strategy is primary damage of massive tumors *via* β⁻ radiation with subsequent treatment enhancement due to the tumor subpopulations (such as stem cell-like cells), metastatic sites, or single tumors targeting with Auger electrons or α emitters (Stokke et al. 2022; Haberkorn et al. 2017). The mentioned approach is frequently used in the tandem treatment of metastatic prostate cancer, where ^{177}Lu-labeled PSMA-617 is followed by [225]Ac-PSMA-617 therapy (Khreish et al. 2020). Recently published breakthrough findings from Mueller et al. revealed that the application of [161]Tb ($T_{1/2} = 6.95$ d) can induce a considerably greater therapeutic effect than observed in comparable studies with [177]Lu (6.64 d). The uniqueness of [161]Tb is based on the simultaneous emission of β⁻ ($\beta_{max} \sim 550$ keV) and Auger electrons (12.1 e⁻ per decay), being prevailing when compared to almost pure β⁻ emitter [177]Lu ($\beta_{max} = 497$ keV) followed by only a negligible number of Auger/conversion electrons (1.11 e⁻ per decay) (Müller et al. 2019). This phenomenon was also confirmed by dosimetric calculations, which clearly proved the superiority of [161]Tb over ^{177}Lu in the therapeutic management of minor neoplastic lesions (< 200 μm) (Uusijärvi et al. 2006).

In the present study, we introduce the idea for the application [109]Pd (13.7 h) in the form of a [109]Pd/[109m]Ag in vivo generator as an alternative approach to the previously described [161]Tb. Our concept is to use β⁻ and Auger electron emitters in the form of in vivo generator, thus it follows most recent trends in radiopharmaceuticals design. This primarily includes innovative deposition pathways of different types of emitted

radiation, especially as one of radionuclides is produced in vivo. Proposed in these studies ^{109}Pd decays via β$^-$ transition (β$_{max}$ = 1.12 MeV, 100% yield) to ^{109m}Ag (39.6 s) (Fig. 1).

Subsequently, already formed metastable intermediate decays to stable ^{109}Ag which is accompanied by the emission of 88-keV photons (3.6%), followed by cascade emission of conversion and Auger electrons. Therefore, ^{109m}Ag combined with ^{109}Pd leads to the formation of an in vivo generator being beneficial against ^{161}Tb with the greater number of Auger/conversion electrons (18 vs. 12.1) and higher β$^-$ particles energy (http://www.lnhb.fr/nuclides/Pd-109_tables.pdf) (Müller et al. 2019, Müller et al. 2022). Furthermore, in contrast to ^{161}Tb, ^{109}Pd can be simply produced by thermal neutron irradiation. Activation of the enriched metallic Pd target (98% in ^{108}Pd) for a duration of 3 days in a neutron flux of 3×10^{13} n/cm^2 s results in a specific activity of 1.85 GBq/mg and nearly 100% radionuclide purity (Das et al. 2008). How easy it is to estimate this yield can be improved with a high-flux reactor, increasing specific activity up to 50 GBq/mg.

The application of radiopharmaceuticals with very high specific activity possessing is necessary for efficient Auger electron therapy. Therefore, we decided to label bioconjugates using nanotechnology. In previous studies involving ^{111}In, it was found that the utilization of nanoparticles as carriers significantly enhanced the efficacy of Auger electron therapy, without compromising specificity (Sung et al. 2016; Ngo Ndjock Mbong et al. 2015; Chattopadhyay et al. 2012). In our studies, we decided to use ^{109}Pd in the form of gold nanoparticles (15 nm) coated with a monolayer of ^{109}Pd (Wicaksono et al. 2020). In this case, the ^{109}Pd atoms will stay on the surface of the nanoparticle and the ^{109m}Ag atoms which formed in the decay reaction will have the capability of unhindered emission of Auger electrons. Our particular attention was aimed to verify whether ^{109m}Ag after ^{109}Pd decay is able to diffuse from the NPs surface which may result in deeper intracellular penetration of its Auger electrons.

We have estimated that it is possible to deposit over 11,000 palladium atoms (assuming an atomic radius of 140 pm) onto a single gold nanoparticle surface. This could lead to a significant (300-fold) increase in specific activity compared to the method of ^{111}In chelation by DOTA, as proposed by Cai et al. (Cai et al. 2016). Therefore, application of ^{109}Pd-coated AuNPs (Au@^{109}Pd) which we introduce in this paper should allow to obtain high specific activity of potential radiopharmaceutical with valuable radiochemical properties for combined β$^-$ and Auger electron therapy. In order to enhance the precise targeting of in vivo generator, we utilized trastuzumab,
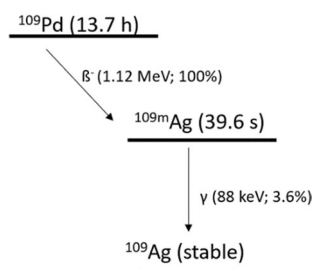

Fig. 1 Decay scheme of ^{109}Pd/^{109m}Ag in vivo generator

a well-known monoclonal antibody specifically binding to HER2 transmembrane receptors overexpressed in tumors with HER2+ status (Tan et al. 2003).

Methods

Reagents

The following chemical reagents were used: gold (III) chloride trihydrate ($HAuCl_4·3H_2O$), trisodium citrate dihydrate ($C_6H_9Na_3O_9$), HS–PEG–COOH (poly(ethylene glycol), 5 kDa) from Sigma-Aldrich (St. Louis, MO, USA), and OPSS–PEG–NHS (alpha-pyridyl-2-disulfid-omega-carboxy succinimidyl ester poly(ethylene glycol), 5 kDa) from Creative PEGworks (Chapel Hill, NC, USA). Trastuzumab was isolated from Herceptin (Roche Pharmaceuticals, Basel, Switzerland). Iodogen (1,3,4,6-tetrachloro-3R,6R-diphenylglycouril) from Thermo Fischer Scientific (Waltham, MA, USA), and PD-10 column (GE Healthcare, Piscataway, NJ, USA). Hydrochloric acid and sodium hydroxide were purchased from POCH (Gliwice, Poland). Fluorescence mounting medium was obtained from Dako (Carpinteria, CA, USA). The following materials were also used in cell studies: McCoy's, DMEM, MEM-EAGLE, and RPMI mediums and fetal calf serum from Biological Industries (Beth Haemek, Israel), phosphate-buffered saline (PBS), dimethyl-sulfoxide (DMSO), and the CellTiter 96® Aqueous One Solution Reagent (MTS compound) from Promega (Mannheim, Germany). SKOV-3 and MDA-MB231 cells were also purchased from the American Type Tissue Culture Collection (ATCC, Rockville, MD, USA) and maintained based on the ATCC protocol. Additionally, all solutions were prepared using double-distilled water (18.2 MΩ·cm, Hydrolab, Straszyn, Poland).

Radionuclides

^{109}Pd was obtained by thermal neutron ($1–2 \times 10^{14}$ n/cm^2 s) irradiation of a natural palladium target (~2 mg, metal powder) in the Maria nuclear reactor (Otwock-Świerk, Poland) for 1 h. After cooling for 12 h, the radioactive palladium was dissolved in 200–400 μL of aqua regia (HNO_3:HCl—1:3) and heated at 130 °C until almost complete evaporation, with slight liquid residues to avoid sintering. Remaining nitrate $[Pd(NO_3)_2·(H_2O)_x]_{(x=0\ or\ 2)}$ removal was achieved through 3×200 μL 0.1 M HCl portions, followed by sample heating (130 °C) until almost complete evaporation. The procedure was then repeated using dd H_2O, finally suspending the target in the mixture of 0.1 M HCl and 0.5 M NaOH (7:1) in order to obtain palladium (II) sodium salt. The activity and radionuclidic purity of the obtained ^{109}Pd were determined by gamma-ray spectrometry. Diluted solutions gained after radiochemical processing of the irradiated target were measured with an HPGe detector connected to a PC-based Multichannel Analyzer (MCA, Canberra). The 88 keV (3.67%) gamma peak was used for the determination of ^{109m}Ag.

^{131}I-radionuclide (no carrier added) was used for the radioiodination of trastuzumab. Na^{131}I (with a specific activity of about > 550 GBq/mg) was obtained from POLATOM Radioisotope Centre Świerk, Poland. ^{125}I-radionuclide (no carrier added, >600 GBq/mg, POLATOM Radioisotope Centre Świerk, Poland) was used for the synthesis of Au@Pd^{125}I-trastuzumab radiobioconjugate, which was applied for comparative cytotoxicity studies.

Synthesis of radioactive Au@^{109}Pd NPs, Au@^{109}Pd -PEG-trastuzumab, and Au@ Pd-^{125}I-PEG-trastuzumab bioconjugates

Radioactive nanoparticles (Au@^{109}Pd NPs) or their bioconjugates (Au@^{109}Pd-PEG-trastuzumab and Au@Pd-^{125}I-PEG-trastuzumab) were synthesized following the same procedure as described for non-radioactive compounds (Additional file 1). After completing the target material processing, ^{109}Pd in the form of Na$_2$^{109}PdCl$_4$ was used as a palladium precursor for metal deposition on the NPs surface. The previously synthesized Au@Pd-^{125}I was utilized to obtain Au@Pd-^{125}I-PEG-trastuzumab. The subsequent steps involving the PEGylation and conjugation with the PEG-trastuzumab bioconjugate were carried out without any modifications, as described in the Additional file 1.

Stability studies of Au@Pd-PEG-trastuzumab bioconjugate colloid

The chemical stability of the bioconjugate in physiological conditions was measured at 37 °C for 16 days after centrifugation and dispersing the Au@Pd-PEG-trastuzumab in PBS buffer and saline (0.9% NaCl). The tendency for aggregation was investigated by measuring changes in hydrodynamic diameter and zeta potential using the Dynamic Light Scattering (DLS) technique.

Radiochemical stability assay was assessed with ɣ spectrometry in order to find ^{109}Pd or ^{109m}Ag detached from the core surface. For this purpose, radiobioconjugates incubated in 0.9% NaCl and human serum (HS) were centrifuged, and both separated fractions (supernatant and nanoparticles) were measured by gamma spectrometry.

Liberation of ^{109m}Ag from Au@^{109}Pd NPs

Nanoparticles were incubated in water and PBS buffer (1 mM) to evaluate the liberation of ^{109m}Ag, as the decay product, on Au@^{109}Pd nanoparticles after β$^-$ decay of ^{109}Pd. The samples were centrifuged for 40 s, and the supernatant fraction was measured to find the liberated ^{109m}Ag from NPs. The supernatant was measured immediately after separation by ɣ spectrometry at 88 keV, with a characteristic peak of ^{109m}Ag.

Internalization studies

Internalization studies were performed on SKOV-3 cells, as no binding was observed for MDA-MB-231 cell line (Additional file 1). Briefly, the day before the experiment, 6×10^5 cells/well were seeded into 6-well plates. After completing this step, cells were washed once with PBS and tested compounds (1 mL) were added. Incubation was performed at 4 °C for 1 h in order to prevent internalization at this step. Next, medium was collected as an unbound fraction and 1 mL of fresh media was added. Plates were then incubated (37 °C, 5% CO$_2$) for the desired time periods, being: 1, 6, and 24 h, respectively. To determine the membrane-bound fraction, cells were washed twice with glycine-HCl buffer (pH ~ 2.8; 0.05 M) and incubated for 5 min at 4 °C. Finally, the internalized fraction was collected after prior lysing the cells with 1 M NaOH. Non-specific binding was assessed with the same procedure as implemented for receptor binding affinity (Additional file 1).

Gharibkandi *et al. EJNMMI Radiopharmacy and Chemistry* (2023) 8:26

Page 6 of 16

Confocal microscopy imaging

SKOV-3 cells (2×10^5 per well) were seeded on sterile glass coverslips (diameter 12 mm, Thermo Fischer Scientific, Waltham, MA, USA) in six-well plates and incubated for 24 h. Next day, the medium was removed, and the cells were treated with trastuzumab (73 μg/mL), Au@Pd-PEG-COOH (1.62×10^{12} NPs/mL), and Au@Pd-PEG-trastuzumab bioconjugate (1.62×10^{12} NPs/mL), and incubated overnight. The applied protocol was similar to that reported previously (Dziawer et al. 2019. The cells were stained with Hoechst 33,258 ($\lambda_{ex/em} = 352/454$ nm) and an anti-human IgG secondary antibody conjugated to FITC ($\lambda_{ex/em} = 490/525$ nm), while bright-field images for nanoparticles were acquired using a transmitted light detector (T-PMT). All analysis was performed using Image J software.

Cytotoxicity studies

Cytotoxicity experiments were conducted on SKOV-3 and MDA-MB-231 cells (3×10^3 cells per well in 96-well plates) using the MTS assay. The preparation procedure was similiar as described for the binding and internalization assays. Tested non-radioactive (9-150 μg Pd/mL) and radioactive compounds in desired concentrations (180 μg Pd/mL for 40 MBq/mL; 90 μg Pd/mL for 20 MBq/mL; 45 μg Pd/mL for 10 MBq/mL) were suspended in fully supplemented growing medium and 100 μL per well was added for 24–72 h incubation. MTS reagent addition was preceded by medium exchange with one-time PBS washing as an intermediate step. The percentage of metabolically active cells was determined by addition of CellTiter96® Aqueous One Solution Reagent and measurement of the absorbance at 490 nm.

Statistical analysis

Statistical analysis, one-way ANOVA, and t-Student tests were performed with GraphPad Prism v.8 Software (GraphPad Software, San Diego, CA, USA). The results are presented as mean ± SD. p values are presented as: (*) $p \leq 0.05$, (**) $p \leq 0.01$, (***) $p \leq 0.001$, and (****) $p \leq 0.0001$.

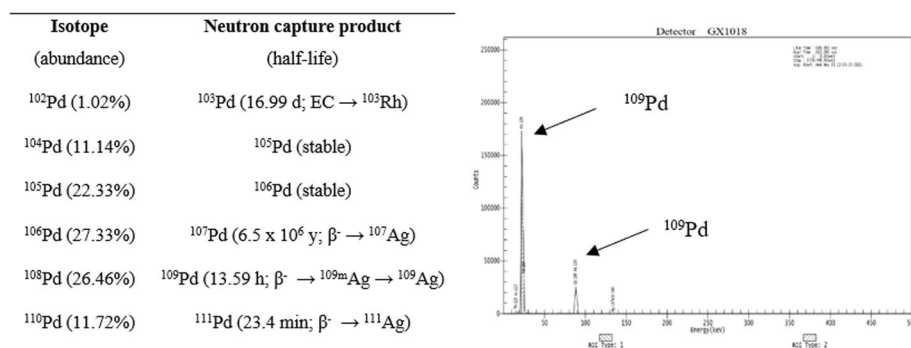| Isotope (abundance)	Neutron capture product (half-life)
^{102}Pd (1.02%)	^{103}Pd (16.99 d; EC $\rightarrow$ ^{103}Rh)
^{104}Pd (11.14%)	^{105}Pd (stable)
^{105}Pd (22.33%)	^{106}Pd (stable)
^{106}Pd (27.33%)	^{107}Pd (6.5 x 10^6 y; β⁻ $\rightarrow$ ^{107}Ag)
^{108}Pd (26.46%)	^{109}Pd (13.59 h; β⁻ $\rightarrow$ ^{109m}Ag $\rightarrow$ ^{109}Ag)
^{110}Pd (11.72%)	^{111}Pd (23.4 min; β⁻ $\rightarrow$ ^{111}Ag)

Fig. 2 Expected radionuclides produced by thermal neutron irradiation and gamma spectrum of a 2 mg sample of natural Pd irradiated for 1 h in a neutron flux of $1-2 \times 10^{14}$ n/cm^2 s

Results and discussion

Production of ^{109}Pd radionuclide

One hour irradiation of 1.92 mg of natural Pd metallic target resulted in 124 MBq of total ^{109}Pd activity. As we described in Fig. 2 three other Pd-radionuclides can be theoretically co-produced during the irradiation of a natural metal target. ^{103}Pd production yield due to the low (~ 1%) abundance of ^{102}Pd is negligible, while long-lived ^{107}Pd is not produced due to a very low cross-Sect. (0.36 b). The co-produced ^{111m}Pd (5.5 h; E_γ ~70.44 keV/7.9%) and its daughter radionuclide ^{111}Ag (7.45 d; E_γ ~342.13 keV/6.7%) activity was insignificant due to the low cross-Sect. (0.10 ± 0.03 b) for the ^{110}Pd(n,γ)^{111}Pd reaction. This was confirmed *via* gamma spectrometry as no characteristic γ-rays line were found (Fig. 2). Target material processing was completed in approximately 40 min and resulted in only 5% of the initial activity loss.

Synthesis of Au@^{109}Pd NPs

Palladium deposition on 15-nm gold nanoparticles (Fig. 3a) was performed with a high yield of over 95%. Gradual and controlled deposition of reduced palladium, followed by rapid diffusion of Pd-metal through the AuNP surface, allowed to obtain a homogenous and thin layer of radionuclide on the nanoparticle surface. High-resolution TEM images acquired in order to visualize Pd deposition confirmed its uniform distribution without any locally increased palladium clusters (Fig. 3b, c). Due to the very short tissue range of Auger and conversion electrons, covering AuNPs with a thin Pd layer was essential to ensure their effective biological activity against cancer cells. According to our calculations, it is anticipated that the resultant AuNPs will be coated with an average of 7 layers of Pd atoms. The thickness of each layer does not exceed 2 nm, and it is presumed that it should not be a barrier to the majority of the emitted Auger electrons. Additionally, with greater activities, it will be obviously feasible to diminish the thickness to a monolayer.

Synthesis of Au@Pd-PEG-COOH and Au@Pd-PEG-trastuzumab bioconjugate

To obtain a radio-bioconjugate having affinity to HER2 receptors, the polyethylene glycol (PEG) chains and the monoclonal antibody trastuzumab have been attached to the Au@Pd nanoparticles. The synthesis was performed as reported previously for the synthesis of Au@DOTA^{177}Lu-PEG-trastuzumab bioconjugate (Cai et al. 2016). PEG (ortho pyridyldisulfide-PEG-succinimidyl carboxymethyl ester; OPSS-PEG-NHS), comprising a
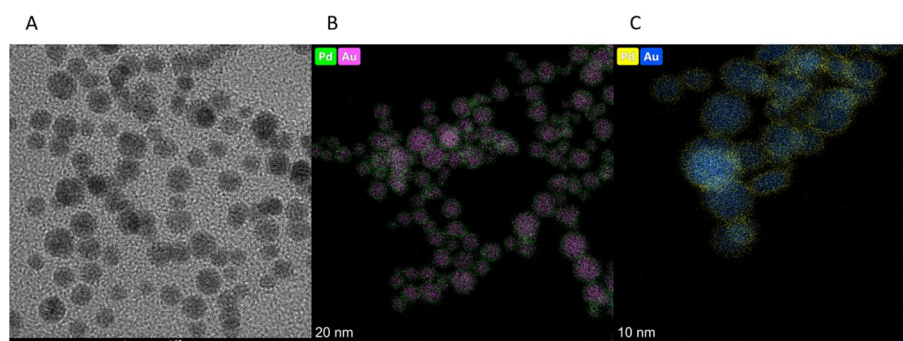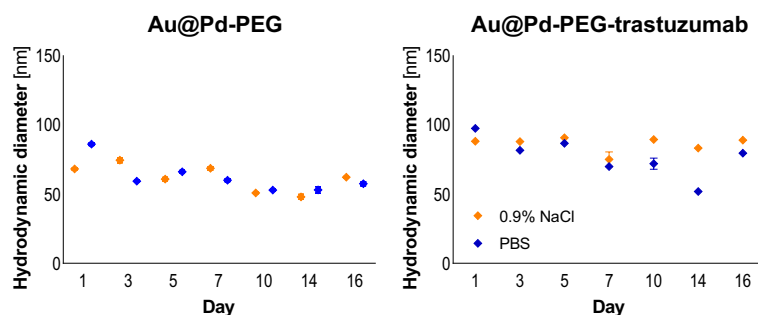

Fig. 3 TEM image of AuNP (**A**) and HR-TEM image of Au@PdNP (**B**, **C**)

Table 1 Hydrodynamic size and zeta potential of the synthesized bioconjugate

	Au@PdNPs	Au@Pd-PEG-trastuzumab
Hydrodynamic diameter (nm)	33.65 ± 0.14	90.88 ± 0.66
Zeta potential (mV)	-36.9 ± 2.5	-25.1 ± 1.6

Fig. 4 Changes in the hydrodynamic diameter of the Au@Pd-PEG (left) and Au@Pd-PEG-trastuzumab conjugates incubated in 0.9% NaCl (yellow line) and 10 mM PBS buffer (blue line) at 37 °C

disulfide bridge, was initially linked with the amine group of lysine in trastuzumab. After that, the conjugate was attached to the Au@Pd NPs, leading to the disruption of the disulfide bridge and the formation of robust gold-sulfur bonds. Finally, to increase the dispersity of the bioconjugate, PEGylation with HS-PEG-COOH (5 kDa) was performed.

In order to determine the mean number of attached trastuzumab molecules to a single AuNP, ^{131}I-labeled trastuzumab molecules were conjugated to Au@Pd NPs (Additional file 1). Using this method, we calculated that average 9.5 trastuzumab molecules were conjugated to a single nanoparticle. This calculation was performed assuming a spherical shape for the nanoparticle with an average diameter of 15 nm, as determined by TEM, with a gold density of 19.28 g/cm³.

Chemical and radiochemical stability studies

The chemical and radiochemical stability of synthesized radiobioconjugates was essential for considering this compound as a potential radiopharmaceutical. Nanoparticle-based compounds stability studies usually concern on the evaluation of their tendency (or not) to agglomerate in biological fluids. The hydrodynamic diameter and zeta potential of the obtained bioconjugate were measured using DLS. The results are shown in Table 1. The rise in the hydrodynamic diameter following the introduction of PEG and trastuzumab proves successful biomolecule conjugation, as in trastuzumab-modified AuNPs (Gawęda et al. 2020; Wawrowicz et al. 2021). The difference within zeta potential values of citrate-coated AuNPs and AuNP-HS-PEG-trastuzumab validates the surface modification as well. The zeta potential of AuNP-PEG-trastuzumab was -25.1 ± 1.6 mV, providing valuable insights into the stability of AuNP-S-PEG-trastuzumab dispersion.

As presented in Fig. 4, colloidal stability over 16 days was studied for Au@Pd-PEG and Au@Pd-PEG-trastuzumab in PBS and saline solutions. Any meaningful differences were observed between the two tested media. Our results revealed that no tendency to

agglomeration or bioconjugate decomposition occurs during evaluation time, thus confirming high stability of the obtained product.

Radiochemical stability studies were performed based on γ-spectrometry, as two types of radionuclides could be potentially identified in measured samples. Any presence of ^{109}Pd or its decay product (^{109m}Ag) was not observed in PBS, saline, and HS solutions for at least 5 h.

Liberation of ^{109m}Ag

The possibility of a daughter radionuclide release from the carrier after nuclear decay is essential in terms of using in vivo generators in nuclear medicine. Enhanced radiation-achievable distance associated with increased tumor cell penetration may significantly improve overall therapeutic effectiveness. In our studies, no liberated ^{109m}Ag was detected in water or a 1 mM PBS buffer in all analyzed samples (1 and 24 h in at least three replicates). The results show that the radionuclide ^{109m}Ag formed as a result of the decay of ^{109}Pd remains on the surface of AuNPs.

Internalization—radiometric assay and confocal imaging

Once we confirmed, that synthesized Au@Pd-PEG-trastuzumab radiobioconjugate similarly as Au@Pt-PEG-trastuzumab (Wawrowicz et al. 2021) and Au@-PEG-trastuzumab (Żelechowska-Matysiak et al. 2023) show its ability to recognize and specifically bind to transmembrane HER2 receptors (Additional file 1), we investigated whether are they able to penetrate the cell membrane and successfully localize inside target cells. Because of the limited range of Auger electrons, radiobioconjugates internalization is essential to obtain optimal therapeutic effects. To achieve trustworthy data, we implemented two independent techniques to specify the internalization: radiometric uptake assay and confocal imaging.

Due to the limited range of Auger electrons, the internalization of radiobioconjugates is essential to attain optimal therapeutic effects. As we observed, complete (>99%) internalization was found to occur after 1 h. This result is in agreement with our previously published papers (Gawęda et al. 2020), where similar radiobioconjugates were investigated against HER2+ breast/ovarian cancer cells. Evaluation of further time points (6 and 24 h) confirmed, that synthesized radiobioconjugates remain inside cancer cell for at least 24 h.

Acquired confocal images (Fig. 5) clearly indicated that only trastuzumab-conjugated NPs are able to locate inside HER2+ breast/ovarian cancer cells. As shown, PEG-ylated NPs (Au@Pd-PEG-COOH) were not detected inside the SKOV-3 cells, thus revealing the fundamental role of trastuzumab as a targeting vector. The dark spots visible on the bright background in Fig. 5, panel C/2, represent Au@Pd particles, whereas the green fluorescence (Fig. 5, panel C/3) signals indicate secondary Ab conjugated to trastuzumab being an integral part of the bioconjugate. Merged signals in Fig. 5, columns 4 and 5, demonstrated the successful penetration of the bioconjugate particles into the SKOV-3 cells and precise localization nearly to the nuclear envelope area. Hence, NPs accumulation in close proximity to the most sensitive cellular organelle allowed us to expect high cytotoxicity induced by radioactive bioconjugates.
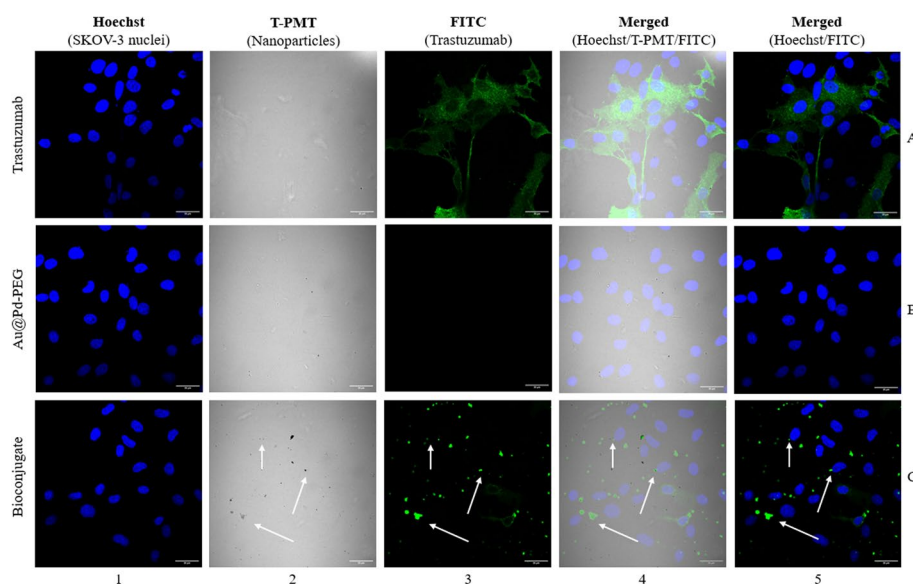
Fig. 5 Internalization of trastuzumab, Au@Pd-PEG-COOH, and Au@Pd-trastuzumab by SKOV-3 cells determined by confocal microscopy. Fluorescence signals indicate: (green)—subcellular trastuzumab distribution; (blue)—nuclei intracellular localization. Au@Pd-containing particles (dark spots) were visualized with a transmitted light detector (T-PMT). Arrows mark the subcellular localization of the Au@Pd-trastuzumab bioconjugate
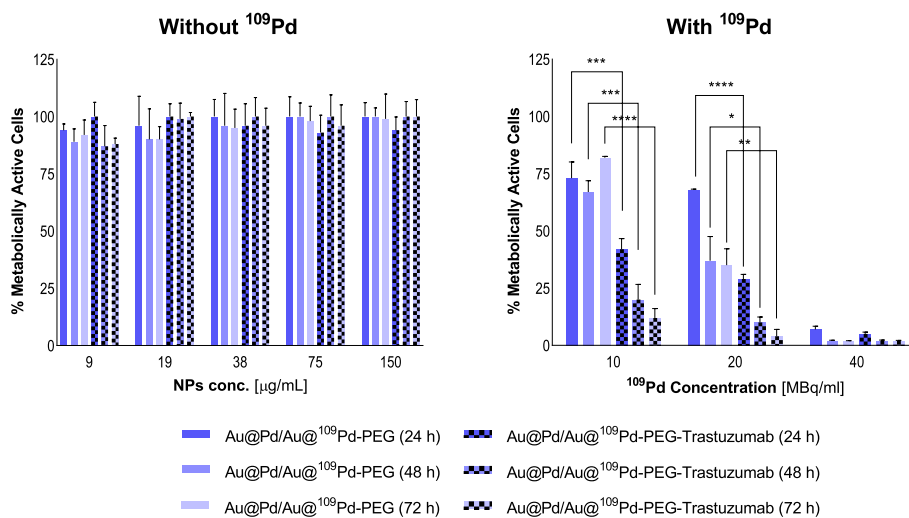

Fig. 6 Metabolic viability of SKOV-3 cells after treatment with different concentrations of Au@Pd-PEG and Au@Pd-PEG-trastuzumab nonradioactive conjugates (left) and radioactive doses of Au@^{109}Pd-PEG and Au@^{109}Pd-trastuzumab conjugates (right) after 24 h, 48 h, and 72 h of treatment.

Cytotoxicity

Initial cytotoxicity studies concerned on non-radioactive compounds evaluation. The aim of these studies was to find out whether Au@Pd-PEG or Au@Pd-PEG-trastuzumab without ^{109}Pd induce mitochondrial dysfunction leading to cell death. As shown in Figs. 6a and 7a, no significant decrease in mitochondrial activity was found with doses up to 150 μg/mL of Pd immobilized in conjugates or bioconjugates. This
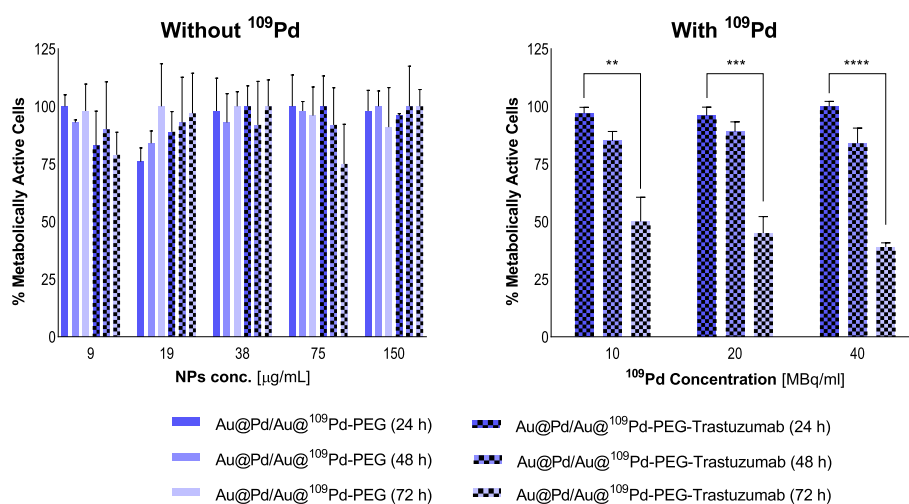
Fig. 7 Metabolic viability of MDA-MB-231 cells after treatment with different concentrations of Au@Pd-PEG and Au@Pd-PEG-trastuzumab nonradioactive conjugates (left) and radioactive doses of Au@^{109}Pd-trastuzumab conjugates (right) after 24 h, 48 h, and 72 h of treatment

result is in agreement with our expectations since cold Pd nanoparticles induce a cytotoxic effect only after specific modifications (Ramalingam et al. 2020).

Metabolic viability of SKOV-3 and MDA-MB-231 (Figs. 6b and 7b) cells after exposure to diverse radioactivity doses of Au@^{109}Pd-trastuzumab and Au@^{109}Pd-PEG conjugates was verified at 24 h, 48 h, and 72 h.

According to the presented results, the use of Au@^{109}Pd-trastuzumab radioconjugate leads to a substantial reduction in the metabolic activity of SKOV-3 cells in a dose-dependent manner. Observed changes were also found to be progressing over time. A double half-life of ^{109}Pd ($\sim$ 26 h) resulted in over 50% toxicity with a slightly ($p \leq 0.05$) stronger effect for 20 MBq/mL when compared to 10 MBq/mL. Prolonged incubation resulted in constantly decreasing the mitochondrial activity, leading after 72 h to almost complete cell death with $12.0 \pm 4.3\%$ and $< 5\%$ of unaffected mitochondrial function for 10 MBq/mL and 20 MBq/mL, respectively. Interestingly, even without the presence of trastuzumab, the Au@^{109}Pd conjugate still exhibited a noticeable decrease in cell viability, observed partially for 20MBq/mL and dominantly for 40 MBq/mL. Nevertheless, the impact was much less severe than in the case of 20 MBq/mL radioboconjugates with the targeting vector. This is related to the crossfire effect of long-range β^- radiation, where Auger and conversion electrons exclusively affect only target cells.

Triple-negative cells (MDA-MB-231) used as reference for comparable analysis, similarly to SKOV-3 cells were usually not affected with non-radioactive conjugates. Some deviations from the overall outcome were observed, but taking into account high SD values, this cannot be considered an induced effect. For the radioactive radiobioconjugate, despite the lack of targeting and internalization, a cytotoxic effect is still apparent, although notably less pronounced compared to the SKOV-3 cell case. The observed cytotoxicity is solely attributed to the impact of long-range β^- radiation, where targeting and internalization are not necessary.

Discussion

The well-established use of ^{125}I and ^{111}In, Auger-emitting radioisotopes, has also stimulated the search for other Auger emitters that may be more practical to use from the perspective of availability, physical half-life, and cost. In our work, we proposed a [109]Pd/[109m]Ag in-vivo generator that combines β^- emission from the parent [109]Pd radionuclide with a high emission of Auger electrons from the daughter [109m]Ag. In our concept, the [109]Pd/[109m]Ag in-vivo generator was applied in the form of Au@[109]Pd core–shell nanoparticles. We found that complete retention of [109m]Ag was accomplished following the nuclear decay of the immobilized [109]Pd on the AuNPs surface. This contrasts with previously published data for chelator-based in-vivo generators. Studies conducted on in vivo generators, such as [103]Pd/[103m]Rh (Jensen et al. 2020), [166]Dy/[166]Ho (Wang et al. 2022) and [212]Pb/[212]Bi (Mirzadeh et al. 1993), have demonstrated that a significant percentage of daughter radionuclides are liberated when chelators are employed to immobilize parent radionuclides. According to (Wang et al. 2022), the loss of daughter radionuclides was attributed to their de-excitation through the internal conversion, resulting in Auger electron emission, rather than to the recoil energy associated with the emission of ß^- particles and neutrinos. As a result, the de-excited daughter radionuclides become highly charged what leads to electrons uptake from the surrounding chelator donor atoms. Moreover, due to the electron transfer to highly charged atoms, donor atoms of chelators acquire a positive charge. The metal-ligand bonds are then broken as a result of the repulsive force between the positively charged atoms, and the daughter radionuclides are released as free cations.

The situation changes dramatically when the parent radionuclide is immobilized on a metallic surface instead of a chelate complex. The application of a metallic surface such as AuNPs as the carrier of the mother radionuclides facilitates the availability of several delocalized electrons. After nuclear decay, highly positively charged daughter radionuclide takes electrons from neighboring Au atoms on the surface. As a result, the positive charge is rapidly transferred to the entire nanoparticle, causing only a marginal change in the surface charge. Therefore, the release of [109m]Ag from the nanoparticles surface is not achievable. The same effect was also observed] with the [166]Dy/[166]Ho in vivo generator deposited on the AuNPs surface (Wang et al. 2022).

This phenomenon is advantageous from the perspective of potential applications. As [109m]Ag remains in the NPs structure, there is negligible risk of [109]Ag unspecific accumulation in different tissues after treatment. Thus, it significantly limits the risks of post treatment side-effects related to increased and difficult to detect silver accumulation throughout the patient organism.

In performed in vitro studies, we observe the crucial role of the trastuzumab vector, which facilitates the cell internalization and cytoplasm localization of Au@[109]Pd-trastuzumab conjugate into the SKOV-3 cells. As presented in confocal images (Fig. 5), the conjugate accumulates in the perinuclear area surrounding the cell nucleus. In the case of β^- radiation, due to the fact that the range of β^- radiation emitted by [109]Pd is a few millimeters, cell internalization is not necessary, and the β^- particles are capable of targeting DNA without cell internalization of [109]Pd. This explains why we observed also cytotoxicity for Au@[109]Pd-PEG nanoparticles. Considering the low-LET characteristics of β^- radiation, a significantly lower DNA DSB generation yield is expected,

leading to a lower overall toxicity ratio. However, the interaction of Auger electrons with the essential cell components is required to induce the cytotoxic effect correlated with the Auger electron emission from ^{109m}Ag as the daughter radionuclide. Cellular DNA is typically considered to be the most sensitive target of Auger electron emitters. The double-stranded DNA helix possesses a diameter of 2 nm. During a typical Auger emission, the greatest release of energy happens in 1–2 nm spheres around the decay site (Buchegger et al. 2006). Similar to the α-radiation path through the cell nucleus, the loss of genetic information occurs in these double-strand breaks, which is attributed to the nucleotide breakdown on both strands (Lobachevsky, et al. 2000). For ^{125}I decays associated with DNA, it means "One decay = one double-strand break" (Elmroth et al. 2005). Furthermore, as has been proposed in some publications, since the cell membrane plays a key role in cell viability, the effects of Auger electrons generated by membrane-bound radiolabeled mAbs should not be overlooked (Pouget et al. 2008; Paillas et al. 2016, Muller et al. 2022). Considering the significant accumulation of nanoparticles on the nuclear membrane within the range of Auger and conversion electron interaction as depicted in confocal microscopy images (Fig. 5), it has been concluded that nuclear envelope damage caused by Auger electrons may be one of numerous reasons of cell death. In order to verify the therapy enhancement for simultaneous β$^-$ particle emission and conversion/Auger electrons, we decided to perform a comparable analysis with ^{125}I (Auger) and ^{198}Au (β$^-$) radionuclides. Both of them were directly implemented into the nanoparticle structure by chemisorption of iodine (^{125}I-labeled Au@Pd-trastuzumab (Additional file 1) or by using radioactive ^{198}AuNPs-trastuzumab radiobioconjugates, as we previously described (Żelechowska-Matysiak et al. 2023).

The comparison provided in Table 2 is undoubtedly an approximation. It does not take into account several parameters, including radionuclide half-life, radiation intensity and energy. In addition, the emitted γ radiation was not taken into account, considering its insignificance in relation to the corpuscular radiation. We intended to compare the obtained data with currently existing alternative pathways. The acquired results, however, clearly reveal that the cytotoxicity of the ^{109}Pd/^{109m}Ag in vivo generator-based conjugate (β$^-$ and Auger electron emitter) is significantly higher than that of the conjugates radiolabeled with the same activities of β$^-$ or Auger electron emitters. This effect will be much greater if the considerably shorter half-life of ^{109}Pd is taken into account.

Table 2 Comparison of cytotoxicity of radiobioconjugates labeled with Auger electron emitter (^{125}I), β-emitter (^{198}Au) and Auger and β-electron emitter (^{109}Pd/^{109m}Ag in vivo generator)

Radiobioconjugate	T$_{1/2}$ (days)	Decay mode	Decay numer in 48 h	Radiation emitted	% of metabolic activity in MTS test
Au@Pd^{125}I-trastuzumab	59.49	EC	3.42×10^{12}	Auger, low energy gamma	60
^{198}Au-trastuzumab	2.69	β$^-$	2.70×10^{12}	β$^-_{avg}$ (315 keV)	53
Au@^{109}Pd-trastuzumab	0.57	β$^-$, IT	1.30×10^{12}	β$^-_{avg}$ (436 keV) + Auger/conversion	10

Activity concentration: 20 MBq/ml, incubation time: 48 h

Conclusion

The ^{109}Pd/^{109m}Ag in vivo generator in the form of trastuzumab conjugated core−shell Au@^{109}Pd nanoparticles used in this paper generated significantly better in vitro cytotoxicity results than Au@PdNPs labeled with either ^{125}I (Auger emitter) or ^{198}Au (β$^−$ emitter). Due to both components decay (β$^−$ and conversion/Auger electrons), the ^{109}Pd/^{109m}Ag in vivo generator presents unique potential in this field. Despite the lack of nuclear localization, which is highly required for efficient Auger electron therapy (Costantini et al. 2010), an adequate cytotoxic effect was attained.

We assume that the toxic effect could have been induced apart of β$^−$ particles by Auger/conversion electrons emitted from the nanoparticles in the perinuclear area efficiently damaging the nuclear envelope. Therefore, radiobioconjugates labeled with the ^{109}Pd/^{109m}Ag radionuclide generator might show the advantages of both β$^−$ emitters (a few millimeters range of radiation, crossfire effect) and Auger electrons (large LET, double-stranded DNA breaks). Therefore, it can be expected, that ^{109}Pd/^{109m}Ag-labeled vectors may have a more substantial antitumor performance, when used either for the treatment of small tumor clusters or targeting of medium-sized tumors.

Nonetheless, the development of this concept requires clarifying its disadvantages, limitations and challenges that need to be overcome. Due to the quite large size and considerable accumulation of the radiolabeled nanoconstructs in the liver, lungs, and spleen, as well as fast blood clearance, toxic radiation exposure of these organs, and reduced tumor uptake, intravenous administration route of Au@^{109}Pd-trastuzumab is excluded. One possible concept which can be implemented is strictly localized administration i.e., directly into the tumor or post-surgery resection cavity. This strategy can also be investigated for the synthesis of Au@^{109}Pd nanoparticles conjugated with other different biological vectors, which, in turn, would broaden the applicability of this approach for targeting a diverse variety of tumors. Nevertheless, the presented concept and obtained results are highly promising and encouraging for further development of the described treatment strategy.

Supplementary Information

The online version contains supplementary material available at https://doi.org/10.1186/s41181-023-00212-4.

> **Additional file 1.** Supplementary information.

Availability of data and meterials
Data is available upon reasonable request to the corresponding author.

Declarations

Ethics approval and consent to participate
Not applicable.

Consent for publication
Not applicable.

Competing interests
The authors declare that they have no competing interests.

References

Buchegger F, Perillo-Adamer F, Dupertuis YM, Bischof Delaloye A. Auger radiation targeted into DNA: a therapy perspective. Eur J Nucl Med Mol Imaging. 2006;33:1352–63.

Cai Z, Chattopadhyay N, Yang K, Kwon YL, Yook S, Pignol J-P, Reilly RM. ^{111}In-labeled trastuzumab-modified gold nanoparticles are cytotoxic in vitro to HER2-positive breast cancer cells and arrest tumor growth in vivo in athymic mice after intratumoral injection. Nucl Med Biol. 2016;43:818–26.

Chattopadhyay N, Fonge H, Cai Z, Scollard D, Lechtman E, Done SJ, Pignol J-P, Reilly RM. Role of antibody-mediated tumor targeting and route of administration in nanoparticle tumor accumulation in vivo. Mol Pharm. 2012;9:2168–79.

Costantini DL, McLarty K, Lee H, Done SJ, Vallis KA, Reilly RM. Antitumor effects and normal-tissue toxicity of ^{111}In-nuclear localization sequence-trastuzumab in athymic mice bearing HER positive human breast cancer xenografts. J Nucl Med. 2010;51:1084–91.

Das T, Chakraborty S, Sarma HD, Barnejee S. A novel [[109]Pd] palladium labeled porphyrin for possible use in targeted radiotherapy. Radiochim Acta. 2008;96:427–33.

Dziawer Ł, Majkowska-Pilip A, Gaweł D, Godlewska M, Pruszyński M, Jastrzębski J, Wąs B, Bilewicz A. Trastuzumab-modified gold nanoparticles labeled with [211]At as a prospective tool for local treatment of HER2-positive breast cancer. Nanomaterials. 2019;9:632–47.

Elmroth K, Stenerlöw B. DNA-incorporated ^{125}I induces more than one double-strand break per decay in mammalian cells. Radiat Res. 2005;163:369–73.

Gawęda W, Pruszyński M, Cędrowska E, Rodak M, Majkowska-Pilip A, Gaweł D, Bruchertseifer F, Morgenstern A, Bilewicz A. Trastuzumab modified barium ferrite magnetic nanoparticles labeled with radium-223: a new potential radiobioconjugate for alpha radioimmunotherapy. Nanomaterials. 2020;10:2067–88.

Haberkorn U, Giesel F, Morgenstern A, Kratochwil C. The future of radioligand therapy: α, β, or both? J Nucl Med. 2017;58:1017–8.

Jensen AI, Zhuravlev F, Severin G, Magnus CB, Fonslet J, Koester U, Jensen M. A solid support generator of the Auger electron emitter rhodium-103m from [[103]Pd]palladium. Appl Radiat Isot. 2020;156:108985.

Khreish F, Ebert N, Ries M, Maus S, Rosar F, Bohnenberger H, Stemler T, Saar M, Bartholomä M, Ezziddin S. [225]Ac-PSMA-617/^{177}Lu-PSMA-617 tandem therapy of metastatic castration-resistant prostate cancer: pilot experience. Eur J Nucl Med Mol Imaging. 2020;47:721–8.

Lobachevsky PN, Martin RF. Iodine-125 decay in a synthetic oligodeoxynucleotide. I. Fragment size distribution and evaluation of breakage probability. Radiat Res. 2000;153:263–70.

Mirzadeh S, Krishan K, Gansow OA. The chemical fate of [212]Bi-DOTA formed by β decay of [212]Pb(DOTA)[2]. Radiochim Acta. 1993;60:1–10.

Müller C, Umbricht CA, Gracheva N, Tschan VJ, Pellegrini G, Bernhardt P, Zeevaart JR, Köster U, Schibli R, van der Meulen NP. Terbium-161 for PSMA-targeted radionuclide therapy of prostate cancer. Eur J Nucl Med Mol Imaging. 2019;46:1919–30.

Müller C, Busslinger S, Fluehmann F, Borgna F, Koester U, Zeevaart J, Grundler P, van der Meulen N, Schibli R. Cell membrane localization of terbium-161 using peptide receptor antagonists: Can we profit from Auger electron emission with non-internalizing targeting agents? Nucl Med Biol. 2022;114:26–6.

Ngo Ndjock Mbong G, Lu Y, Chan C, Cai Z, Liu P, Boyle AJ, et al. Trastuzumab labeled to high specific activity with (111)in by site-specific conjugation to a metal-chelating polymer exhibits amplified Auger electron-mediated cytotoxicity on Her2-positive breast cancer cells. Mol Pharm. 2015;12:1951–60.

Paillas S, Ladjohounlou R, Lozza C, Pichard A, Boudousq V, Jarlier M, Deshayes E, Sosabowski J, Chardes T, Navarro-Teulon I, Mairs R, Pouget J. Localized irradiation of cell membrane by Auger electrons is cytotoxic through non-targeted effects involving p38 and JNK signaling pathways. EJNMMI. 2016;43:163–4.

Pouget J-P, Santoro L, Raymond L, Chouin N, Bardies M, Bascoul-Mollevi C, Huguet H, Azria D, Kotzki PO, Pelegrin M, Vives E, Pelegrin A. Cell membrane is a more sensitive target than cytoplasm to dense ionization produced by Auger electrons. Radiat Res. 2008;170:192–200.

Ramalingam V, Sakthivel R, Mohan H. In-situ one step synthesis of polymer functionalized palladium nanoparticles: an efficient anticancer agent against breast cancer. Dalton Trans. 2020;49:3510–8.

Sgouros G, Bodei L, McDevitt MR, Nedrow JR. Radiopharmaceutical therapy in cancer: clinical advances and challenges. Nat Rev Drug Discov. 2020;19:589–608.

Stokke C, Kvassheim M, Blakkisrud J. Radionuclides for targeted therapy: physical properties. Molecules. 2022;27:5429–49.

Sung W, Jung S, Ye SJ. Evaluation of the microscopic dose enhancement for nanoparticle-enhanced auger therapy. Phys Med Biol. 2016;6:7522–35.

Tan A, Swain S. Ongoing adjuvant trials with trastuzumab in breast cancer. Semi Oncol. 2003;30:54–64.

Uusijärvi H, Bernhardt P, Rösch F, Maecke HR, Forssell-Aronsson E. Electron- and positron-emitting radiolanthanides for therapy: aspects of dosimetry and production. J Nucl Med. 2006;47:807–14.

Wang R, Ponsard B, Wolterbeek H, Denkova A. Core–shell structured gold nanoparticles as carrier for [166]Dy/[166]Ho in vivo generator. EJNMMI Radiopharm Chem. 2022;7:16–32.

Wawrowicz K, Majkowska-Pilip A, Gaweł D, Chajduk E, Pieńkowski T, Bilewicz A. Au@Pt core-shell nanoparticle bioconjugates for the therapy of Her2+ breast cancer and hepatocellular carcinoma. Model studies on the applicability of [193m]Pt and [195m]Pt radionuclides in Auger electron therapy. Molecules. 2021;26:2051–71.

Wicaksono WP, Kadja GTM, Amalia D, Uyun L, Rini WP, Hidayat A, Fahmi RL, Nasriyanti D, Leun SGV, Ariyanta HA, Ivandini Tribidasari A. A green synthesis of gold–palladium core–shell nanoparticles using orange peel extract through two-step reduction method and its formaldehyde colorimetric sensing performance. Nano-Struct Nano-Objects. 2020;24:100535.

Żelechowska-Matysiak K, Salvanou E-A, Bouziotis P, Bilewicz A, Majkowska-Pilip A. Doxorubicin and trastuzumab modified radioactive gold nanoparticles as potential multimodal agents for targeted therapy of HER2+ breast cancer. Mol Pharm. 2023;20:4676–86.

Publisher's Note

Springer Nature remains neutral with regard to jurisdictional claims in published maps and institutional affiliations.

PUBLICATION NO. 3

Nasrin Abbasi Gharibkandi, Agnieszka Majkowska-Pilip, Rafał Walczak, Mateusz Wierzbicki, Aleksander Bilewicz

Article

Au@^{109}Pd Core–Shell Nanoparticles Conjugated to Panitumumab for the Combined β$^−$—Auger Electron Therapy of Triple-Negative Breast Cancer

Nasrin Abbasi Gharibkandi [1], Agnieszka Majkowska-Pilip [1,2,*], Rafał Walczak [1], Mateusz Wierzbicki [3] and Aleksander Bilewicz [1,*]

[1] Centre of Radiochemistry and Nuclear Chemistry, Institute of Nuclear Chemistry and Technology, Dorodna 16 St., 03-195 Warsaw, Poland; n.abbasi@ichtj.waw.pl (N.A.G.); r.walczak@ichtj.waw.pl (R.W.)

[2] Department of Nuclear Medicine, Central Clinical Hospital of the Ministry of the Interior and Administration, Wołoska 137 St., 02-507 Warsaw, Poland

[3] Institute of Biology, Warsaw University of Life Sciences, Ciszewskiego 8 St., 02-786 Warsaw, Poland; mateusz_wierzbicki@sggw.edu.pl

[*] Correspondence: a.majkowska@ichtj.waw.pl (A.M.-P.); a.bilewicz@ichtj.waw.pl (A.B.)

Abstract: Apart from HER2-positive, triple-negative breast cancer (TNBC) is the second most highly invasive type of breast cancer. Although TNBC does not overexpress HER2 receptors, it has been observed that EGFR protein expression is present in this specific type of tumor, making it an attractive target for immune and radiopharmaceutical treatments. In our current study, we used ^{109}Pd ($T_{1/2}$ = 13.7 h) in the form of a ^{109}Pd/^{109m}Ag in vivo generator as a source of β$^−$ particles and Auger electrons in targeted radionuclide therapy for TNBC. ^{109}Pd, obtained through neutron irradiation of the ^{108}Pd target, was deposited onto 15 nm gold nanoparticles to form Au@^{109}Pd core–shell nanoparticles, which were then conjugated to the panitumumab antibody. Au@^{109}Pd-PEG-panitumumab nanoparticles were bound, internalized, and partially routed to the nucleus in MDA-MB-231 human breast cancer cells overexpressing EGFR receptors. The Au@^{109}Pd-panitumumab radioconjugate significantly reduced the metabolic activity of MDA-MB-231 cells in a dose-dependent manner. In conclusion, we have found that Au@^{109}Pd-PEG-panitumumab nanoparticles show potential as a therapeutic agent for combined β$^−$–Auger electron targeted radionuclide therapy of TNBC. The simultaneous emission of β$^−$, conversion, and Auger electrons from the ^{109}Pd/^{109m}Ag generator, similar to ^{161}Tb conjugates, significantly enhances the therapeutic effect. The partial localization of these nanoparticles into the cell nucleus, provided by the panitumumab vector, ensures effective therapy with Auger electrons. This is particularly important for the treatment of drug-resistant TNBC cells.

Keywords: ^{109}Pd/^{109m}Ag in vivo generator; radioimmunotherapy; triple-negative breast cancer

1. Introduction

Breast cancer is the most prevalent cancer in women, with 2,296,840 new cases and 670,000 fatalities worldwide recorded in 2022 [1]. The molecular classification of breast cancer relies on the overexpression pattern of estrogen, progesterone, and human epidermal growth factor receptor 2 (HER2). Among all types of breast cancer, 15–20% are HER2-positive, characterized by their highly aggressive and metastatic nature. This form of cancer progresses rapidly and frequently leads to distant metastases. However, due to the high concentration of the HER2 antigen on the cell surface, the cancer responds favorably to targeted therapy.

The second type of invasive breast cancer is known as triple-negative breast cancer (TNBC). This aggressive form of breast cancer is characterized by the absence of estrogen, progesterone receptors, and HER2 overexpression [2]. TNBC accounts for around 10–15%

of all breast cancer cases, often showing rapid growth and a higher likelihood of having spread by the time of diagnosis, limited treatment options, and typically poor prognosis. Additionally, it has a greater tendency to recur after treatment compared to other forms of breast cancer. Due to the absence of specific receptors, hormone therapy and HER2-targeted drugs are not effective for women with triple-negative breast cancer. Therefore, cytotoxic chemotherapy is the only form of systemic therapy currently available for patients with TNBC. The FDA has approved anti-metabolites, paclitaxel, and anthracyclines as adjuvant and neoadjuvant chemotherapy regimens for patients with TNBC [3,4]. However, the toxicity of chemotherapy is harmful to patients, and many still do not receive clinical benefit. Therefore, there is a strong interest in identifying new targets for treating patients with TNBC [5].

Although TNBC does not overexpress HER2 receptors, it has been observed that EGFR protein expression is present in this specific type of tumor. EGFR, also known as HER1, is one of the four members of the HER family of receptors, along with HER2, HER3, and HER4. Further evidence supporting the significance of EGFR in TNBC comes from the discovery that high expression of EGFR predicts a poor prognosis in patients with this type of cancer. Like HER2, there are now multiple therapies available that target EGFR. These therapies include monoclonal antibodies such as cetuximab and panitumumab. They work by preventing ligand binding. Both of these antibodies have been approved for treating advanced colorectal cancers. Currently, intensive preclinical and phase I and II clinical trials are being conducted on their application in TNBC therapy.

Panitumumab, a fully humanized monoclonal antibody, exhibits a high affinity ($K_d = 5 \times 10^{-11}$ M) for the EGFR receptor. By blocking the binding of EGF ligands and TGF-α to EGFR, panitumumab inhibits tumor growth and triggers tumor regression [3]. Therapeutic properties of both panitumumab itself and its conjugates with radionuclides, in which it acts as a targeting vector to EGFR receptors, are under study.

In a series of studies, Reilly's group at the University of Toronto has been investigating the use of panitumumab labeled with ^{111}In, an Auger electron emitter, for targeted radionuclide therapy (TRT) of TNBC. The ^{111}In radionuclide (with a half-life of 2.8 days) decays by electron capture, emitting 7.4 Auger electrons and 0.2 low-energy internal conversion (IC) electrons per decay which can be utilized for TRT. The Auger electron releases all of its energy over very short distances, leading to high linear energy transfer (LET: 1–23 keV/μm). This is effective in causing lethal DNA double-strand breaks in cancer cells, especially when the electrons are emitted close to DNA strands [6]. The AE can also be targeted at the cell membrane when radiolabeled antagonists of this receptor are used. The short range of AE and high LET make these electrons attractive for treatment of single tumor cells and micrometastases, preventing TNBC relapse. In one study [7], the use of panitumumab conjugated with the DOTA chelator and labeled with ^{111}In resulted in high binding affinity to EGFR ($K_D = 0.6 \pm 0.2 \times 10^{-9}$ M). This conjugate was found to be bound, internalized, and partially imported into the nucleus of human TNBC MDA-MB-231 and MDA-MB-468 cells. The emission of AE by ^{111}In inside the nucleus of TNBC cells caused a significant increase in DNA DSBs, leading to cell cycle arrest in the G2/M phase and promoting apoptosis, which in turn reduced clonogenic survival in vitro. Additionally, in a mouse model with induced MDA-MB-231 cell tumors in the mammary fat pad, it significantly slowed tumor growth and prolonged survival compared with control mice. Subsequent studies [8] continued these investigations in the context of using ^{111}In-DOTA-panitumumab in adjuvant therapy to improve survival in the relapse and metastatic progression treatment model.

Due to the limited number of chelator molecules that can be attached to a protein like panitumumab, the specific activity that can be achieved is limited. As a result, as few as one in 50 antibody molecules may be radiolabeled [9]. One strategy to overcome this delivery barrier may be to increase the number of chelators attached to the antibody molecules carrying a radionuclide, thereby increasing the amount of radioactivity targeted to tumor cells per receptor. To achieve this, panitumumab was attached to a chelating block polymer [10] or gold nanoparticles [11] carrying a large number of chelators.

In several of our previous publications, we have enhanced the specific activity of similar antibody (trastuzumab) conjugates by utilizing radioactive metallic gold, platinum, or palladium nanoparticles, which are synthesized from radioactive ^{198}Au [12,13], $^{193/195m}$Pt [14], or $^{109/103}$Pd [15] salts. In this way, we significantly increased the specific activity of trastuzumab radiobioconjugates, up to 40,000 radioactive ^{198}Au atoms, when using 30 nm Au nanoparticles [13].

In our last published work in this field [15], we presented the outcomes of our studies exploring the application of a radiobioconjugate consisting of gold nanoparticles coated with a layer of ^{109}Pd (Au@^{109}Pd). This radiobioconjugate was conjugated with the monoclonal antibody trastuzumab and was applied in the targeted radionuclide therapy of HER2+ cancer.

Palladium-109 exhibits significant potential for application in radionuclide therapy. It undergoes β$^-$ decay (β$_{max}$ = 1.12 MeV, 100% yield) to form ^{109m}Ag, which has a half-life of 39.6 s. The resulting metastable ^{109m}Ag decays to the stable isotope ^{109}Ag, emitting photons at 88 keV (3.6%), followed by a cascade emission of both conversion and Auger electrons. The combination of ^{109m}Ag with ^{109}Pd forms an in vivo generator that emits medium-energy β$^-$ particles along with a high quantity (18) of Auger/conversion electrons. The described properties of ^{109}Pd closely resemble those of the widely used ^{161}Tb (β$^-$ and Auger electron emitter), which is currently the preferred option in targeted radiotherapy [16]. It allows for the use of ^{161}Tb in both low- and high-linear energy transfer (LET) internal radiation therapy. Such treatment can simultaneously destroy large tumors using beta radiation and also allow for the destruction of small tumor metastases and subpopulations of treatment-resistant cancer stem cells using Auger electrons.

The results from our studies on the core–shell Au@^{109}Pd nanoparticles–trastuzumab conjugate [15,17] showed that the ^{109}Pd/^{109m}Ag in vivo generator is more cytotoxic compared to Au@PdNPs labeled with either ^{125}I (Auger emitter) or ^{198}Au (β$^-$ emitter). It is worth noting that despite the lack of nuclear localization, which is crucial for efficient Auger electron therapy [18], an adequate cytotoxic effect was achieved. These encouraging properties of the ^{109}Pd@^{109m}Ag-trastuzumab radiobioconjugate for treating HER2+ tumors prompted us to expand our studies to another aggressive form of breast cancer described above, TNBC. By substituting trastuzumab with panitumumab in the radioconjugate, we anticipated achieving improved cytotoxicity outcomes. Our optimism was based on the ability of panitumumab to partially localize (>10%) in the nucleus of MDA-MB-231 cells, potentially allowing it to be close to the DNA strand. It also extensively localizes in the cell membrane (70%), which is also a good target for Auger electron therapy [7]. This contrasts with the trastuzumab conjugate, which mainly localizes in the cytoplasm in the perinuclear region.

2. Results and Discussion

2.1. Production of ^{109}Pd Radionuclide

A large amount of ^{109}Pd activity can be produced in a nuclear reactor through the ^{108}Pd (n,γ)^{109}Pd reaction, with a cross-section of 12.2 b. When natural palladium is used as the target material, more than 500 MBq/mg of ^{109}Pd was obtained after 7 h of irradiation at a flux of 1.5 × 10^{14} n cm^{-2} s^{-1}. Using a 98%-enriched ^{108}Pd target, the obtained radioactivity exceeded 2 GBq/mg. When natural Pd targets are irradiated, a small amount of ^{111}Ag (T$_{1/2}$ = 7.45 d) is formed in the reaction ^{110}Pd(n,γ)^{111m}Pd→^{111}Ag. The separation of ^{111}Ag by co-precipitation with AgCl, as proposed by Das et al. [19], was highly effective. After the radiochemical processing, the gamma-ray spectrum did not show any characteristic gamma photo-peaks from ^{111}Ag and other radioactive impurities. The target material was processed in about 40 min, resulting in only a 5% decrease in the initial activity. In the case of irradiating the isotopically enriched target, the negligible radioactivity of ^{111}Ag made the removal procedure unnecessary.

2.2. Synthesis of Au@^{109}PdNPs

To ensure that Auger electrons can travel a minimal distance (2–500 nm [20]), it is crucial for the emitter's atoms to be located on the surface of the nanoparticle or in close proximity to it. Therefore, in our approach, to immobilize ^{109}Pd atoms in nanoparticles, we selected 15 nm gold nanoparticles covered with one or a few palladium layers. The process of creating these core–shell nanoparticles involves the gradual, uniform deposition and rapid spread of reduced palladium atoms over the core region. Subsequently, the palladium atoms can migrate to the gold region and form a homogeneous layer, covering most of the AuNP surface [21]. The TEM images confirmed that the distribution of Pd was homogeneous and there were no locally elevated palladium clusters presented in our previous publication [15]. Due to the very short path length of Auger and conversion electrons, covering AuNPs with a thin layer of Pd was crucial to ensure their beneficial biological effects on tumor cells. Our calculations show that the obtained Au@Pd nanoparticles have an average of seven layers of Pd atoms on their surface. Considering the diameter of a Pd atom to be 0.274 nm, the total thickness of seven layers of Pd atoms should not exceed 2 nm. Furthermore, this should not significantly affect the energy of most Auger and conversion electrons emitted by ^{109}Pd. By increasing the specific activity, it would be feasible to reduce the thickness to just a single layer.

2.3. Synthesis of Au@Pd-PEG-COOH and Au@Pd-PEG-Panitumumab Bioconjugate

In order to generate a radiobioconjugate having high affinity to EGFR receptors, the Au@Pd nanoparticles have been modified by the monoclonal antibody panitumumab using a polyethylene glycol (PEG) linker. Panitumumab was conjugated with PEG (ortho-pyridyldisulfde-PEG-succinimidyl carboxymethyl ester, OPSS-PEG-NHS) through lysine and next was attached to the Au@PdNPs by the formation of strong gold–thiol bonds. At last, to improve the dispersity of the bioconjugate, PEGylation was carried out with HS-PEG-COOH (5 kDa). The scheme of the developed Au@^{109}Pd-PEG-panitumumab radiobioconjugate is shown in Figure 1. The increase in hydrodynamic diameter, along with the addition of PEG and panitumumab, demonstrates the effective conjugation of biomolecules, as shown in Table 1. Also, the difference in zeta potential values between citrate-coated AuNPs and AuNP-HS-PEG-panitumumab confirms the effectiveness of the surface modification. The radiochemical purity of the Au@^{109}PdNP-PEG-panitumumab radiobioconjugate, after centrifugation from the reaction mixture, exceeds 99%.
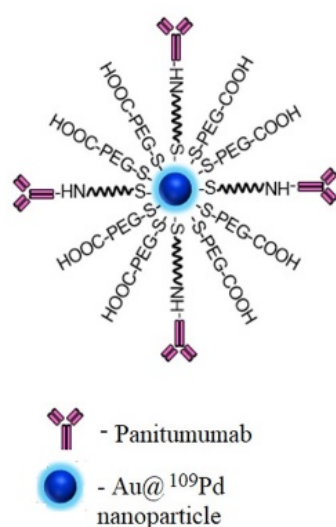

**Figure 1.** The scheme of the developed Au@^{109}Pd-PEG-panitumumab radiobioconjugate.

Table 1. Hydrodynamic diameter and zeta potential of the synthesized conjugates.

	Au@PdNPs	**Au@Pd-PEG-Panitumumab**
Hydrodynamic diameter (nm)	23.78 ± 0.38	82.79 ± 0.43
Zeta potential (mV)	-35.6 ± 1.5	-25 ± 1.8

In order to determine the mean number of attached panitumumab molecules to a single Au@PdNP, ^{131}I-labeled panitumumab molecules were conjugated to Au@PdNPs [22]. Using this method, we calculated that an average of 19 panitumumab molecules were conjugated to a single nanoparticle. This calculation was performed assuming a spherical shape for the nanoparticle with an average diameter of 15 nm, as determined by TEM, with a gold density of 19.28 g/cm^3. The data obtained from the DLS analysis indicate that the distribution is random.

2.4. Colloidal, Chemical, and Radiochemical Stability of Au@Pd-PEG-Panitumumab Conjugate

As the stability of synthesized radiobioconjugates is crucial for their potential use as radiopharmaceuticals, we conducted an assessment of their tendency to agglomerate in biological fluids. The zeta potential of Au@PdNP-PEG-panitumumab of -25.0 ± 1.8 mV should indicate a lack of stability of the bioconjugate, as ζ-potential values > ± 30 mV are considered to indicate colloidal stability. However, our observation of the hydrodynamic diameter of Au@PdNP-PEG-panitumumab over 16 days (Figure 2) indicates no agglomeration or disintegration of the bioconjugates within the evaluation interval, indicating their high stability. This indicates that panitumumab and PEG molecules do not dissociate from the nanoparticle.
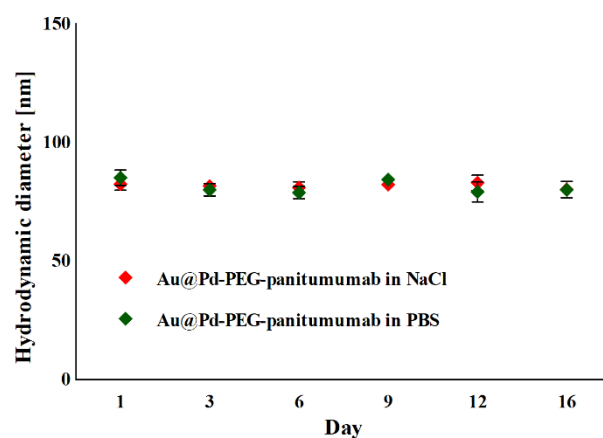
Figure 2. Changes in the hydrodynamic diameter of the Au@Pd-PEG-panitumumab nanoparticles incubated in 10 mM PBS buffer and 0.9% NaCl.

The radiochemical stability of Au@[109]PdNPs was tested using γ-spectrometry. After centrifugation, we did not observe the release of [109]Pd and [109m]Ag from the nanoparticles. The potential release of the daughter radionuclide due to nuclear decay is crucial for the use of in vivo generators in nuclear medicine. Our previous studies [17] show that, unlike chelator-based in vivo [109]Pd/[109m]Ag generators, we observed complete retention of [109m]Ag on Pd nanoparticles. This means that the parent radionuclide is integrated into a metallic nanoparticle rather than a chelate complex, and we did not detect any traces of [109m]Ag released in water, PBS buffer (1 mM), or human serum.

2.5. EGFR Immunoreactivity

Increasing concentrations (0 to 20 nM) of Au@[109]PdNP-PEG-panitumumab were incubated with EGFR-overexpressing MDA-MB-231 cells, either in the presence or absence of a 500-fold molar excess of panitumumab. Figure 3 shows significant differences in binding

with or without free panitumumab used to block the receptors, indicating specific EGFR-dependent binding to MDA-MB-231 cells; however, the SB (specific binding) curve did not reach saturation or even come close to saturation over the entire range of concentrations tested. The shape of the dependency curve shows notable distinctions compared to those of labeled antibodies or peptides, but it closely resembles the curves for nanoparticle conjugates with trastuzumab [14,23]. The characteristics of these curves are straightness across a broad concentration range and very large nonspecific binding that exceeds the specific binding. The phenomenon can be explained by the significant adhesion of nanoparticles on cell membranes, as demonstrated in multiple studies [24]. In contrast, the nonspecific binding of the tested monoclonal antibodies is typically minimal.
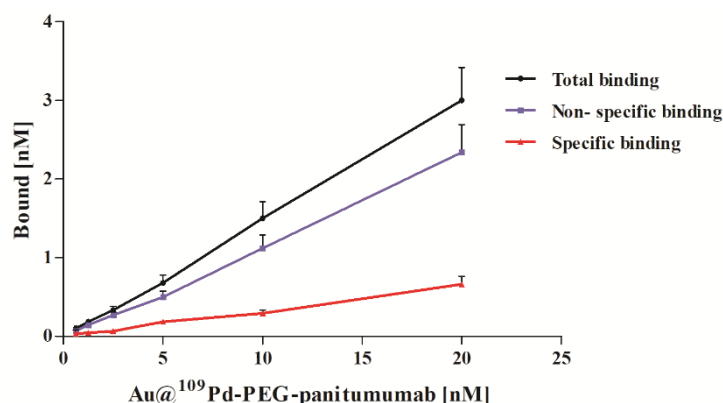

Figure 3. Binding studies of Au@[109]PdNP-PEG-panitumumab on MDA-MB-231 cell line.

2.6. Internalization by Radiometric Assay and Confocal Imaging

In order to achieve optimal treatment results, it is crucial to deliver Auger-electron-emitting radionuclides to the cell nucleus, preferably close to the DNA. It has also been found that localization of the Auger electron emitter in the cell membrane can also cause cell death [6]. Nanoparticles carrying Auger emitters can be transported into the cell nucleus in two ways. The first way is through passive transport via nuclear pore complexes. These complexes allow the diffusion of ions, small molecules, and nanoparticles through aqueous channels with a diameter of approximately 9 nm. The main condition for transportation is that the substances must be hydrophilic. The second route is known as active transport. During this process, certain macromolecules are actively transported across the nuclear envelope. This transport is a highly selective process that can be divided into two steps: receptor binding, followed by translocation across the nuclear envelope [25]. Receptor binding is facilitated by nuclear localization signals, which have been identified in many nuclear proteins.

In our previous studies [15], as well as in the studies conducted by Cai et al. [23], it was observed that trastuzumab and trastuzumab-modified Au@Pd and Au nanoparticles exhibited very high internalization (>90%) into SKOV-3, SKBR-3, and MDA-361 cells overexpressed the HER2 receptors. However, the localization of these conjugates into the cell nucleus was not observed. In the case of the behavior of Au@Pd-PEG-panitumumab NPs in the MDA-MB-231 cell overexpressing the EGFR receptor, the situation is different. Results of radiometric studies presented in Figure 4 indicated similar internalization into the cell; however, there is also a significant transport into the cell nucleus, in contrast to trastuzumab-modified nanoparticles in HER2+ cells, where transportation to the nucleus does not occur.

These results are well supported by confocal and dark-field microscopy images (Figure 5). The dark spots visible on the bright background represent agglomerated Au@Pd particles, whereas the green fluorescence signals indicate secondary mAb conjugated to panitumumab as an integral part of the bioconjugate. In dark-field microscopy, agglomerated Au@Pd-PEG-panitumumab NPs were observed in EGFR-targeted MDA-MB-231 cells, but

not in untargeted Au@Pd-PEG. The possibility of observing Au@Pd-PEG-panitumumab NPs in dark-field mode in the absence of a signal for Au@Pd-PEG may be due to the clustering of receptor-bound Au@Pd-PEG-panitumumab NPs. This clustering could occur because some receptors have been found to cluster on lipid rafts on the cell surface [23]. In confocal microscopy images, we can also observe the accumulation of Au@Pd-PEG-panitumumab NPs inside cells, revealing the crucial role of panitumumab as a targeting vector for EGFR-overexpressed breast cancer cells. In contrast to the confocal microscopy images recorded for Au@Pd-PEG-trastuzumab in SKOV-3 cells, which displayed accumulation in the perinuclear area nearly to the nuclear envelope [15], we now observe a localization of the Au@Pd-PEG-panitumumab conjugate inside the cell nucleus. Therefore, the accumulation of NPs in close proximity to the most sensitive cellular organelle led us to expect high cytotoxicity induced by radioactive bioconjugates.
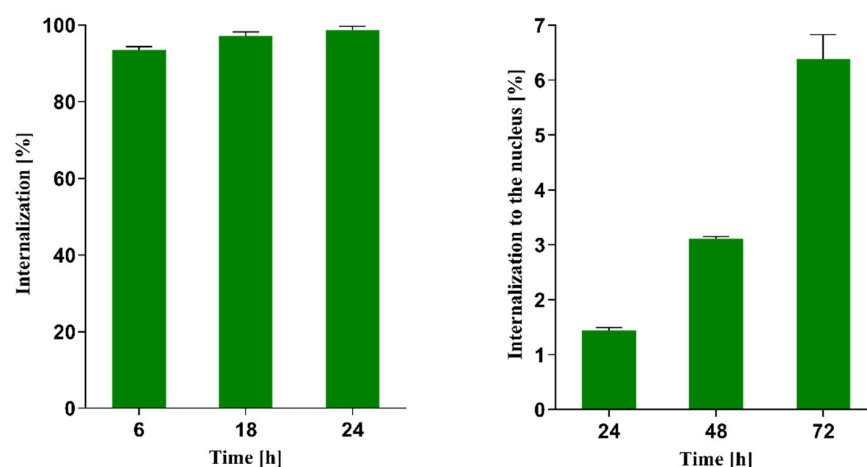
Figure 4. Internalization of Au@Pd-PEG-panitumumab NPs into the MDA-MB-231 cell overexpressing EGFR receptor (**left**) and intranuclear uptake of radioconjugate (**right**).
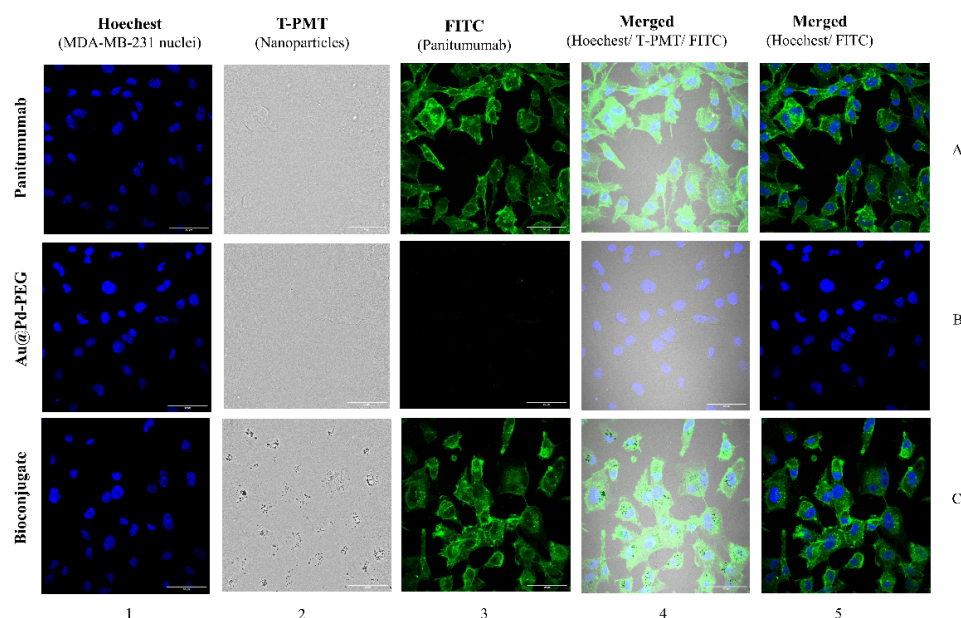
Figure 5. Internalization of panitumumab, Au@Pd-PEG-COOH, and Au@Pd-PEG-panitumumab in MDA-MB-231 cells determined by confocal microscopy. The fluorescence signals indicate the following: subcellular panitumumab distribution (green) and nuclei intracellular localization (blue). Au@Pd-containing particles (dark spots) were also visualized with a transmitted light detector (T-PMT).

2.7. Cytotoxicity

The viability of MDA-MB-231 cells overexpressing EGFR and incubated with non-radioactive Au@Pd-PEG-panitumumab NPs and Au@^{109}Pd-PEG-panitumumab NPs was evaluated using the MTS assay. The bioconjugates of non-radioactive Au@Pd-PEG-panitumumab NPs were used at concentrations ranging from 11.25 µg/mL (3×10^{-3} nmol/mL NP) to 180 µg/mL (5×10^{-2} nmol/mL NP). The goal of this study was to investigate whether this bioconjugate could cause mitochondrial dysfunction and cell death. As shown in Figure 6a, the effect of non-radioactive Au@Pd-PEG-panitumumab NPs on the viability of MDA-MB-231 cells was observed across all tested concentrations. However, the most significant effect was observed for concentrations above 22.5 µg/mL. A similar cytotoxic effect of Au-PEG-panitumumab NP conjugates on TNBC was also observed by Yook et al. [11]. The authors suggested that the cytotoxicity of panitumumab nanoparticle conjugates on MDA-MB-231 cells may be due to the immunotoxic effect of the panitumumab antibody linked to the nanoparticles, as indicated by several clinical studies. They also proposed that the internalization of Au-PEG-panitumumab nanoparticles into the cell nucleus could potentially cause nuclear damage in cells, similar to what has been observed with AuNPs [26]. The cytotoxicity of PdNPs is significantly higher than that of AuNPs. Therefore, Au@Pd-PEG-panitumumab demonstrates increased cytotoxicity. This is consistent with our previous studies on the Au@Pd-PEG-trastuzumab conjugates on SKOV-3 cells [15], where nuclear localization of the conjugate in cell nuclei was not observed, and therefore, no nuclear damage caused by nanoparticles in cells was detected.
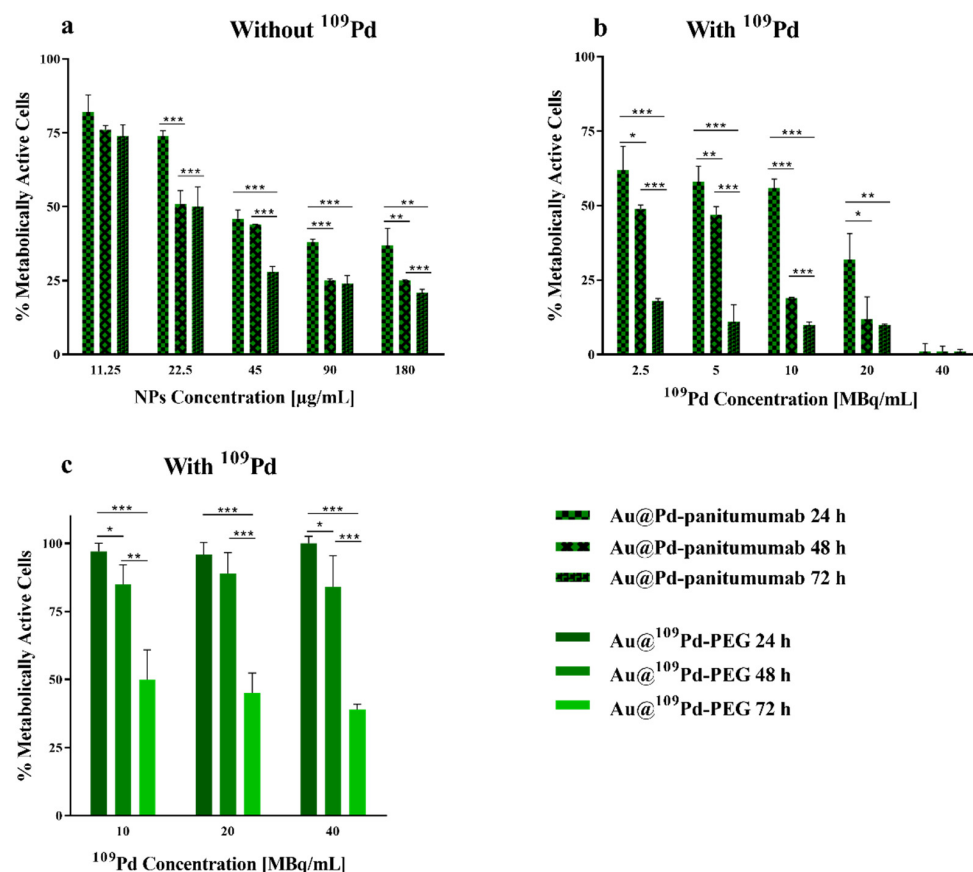
Figure 6. Metabolic viability of MDA-MB-231 cells after treatment with different concentrations of Au@Pd-PEG-panitumumab non-radioactive conjugates (**a**) and with different radioactive doses of Au@^{109}Pd-PEG-panitumumab NPs (**b**) and of Au@^{109}Pd-PEG radioactive conjugates (**c**) after 24 h, 48 h, and 72 h of incubation.). The results are expressed as mean $\pm$ SD. *p*-values are presented as follows: (*) $p \leq 0.05$, (**) $p \leq 0.001$, (***), and $p \leq 0.0001$.

The effects of different levels of radioactivity concentrations of Au@^{109}Pd-PEG-panitumumab and Au@^{109}Pd-PEG conjugates on the metabolic viability of MDA-MB-231 cells at 24, 48, and 72 h after exposure are illustrated in Figure 6b,c. It is evident that the use of the Au@^{109}Pd-panitumumab radiobioconjugate significantly reduced the metabolic activity of MDA-MB-231 cells, with the reduction depending on the dosage and time interval after administration. Increasing the radioactivity of the radiobioconjugate caused a gradual reduction in mitochondrial activity, leading to almost complete cell death for an activity of 40 MBq/mL. When analyzing the results shown in Figure 6b, it is important to consider that the individual solutions of Au@^{109}Pd-panitumumab used in cytotoxic tests were obtained by diluting the initial solution of 40 MBq/mL, which contained 180 µg/mL of the conjugate. As a result, the observed total cytotoxic effect comprises a chemotoxic effect caused by the non-radioactive conjugate (Figure 6a) and a radiotoxic effect caused by β$^-$ particles and Auger electrons emitted by ^{109}Pd.

In the case of Au@^{109}PdNPs, despite the lack of panitumumab, a significant reduction in cell viability was found, particularly 72 h after exposure (Figure 6c). The range of β$^-$ particles emitted by ^{109}Pd in the body is approximately 4 mm. Therefore, the cross-fire effect of these particles could potentially target TNBC cells in tumors with low or moderate EGFR expression, or cells that are not effectively targeted by Au@^{109}Pd-PEG-panitumumab NPs due to their uneven distribution within the tumor. However, this effect is much smaller compared to the vector-attached radiobioconjugates, where due to internalization, the chemotoxicity of panitumumab, Au@Pd nanoparticles, and the radiotoxicity of Auger electrons are additionally involved.

2.8. DNA Double-Strand Breaks (DSBs)

Lethal and irreparable damage to genetic material is considered one of the most desired outcomes of radiopharmaceutical anticancer activity [27]. These damages can occur through direct ionization of DNA caused by ionizing radiation or by the interaction of reactive oxygen species (ROS) generated from water with the DNA strand. In our study, we investigated the formation of DSBs following exposure to Au@^{109}Pd-PEG-panitumumab nanoparticles. These nanoparticles can induce DSBs through direct and indirect interactions of β$^-$ and Auger electron radiation, as well as through the generation of ROS by Pd nanoparticles [28]. The presence of DSBs in MDA-MB-231 cells was confirmed by the detection of γH2A.X foci, offering a fast and sensitive method for detecting DSBs induced by various cytotoxic agents, including ionizing radiation. DNA double-strand breaks in MDA-MB-231 cells are visualized with γH2A.X foci after treatment with Au@^{109}Pd-PEG-panitumumab NPs (Figure 7). Quantification of these foci, represented as the integrated density of γH2AX foci per nucleus area, is shown in Figure 8.

The presence of DSBs in the MA-MB-231 cells treated with Au@^{109}Pd-PEG-panitumumab NPs is consistent with the cytotoxicity results shown in Figure 6b. Similarly, as observed in HepG2 cells treated with ^{109}Pd-PEG NPs [17], the high-LET Auger and conversion electrons emitted by the ^{109}Pd/^{109m}Ag in vivo generator lead to the formation of a high number of DSBs. However, when comparing our results with those of ^{109}Pd-PEG NPs on HepG2 cells, a significantly higher number of γH2A.X foci is observed for the Au@^{109}Pd-PEG-panitumumab radiobioconjugate. For instance, at an activity of 20 MBq/mL, the average number of γH2A.X foci in the cell nucleus reaches eight for Au@^{109}Pd-PEG-panitumumab; however, it was only three for ^{109}Pd-PEG NPs on HepG2 cells. This effect is likely due to the additional immunotoxicity effect on MDA-MB-231 cells generated by the panitumumab antibody conjugated to the nanoparticles. In the studies of DSBs caused by the ^{111}In-labeled conjugate of trastuzumab with dendrimers derivatized with multiple DTPA chelators [29], a similar number of γH2A.X foci was observed on cells overexpressing HER2 receptors (SK-Br-3 cells). There were six γH2A.X foci in the cell nucleus at 12 MBq/mL activity, while our study showed seven γH2A.X foci at 10 MBq/mL Au@^{109}Pd-PEG-panitumumab on MDA-MB-231 cells. As ^{111}In does not emit beta particles, in contrast to the ^{109}Pd/^{109m}Ag

in vivo generator, it can be deduced that the presence of DSBs is associated with Auger electron radiation.
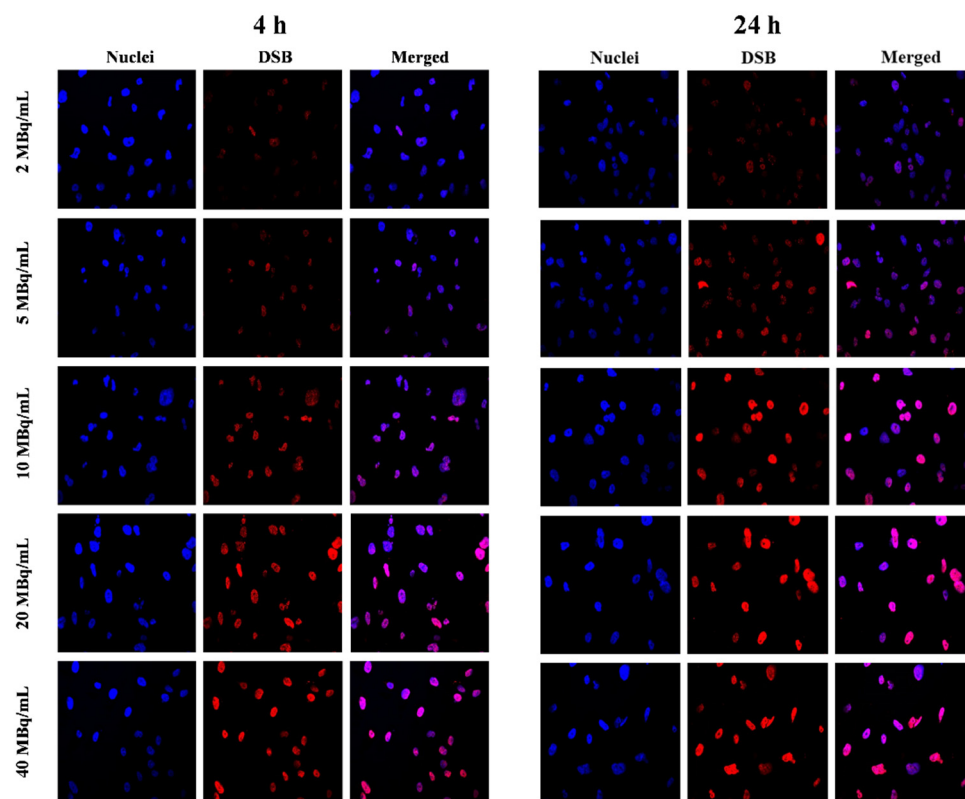
Figure 7. Confocal immunofluorescence microscopy exhibiting γH2A.X foci (red) in the nucleus (counterstained blue with DAPI) and merged (purple) of MDA-MB-231 breast cancer cells treated with various radioactivity of Au@^{109}Pd-PEG-panitumumab recorded after 4 h (**left**) and 24 h (**right**) of incubation.
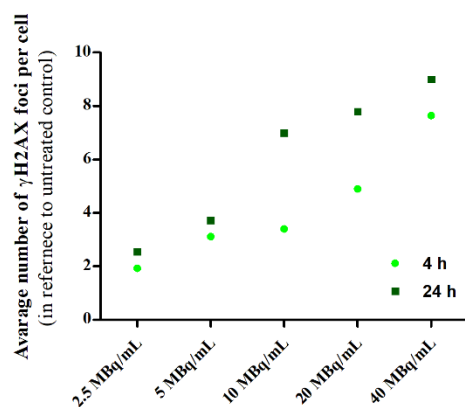
Figure 8. Quantification of γH2AX foci from the images shown in Figure 7.

3. Materials and Methods

3.1. Chemical Reagents

Gold (III) chloride trihydrate (HAuCl$_4$·3H$_2$O), trisodium citrate dihydrate (C$_6$H$_9$Na$_3$O$_9$), and HS-PEG-COOH (poly(ethylene glycol), 5 kDa) were purchased from Sigma-Aldrich (St. Louis, MO, USA), and OPSS-PEG-NHS (alpha-pyridyl2-disulfd-omega-carboxy succinimidyl ester poly(ethylene glycol), 5 kDa) was obtained from Creative PEGworks (Chapel Hill, NC, USA). Panitumumab (Vectibix®) from Amgen (Thousand Oaks, CA, USA) and a PD-10 column (GE Healthcare, Piscataway, NJ, USA) were also utilized in such stud-

ies. Hydrochloric acid and sodium hydroxide were purchased from POCH (Gliwice, Poland). Fluorescence mounting medium was obtained from Dako (Carpinteria, CA, USA). The following materials were used in cell studies: phosphate-buffered saline (PBS) and dimethylsulfoxide (DMSO) from Sigma-Aldrich (St. Louis, MO, USA), and the CellTiter 96® Aqueous One Solution Reagent (MTS compound) from Promega (Mannheim, Germany). MDA-MB-231 cells were purchased from the American Type Tissue Culture Collection (ATCC, Rockville, MD, USA), cultured in DMEM medium supplemented with 10% FBS and 1% penicillin−streptomycin (all from Beth Haemek, Israel), and maintained at 37 °C and 5% CO_2. Furthermore, the solutions were generated using double-distilled water (18.2 MΩ·cm, Hydrolab, Straszyn, Poland).

3.2. Radionuclides

[109]Pd was obtained by thermal neutron ($1–2 \times 10^{14}$ n/cm^2 s) irradiation of a natural palladium target (~2 mg, metal powder) or ~1 mg, metal powder enriched to >99% [108]Pd in the Maria nuclear reactor (Otwock-Świerk, Poland) for 7 h. After a cooling time of 12 h, the radioactive palladium target was dissolved in aqua regia (HNO_3: HCl—1:3, 200–400 μL) and heated at 130 °C until near-evaporation.

The elimination of the remaining nitrate was accomplished by using three 200 μL portions of 0.1 M HCl and double-distilled H_2O, respectively, and then heating at 130 °C until near-evaporation. At last, the target was suspended in 0.1 M HCl and 0.5 M NaOH in a ratio of 7:1, to generate Na_2PdCl_4. Neutron irradiation of the natural Pd target can lead to the formation of [111]Ag as an impurity in the reaction of [110]Pd (n,γ)[111m]Pd→[111]Ag. It is essential to remove it from the solution before use, which was achieved by precipitating [111]Ag as AgCl using $AgNO_3$ in the modified procedure described by Das et al. [17,19].

[131]I radionuclide (no carrier added) was utilized for radioiodination of panitumumab, which was used to determine the number of panitumumab molecules attached to the Au@Pd surface. Na[131]I (with a specific activity of about >550 GBq/mg) was obtained from POLATOM Radioisotope Centre in Świerk, Poland.

3.3. Synthesis of Core–Shell Au@Pd and Radioactive Au@[109]PdNPs

Core–shell Au@Pd nanoparticles (NPs) were synthesized using the same procedure as described in [15]. Initially, gold nanoparticles with a diameter of 15 nm were synthesized based on the Turkevich method, with slight modifications by our group. In the next step, AuNPs were coated with an ultrathin layer of palladium via the chemical reduction of Na_2PdCl_4 by ascorbic acid using the procedure described before for the synthesis of Au@Pt [20]. Briefly, AuNPs solution was heated to 90 °C for 10 min. Subsequently, Na_2PdCl_4 (0.27 mg, 1 mM) or Na_2[109]$PdCl_4$ were added as the palladium precursors, along with ascorbic acid (7.5 mg, 2 M) as the reducing agent, at 10 min and 30 min intervals. The reaction mixture was then heated for 30 min at 90 °C, cooled to room temperature, and characterized using DLS and UV–Vis techniques.

3.4. Synthesis of Non-Radioactive and Radioactive Au@[109]Pd-PEG-Panitumumab Radiobioconjugate

The radioactive antibody-conjugated nanoparticles Au@[109]Pd-PEG-panitumumab were synthesized using the same procedure as for Au@[109]Pd-PEG-trastuzumab [15]. Panitumumab (1 mg) was combined with a 25-fold molar excess of OPSS-PEG-NHS (5 kDa) in carbonate buffer (100 mM) and allowed to react overnight. Afterward, the purified OPSS-PEG-panitumumab was conjugated to Au@Pd or Au@[109]Pd in carbonate buffer (20 mM) for 45 min. A 15000-molar excess of HS-PEG-COOH (5 kDa) was added to increase bioconjugate dispersity for 30 min at room temperature. At last, the product was purified by centrifugation, dispersed in deionized water, and characterized.

3.5. Determination of Number of Panitumumab Molecules Conjugated to Au@Pd Nanoparticles

We used iodinated panitumumab to calculate protein molecules conjugated to nanoparticles ([^{131}I]I-panitumumab). The ^{131}I labeling was performed using the Iodogen method [22].

In brief, 2 mg of panitumumab, 64 MBq of ^{131}I, and 0.1 M PBS buffer were mixed with Iodogen reagent for 10 min in room temperature. The mixture was purified using a PD-10 column (Sephadex G-25 resin) and PBS buffer (10 mM) as a mobile phase. Consequently, buffer exchange was carried out using Vivaspin®500 centrifugal concentrators and the product was then transferred into an aqueous solution. Afterwards, 250 μg of [^{131}I]I-panitumumab was mixed with OPSS-PEG-NHS (5 kDa, 25-fold molar excess) in carbonate buffer (100 mM) overnight, purified, and conjugated to nanoparticles. To determine the yield of conjugation, after centrifuging of nanoparticles, the obtained supernatant was collected, and the activity of both—nanoparticles and supernatant—portions was measured. Finally, the number of iodinated panitumumab molecules attached to one Au@PdNP was calculated by dividing the moles of protein by that of nanoparticles.

3.6. Stability Studies of Au@Pd-PEG-Panitumumab Bioconjugate Colloid

The stability of the bioconjugate in physiological conditions was evaluated at 37 °C over a period of 16 days following centrifugation and dispersion of the Au@Pd-PEG-panitumumab in both PBS buffer and saline (0.9% NaCl). The aggregation tendency was investigated by measuring the hydrodynamic diameter and zeta potential using the DLS technique. The radiochemical stability was evaluated using γ spectrometry to detect any detachment of either ^{109}Pd or ^{109m}Ag from the core surface. For this purpose, radiobioconjugates were centrifuged after incubation in PBS, 0.9% NaCl, and human serum (HS), and the obtained fractions (supernatant and nanoparticles) were then quantified using gamma spectrometry.

3.7. Determination of EGFR Immunoreactivity

The immunoreactivity of Au@^{109}Pd-PEG-panitumubab with EGFR-overexpressing MDA-MB-231 cells was determined in a direct (saturation) binding assay. MBA-MB-231 cells (7.5 × 10^3 cells/well) were seeded in 24-well plates and incubated overnight. The following day, plates were washed twice with cold PBS and incubated with increasing concentrations of Au@^{109}Pd-PEG-panitumubab (0−20 nM) at 4 °C for 2 h. To determine non-specific binding, one of the plates was incubated with an excess of 500-fold molar of unlabeled mAb. After incubation, cells were washed twice with cold PBS and collected in tubes. The cells were then lysed twice with 800 μL of 1 M NaOH and collected in separate tubes. The samples were counted using the Wizard2 system.

3.8. Internalization Studies

Internalization studies were performed on MDA-MB-231 cells. Briefly, the day before the experiment, 6× 10^5 cells/well were seeded into 6-well plates. After 24 h of incubation, cells were rinsed with PBS and then treated with tested compounds (1 mL). To avoid internalization, the cells were incubated at 4 °C for 1 h. After that, the medium was collected as the unbound portion, and then the cells were washed with PBS and a fresh medium (1 mL) was added. Plates were then incubated (37 °C, 5% CO$_2$) for various time points of interest, including 6, 18, and 24 h. To evaluate the membrane-bound portion, cells were rinsed twice with glycine-HCl buffer (pH ~2.8, 0.05 M) and then kept at 4 °C for 5 min. Finally, the internalized portion was collected by lysing the cells with 1 M NaOH. Non-specific binding was assessed with the same procedure as implemented for receptor binding affinity.

3.9. Confocal Microscopy Imaging

MDA-MB-231 cells (2 × 10^5 cells per well) were cultured on sterile glass coverslips with a diameter of 12 mm (Thermo Fischer Scientific, Waltham, MA, USA) in 6-well plates and then left to incubate over 24 h. The following day, after removal of the medium, cells were administered with panitumumab (73 μg/mL), Au@Pd-PEG-COOH (1.62 × 10^{12} NPs/mL), and Au@Pd-PEG-panitumumab bioconjugate (1.62 × 10^{12} NPs/mL), and incubated overnight. The cells were stained with both Hoechst 33,258 (λex/em = 352/454 nm) and an anti-human

IgG secondary antibody coupled to FITC (λex/em = 490/525 nm), and bright-field images for nanoparticles were obtained by a transmitted light detector (T-PMT). All analysis was performed using Image J 1.54i software.

3.10. Cytotoxicity Studies

Cytotoxicity experiments were conducted on MDA-MB-231 cells using the MTS assay. Briefly, cells were seeded at a density of 3×10^3 cells per well in 96-well plates and incubated overnight at 37 °C with 5% CO_2 atmosphere. The next day, after aspirating the medium, the cells were washed with PBS. Subsequently, antibody-conjugated nanoparticles at the concentrations of (11–180 µg/mL, for non-radioactive) and (180 µg/mL for 40 MBq/mL, 90 µg/mL for 20 MBq/mL, 45 µg/mL for 10 MBq/mL, for radioactive compounds) were suspended in fully supplemented growing medium and 100 µL per well was added and incubated for 24–72 h at 37 °C with 5% CO_2 atmosphere. Before adding the MTS reagent, the medium was aspirated, the cells were washed with PBS, and fresh medium was added to the wells. Finally, the percentage of metabolically active cells was determined by the addition of CellTiter96® AQueous One Solution Reagent and measurement of the absorbance at 490 nm.

3.11. DNA Double-Strand Break Study

γ-H2AX nuclear staining was performed to evaluate the intensity of DNA damage (double-strand breaks) induced by treatment with Au@^{109}PdNPs-PEG-panitumumab. MDA-MB-231 cells (2×10^5/well) were cultured in 6-well plates. Each well is covered with five sterile glass coverslips with a diameter of 12 mm. After 24 h of incubation, the medium was removed, and the cells were exposed to various concentrations (ranging from 0 to 40 MBq/mL) and staurosporine (0.5 µM) as a positive control. The cells were then incubated for 4 and 24 h. To identify γH2A.X foci 350 µL of a primary antiphospho-histone H2A.X (Ser139) antibody, clone JBW301 (with a dilution ratio of 1:100) was added to each well and left overnight at 4 °C. On the following day, the primary antibody was replaced with a secondary antibody (anti-mouse IgG), which was dissolved in blocking buffer (BB-4% BSA in TBS) and labeled with CF™ 633. Subsequently, the cells were incubated at room temperature for 2 h. Afterward, the cells were washed with water and then stained with Hoechst 33258. The imaging study was carried out using an FV-1000 confocal microscope (Olympus Corporation, Tokyo, Japan) with ex/em maxima of 630/650 nm for CF633 and ex/em maxima of 352/454 nm for Hoechst 33258. The results were analyzed using the Fiji 2.9.0 version.

3.12. Statistical Analysis

Statistical analysis, one-way ANOVA, and Student's t-tests were carried out with GraphPad Prism v.8 (GraphPad Software, San Diego, CA, USA). The results are expressed as mean $\pm$ SD. p-values are presented as follows: (*) $p \leq 0.05$, (**) $p \leq 0.001$, (***), and $p \leq 0.0001$.

4. Conclusions

In this article, we discuss the potential application of ^{109}Pd-PEG-panitumumab nanoparticle conjugates as an in vivo ^{109}Pd/^{109m}Ag generator for targeted therapy of TNBC. Similar to previous studies, we show that, unlike most chelator-based generators, we observed complete retention of the daughter isotope on the nanoparticles. This has important implications for targeted therapy, as it does not result in the displacement of radioactivity outside the targeting area. The Au@^{109}Pd-PEG-panitumumab nanoparticle conjugates have been found to exhibit multiple toxic interactions with cancer cells. They are both radiotoxic, emitting β^- and Auger electrons, and exhibit immunotoxicity due to the presence of the panitumumab antibody. Additionally, they demonstrate chemotoxicity as a result of the catalytic generation of ROS on PdNPs. However, the radiotoxic effects of Auger electrons become dominant due to the relatively high internalization of the radiobioconjugate

into the cell nucleus, which is caused by the presence of the panitumumab vector. The emission of this high-LET radiation is particularly important for the treatment of resistant triple-negative breast cancer cells.

It is important to note that using radioactive bioconjugates based on metallic nanoparticles poses challenges for systemic administration. The accumulation of radioactively labeled nanobioconjugates in the liver, lungs, and spleen can expose these organs to radiation and reduce the accumulation of these radiobioconjugates by tumors. As a result, intravenous administration of Au@^{109}Pd-PEG-panitumumab is not feasible. Many studies suggest that for these types of radiobioconjugates, localized administration directly to the tumor or to the resection cavity is more effective [9,11,13,15]. Despite these limitations, the concept of using an in vivo ^{109}Pd/^{109m}Ag generator and the promising results obtained encourage further exploration of this treatment strategy.

Author Contributions: Conceptualization: A.B. and A.M.-P.; formal analysis: N.A.G.; funding acquisition: A.M.-P. and A.B.; investigation: N.A.G., M.W., R.W., A.M.-P. and A.B.; methodology: N.A.G., M.W., R.W., A.M.-P. and A.B.; project administration: A.M.-P. and A.B.; resources: A.M.-P. and A.B.; supervision: A.B. and A.M.-P.; visualization: N.A.G. and A.M.-P.; writing—original draft: A.B. and N.A.G.; writing—review and editing: N.A.G., A.M.-P. and A.B. All authors have read and agreed to the published version of the manuscript.

Institutional Review Board Statement: Not applicable.

Informed Consent Statement: Not applicable.

Data Availability Statement: The data presented in this study are available on request from the corresponding authors due to (specify the reason for the restriction).

Conflicts of Interest: The authors declare no conflict of interest.

References

1. Xu, Y.; Gong, M.; Wang, Y.; Yang, Y.; Liu, S.; Zeng, Q. Global trends and forecasts of breast cancer incidence and deaths. *Sci. Data* **2023**, *10*, 334. [CrossRef] [PubMed]
2. Borri, F.; Granaglia, A. Pathology of triple negative breast cancer. *Semin. Cancer Biol.* **2021**, *72*, 136–145. [CrossRef] [PubMed]
3. Schmid, P.; Adams, S.; Rugo, H.S.; Schneeweiss, A.; Barrios, C.H.; Iwata, H.; Diéras, V.; Hegg, R.; Im, S.-A.; Shaw Wright, G.; et al. Atezolizumab and Nab-Paclitaxel in Advanced Triple-Negative Breast Cancer. *N. Engl. J. Med.* **2018**, *379*, 2108–2121. [CrossRef]
4. Emens, L.; Molinero, L.; Loi, S.; Rugo, H.S.; Schneeweiss, A.; Diéras, V.; Iwata, H.; Barrios, C.H.; Nechaeva, M.; Duc, A.N.; et al. Atezolizumab and nab-Paclitaxel in Advanced Triple-Negative Breast Cancer: Biomarker Evaluation of the IMpassion130 Study. *J. Natl. Cancer Inst.* **2021**, *113*, 1005–1016. [CrossRef]
5. Duffy, M.J.; McGowan, P.M.; Crown, J. Targeted therapy for triple-negative breast cancer: Where are we? *Int. J. Cancer* **2012**, *131*, 2471–2477. [CrossRef]
6. Ku, A.; Facca, V.J.; Cai, Z.; Reilly, R.M. Auger electrons for cancer therapy—A review. *EJNMMI Radiopharm. Chem.* **2019**, *4*, 27. [CrossRef]
7. Facca, V.J.; Cai, Z.; Gopal, N.E.K.; Reilly, R.M. Panitumumab-DOTA-(111)In: An Epidermal Growth Factor Receptor Targeted Theranostic for SPECT/CT Imaging and Meitner-Auger Electron Radioimmunotherapy of Triple-Negative Breast Cancer. *Mol. Pharm.* **2022**, *19*, 3652–3663. [CrossRef]
8. Facca, V.J.; Cai, Z.; Ku, A.; Georgiou, C.J.; Reilly, R.M. Adjuvant Auger Electron-Emitting Radioimmunotherapy with [(111)In]In-DOTA-Panitumumab in a Mouse Model of Local Recurrence and Metastatic Progression of Human Triple-Negative Breast Cancer. *Mol. Pharm.* **2023**, *20*, 6407–6419. [CrossRef]
9. Mbong, G.N.N.; Lu, Y.; Chan, C.; Cai, Z.; Liu, P.; Boyle, A.J.; Winnik, M.A.; Reilly, R.M. Trastuzumab Labeled to High Specific Activity with (111)In by Site-Specific Conjugation to a Metal-Chelating Polymer Exhibits Amplified Auger Electron-Mediated Cytotoxicity on HER2-Positive Breast Cancer Cells. *Mol. Pharm.* **2015**, *12*, 1951–1960. [CrossRef]
10. Aghevlian, S.; Lu, Y.; Winnik, M.A.; Hedley, D.W.; Reilly, R.M. Panitumumab Modified with Metal-Chelating Polymers (MCP) Complexed to (111)In and (177)Lu-An EGFR-Targeted Theranostic for Pancreatic Cancer. *Mol. Pharm.* **2018**, *15*, 1150–1159. [CrossRef]
11. Yook, S.; Cai, Z.; Lu, Y.; Winnik, M.A.; Pignol, J.-P.; Reilly, R.M. Radiation Nanomedicine for EGFR-Positive Breast Cancer: Panitumumab-Modified Gold Nanoparticles Complexed to the β-Particle-Emitter, (177)Lu. *Mol. Pharm.* **2015**, *12*, 3963–3972. [CrossRef] [PubMed]

12. Gharibkandi, N.A.; Żuk, M.; Muftuler, F.Z.B.; Wawrowicz, K.; Żelechowska-Matysiak, K.; Bilewicz, A. (198)Au-Coated Superpara-magnetic Iron Oxide Nanoparticles for Dual Magnetic Hyperthermia and Radionuclide Therapy of Hepatocellular Carcinoma. *Int. J. Mol. Sci.* **2023**, *24*, 5282. [CrossRef] [PubMed]

13. Żelechowska-Matysiak, K.; Salvanou, E.-A.; Bouziotis, P.; Budlewski, T.; Bilewicz, A.; Majkowska-Pilip, A. Improvement of the Effectiveness of HER2+ Cancer Therapy by Use of Doxorubicin and Trastuzumab Modified Radioactive Gold Nanoparticles. *Mol. Pharm.* **2023**, *20*, 4676–4686. [CrossRef]

14. Wawrowicz, K.; Majkowska-Pilip, A.; Gaweł, D.; Chajduk, E.; Pieńkowski, T.; Bilewicz, A. Au@Pt Core-Shell Nanoparticle Bioconjugates for the Therapy of HER2+ Breast Cancer and Hepatocellular Carcinoma. Model Studies on the Applicability of (193m)Pt and (195m)Pt Radionuclides in Auger Electron Therapy. *Molecules* **2021**, *26*, 2051. [CrossRef]

15. Gharibkandi, N.A.; Wawrowicz, K.; Majkowska-Pilip, A.; Żelechowska-Matysiak, K.; Wierzbicki, M.; Bilewicz, A. Au@(109)Pd core-shell nanoparticle conjugated to trastuzumab for the therapy of HER2+ cancers: Studies on the applicability of (109)Pd/(109m)Ag in vivo generator in combined β(-) auger electron therapy. *EJNMMI Radiopharm. Chem.* **2023**, *8*, 26. [CrossRef]

16. Müller, C.; Umbricht, C.A.; Gracheva, N.; Tschan, V.J.; Pellegrini, G.; Bernhardt, P.; Zeevaart, J.R.; Köster, U.; Schibli, R.; van der Meulen, N.P. Terbium-161 for PSMA-targeted radionuclide therapy of prostate cancer. *Eur. J. Nucl. Med.* **2019**, *46*, 1919–1930. [CrossRef]

17. Gharibkandi, N.A.; Wawrowicz, K.; Walczak, R.; Majkowska-Pilip, A.; Wierzbicki, M.; Bilewicz, A. (109)Pd/(109m)Ag in-vivo generator in the form of nanoparticles for combined β(-)—Auger electron therapy of hepatocellular carcinoma. *EJNMMI Radiopharm. Chem.* **2024**, *9*, 59. [CrossRef]

18. Costantini, D.L.; McLarty, K.; Lee, H.; Done, S.J.; Vallis, K.A.; Reilly, R.M. Antitumor effects and normal-tissue toxicity of 111In-nuclear localization sequence-trastuzumab in athymic mice bearing HER-positive human breast cancer xenografts. *J. Nucl. Med.* **2010**, *51*, 1084–1091. [CrossRef]

19. Das, T.; Chakraborty, S.; Sarma, H.D.; Banerjee, S. 109Pd labeled 5,10,15,20-tetrakis[4-carboxymethyleneoxyphenyl]porphyrin: A potential agent for targeted tumor therapy. *Curr. Radiopharm.* **2012**, *5*, 340–347. [CrossRef]

20. Kassis, A.I.; Adelstein, S.J. Radiobiologic principles in radionuclide therapy. *J. Nucl. Med.* **2005**, *46* (Suppl. S1), 4s–12s. [PubMed]

21. Gao, Z.; Ye, H.; Tang, D.; Tao, J.; Habibi, S.; Minerick, A.; Tang, D.; Xia, X. Platinum-Decorated Gold Nanoparticles with Dual Functionalities for Ultrasensitive Colorimetric in Vitro Diagnostics. *Nano Lett.* **2017**, *17*, 5572–5579. [CrossRef] [PubMed]

22. Gupta, S.; Batra, S.; Jain, M. Antibody labeling with radioiodine and radiometals. *Methods Mol. Biol.* **2014**, *1141*, 147–157. [CrossRef] [PubMed]

23. Cai, Z.; Chattopadhyay, N.; Yang, K.; Kwon, Y.L.; Yook, S.; Pignol, J.-P.; Reilly, R.M. (111)In-labeled trastuzumab-modified gold nanoparticles are cytotoxic in vitro to HER2-positive breast cancer cells and arrest tumor growth in vivo in athymic mice after intratumoral injection. *Nucl. Med. Biol.* **2016**, *43*, 818–826. [CrossRef] [PubMed]

24. Lesniak, A.; Salvati, A.; Santos-Martinez, M.J.; Radomski, M.W.; Dawson, K.A.; Åberg, C. Nanoparticle adhesion to the cell membrane and its effect on nanoparticle uptake efficiency. *J. Am. Chem. Soc.* **2013**, *135*, 1438–1444. [CrossRef]

25. Wagner, P.; Kunz, J.; Koller, A.; Hall, M.N. Active transport of proteins into the nucleus. *FEBS Lett.* **1990**, *275*, 1–5. [CrossRef]

26. Surapaneni, S.K.; Bashir, S.; Tikoo, K. Gold nanoparticles-induced cytotoxicity in triple negative breast cancer involves different epigenetic alterations depending upon the surface charge. *Sci. Rep.* **2018**, *8*, 12295. [CrossRef]

27. Buchegger, F.; Perillo-Adamer, F.; Dupertuis, Y.M.; Delaloye, A.B. Auger radiation targeted into DNA: A therapy perspective. *Eur. J. Nucl. Med. Mol. Imaging* **2006**, *33*, 1352–1363. [CrossRef]

28. Liu, Y.; Li, J.; Chen, M.; Chen, X.; Zheng, N. Palladium-based nanomaterials for cancer imaging and therapy. *Theranostics* **2020**, *10*, 10057–10074. [CrossRef]

29. Chan, C.; Cai, Z.; Reilly, R.M. Trastuzumab labeled to high specific activity with 111In by conjugation to G4 PAMAM dendrimers derivatized with multiple DTPA chelators exhibits increased cytotoxic potency on HER2-positive breast cancer cells. *Pharm. Res.* **2013**, *30*, 1999–2009. [CrossRef]

PUBLICATION NO. 4

Nasrin Abbasi Gharibkandi, Kamil Wawrowicz, Rafał Walczak, Agnieszka Majkowska-Pilip,

Mateusz Wierzbicki, Aleksander Bilewicz

^{109}Pd/^{109m}Ag in-vivo generator in the form of nanoparticles for combined β⁻ - Auger electron therapy of hepatocellular carcinoma

Nasrin Abbasi Gharibkandi[1], Kamil Wawrowicz[2,3], Rafał Walczak[1], Agnieszka Majkowska-Pilip[1,4*], Mateusz Wierzbicki[5] and Aleksander Bilewicz[1*]

*Correspondence:
Agnieszka Majkowska-Pilip
a.majkowska@ichtj.waw.pl
Aleksander Bilewicz
a.bilewicz@ichtj.waw.pl
[1]Centre of Radiochemistry and
Nuclear Chemistry, Institute of
Nuclear Chemistry and Technology,
Dorodna 16 St, Warsaw
03-195, Poland
[2]Department of Medical Physics, M.
Smoluchowski Institute of Physics,
Faculty of Physics, Astronomy
and Applied Computer Science,
Jagiellonian University, Kraków,
Poland
[3]Center for Theranostics,
Jagiellonian University, Kraków,
Poland
[4]Department of Nuclear Medicine,
National Medical Institute of
the Ministry of the Interior and
Administration, Wołoska 137 St,
Warsaw 02-507, Poland
[5]Institute of Biology, Warsaw
University of Life Sciences,
Ciszewskiego 8 St, Warsaw
02-786, Poland

Abstract

Background Convenient therapeutic protocols for hepatocellular carcinoma (HCC) are often ineffective due to late diagnosis and high tumor heterogeneity, leading to poor long-term outcomes. However, recently performed studies suggest that using nanostructures in liver cancer treatment may improve therapeutic effects. Inorganic nanoparticles represent a unique material that tend to accumulate in the liver when introduced in-vivo. Typically, this is a major drawback that prevents the therapeutic use of nanoparticles in medicine. However, in HCC tumours, this may be advantageous because nanoparticles may accumulate in the target organ, where the leaky vasculature of HCC causes their accumulation in tumour cells *via* the EPR effect. On the other hand, recent studies have shown that combining low- and high-LET radiation emitted from the same radionuclide, such as ^{161}Tb, can increase the effectiveness of radionuclide therapy. Therefore, to improve the efficacy of radionuclide therapy for hepatocellular carcinoma, we suggest utilizing radioactive palladium nanoparticles in the form of ^{109}Pd/^{109m}Ag in-vivo generator that simultaneously emits β⁻ particles and Auger electrons.

Results Palladium nanoparticles with a size of 5 nm were synthesized using ^{109}Pd produced through neutron irradiation of natural palladium or enriched ^{108}Pd. Unlike the ^{109}Pd-cyclam complex, where the daughter radionuclide diffuses away from the molecules, ^{109m}Ag remains within the nanoparticles after the decay of ^{109}Pd. In vitro cell studies using radioactive ^{109}Pd nanoparticles revealed that the nanoparticles accumulated inside cells, reaching around 50% total uptake. The ^{109}Pd-PEG nanoparticles exhibited high cytotoxicity, even at low levels of radioactivity (6.25 MBq/mL), resulting in almost complete cell death at 25 MBq/mL. This cytotoxic effect was significantly greater than that of PdNPs labeled with β⁻ (^{131}I) and Auger electron emitters (^{125}I). The metabolic viability of HCC cells was found to be correlated with cell DNA DSBs. Also, successful radioconjugate anticancer activity was observed in three-dimensional tumor spheroids, resulting in a significant treatment response.

Conclusion The results indicate that nanoparticles labeled with ^{109}Pd can be effectively used for combined β⁻ - Auger electron-targeted radionuclide therapy of

HCC. Due to the decay of both components (β⁻ and Auger electrons), the ^{109}Pd/^{109m}Ag in-vivo generator presents a unique potential in this field.

Keywords ^{109}Pd/^{109m}Ag in-vivo generator, Hepatocellular carcinoma, Auger electron therapy, Nanotechnology

Background

Hepatocellular carcinoma (HCC) is the fifth most common cancer and one of the three deadliest cancers worldwide (Torre et al. 2015). Despite considerable progress in cancer therapy, such as targeted and immunotherapies, liver transplantation is still the most efficient option to prolong the life quality in patients with HCC. Surgical resection, radiofrequency ablation, transarterial chemoembolization, radioembolization, and combination approaches are approved treatments for advanced HCC. However, these modalities do not significantly extend life expectancy or prevent disease recurrence (Medavaram and Zhang 2018). Another option - chemotherapy involves drug infusion into the hepatic artery, which is designed to limit side effects to the rest of the body (Chakraborty and Sarkar 2022). Once delivered in this way, a significant dosage of anticancer drugs will be broken down by the healthy liver cells. Although the overall effects of the chemotherapeutic drugs have decreased, some treatment-associated adverse effects still persist, such as hair loss, nausea, and fatigue (Medavaram and Zhang 2018). Additional therapy commonly used for advanced HCC includes broad-spectrum tyrosine kinase inhibitors, such as sorafenib and lenvatinib, as well as a combination of immunotherapy and anti-angiogenesis therapy (Fu and Wang 2018; Greten and Sangro 2018). These strategies offer a nominal extension of the survival curve, but these improvements can be measured in months and result in widely observed toxic side effects, ultimately leading to patients developing resistance to therapy. For this reason, there is a a significant need to design novel therapy options for liver cancer patients who cannot undergo surgical treatment.

Many researchers have shifted their focus to the field of nanotechnology with the aim of addressing this issue. In a review article, Mintz and Leblanc (Mintz and Leblanc 2021) presented over a hundred studies on the possibility of using nanostructures for liver cancer therapy. According to Web of Science, only in 2023, 567 papers containing the keywords "nanoparticles" and "liver cancer" were published. The studies were conducted with both inorganic nanoparticles and carbon-based nanostructures, where the role of nanostructures was either as a drug carrier or the nanoparticles themselves were therapeutic.

The application of nanostructures in liver cancer treatment offers significant advantages, such as reducing therapy-related toxicity and increasing the possibility of precise drug delivery. The common feature of nanoparticles is accumulation in the liver after systemic injection, but this phenomenon depends highly on their properties (Blanco et al. 2015). This remains valid for the majority of nanoparticles, mainly inorganic; however depending on size and charge, some may accumulate in the kidneys and spleen as well (Demoy et al. 1999). As commonly known, blood from the circulation reaches the liver before reaching the kidneys, but not all of the blood supply passes through the liver. Accumulation in the kidneys can be prevented by using negatively charged very small nanoparticles with a hydrodynamic diameter of 6–8 nm, which are not filtered by the kidneys and pass to the liver, where their accumulation is observed (Mintz and Leblanc 2021). Specificity to cancer cells in the liver can be ensured through passive targeting by

utilizing the enhanced permeability and retention (EPR) effect. Due to the EPR effect, small-sized nanoparticle drugs can accumulate more effectively in the tumor than in healthy tissues (Yhee et al. 2013). This phenomenon is possible due to the leaky tumor vasculature through which nanostructures can leave the bloodstream, pass through the gaps in the vessels' endothelial lining, and enter the tumors.

A variety of nanoparticle types, including various metallic ones, have been utilized for the treatment of HCC. Among the ranges studied, platinum nanoparticles proved to be the most advantageous. The use of platinum nanoparticles in cancer therapy seems logical, considering the extensive application of cisplatin in cancer therapy. For instance, Medhat et al. (Medhat et al. 2017) reported that platinum nanoparticles displayed an IC50 value of 10.3 μM, whereas cisplatin showed a value of 26.5 μM, indicating increased chemotherapeutic efficacy of platinum nanoparticles. Moreover, the measured parameters for liver function were notably closer to the control group for platinum nanoparticles compared to cisplatin, indicating reduced side effects.

The main inspiration for our studies described in the present publication was the paper by Wennemers et al. (Shoshan et al. 2019) on the selective toxicity of small platinum nanoparticles against hepatocellular carcinoma cells. The authors explained the strong and selective cytotoxic effect by intracellular oxidation of Pt^0 to Pt^{2+} followed by the release of Pt^{2+} ions from nanoparticles that block cell division by binding to DNA, inducing DNA damage. Therefore, PtNPs are expected to cause substantially higher toxicity in cells with a high oxidation state, thus being highly selective and safe for healthy tissues. Taking into account the redox potential of the reaction $Pt^{2+} + 2e \rightarrow Pt^0 = 1.18$ V, the oxidation of metallic platinum in H_2O_2 solutions cannot be expected. However, as was found in the case of noble metal nanoparticles, small nanoparticles, and metal clusters show significantly greater reactivity in redox (e.g. with H_2O_2) systems than in bigger block structures (Ye et al. 2016).

Since platinum has two radioisotopes, [193m]Pt and [195m]Pt, which are Auger electron emitters, nanoparticles synthesized with these radionuclides should have a multiplied cytotoxic effect. It was found in the metastatic tumor cell studies that both the non-radioactive Pt and [195m]Pt complexes had a considerable therapeutic anticancer effect (expressed as DNA damage in tumor cells). Notably, it was 11-fold higher when Auger-emitting [195m]Pt was used instead of non-radioactive Pt (Nadar et al. 2021). As low-energy Auger electrons exhibit high toxicity only upon intercalation into DNA strands (Aghevlian et al. 2017; Ku et al. 2019), in the case of [193m,195m]Pt nanoparticles, this effect should specifically affect cells with a high concentration of H_2O_2, such as HepG2, whereas postulated (Shoshan et al. 2019) Pt nanoparticles can undergo at least partial dissolution. Consequently, a high selectivity of cytotoxic effects can be achieved. Unfortunately, our recent studies have clearly demonstrated that it is basically impossible to generate sufficient activity of [193m,195m]Pt for application in Auger electron therapy (Wawrowicz and Bilewicz 2023). Due to the expected minimal bone marrow and normal tissue toxicity, very high activities of the radioisotope per patient are administered in targeted Auger radionuclide therapy. For instance, in clinical studies concerning neuroendocrine tumour therapy, patients have received accumulative ^{111}In radioactivity of up to 100 GBq to boost the therapeutic response without any notable side effects (Kwekkeboom et al. 2003). Hence, it can be concluded that it is currently impractical to obtain such activities

of ^{193m,195m}Pt to perform Auger electron therapy, as we discussed previously (Wawrow-icz and Bilewicz 2023) .

Due to the similar d^8 electron configurations and the high chemical similarity of Pt^{2+} and Pd^{2+} cations, palladium nanoparticles are interesting candidates for Auger electron therapy. This includes possible solubility in higher H_2O_2 concentrations. Furthermore, many publications have confirmed the anti-cancer properties of Pd^{2+} cations and their complexes. As a result, the two palladium radionuclides,^{103}Pd and ^{109}Pd, can serve as great alternatives for $^{193\ m,195m}$Pt. Palladium-103, due to the emission of X-ray radiation in the 20–23 keV range, is widely used in seed form for prostate brachytherapy There-fore the methods of its production on both research and industrial scale have already been developed. This radionuclide can be produced by thermal neutron irradiation of the isotopically-enriched ^{102}Pd target in the nuclear reactor or by proton irradiation of ^{103}Rh monoisotopic target. Although ^{103}Pd emits a limited number of Auger electrons, its decay product $-^{103m}$Rh is one of the most promising candidates for Auger electron radiotherapy, according to the reaction (Filosofov et al. 2021; Peter Bernhardt 2001) .

$$^{103}Pd \xrightarrow{EC(branching\ ratio\ 99.97\%)} {}^{103m}Rh \xrightarrow{IT,\ Auger\ electrons} {}^{103}Rh$$
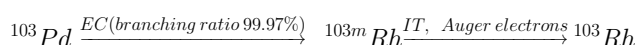
Unfortunately, the short half-life of ^{103m}Rh ($t_{1/2}$=56.11 min) causes challenges and makes it almost impracticable to prepare the ^{103m}Rh radiopharmaceuticals. Nevertheless, it can serve as an in-vivo generator of ^{103}Pd/^{103m}Rh for targeted therapy.

Second palladium radionuclide $-^{109}$Pd, has excellent potential for use in radionuclide therapy. Palladium-109 undergoes β^- decay (β_{max}=1.12 MeV, 100% yield) to ^{109m}Ag ($t_{1/2}$=39.6 s). The formed metastable ^{109m}Ag decays to stable isotope ^{109}Ag which is accompanied by photon emission of 88-keV(3.6%), followed by cascade emission of both conversion and Auger electrons. Such properties enable its simultaneous application in both low- and high-LET internal radiation therapy. This approach relies on the simul-taneous destruction of large tumors using β^- radiation while additionally improving the treatment for tumor subpopulations, including resistant cancer stem cells or small metastases by either Auger electrons or α emitters (Stokke et al. 2022). Recently pub-lished groundbreaking studies by Mueller et al. (Müller et al. 2019) have demonstrated that the utilization of ^{161}Tb can lead to a significantly greater therapeutic effect com-pared to similar studies involving ^{177}Lu. This distinctive feature of ^{161}Tb is based on the simultaneous emission of β^- ($\beta_{max} \sim 550$ keV) and Auger electrons (12.1 e$^-$ per decay), which prevails over the nearly pure β^- emitter ^{177}Lu (β_{max}=497 keV) followed by only a minimal number of Auger/conversion electrons (~ 1.11 electrons per decay) (Müller et al. 2019) .

In this study, we propose the utilization of ^{109}Pd in the form of a ^{109}Pd/^{109m}Ag in-vivo generator as an alternative to ^{161}Tb produced via the indirect route by neutron irradia-tion of ^{160}Gd. The proposed approach involves the application of ^{109}Pd/^{109m}Ag in-vivo generators, which offer advantages over ^{161}Tb due to a greater number of Auger/con-version electrons emission (18 vs. 12.1). Furthermore, in contrast to ^{161}Tb, ^{109}Pd can be simply produced by thermal neutron irradiation. Activation of the enriched metallic Pd target (98% in ^{108}Pd) with a thermal neutron flux of 3×10^{13} n cm^{-2} s^{-1} for three days results in a specific activity of 1.85 GBq/mg and almost 100% radionuclide purity (Das et al. 2008). A high-flux reactor ($>10^{15}$ n cm^{-2} s^{-1}) can boost this yield, increasing the specific activity up to 40 GBq/mg. Contrary to ^{161}Tb, palladium, due to its chemistry,

cannot be used in the form of complexes with the most commonly used chelators, thus its application in NP-based radioconjugates makes it especially convenient to liver cancer therapy.

In previous work, we presented the results of our studies on the use of a radiobioconjugate of gold nanoparticles covered with a [109]Pd layer and attached to the monoclonal antibody trastuzumab (Gharibkandi et al. 2023). The positive results obtained encouraged us to continue our studies oriented at hepatocellular carcinoma (HCC) therapy with small pegylated radioactive [109]Pd nanoparticles. Due to the anticipated dissolution of nanoparticles in HepG2 cells containing elevated levels of H_2O_2, we expected a significant cytotoxic effect. Additionally, our study aimed to deeper investigate whether the radionuclide [109m]Ag formed during the decay of [109]Pd remains within the palladium nanoparticles or diffuses away from them.

Materials and methods

Reagents

The used chemical reagents include: Palladium(II) chloride, (HS–PEG–COOH (poly(ethylene glycol), 5 kDa) from Sigma-Aldrich (St. Louis, MO, USA). Enriched palladium [108]Pd (>99%) was acquired from Isoflex (San Francisco, CA USA). Hydrochloric acid, sodium hydroxide, and hydrogen peroxide 30% were purchased from POCH (Gliwice, Poland).

The following materials were utilized in cell studies: MEM-EAGLE medium, trypsin EDTA solution C, fetal bovine serum (FBS) from Biological Industries (Beth Haemek, Israel); phosphate-buffered saline (PBS), w/o calcium and magnesium, dimethylsulfoxide (DMSO), and the CellTiter 96® Aqueous One Solution Reagent (MTS compound) from Promega (Mannheim, Germany). HepG2 cells were obtained from the American Type Tissue Culture Collection (ATCC, Rockville, MD, USA) and cultured following the ATCC protocol. For experimental applications, over 80% confluent cells were used. Cells were maintained in MEM-EAGLE medium enriched with 10% heat-inactivated fetal bovine serum, 1% L-glutamine (200 mM), and antibiotics (penicillin 100 IU/mL and streptomycin 100 μg/mL).

Anti-phospho-Histone H2A.X (Ser139) antibody, clone JBW301; anti-mouse IgG (H+L), CF™ 633 antibody produced in goat were used to prepare samples for DNA double strand breaks study. Other reagents for DNA double strand breaks study included 4% paraformaldehyde (PFA) in PBS as fixative, bovine serum albumin (BSA), Triton X-100, and TBS (tris buffered saline) purchased from Merck & Co., Inc. (Kenilworth, NJ, USA). DAKO Fluorescent Mounting Medium was obtained from Agilent Technologies (Santa Clara, CA, USA). For DNA staining, Hoechst 33,258, purchased from Thermo Fischer Scientific (Waltham, MA, USA), was used. All solutions were prepared using double-distilled water (18.2 MΩ·cm, Hydrolab, Straszyn, Poland).

Instruments

The size and morphology of nanoparticles were examined using a Zeiss Libra 120 Plus TEM operating at 120 kV (Zeiss, Stuttgart, Germany). The DLS method was used to analyze the hydrodynamic size of the synthesized nanoparticles and their conjugates with PEG. The hydrodynamic diameter and zeta potential measurements were conducted in 1 mM PBS pH 7.4 buffer using a Zetasizer Nano ZS (Malvern Panalytical, Malvern,

Worcestershire, UK). The MTS assay absorbance values were evaluated at 490 nm *via* an Apollo 11LB913 microplate reader (Berthold, Bad Wildbad, Germany). The radioactivity of samples was measured using Wizard® 2 automatic gamma counter (Perkin Elmer, Waltham, MA, USA) and an HPGe detector connected to a PC-based Multichannel Analyzer (MCA, Canberra).

Instrumental thin layer chromatography (iTLC) analyses were performed with the use of Storage Phosphor System Cyclone Plus (Perkin Elmer, Waltham, MA, USA), glass microfiber chromatography paper impregnated with silica gel (iTLC SG, Agilent Technologies, Santa Clara, CA, USA), and methyl alcohol (MeOH) as mobile phase. Analyses were performed in experiments of ^{109}PdNPs dissolution in H_2O_2 as well as, during stability studies. For additional radiochemical yield evaluation, we centrifuged nanoparticles after each synthesis step and measured the activity of collected fractions.

Radionuclides

^{109}Pd was produced by thermal neutron ($1-2\times10^{14}$ n cm^{-2} s^{-1}) irradiation of a natural palladium target (~3 mg, metal powder) or enriched ^{108}Pd (>99%) (~1 mg, metal powder) in the Maria nuclear reactor (Otwock-Świerk, Poland) for 7 h. Following an 8-hour cooling time, the radioactive palladium was dissolved in 200–400 µL of aqua regia (HNO$_3$:HCl–1:3) and heated at 130 °C to get almost completely evaporated. The remaining nitrates were removed by dissolving the residues in 0.1 M HCl three times (100 µL) and heating at 130 °C until almost complete evaporation. Finally, the residual material was reconstituted in 1 mL of 6 M HCl resulting in the formation of H_2PdCl_4.

Since the neutron irradiation of the natural Pd target can result in the formation of ^{111}Ag as an impurity in the reaction of ^{110}Pd(n,γ)^{111}Pd $\rightarrow$ ^{111}Ag, it is essential to remove it from the solution before application (Das et al. 2012). The removal of ^{111}Ag can be accomplished by precipitating it as AgCl using AgNO$_3$ in the modified procedure reported by Das et al. (Das et al. 2012). Briefly, 100 µL of 0.1 M AgNO$_3$ solution in 0.1 M HNO$_3$ (20 mg/ mL) was added to 1 mL solution of PdCl$_4^{2-}$ in 6 M HCl. After 2 min, the AgCl precipitate was centrifuged (4600 rpm, 5 min), and the obtained supernatant was carefully separated from the precipitate AgCl through the pipette. followed by evaporation until complete drying. Subsequently, the procedure was repeated using deionized H_2O. At last, the palladium was suspended in a 0.1 M HCl (100 µL). The activity and radionuclide purity of the obtained ^{109}Pd were determined by gamma-ray spectrometry. The diluted solutions gained after radiochemical processing of the irradiated target were measured using an HPGe detector connected to a PC-based Multichannel Analyzer (MCA, Canberra). The 88 keV (3.67%) gamma peak emitted by ^{109m}Ag was used for the estimation of the radioactivity of ^{109}Pd. Nevertheless, due to the very low content of the ^{111}Ag radionuclide, the silver removal procedure is unnecessary when using an isotopically enriched ^{108}Pd target.

Iodine radionuclides, ^{125}I (t$_{1/2}$ = 59.5 d) and ^{131}I (t$_{1/2}$ = 8.01 d), which were utilized for comparative cytotoxicity studies, were obtained from the National Centre for Nuclear Research, POLATOM Radioisotope Centre (Świerk, Poland). The specific activity was >600 GBq/mg and >550 GBq/mg for ^{125}I and ^{131}I, respectively. Both radionuclides were supplied in an aqueous solution of sodium iodide (NaI) with a pH of around 10–12, adjusted using sodium hydroxide or sodium carbonate buffer.

Synthesis of 5 nm palladium – PEG nanoparticles

Palladium nanoparticles (PdNPs) were synthesized according to the modified method described in the paper (Jung et al. 2017). Briefly, 5.3 mg of $PdCl_2$ was dissolved in HCl (1.2 M, 500 µL) and stirred at room temperature. Following dissolution, the Pd solution was diluted by adding 53.5 mL of H_2O. Subsequently, a freshly prepared $NaBH_4$ solution (3.5 M, 5mL) was added to the mixture and stirred for 20 min. Finally, an aqueous solution of polyvinylpyrrolidone (PVP) (4.8 M, 21mL) was added, and stirring was continued for 1 h at room temperature. Considering the spherical shape, 5 nm diameter of the nanoparticles, and a Pd density of 12.02 g/cm^3, the concentration of nanoparticles was calculated to be about 2.9×10^{13} PdNPs in 1 mL.

Radioactive nanoparticles were synthesized through the same procedure, using correspondingly smaller amounts of reagents. Both radioactive and non-radioactive PdNPs were stabilized by polyethylene glycol (PEG-COOH) chains using the following procedure: the synthesized PdNPs (5 nm) were combined with a 200 molar excess of HS−PEG−COOH (5 kDa) and stirred for 30 min. Afterwards, the nanoparticles were purified by centrifugation at 10,000 rpm for 10 min using Vivaspin 500 centrifugal filters with a 10,000 MWCO polyethersulfone (PES) membrane.

To conduct comparative experiments, the PEGylated Pd nanoparticles labelled with radionuclides ^{125}I (Auger emitter) and ^{131}I (β^- and γ emitter) were synthesized as well. To accomplish this, 10 mL of the previously obtained Pd-PEG NPs (5 nm) were redispersed in deionized water. Subsequently, either ^{125}I or ^{131}I was added (300MBq), and the reaction was kept at room temperature for 1 h with continuous stirring. At last, HS-PEG-COOH (MW=5 kDa) was introduced to the solution of NPs with the desired excess, and the reaction was continued for the next 30 min.

Stability studies of Pd-PEG nanoparticles

The colloidal stability of the PEGylated PdNPs dispersion in 10 mM PBS buffer was evaluated at 37 °C for 16 days. The aggregation tendency was examined by assessing hydrodynamic diameter and zeta potential variations using the Dynamic Light Scattering (DLS) technique. Due to technical limitations, the application of protein-containing solutions, such as serum, was not allowed.

Studies on the recoil of ^{109m}Ag from ^{109}Pd nanoparticles and ^{109}Pd-cyclam complex

To investigate the liberation of ^{109m}Ag from $^{109}PdNPs$, they were incubated in both water and PBS buffer (1 mM). The initial radioactivity of the $^{109}PdNPs$ solution was 4.8×10^4 cpm. The nanoparticles were precipitated from the solution by adding 1 M NaCl and subsequent centrifugation (13 400 rpm, 40 s). To determine the released ^{109m}Ag from NPs, the supernatant was immediately measured after separation using NaI (Tl) scintillation detectors at 15 s intervals. The measurement started 164 s after the precipitation of nanoparticles, which is comparable to four half-lives of ^{109m}Ag.

For comparison, we examined a system in which $^{109}Pd^{2+}$ was complexed with cyclam (1,4,8,11-tetraazacyclotetradecane; $C_{10}H_{24}N_4$; 200.33 g/mol) to form a stable complex (log K_{ML}=56.9 (Harrington et al. 2005)). In this case, the following original procedure for studies of liberation ^{109m}Ag was applied: 10 µL of ^{109}Pd-cyclam complex was added into a centrifuge tube containing 1 mL of NaCl solution, resulting in radioactivity of ^{109}Pd-cyclam solution around 7.5×10^4 cpm. Following that, 100 µL of 0.1 M $AgNO_3$ solution

in 0.1 M HNO_3 (20 mg/ mL) was added, and the solution was promptly mixed using a vortex shaker. The formed AgCl precipitate was then centrifuged (13 400 rpm, 40 s). The obtained supernatant was carefully separated from the precipitate, and AgCl was dispersed in 1 mL H_2O. The radioactivity measurement began 139 s after the precipitation of nanoparticles, i.e. after 3.5 half-lives of ^{109m}Ag, and was measured successively at 15 s intervals.

PdNPs dissolution in a highly oxidative environment

To verify the concept of the dissolution of PdNPs in elevated concentrations of H_2O_2, selected concentrations of hydrogen peroxide were prepared by diluting a stock solution (30%) with deionized water. Then, nanoparticles were dispersed directly in prepared H_2O_2 solutions and incubated for 24 h at 37°C. Afterwards, the radioactivity of $^{109}PdNPs$ and the released free $^{109}Pd^{2+}$ cations were measured using iTLC, as described above.

Internalization studies

Internalization studies were conducted on HepG2 cells. Briefly, a total of 6×10^5 cells/ well were seeded into 6-well plates and incubated overnight at 37 °C and 5% CO_2. Following this step, the cells were rinsed with PBS, and the main test compounds (1 mL) were added and incubated at 4 °C for 1 h to prevent any internalization. Subsequently, the medium was collected into the tubes as the unbound portion and replaced with 1 mL of fresh medium. The plates were then incubated (37 °C, 5% CO_2) at different time points of 6, 18, and 24 h. To determine the membrane-bound fraction, cells were rinsed twice with glycine-HCl buffer (pH ~ 2.8; 0.05 M) for 5 min at 4 °C. Eventually, the internalized fraction was collected by lysing the cells with a solution of 1 M NaOH.

Cytotoxicity studies

The MTS test was used to perform cytotoxicity assays on HepG2 cells (10^4 cells per well in 96-well plates). The preparation procedure was analogous to that described for the internalization studies. Both non-radioactive (9–150 μg Pd/mL) and radioactive compounds (180 μg Pd/mL for 40 MBq/mL, 90 μg Pd/mL for 20 MBq/mL, 45 μg Pd/mL for 10 MBq/mL) were suspended in fully supplemented growing medium, and 100 μL per well was added for 24–72 h incubation. Afterwards, the medium was replaced with fresh medium (100 μL/well) prior to MTS reagent addition (20 μL/well). The percentage of metabolically active cells was assessed by the addition of CellTiter96® Aqueous One Solution Reagent and the measurement of the absorbance at 490 nm.

Double-strand breaks analysis

To assess the extent of DNA DSBs (double-strand breaks) induced by $^{109}PdNPs$ treatment, staining of phosphorylated H2A histone family member X (γH2A.X) was conducted. HepG$_2$ cells with a density of 2.5×10^5 per well were seeded into six-well plates with five sterile glass coverslips per well (∅ 12 mm, Thermo Fischer Scientific (Waltham, MA, USA) and then incubated overnight. After the removal of the medium, cells were treated with compounds at different concentrations (0–180 μg/mL, 0–20 MBq/mL, and 0-100 MBq/mL of Pd-PEG, ^{109}Pd-PEG, and ^{131}I-Pd-PEG NPs, respectively), and staurosporine (0.5 μM) as a positive control, followed by incubation for 4 and 24 h. The protocol used was similar to the one described in a previous report (Wawrowicz et al. 2023).

For γH2A.X foci detection, the primary antiphospho-Histone H2A.X (Ser139) antibody, clone JBW301, was diluted to a ratio of 1:100 with blocking buffer (BB- 4% BSA in TBS) and 350 μL of that was added to each well and incubated overnight at 4 ℃. The next day, the primary antibody was switched with an anti-mouse IgG secondary antibody conjugated with CFTM 633. The antibody was dissolved in a blocking buffer according to the manufacturer's instructions. The cells were then incubated for two h at room temperature with mixing. Finally, cells were rinsed 3 times with water, followed by nuclei staining with Hoechst 33258. The imaging was performed using an FV-1000 confocal microscope (Olympus Corporation, Tokyo, Japan) with ex/mm maxima: 630/650 nm for CF633 and ex/em maxima: 352/454 nm for Hoechst 33258. The results were analysed using the Fiji 2.9.0 version.

^{109}PdNPs effects on 3D tumor spheroid model

HepG2 cells (1×10^3) were cultured on 96-well U-bottom ultra-low adherent plates (Corning®, Corning, NY, USA) with 200 μL of growing medium for seven days ahead of the experiment, as previously reported (Wawrowicz et al. 2023). During the incubation period, 100 μL of the medium was replaced with fresh medium every two days. After seven days, both radioconjugates and non-radioactive compounds were added into the growing medium (100 μL). All the images were taken and analyzed with a ZEISS Axio-Vert. A1 Microscope and ZEN 2.1 software (Zeiss, Jena, Germany).

Statistical analysis

For statistical analysis, one-way ANOVA and t-Student tests were performed with GraphPad Prism v.8 Software (GraphPad Software, San Diego, CA, USA). The results are presented as mean $\pm$ SD. *p* values are presented as: (*) $p \leq 0.05$, (**) $p \leq 0.01$, (***) $p \leq 0.001$, and (****) $p \leq 0.0001$.

Results and discussion

Production of ^{109}Pd

Due to a cross-section of 12.2 b (Boros and Packard 2019), large quantities of ^{109}Pd can be produced in a nuclear reactor through the ^{108}Pd(n,γ) reaction. Using natural palladium as a target material, after seven hours of irradiation at a flux of $1-2 \times 10^{14}$ n cm^{-2} s^{-1}, more than 500 MBq/mg of ^{109}Pd was obtained. In the case of enriched 98% ^{108}Pd target material, the obtained radioactivity exceeded 2 GBq/mg. In the gamma-ray spectrum of the irradiated natural target recorded before radiochemical processing, photopeaks characteristic of ^{109}Pd (22.1 and 24.8 keV) and ^{109m}Ag (88.2 keV) can be seen. Additionally, small peaks from ^{111}Ag (96, 245, and 342 keV) impurity formed in reaction ^{110}Pd(n,γ)^{111}Pd $\rightarrow$ ^{111}Ag can be obseʳved. The impurity from ^{103}Pd formed from the ^{102}Pd(n,γ) reaction is negligible due to the low abundance of ^{102}Pd (1%) and neutron low cross section. The separation of ^{111}Ag by co-precipitation with AgCl was very effective, and the gamma-ray spectrum of the ^{109}Pd solution after radiochemical processing did not show any gamma photo-peaks characteristic of ^{111}Ag. This indicates that ^{109}Pd was obtained with nearly 100% radionuclidic purity. The average radiochemical yield of ^{109}Pd after the radiochemical separation of silver was found to be approximately 80%.

^{109}Pd, which was obtained by neutron activation, was utilized in the synthesis of 5 nm radioactive PdNPs. It is estimated that the mass of one of the 5 nm nanoparticles is

7.9×10^{-18} g, and it can be assumed that it contains 4.4×10^4 Pd atoms, with 1–2 being radioactive. By using a high-flux reactor with a neutron flux of 10^{15} n/cm^2/s and a longer irradiation time, the number of ^{109}Pd atoms in the nanoparticle increases to 20–30.

Synthesis and characterization of 5 nm Pd-PEG nanoparticles

Due to the strong affinity of thiol groups to palladium atoms, PVP molecules were completely displaced on the surface of nanoparticles. The synthesized PEGylated 5 nm (Pd-PEG NPs) are stable in solutions because the PEG molecules stopping layer on the PdNPs surface provides an electrostatic repulsion force resulting from the electric double layer.

The same procedure was followed to synthesize radioactive nanoparticles using ^{109}PdCl$_2$. As a result of the synthesis, ^{109}PdNP-PEG–COOH nanoparticles with activity 10 MBq/mg (0.9 GBq/nmol NP) were obtained.

Synthesized PdNP-PEG–COOH nanoparticles were characterized using TEM and DLS methods. Figure 1 shows that the particles have a size of approximately 5 nm based on transmission electron microscopy. It was not possible to observe the "corona" around the Pd-NPs due to the poor interaction of the electron beam with the PEG molecules (low electron density), in contrast to the strong scattering of the electron beam when it interacted with metallic nanoparticles.

The hydrodynamic diameter of PEGylated PdNPs was around 40 nm, as determined by DLS in PBS solution, and was notably larger than the diameter measured by TEM. As both of the applied techniques are based on different approaches, within DLS it is possible to identify the polymer presence on the outer surface of nanoparticles, thus the diameter measured with this method directly reflects the PEG chains located on PdNPs surface, leading to increased size. The zeta potential of PdNP-PEG-COOH was -19.9 ± 1.57 mV and the negative value of this potential indicates that the particles repel each other, contributing to the considerable stability of the colloid. Moreover, negative surface charge makes them suitable candidates for liver treatment by preventing kidney accumulation. As shown in Fig. 2, the particles do not tend to aggregate until 10 days, which was confirmed by the lack of changes in hydrodynamic diameter during a whole experimental assessment.

Liberation of ^{109m}Ag from ^{109}Pd nanoparticles

When using in-vivo generators in nuclear medicine, it is important to consider the behavior of the daughter radionuclide after radioactive decay. In our previously published paper, we studied liberation of ^{109m}Ag from core-shell Au@^{109}Pd nanoparticles (Gharibkandi et al. 2023). Current research aimed for deeper investigation of this topic
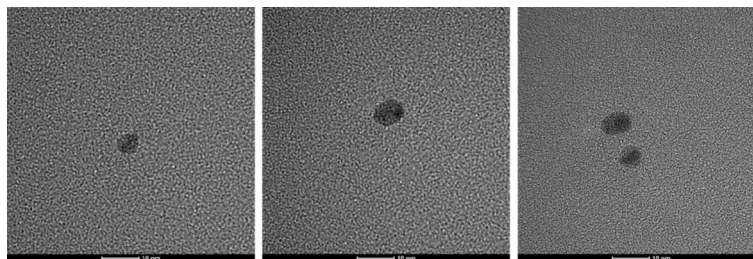

Fig. 1 Transmission electron microscopy images of PdNP-PEG–COOH nanoparticle. Scale bars correspond to 10 nm
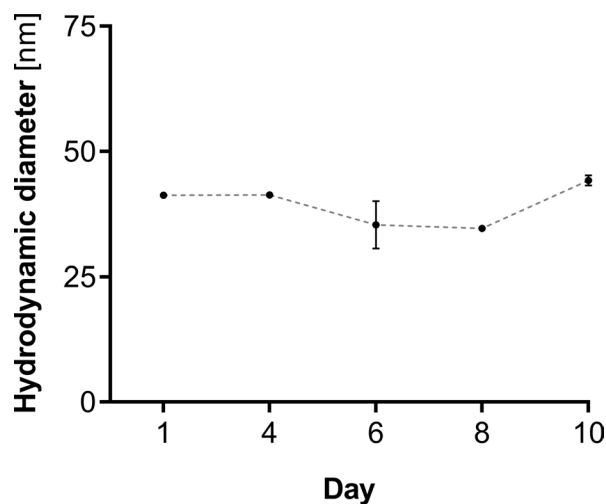
Fig. 2 Changes in the hydrodynamic diameter of the Pd-PEG nanoparticles incubated in 10 mM PBS buffer
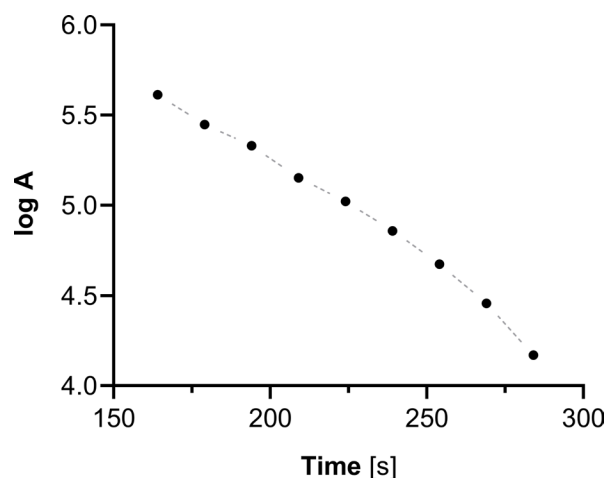

Fig. 3 Decay curve of AgCl precipitated from the ^{109}Pd-cyclam complex solution. The measurement started 2 min and 44 s after the addition of AgNO$_3$, which corresponds to four half-lives of ^{109m}Ag. The radioactivity of the AgCl was measured successively at 15-second intervals. Activity in cpm

and comparison the behavior of the ^{109m}Ag daughter radionuclide after the radioactive decay of ^{109}Pd on ^{109}PdNPs (5 nm) and in the ^{109}Pd-cyclam complex.

Our initial studies, which involved binding of ^{109}Pd to a biomolecule using the macrocyclic cyclam, demonstrated the complete release of ^{109m}Ag from the complex. Figure 3 illustrates the decay curve of ^{109m}AgCl precipitated from the solution of the ^{109}Pd-cyclam complex. By extrapolating the activity to time zero, we observed that the estimated activity of ^{109m}Ag is equivalent to the activity of ^{109}Pd in the complex. Therefore, despite its short half-life of 39 s, ^{109m}Ag can diffuse away from the target site and affect healthy cells.

To prevent the diffusion of ^{109m}Ag from the target site, we propose a solution involving the use of a ^{109}Pd/^{109m}Ag in-vivo generator in the form of 5 nm ^{109}Pd nanoparticles. In contrast to chelator-based in-vivo generators, we found complete retention of ^{109m}Ag on Pd nanoparticles. While the parent radionuclide is incorporated into a metallic nanoparticle instead of a chelate complex, we do not observe the liberation of ^{109m}Ag from the

nanoparticles, as shown in Fig. 4. The constant level of radioactivity is attributed to the presence of nanoparticle residues after a short centrifugation time (13400 rpm, 40 s.).

^{109}PdNPs dissolution in a highly oxidative environment

To verify the concept of PdNPs dissolution in HepG2 cells with elevated H_2O_2 concentrations, as described in the introduction, we conducted studies of the behavior of PdNPs in a wide range of H_2O_2 concentrations. The concentration of H_2O_2 in normal cells is generally in the nanomolar range (Sies 2017). Therefore, we launched our investigations at a concentration of 10 nM and implemented also higher concentrations of up to 10 mM. Figure 5 shows iTLC strips for different H_2O_2 concentrations. If the ^{109}PdNPs nanoparticles were dissolved, we would observe migrating $^{109}Pd^{2+}$ cations with the solvent front. However, for all of the tested H_2O_2 concentrations, radioactivity remained at the site of application. This indicates the lack of dissolution of ^{109}PdNPs, even in solutions with high H_2O_2 levels.

Internalization of ^{109}Pd-PEG nanoparticles

Internalization to the cell nucleolus or localization on the cell membrane is crucial for effective Auger electron radionuclide therapy (Ku et al. 2019b). As investigated NPs do not undergo even partial dissolution in highly oxidative environment, we aimed to verify whether, due to their small diameter, they are able to passively penetrate the nuclear membrane. The performed studies using radioactive ^{109}Pd nanoparticles revealed that the nanoparticles accumulated inside the cells in a time-dependent manner. Radioconjugate uptake, reaching approximately 5% after six h, was significantly ($p \leq 0.01$) enhanced after 18 h ($\sim$15%) and maintained almost unchanged ($p = 0.9379$) after 24 h (Fig. 6A). As shown in Fig. 6B, over 75% of the total bound fraction was subsequently internalized starting from first investigated time point. This process progressed over time, leading to over 95% and 98% internalization after 18 and 24 h, respectively. Therefore, our studies showed that PEGylated nanoparticles can successfully penetrate the HCC cell membrane without the need for internalizing vectors.

In our subsequent studies, we aimed to determine the proportion of Pd internalized into the nucleus from the cell cytosol. To assess the efficiency of internalization, we extracted cell nuclei fractions from HepG2 cells that were treated with ^{109}Pd-PEG
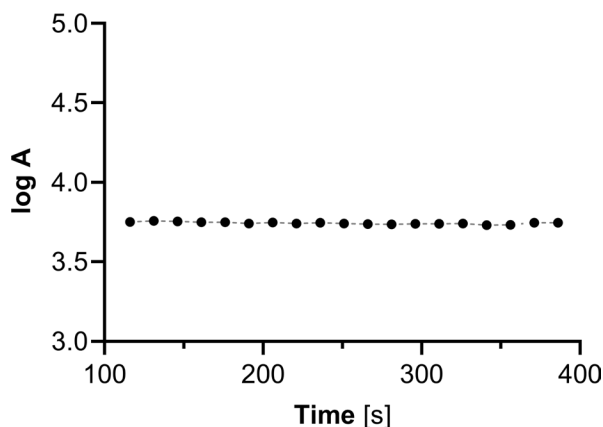

Fig. 4 Activity of the supernatant after precipitation of the nanoparticles by 1 M NaCl solution. The measurement started 116 s after the addition of NaCl, which corresponds to three half-lives of ^{109m}Ag. The radioactivity of the supernatant was measured successively at 15-second intervals. Activity in cpm
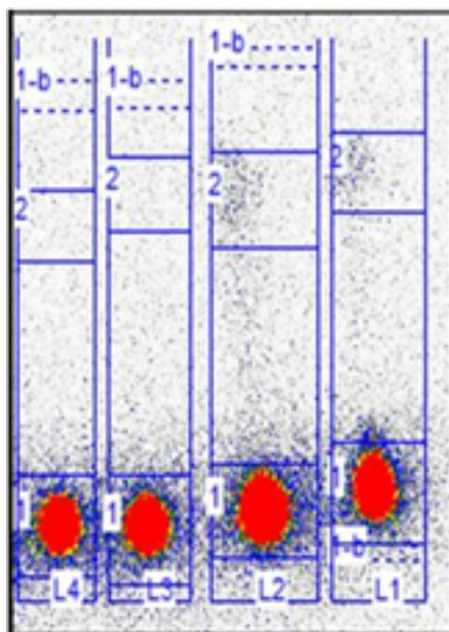
Fig. 5 The iTLC strips illustrate the lack of dissolution of 109PdNPs in H2O2 solutions. L4 strip is for concentration H$_2$O$_2$ 10 mM, L3 for 10μM, L2 for 10 nM and L1 for human serum. Incubation time 24 h at 37°C
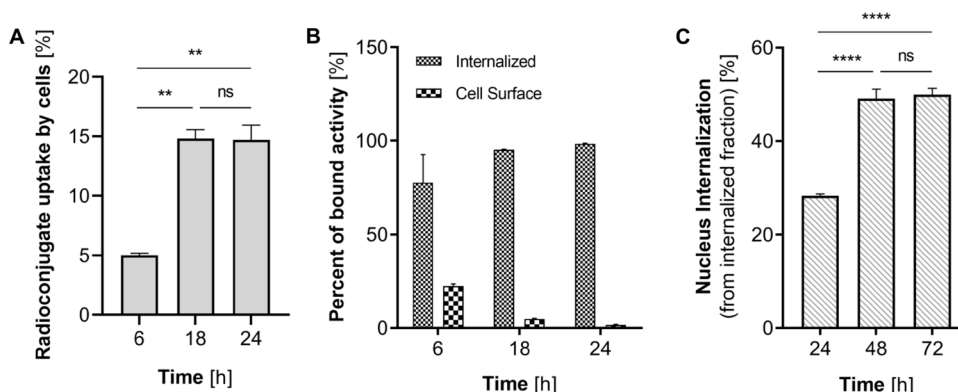

Fig. 6 ^{109}PdNPs bound to HepG2 cells (**A**); percent of bound activity that was later internalized to the cells (**B**); intranuclear uptake of synthesized radioconjugates (**C**)

NPs and measured the intracellular ^{109}Pd radioactivity after 24, 48, and 72 h of incubation (Fig. 6C). Approximately 28% of the internalized ^{109}Pd in the cytosol was efficiently transferred to the nucleus after 24 h. This process significantly increased to almost 50% after 48 h ($p \leq$ 0.0001).

As it is well-known, the nucleus is separated from the cytosol by the double nuclear membrane, which contains 2000 to 5000 specialized channels called nuclear pore complexes through which transport to and from nucleus occurs. The 5 nm Pd-PEG nanoparticles are hydrophilic and thus able to passively diffuse into the cell nucleus, as confirmed by Fig. 6C and previously discussed research. Due to the presence of radioactive ^{109}Pd-PEG nanoparticles in the nucleus, it was expected to effectively increase its cytotoxicity through the interaction of Auger electrons or formed oxygen radicals with DNA.

In vitro toxicity

The viability of HepG2 cells incubated with non-radioactive Pd-PEG-NPs and ^{109}Pd-PEG-NPs was evaluated using the MTS assay. Nonradioactive Pd–PEG bioconjugates were used with various concentrations 11.25 µg/mL (3×10^{-3} nmol/mL NP) to 180 µg/mL (0.05 nmol/mL NP). These studies aimed to investigate whether non-radioactive Pd-PEG can lead to mitochondrial dysfunction and cell death. As shown in Fig. 7, almost no significant reduction in mitochondrial activity was found with doses up to 45 µg/mL of Pd-PEG NPs. In higher concentrations, the viability of cells gradually decreased with the increase of Pd concentration, reaching below 25% viability at the remarkably high concentration of 180 µg/mL. It is important to note that the most meaningful changes were identified after 72 h. Similar results were obtained by Rajakumar et al.(Rajakumar et al. 2015) studying 60 nm PdNPs on HepG2 cells. Interestingly, the toxicity levels were found to be similar to that of cationic Pd^{2+}. The comparison between the cytotoxicity of PdNPs and 2 nm platinum nanoparticles and 30 nm core shell Au@PtNPs on HepG2 cells indicated slightly higher cytotoxicity induced by PdNPs compared to both 2 nm PtNPs and 30 nm Au@PtNPs (Wawrowicz et al. 2022).

In the cytotoxicity studies of radioactive ^{109}Pd-PEG, we used nanoparticles with radio-activities ranging from 11.25 MBq/mL to 100 MBq/mL. In these experiments, the concentration of PdNPs varied from 22.5 µg/mL to 180 µg/mL. Figure 7 shows that if the mass concentration exceeds 22.5 µg/mL, PdNPs may exhibit chemical toxicity in addition to radiotoxicity, especially after 72 h of incubation.

We observed a significantly stronger cytotoxic effect when the radioactive ^{109}Pd-PEG interacted with HepG2 cells than nonradioactive compounds. Figure 8 illustrates the dependence of cell viability on the radioactivity of ^{109}Pd-PEG. As demonstrated, toxicity in a dose-dependent manner, progressing over time was observed. Furthermore, even at the lowest radioactivity level of 6.25 MBq/mL ^{109}PdNP-PEG, a significant inhibition of cell metabolic activity was observed (6% after 72 h, $p \leq 0.001$). Extended incubation resulted in a constant reduction in mitochondrial activity, leading to almost complete cell death with <5% of unaffected mitochondrial function at 25 MBq/mL. By comparing the data presented in Figs. 7 and 8, it is obvious that the cytotoxic effect caused by the chemical generation of reactive oxygen species (ROS) is negligible compared to the radiotoxic effect presented in Fig. 8.

As we discussed earlier, the ^{109}Pd/^{109m}Ag in-vivo generator, similarly to ^{161}Tb, emits together β$^-$ particles and Auger electrons. To verify the superior therapeutic efficacy
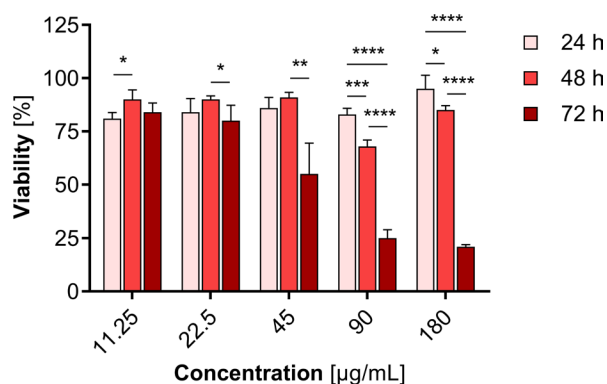

Fig. 7 Metabolic activity of HepG2 cells after treatment with different concentrations of nonradioactive Pd-PEG after 24 h 48 h and 72 h
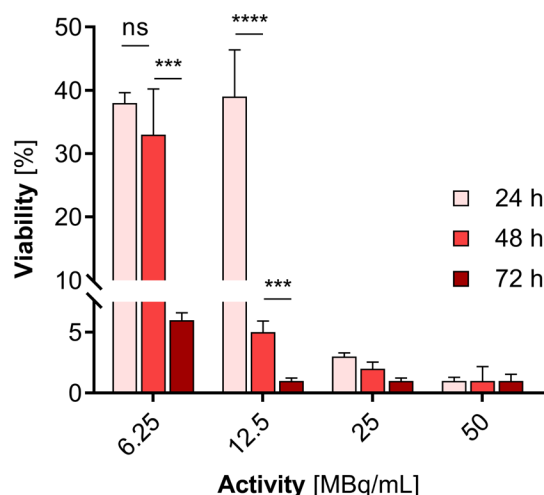
Fig. 8 Metabolic viability of HepG2 cells after treatment with different radioactive doses of [109]Pd-PEG after 24 h, 48 h, and 72 h treatment
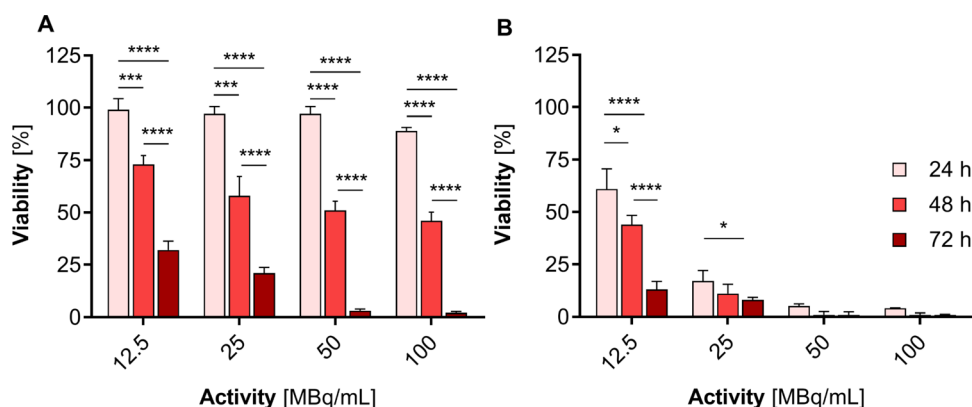

Fig. 9 Metabolic viability of HepG2 cells after treatment with different radioactive doses of ^{125}I-Pd-PEG (**A**) and ^{131}I-Pd-PEG (**B**) radio conjugates

with simultaneous emission of β^- particles, conversion, and Auger electrons in comparison with using β^- or Auger electron emitters with the same activity alone, we performed cytotoxicity experiments using Pd nanoparticles labeled with [125]I (Auger electrons, γ emitters) and [131]I (β^-, γ emitters) radionuclides.

It was possible to attach ^{125}I and ^{131}I to the surface of Pd NPs by exploiting the strong affinity between noble metals and iodine atoms. Figure 9 presents the results of MTS tests conducted on HepG2 cells using both ^{131}I-Pd-PEG and ^{125}I-Pd-PEG radioactive NPs. Our findings indicate that PdNPs labeled with [109]Pd, despite its shorter half-life and the smallest number of radioactive decays during cytotoxicity examination, were significantly more cytotoxic than those labeled with either ^{131}I or [125]I. We observed a similar effect in cytotoxicity studies of the Au@[109]Pd core–shell nanoparticles conjugated to trastuzumab, which showed greater efficacy compared to [198]AuNPs-trastuzumab (emitting β^- particles) (Gharibkandi et al. 2023). These findings prove that the therapeutic efficacy of medium-energy β electrons can be significantly improved by adding short-range Auger electrons, as is in the case with [161]Tb-based radiopharmaceuticals.

It should be noted that the comparison of cytotoxicity between the data presented in Figs. 8 and 9 is only an approximation because the half-life of the radionuclides and the energy have not been considered. Furthermore, the emitted γ radiation was neglected due to its insignificance in comparison to corpuscular radiation. However, the obtained results clearly demonstrate that the cytotoxicity of [109]Pd - a mixed radiation emitter (β[-], Auger) is much greater than that of Auger electron and β[-] radiation emitters, assuming the same activities.

Radiotoxicity studies on 3D tumor spheroid model

In contrast to monolayer cultures, three-dimensional (3D) cell cultures better mimic tissue physiology and exhibit the characteristics of poorly perfused tumors. These models are suitable for evaluating the effectiveness of anticancer drugs (Białkowska et al. 2020). Hence, we also conducted cytotoxicity studies on spheroids formed from HepG2 cells incubated with [109m]Pd-PEG nanoparticles. In Fig. 10 we present microscopic images of the spheroids treated with [109]Pd-PEG NPs and changes in tumor areas continuously measured for 30 days. Remarkable surface changes were observed in the spheroids of both treated and control samples. The area of the control samples increased ∼ 2.5 times during the 30 days of observation. In the treated samples, the initial signs of tumor growth inhibition were observed 72 h after NPs injection. Despite the relatively short half-life of [109]Pd (13.7 h), the growth of spheroids was inhibited until day 30 of the study. For all tested concentrations, inhibition of tumor growth was found. However, we also observed the shrinkage of spheroids for samples treated with higher activities of 25 MBq/mL and 50 MBq/mL.

DNA double-strand breaks (DSBs)

Damage to the genetic materials is considered as one of the most important effects in radionuclide therapy. Single-strand breaks (SSBs) and especially double-strand breaks (DSBs) are the two primary and most desired damages that can occur in the DNA molecule. These breaks can occur through direct ionization of the DNA caused by ionizing radiation (direct effects) or by the interaction of reactive oxygen radicals generated from water with the DNA strand (indirect effects). In our study, we compared the induction of DSBs following exposure to β[−] radiation emitted from ^{131}I-PdNPs and β[−] and Auger electrons emitted by [109]Pd. The phosphorylation of the H2A.X occurs at one of the initial
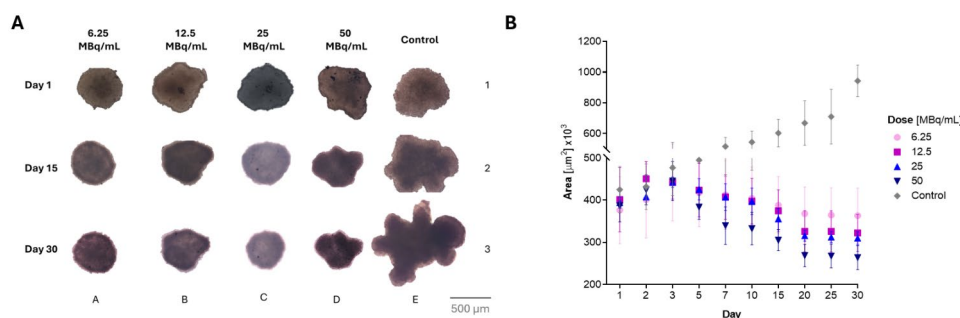
Fig. 10 Effects of [109]Pd-PEG radioconjugates against HepG2 tumor spheroid model. (**A**). Microscope images of representative spheroids - structures extracted from the background due to differences in contrast. All photos were taken using a 10X lens. However, the last photo (panel 3D) was taken using a 4X objective due to the high increase in the spheroid size of the control group and subsequently reconstructed; (**B**) Time dependence spheroids growth

stages in the DSB repair pathway. As a result, the scoring of phosphorylated histone (γH2A.X) foci is widely utilized to quantify DSBs. H2A.X phosphorylation happens at the site of DSB immediately after its formation and can be seen under a microscope as distinct foci after antibody labeling as described before (Hernández et al. 2013).

DNA DSBs found in HepG2 cells visualized with γH2A.X foci after treatment with non-radioactive Pd-PEG NPs (A-C), radioactive [109]Pd-PEG (D-F), and ^{131}I-Pd-PEG NPs (G-I) are presented in Fig. 11.

A growing number of DSBs cells was found after treatment of HepG2 cells with [109]Pd-PEG NPs starting from radioactivity 1.25 MBq/mL. In the case of ^{131}I-Pd-PEG nanoparticles, DSBs formation is observed starting from a concentration of 6.25 MBq/mL, with a much smaller DSBs number occurring. Considering the redox activity of PdNPs, we could also expect an increased DSB ratio in cells after treatment with the nonradioactive compound. It is widely reported that ROS may induce severe DNA damage, also including DNA DSBs. However, as can be seen in Fig. 11, in the concentration range up to 90 µg/mL, the number of DSBs remains at the level of the control sample. Only at a concentration of 180 ug/mL we identified a significant number of γH2A.X foci both after 4 h and 24 h.
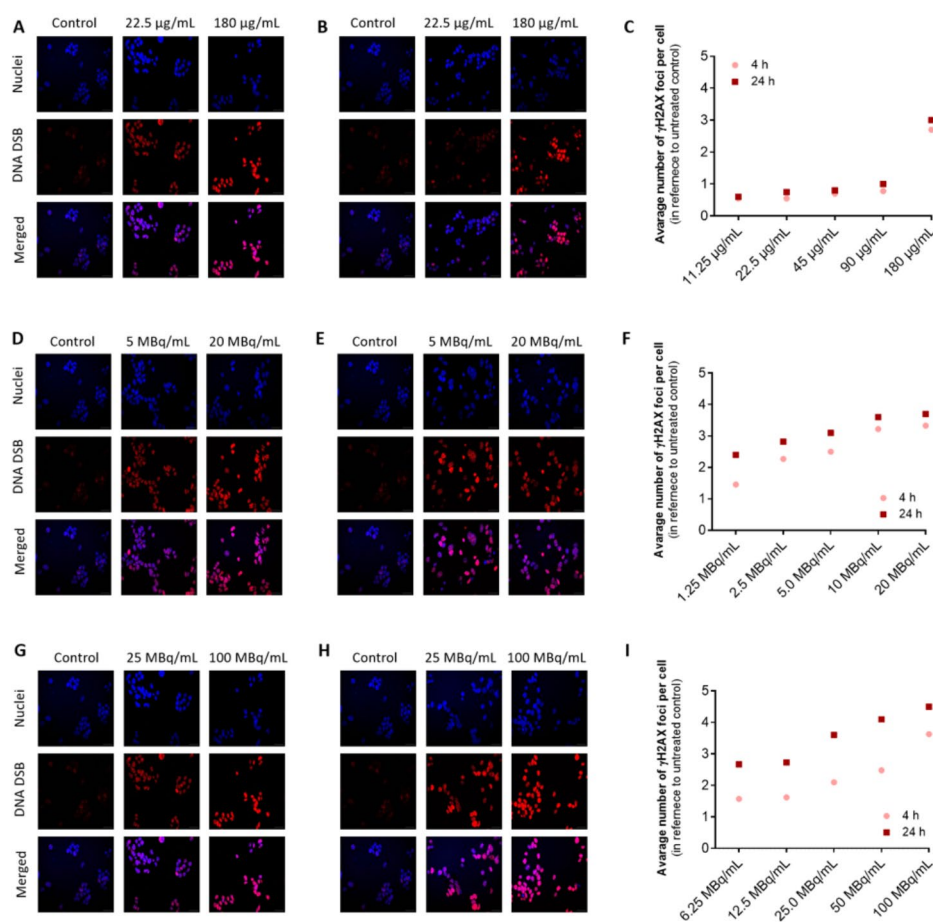

Fig. 11 γH2A.X foci formation in HepG2 cells after treatment with Pd-NPs (**A-C**), [109]Pd-NPs (**D-F**), and ^{131}I-Pd-NPs (**G-I**). Panels A, D, and G – imaging 4 h post-treatment; panels B, E, and H – imaging 24 h post-treatment. Images only of selected compounds doses are shown

Discussion

When using in-vivo generators it is crucial to assess whether after radioactive decay, the daughter radionuclide remains in the bioconjugate or diffuses out of initial structure. There are two opportunities where the daughter can detach from the parent radionuclide: either due to elemental differences between them or as a result of the physical and chemical disturbances caused by the nuclear decay process. In many cases, the chemical change of atomic number (as a result of nuclear decay) is sufficient to induce a difference between parent and daughter chemistry. This occurs for example in the decay of ^{131}I to noble gas ^{131}Xe, when Xe atoms escape from ^{131}I labeled molecules. However, even when the parent and decay product have nearly identical chemical behavior, as with transitions between two lanthanides, there is still a possibility for a chemical change due to the atomic effects of nuclear decay (Edem et al. 2016). Generally, if the nuclear transition recoil energy of the daughter radionuclide exceeds the binding energy in the complex, breaking of the bonds and the daughter radionuclide escape from the original structure can be expected. Alpha transition is one of examples where the recoil energy significantly exceeds the energy of chemical bonds, and the complete release of the daughter radionuclides from the molecules is observed. However, for other decay types, this process is more complex. In a series of articles Szücs, Zeevaart et al. described chemical consequences that may occur in the case of beta, electron capture, and internal transition decay (van Rooyen et al. 2008; Zeevaart et al. 2012b; Zeevaart et al. 2012a). In most β^- decays, where beta and neutrino particles are emitted, the recoil energy imparted to the daughter does not exceed a few eV and is not sufficient to displace the daughter from strong multidentate chelates. For example, in the case of the ^{90}Sr/^{90}Y complexed pair with DOTA, it was shown that only 1% of all β^- decays led to the release of the ^{90}Y daughter (Zeevaart et al. 2012b).

The situation changes significantly when β^- decay is accompanied by the emission of Auger electrons, as seen in the ^{166}Dy/^{166}Ho in-vivo generator. It has been found that following the β^- decay of ^{166}Dy, an excited state of ^{166}Ho* is formed. The de-excitation of ^{166}Ho* occurs *via* internal conversion instead of γ emission and energy is transferred to the electrons of the inner shell, resulting in the creation of electron vacancies. Electrons from the outer shells are organized to fill the vacancies, emitting an Auger electron cascade through the created ^{166}Ho atom. As a result, the de-excited daughter radionuclides become highly charged which leads to electron uptake from the surrounding chelator donor atoms. Moreover, due to the electron transfer to highly charged atoms, donor atoms of chelators acquire a positive charge. The metal-ligand bonds are then broken as a result of the repulsive force between the positively charged atoms, and the daughter ^{166}Ho is released as free cations (Wang et al. 2022).

A similar situation occurs in the case of the proposed in our work ^{109}Pd/^{109m}Ag in-vivo generator, which combines β^- emission from the parent ^{109}Pd radionuclide with a high emission of Auger electrons from the daughter ^{109m}Ag. In the case of the ^{109}Pd/^{109m}Ag macrocyclic complexes, an additional factor contributing to the release of the daughter radionuclide is the high chemical difference between Pd^{2+} and Ag$^+$ cations. Furthermore, tetraaza macrocyclic ligands exhibit very weak binding of Ag$^+$ ions - K_{ML} of Pd^{2+}cyclam complex is 56.9 (Harrington et al. 2005), whereas for a very similar Ag$^+$ cylcen it is only 6.6 (Rajakumar et al. 2015) .

Interestingly, in the case of [109]Pd-PEG nanoparticles used in our studies, the release of [109m]Ag is not observed. As it is well recognized that the metallic phase contains several delocalized electrons, after the nuclear decay of [109]Pd, the highly positively charged daughter [109m]Ag radionuclide extracts the delocalized electrons from the Pd nanoparticles. As a result, the positive charge is rapidly transferred to the entire nanoparticle, causing only a negligible change in the whole nanoparticle charge. Consequently, the release of [109m]Ag from the nanoparticles is not achievable. This same effect was also observed by Wang et al. (Wang et al. 2022) in their studies of a [166]Dy/[166]Ho in-vivo generator with radionuclides deposited on the AuNPs surface. This phenomenon is, of course, beneficial in terms of maximizing therapeutic effectiveness. As [109m]Ag remains within the structure of the NPs, there is negligible risk of [109m]Ag unspecific localization in different non-target tissues after treatment. Hence, it significantly reduces the risk of post-treatment side effects.

In order to achieve optimal treatment results, it is crucial to deliver Auger-electron-emitting radionuclides to the cell nucleus, preferably close to the DNA. As previously mentioned, this can be achieved by dissolving the small platinum NPs in the cytoplasm of HepG2 cells, which is commonly known to be a cancer cell line with an increased redox potential in the cytosol (Shoshan et al. 2019; Szatrowski and Nathan 1991). In our work, we intended to investigate whether the described effect of dissolving platinum nanoparticles also applies to PdNPs. If such a phenomenon occurred, easy transport of [109]Pd ions from the cytoplasm to the cell nucleus and incorporation into DNA would be possible, favouring DNA damage and therapeutic response. However, as shown in Fig. 5, Pd-PEG NPs did not dissolve, even when exposed to high concentrations of hydrogen peroxide. Despite this, both non-radioactive and [109]Pd-PEG nanoparticles exhibited high toxicity levels during our studies. This relates to the significant internalization of Pd-PEG NPs into the cytoplasm, followed by their ~50% cell nucleus uptake through the nuclear pore complex. Nuclear pore complexes allow the passive diffusion of ions, small molecules and nanoparticles through aqueous channels with a diameter of ~9 nm (Panté and Kann 2002). The main condition for transportation is that the substances being transported must be hydrophilic (Ma et al. 2012). Therefore, the observed toxicity of non-radioactive Pd-PEG NPs on HepG2 cells could be associated with the catalytic decomposition of H_2O_2 on the surface of PdNPs, resulting in the formation of reactive hydroxyl radicals or singlet oxygen molecules. Of course, for [109]Pd-PEG NPs, the radio-toxic effect of β[-] particles and Auger electrons emitted in the cell nucleus predominates.

In our studies, we have demonstrated that Pd-PEG NPs labelled with [109]Pd have a significantly higher cytotoxic effect on HepG2 cells compared to labelled with [131]I (beta emitter) and [125]I (Auger electron emitter). This effect has been also observed repeatedly when comparing bioconjugates labelled with [161]Tb and [177]Lu. As explained, the higher efficacy of [161]Tb compared to ^{177}Lu and other β[-] radioisotopes like [47]Sc and [67]Cu is mainly due to the larger amount of Auger and low-energy conversion electrons, whose doses are deposited over relatively short distances (Champion et al. 2016). The authors of the study demonstrated that in a 100-μm metastasis, CE and Auger electrons were responsible for 71% of the radiation dose deposited by [161]Tb. This is in contrast to almost pure β[-] emitters, where more than 99% of the absorbed energy is due to β[-] particles for all spheres. For tumors with a 5 mm diameter, the absorbed dose was similar across all three radionuclides. As shown in Figs. 8 and 9 we observed a similar situation when

we compared the cytotoxicity of [109]Pd-PEG with that of ^{131}I-labeled Pd-PEG NPs. Our experiments conducted to determine cytotoxicity involved examining layers of cell colonies (1–2 layers, 10–20 μm) and spheroids with a diameter of ~ 1 mm. In the case of a cell layer, we found that metabolic activity is significantly reduced to 25% for 12.5 MBq/mL. However, for 1 mm spheroids that limit metastases, the effect is not as significant and is limited to inhibiting spheroid growth or slightly decreasing their surface area. The toxicity of [109]Pd-PEG NPs for spheroids is comparable to that of [198]Au nanoparticles x017B;elechowska-Matysiak et al. 2023) which emit β^- radiation with an energy of $\beta_{max} = 961$ keV, a similar energy to that emitted by [109]Pd. However, unlike [109]Pd, [198]Au does not emit Auger electrons. Thus, the advantages of [109]Pd-PEG become visible in the case of small cancer metastases. However, the β radiation component allows for the parallel destruction of larger cancer lesions Therefore, [109]Pd-PEG nanoparticles, similar to [161]Tb radioconjugates, should be intended for applications in metastatic cancers.

Cytotoxicity results of [109]Pd-PEG and ^{131}I-Pd-PEG NPs directly correlate well with the occurrence of DSBs in the HepG2 cells visualized by γH2A.X foci. The high LET Auger and conversion electrons emitted by the [109]Pd/[109m]Ag in-vivo generator are responsible for the high number of DSBs formation. The number of DSBs is significantly reduced following β^- particle irradiation, attributable to the extended interaction range and lower LET of β^- particles (Faraggi et al. 1994). The significance of DSBs in radionuclide therapy was demonstrated by Tounekti et al. (Tounekti et al. 2001) through their studies on Chinese hamster fibroblasts. They found that cell death may occur in the form of apoptosis if there are more than 150 000 SSBs and only 500 DSBs. However, if the number of SSBs and DSBs is less than 150 000 and 500, respectively, cell death does not occur; instead, a reparative process emerges. This information is essential for understanding the effects of radiation on cells during radionuclide therapy, which aims to selectively target and destroy cancer cells while minimizing damage to healthy tissues.

Conclusions

Nanostructures have been proposed as a novel approach for the treatment of HCC that is more effective than traditional methods such as sorafenib, transarterial chemotherapy, and radioembolization. The application of nanostructures can reduce therapeutic toxicity and facilitates more precise targeting of the affected area. In this paper, we discuss the use of [109]Pd-PEG nanoparticles as an in-vivo [109]Pd/[109m]Ag generator. The studies revealed that these nanoparticles were significantly more effective in-vitro than Pd-PEG NPs labeled with either [125]I (Auger emitter) or [131]I (β[-] emitter). This is due to the unique potential presented by the [109]Pd/[109m]Ag in-vivo generator, which emits both β[-] and conversion/Auger electrons.

As presented in the introduction, we expected the dissolution of PdNPs in H_2O_2 solution, the concentration of which is elevated in HepG2 cells. This would allow to Auger electrons emitted from [109]Pd^{2+} to interact directly with the DNA strand. However, studies carried out in a wide range of H_2O_2 solutions have shown that this process does not occur. On the other hand, the approximately 50% accumulation of 5 nm [109]Pd-PEG nanoparticles in the cell nucleus caused a significant cytotoxic effect. The nucleus localization of high-activity Auger emitters can lead to DNA strand damage through direct interaction with conversion electrons, higher energy Auger electrons, and ROS radicals generated within the nucleus. The interaction of β[-] particles emitted by [109]PdNPs

localized in the nucleus with DNA is limited due to their low LET value. However, β⁻ particles can interact with DNA in neighboring cells, expanding the range of cytotoxic effects. Therefore, radiobioconjugates labeled with the ^{109}Pd/^{109m}Ag radionuclide generator, like ^{161}Tb, might show the advantages of both β⁻ emitters (a few millimeters range of radiation, crossfire effect) and Auger electrons (large LET, double-stranded DNA breaks).

The proposed solution also provides another advantage: the accumulation of inorganic nanoparticles in the liver when introduced in-vivo. Typically, this is a major drawback that prevents the therapeutic use of nanoparticles in medicine. However, in the case of HCC tumors, it might be advantageous because it will enable the accumulation of ^{109}Pd-PEG NPs in the targeted organ, where due to the leaky vasculature of HCC tumors (EPR effect), we can expect the accumulation in the cancer cells. In our future studies, we plan to incorporate targeting vectors such as glycyrrhetinic acid, transferrin, folate, or P-glycoprotein 1 (CD44) ligands to specifically target HepG2 cells while avoiding normal liver cells.

In recent years, there have been numerous studies on glypican-3 (GPC3), a highly expressed cell surface antigen found in about 75% of HCC cases. It was also found GC33 (codrituzumab), a humanized monoclonal antibody, has been shown to be specific for GPC3 antigen (Haruyama and Kataoka 2016). Additionally, preclinical studies conducted in the last five years have demonstrated that the α and β⁻emitters labeled GC33 antibody effectively and selectively reduced liver tumor volume in a mouse model (Bell et al. 2021). Consequently, in our future studies with ^{109}Pd, we plan to incorporate GC33 as a targeting vector to specifically target HepG2 cells while avoiding normal liver cells.

Declarations

Ethics approval and consent to participate
Not applicable.

Consent for publication
Not applicable.

Competing interests
The authors declare that they have no competing interests.

References
Aghevlian S, Boyle AJ, Reilly RM. Radioimmunotherapy of cancer with high linear energy transfer (LET) radiation delivered by radionuclides emitting α-particles or Auger electrons. Adv Drug Deliv Rev. 2017;109:102–18.
Bell MM, Gutsche NT, King AP, Baidoo KE, Kelada OJ, Choyke PL, Escorcia FE. Glypican-3-Targeted Alpha Particle Therapy for Hepatocellular Carcinoma. Molecules. 2021;26:4.

Białkowska K, Komorowski P, Bryszewska M, Miłowska K. Spheroids as a type of three-dimensional cell cultures—examples of methods of preparation and the most important application. Int J Mol Sci. 2020;21:6225.

Blanco E, Shen H, Ferrari M. Principles of nanoparticle design for overcoming biological barriers to drug delivery. Nat Biotechnol. 2015;33:941–51.

Boros E, Packard AB. Radioactive Transition metals for imaging and therapy. Chem Rev. 2019;119:870–901.

Chakraborty E, Sarkar D. Emerging therapies for hepatocellular carcinoma (HCC). Cancers (Basel). 2022;14:2798.

Champion C, Quinto MA, Morgat C, Zanotti-Fregonara P, Hindié E. Comparison between three promising ß-emitting radionuclides, [67]Cu, [47]sc and [161]tb, with emphasis on doses delivered to minimal residual disease. Theranostics. 2016;6:1611–8.

Das T, Chakraborty S, Sarma HD, Banerjee S. A novel [[109]pd] palladium labeled porphyrin for possible use in targeted radiotherapy. Radiochim Acta. 2008;96:427–33.

Das T, Chakraborty S, Sarma D, Banerjee H. [109]pd labeled 5,10,15,20-tetrakis[4-carboxymethyleneoxyphenyl]porphyrin: a potential Agent for targeted Tumor Therapy. Curr Radiopharm. 2012;5:340–7.

Demoy M, Andreux J, Weingarten C, Gouritin B, Guilloux V, Couvreur P. Spleen capture of nanoparticles: influence of animal species and surface characteristics. Pharm Res. 1999;16:37–41.

Edem PE, Fonslet J, Kjær A, Herth M, Severin G. Vivo Radionuclide generators for diagnostics and therapy. Bioinorg Chem Appl. 2016;2016:1–8.

Faraggi M, Gardin I, de Labriolle-Vaylet C, Moretti J, Bok B. The influence of tracer localization on the electron dose rate delivered to the cell nucleus. J Nucl Med. 1994;35:113–9.

Filosofov D, Kurakina E, Radchenko V. Potent candidates for targeted Auger Therapy: production and radiochemical considerations. Nucl Med Biol. 2021;94–95:1–19.

Fu J, Wang H. Precision diagnosis and treatment of liver cancer in China. Cancer Lett. 2018;412:283–8.

Gharibkandi NA, Wawrowicz K, Majkowska-Pilip A, Żelechowska-Matysiak K, Wierzbicki M, Bilewicz A. Au@[109]Pd core–shell nanoparticle conjugated to trastuzumab for the therapy of HER2+cancers: studies on the applicability of [109]Pd/[109m]Ag in vivo generator in combined β – auger electron therapy. EJNMMI Radiopharm Chem. 2023;8:26.

Greten TF, Sangro B. Targets for immunotherapy of liver cancer. J Hepatol. 2018;68:157–66.

Harrington JM, Jones SB, Hancock RD. Determination of formation constants for complexes of very high stability: $\log\beta_4$ for the $[Pd(CN)_4]^{2-}$ ion. Inorganica Chim Acta. 2005;358:4473–80.

Haruyama Y, Kataoka H. Glypican-3 is a prognostic factor and an immunotherapeutic target in hepatocellular carcinoma. World J Gastroenterol. 2016;22:275–83.

Hernández L, Terradas M, Martín M, Tusell L, Genescà A. Highly sensitive automated method for DNA damage assessment: Gamma-H2AX foci counting and cell cycle sorting. Int J Mol Sci. 2013;14:15810–26.

Jung SC, Park Y-K, Jung H-Y, Kim SC. Effect of stabilizing agents on the synthesis of palladium nanoparticles. J Nanosci Nanotechnol. 2017;17:2833–6.

Ku A, Facca VJ, Cai Z, Reilly RM. Auger electrons for cancer therapy – a review. EJNMMI Radiopharm Chem. 2019;4:27.

Kwekkeboom DJ, Bakker WH, Kam BL, Teunissen JJM, Kooij PPM, de Herder WW, et al. Treatment of patients with gastro-entero-pancreatic (GEP) tumours with the novel radiolabelled somatostatin analogue [^{177}Lu-DOTA0,Tyr3]octreotate. EJNMMI. 2003;30:417–22.

Ma J, Goryaynov A, Sarma A, Yang W. Self-regulated viscous channel in the nuclear pore complex. PNAS. 2012;109:7326–31.

Medavaram S, Zhang Y. Emerging therapies in advanced hepatocellular carcinoma. Exp Hematol Oncol. 2018;7:17.

Medhat A, Mansour S, El-Sonbaty S, Kandil E, Mahmoud M. Evaluation of the antitumor activity of platinum nanoparticles in the treatment of hepatocellular carcinoma induced in rats. Tumor Biology. 2017;39:101042831771725.

Mintz KJ, Leblanc RM. The use of nanotechnology to combat liver cancer: progress and perspectives. BBA - Reviews Cancer. 2021;1876(2):188621.

Müller C, Umbricht CA, Gracheva N, Tschan VJ, Pellegrini G, Bernhardt P, et al. Terbium-161 for PSMA-targeted radionuclide therapy of prostate cancer. Eur J Nucl Med Mol Imaging. 2019;46(9):1919–30.

Nadar RA, Franssen GM, Van Dijk NWM, Codee-van der Schilden K, de Weijert M, Oosterwijk E, et al. Bone tumor–targeted delivery of theranostic [195m]Pt-bisphosphonate complexes promotes killing of metastatic tumor cells. Mater Today Bio. 2021;9:100088.

Panté N, Kann M. Nuclear pore complex is able to transport macromolecules with diameters of ∼39 nm. Mol Biol Cell. 2002;13:425–34.

Peter Bernhardt EF-A. Low-energy electron emitters for targeted radiotherapy of small tumours. Acta Oncol (Madr). 2001;40:602–8.

Rajakumar G, Rahuman AA, Chung I-M, Kirthi AV, Marimuthu S, Anbarasan K. Antiplasmodial activity of eco-friendly synthesized palladium nanoparticles using Eclipta prostrata extract against Plasmodium berghei in Swiss albino mice. Parasitol Res. 2015;114:1397–406.

Shoshan MS, Vonderach T, Hattendorf B, Wennemers H. Peptide-coated platinum nanoparticles with selective toxicity against liver cancer cells. Angew Chem Int Ed. 2019;58:4901–5.

Sies H. Hydrogen peroxide as a central redox signaling molecule in physiological oxidative stress: oxidative eustress. Redox Biol. 2017;11:613–9.

Stokke C, Kvassheim M, Blakkisrud J. Radionuclides for targeted therapy: physical properties. Molecules. 2022;27:5429.

Szatrowski T, Nathan C. Production of large amounts of hydrogen peroxide by human tumor cells. Cancer Res. 1991;51:794–8.

Torre LA, Bray F, Siegel RL, Ferlay J, Lortet-Tieulent J, Jemal A. Global cancer statistics, 2012. CA Cancer J Clin. 2015;65:87–108.

Tounekti O, Kenani A, Foray N, Orlowski S, Mir LM. The ratio of single- to double-strand DNA breaks and their absolute values determine cell death pathway. Br J Cancer. 2001;84:1272–9.

van Rooyen J, Szucs Z, Rijn Zeevaart J. A possible in vivo generator [103]Pd/[103m]Rh—Recoil considerations. Appl Radiat Isot. 2008;66:1346–9.

Wang R, Ponsard B, Wolterbeek H, Denkova A. Core–shell structured gold nanoparticles as carrier for [166]Dy/[166]Ho in vivo generator. EJNMMI Radiopharm Chem. 2022;7:16.

Wawrowicz K, Bilewicz A. Challenging production of Auger electron emitter platinum-195m via double-neutron capture activation of an iridium-193 target. Bio-Algorithms Med-Systems. 2023;19:35–9.

Wawrowicz K, Majkowska-Pilip A, Szwed M, Żelechowska-Matysiak K, Chajduk E, Bilewicz A. Oxidative status as an attribute for selective antitumor activity of platinum-containing nanoparticles against hepatocellular carcinoma. Int J Mol Sci. 2022;23:14773.

Wawrowicz K, Żelechowska-Matysiak K, Majkowska-Pilip A, Wierzbicki M, Bilewicz A. Platinum nanoparticles labelled with iodine-125 for combined chemo-auger electron therapy of hepatocellular carcinoma. Nanoscale Adv. 2023;5:3293–303.

Ye R, Hurlburt TJ, Sabyrov K, Alayoglu S, Somorjai GA. Molecular catalysis science: Perspective on unifying the fields of catalysis. Proceedings of the National Academy of Sciences. 2016;113(19):5159–66.

Yhee JY, Son S, Son S, Joo MK, Kwon IC. The EPR Effect in Cancer Therapy. Cancer targeted drug delivery. New York, NY: Springer New York; 2013. pp. 621–32.

Zeevaart JR, Szucs Z, Takacs S, van Rooyen J, Jansen D. Recoil and conversion electron implications to be taken into account in the design of therapeutic radiopharmaceuticals utilising *in vivo* generators. J Label Comp Radiopharm 2012b Mar 16;55(3):115–9.

Zeevaart JR, Szücs Z, Takács S, Jarvis NV, Jansen D. Recoil and conversion electron considerations of the ^{166} Dy/ ^{166} Ho *in vivo* generator. Ract. 2012a Feb;100(2):109–13.

Żelechowska-Matysiak K, Salvanou E-A, Bouziotis P, Budlewski T, Bilewicz A, Majkowska-Pilip A. Improvement of the effectiveness of HER2 + Cancer therapy by Use of Doxorubicin and Trastuzumab Modified Radioactive Gold nanoparticles. Mol Pharm. 2023;20(9):4676–86.

Publisher's Note

Springer Nature remains neutral with regard to jurisdictional claims in published maps and institutional affiliations.

Agnieszka Majkowska-Pilip
Imię i nazwisko współautora

Instytut Chemii i Techniki Jądrowej
Miejsce pracy/afiliacja

Oświadczenie współautora

Oświadczam, iż mój udział w przygotowaniu następujących publikacji:

Nasrin Abbasi Gharibkandi, Kamil Wawrowicz, Agnieszka Majkowska-Pilip, Kinga Żelechowska-Matysiak, Mateusz Wierzbicki, Aleksander Bilewicz, Au@^{109}Pd core–shell nanoparticle conjugated to trastuzumab for the therapy of HER2+ cancers: studies on the applicability of ^{109}Pd/^{109m}Ag *in vivo* generator in combined β⁻ Auger electron therapy. EJNMMI Radiopharmacy and Chemistry 8, 26 (2023)

Nasrin Abbasi Gharibkandi, Agnieszka Majkowska-Pilip, Rafał Walczak, Mateusz Wierzbicki, Aleksander Bilewicz, Au@^{109}Pd core-shell nanoparticle conjugated to panitumumab for the combined β⁻ - Auger electron therapy of triple-negative breast cancer. International Journal of Molecular Sciences 25, 13555 (2024).

Nasrin Abbasi Gharibkandi, Kamil Wawrowicz, Rafał Walczak, Agnieszka Majkowska-Pilip, Mateusz Wierzbicki, Aleksander Bilewicz, ^{109}Pd/^{109m}Ag in vivo generator in the form of nanoparticles for combined β⁻ - Auger electron therapy of hepatocellular carcinoma. EJNMMI Radiopharmacy and Chemistry 9, 59 (2024).

wchodzących w skład rozprawy doktorskiej Pani mgr Nasrin Abbasi Gharibkandi polegał na współtworzeniu koncepcji pracy, zaproponowaniu eksperymentów, dyskusji wyników dotyczących przeprowadzonych badań biologicznych i udziale w końcowym przygotowaniu manuskryptu i odpowiedzi recenzentom.

17.01. 25

Data/podpis

Mateusz Wierzbicki,
Imiona i nazwisko współautora

Katedra Nanobiotechnologii – SGGW
Miejsce pracy/afiliacja

Oświadczenie współautora

Oświadczam, iż mój udział w przygotowaniu następujących publikacji:

Nasrin Abbasi Gharibkandi, Agnieszka Majkowska-Pilip, Rafał Walczak, Mateusz Wierzbicki, Aleksander Bilewicz, Au@^{109}Pd core-shell nanoparticle conjugated to panitumumab for the combined β⁻ - Auger electron therapy of triple-negative breast cancer. International Journal of Molecular Sciences 25, 13555 (2024).

Nasrin Abbasi Gharibkandi, Kamil Wawrowicz, Rafał Walczak, Agnieszka Majkowska-Pilip, Mateusz Wierzbicki, Aleksander Bilewicz, ^{109}Pd/^{109m}Ag in vivo generator in the form of nanoparticles for combined β⁻ - Auger electron therapy of hepatocellular carcinoma. EJNMMI Radiopharmacy and Chemistry 9, 59 (2024).

wchodzących w skład rozprawy doktorskiej Pani mgr Nasrin Abbasi Gharibkandi polegał na wykonaniu obrazów mikroskopem konfokalnym i udziale w końcowym przygotowaniu manuskryptu i odpowiedzi recenzentom.

16.01.2025 Mateusz Wierzbicki
Data/podpis

Kamil Wawrowicz
Imiona i nazwisko współautora

Uniwersytet Jagielloński, Wydział Fizyki, Astronomii i Informatyki Stosowanej
Miejsce pracy/afiliacja

Oświadczenie współautora

Oświadczam, iż mój udział w przygotowaniu publikacji:

Nasrin Abbasi Gharibkandi, Joanna Gierałtowska, Kamil Wawrowicz, Aleksander Bilewicz. "Nanostructures as Radionuclide Carriers in Auger Electron Therapy" Materials 15, 2022, 1143.

wchodzącej w skład rozprawy doktorskiej Pani mgr Nasrin Abbasi Gharibkandi polegał na przygotowaniu rozdziału Organic Nanocarriers oraz współudziale w końcowym przygotowaniu manuskryptu i odpowiedzi recenzentom.

Zaś w poniższej publikacji polegał na zaproponowaniu i pomocy w przeprowadzeniu eksperymentów oraz dyskusji wyników i odpowiedzi recenzentom.

Nasrin Abbasi Gharibkandi, Kamil Wawrowicz, Rafał Walczak, Agnieszka Majkowska-Pilip, Mateusz Wierzbicki, Aleksander Bilewicz, ^{109}Pd/^{109m}Ag in vivo generator in the form of nanoparticles for combined β⁻ - Auger electron therapy of hepatocellular carcinoma. EJNMMI Radiopharmacy and Chemistry 9, 59 (2024).

16.01.2025 r.   Kamil Wawrowicz
....
Data/podpis

Rafał Walczak
Imię i nazwisko współautora

Instytut Chemii i Techniki Jądrowej
Miejsce pracy/afiliacja

Oświadczenie współautora

Oświadczam, iż mój udział w przygotowaniu następujących publikacji:

Nasrin Abbasi Gharibkandi, Agnieszka Majkowska-Pilip, Rafał Walczak, Mateusz Wierzbicki, Aleksander Bilewicz, Au@^{109}Pd core-shell nanoparticle conjugated to panitumumab for the combined β⁻ - Auger electron therapy of triple-negative breast cancer. International Journal of Molecular Sciences 25, 13555 (2024).

Nasrin Abbasi Gharibkandi, Kamil Wawrowicz, Rafał Walczak, Agnieszka Majkowska-Pilip, Mateusz Wierzbicki, Aleksander Bilewicz, ^{109}Pd/^{109m}Ag in vivo generator in the form of nanoparticles for combined β⁻ - Auger electron therapy of hepatocellular carcinoma. EJNMMI Radiopharmacy and Chemistry 9, 59 (2024).

wchodzących w skład rozprawy doktorskiej Pani mgr Nasrin Abbasi Gharibkandi polegał na pomocy w przeprowadzeniu eksperymentów i udziale w końcowym przygotowaniu manuskryptu i odpowiedzi recenzentom.

16.01.2025
Data/podpis

Aleksander Bilewicz
Imię i nazwisko współautora

Instytut Chemii i Techniki Jądrowej
Miejsce pracy/afiliacja

Oświadczenie współautora

Oświadczam, iż mój udział w przygotowaniu publikacji:

Nasrin Abbasi Gharibkandi, Joanna Gierałtowska, Kamil Wawrowicz, Aleksander Bilewicz. "Nanostructures as Radionuclide Carriers in Auger Electron Therapy" Materials 15, 2022, 1143.

wchodzących w skład rozprawy doktorskiej Pani mgr Nasrin Abbasi Gharibkandi polegał na współtworzeniu koncepcji pracy i udziale w końcowym przygotowaniu manuskryptu i odpowiedzi recenzentom.

zaś w następujących publikacjach:

Nasrin Abbasi Gharibkandi, Kamil Wawrowicz, Agnieszka Majkowska-Pilip, Kinga Żelechowska-Matysiak, Mateusz Wierzbicki, Aleksander Bilewicz, Au@^{109}Pd core–shell nanoparticle conjugated to trastuzumab for the therapy of HER2+ cancers: studies on the applicability of ^{109}Pd/^{109m}Ag *in vivo* generator in combined β⁻ Auger electron therapy. EJNMMI Radiopharmacy and Chemistry 8, 26 (2023)

Nasrin Abbasi Gharibkandi, Agnieszka Majkowska-Pilip, Rafał Walczak, Mateusz Wierzbicki, Aleksander Bilewicz, Au@^{109}Pd core-shell nanoparticle conjugated to panitumumab for the combined β⁻ - Auger electron therapy of triple-negative breast cancer. International Journal of Molecular Sciences 25, 13555 (2024).

Nasrin Abbasi Gharibkandi, Kamil Wawrowicz, Rafał Walczak, Agnieszka Majkowska-Pilip, Mateusz Wierzbicki, Aleksander Bilewicz, ^{109}Pd/^{109m}Ag in vivo generator in the form of nanoparticles for combined β⁻ - Auger electron therapy of hepatocellular carcinoma. EJNMMI Radiopharmacy and Chemistry 9, 59 (2024).

Mój udział polegał na współtworzeniu koncepcji pracy, zaproponowaniu eksperymentów i dyskusji wyników i udziale w końcowym przygotowaniu manuskryptu i odpowiedzi recenzentom.

15.01.2025

Data/podpis

Jaoanna Gierałtowska
Imię i nazwisko współautora

Sieć Badawcza Łukasiewicz - Instytut Mikroelektroniki i Fotoniki
Miejsce pracy/afiliacja

Oświadczenie współautora

Oświadczam, iż mój udział w przygotowaniu publikacji:

Nasrin Abbasi Gharibkandi, Joanna Gierałtowska, Kamil Wawrowicz, Aleksander Bilewicz. "Nanostructures as Radionuclide Carriers in Auger Electron Therapy" Materials 15, 2022, 1143.

wchodzącej w skład rozprawy doktorskiej Pani mgr Nasrin Abbasi Gharibkandi polegał na współudziale w końcowym przygotowaniu manuskryptu i odpowiedzi recenzentom.

17.01.2025 *Joanna Gierałtowska*
Data/podpis

List of Publications

1. **Nasrin Abbasi Gharibkandi**, Agnieszka Majkowska-Pilip, Rafal Walczak, Mateusz Wierzbicki, and Aleksander Bilewicz; "Au@^{109}Pd Core–Shell Nanoparticles Conjugated to Panitumumab for the Combined β⁻- Auger Electron Therapy of Triple-Negative Breast Cancer" International Journal of Molecular Sciences, (2024), IF: 4.9

2. **Nasrin Abbasi Gharibkandi**, Kamil Wawrowicz, Agnieszka Majkowska-Pilip, Rafal Walczak, Mateusz Wierzbicki, and Aleksander Bilewicz; "^{109}Pd/^{109m}Ag in-vivo generator in the form of nanoparticles for combined β⁻ - Auger electron therapy of hepatocellular carcinoma" EJNMMI Radiopharmacy and Chemistry, 9, 59 (2024), IF: 4.6

3. **Nasrin Abbasi Gharibkandi**, Kamil Wawrowicz, Agnieszka Majkowska-Pilip, Kinga Żelechowska- Matysiak, Mateusz Wierzbicki, and Aleksander Bilewicz; "Au@^{109}Pd core-shell nanoparticle conjugated to trastuzumab for the therapy of HER2+ cancers. Studies on the applicability of ^{109}Pd/^{109m}Ag in vivo generator in combined β−Auger electron therapy" EJNMMI Radiopharmacy and Chemistry, Vol 8, No 26 (2023), IF: 4.6

4. **Nasrin Abbasi Gharibkandi**, Michał Żuk, Fazilet Zumrut Biber Muftuler, Kamil Wawrowicz, Kinga Żelechowska-Matysiak, and Aleksander Bilewicz; "^{198}Au-Coated Superparamagnetic Iron Oxide Nanoparticles for Dual Magnetic Hyperthermia and Radionuclide Therapy of Hepatocellular Carcinoma" International Journal of Molecular Sciences, 24 (6), 5282, (2023), IF: 4.9

5. **Nasrin Abbasi Gharibkandi**, Joanna Gierałtowska, Kamil Wawrowicz, and Aleksander Bilewicz; "Nanostructures as Radionuclide Carriers in Auger Electron Therapy" Materials, 15 (3), 1143, (2022), IF: 3.4

6. Marzena Szwed, Tina Jost, Emilia Majka, **Nasrin Abbasi Gharibkandi**, Agnieszka Majkowska - Pilip, Benjamin Frey, Aleksander Bilewicz, Rainer Fietkau, Udo Gaipl, Agnieszka Marczak, Dorota Lubgan "Pt-Au nanoparticles in combination with near-infrared-based hyperthermia increase the temperature and impact on the viability and immune phenotype of human hepatocarcinoma cells", International Journal of Molecular Sciences, 2025, 26(4), 1574, IF: 4.9

7. **Gharibkandi, Nasrin A**.; Molavipordanjani, Sajjad; Mardanshahi, Alireza; Hosseinimehr, Seyed Jalal; "The Influence of Kidneys Ion Transport Inhibitors on the Pharmacokinetic and Tumor Uptake Behaviors of a HER2-targeted Small Size Radiolabeled Peptide" Current Drug Metabolism, Vol 23, No 1, 82-87 (6), (2022), IF: 2.1

8. Alireza Mardanshahi, **Nasrin Abbasi Gharibkandi**, Samaneh Vaseghi, Seyed Mohammad Abedi, and Sajjad Molavipordanjani; "The PI3K/AKT/mTOR signaling pathway inhibitors enhance radiosensitivity in cancer cell lines" Molecular Biology Reports, Vol 48, 1-14, (2021), IF: 2.6

9. **Nasrin Abbasi Gharibkandi**, J. Michael Conlon, Seyed Jalal Hosseinimehr; "Strategies for Improving Stability and Pharmacokinetic Characteristics of Radiolabeled Peptides for Imaging and Therapy" Peptides, Vol 133, 170385, (2020), IF: 2.4

10. **Gharibkandi NA**, Molavipordanjani S, Akbari J, Hosseinimehr SJ; "Pharmacokinetic evaluation of ^{99m}Tc- radiolabeled solid lipid nanoparticles and chitosan coated solid lipid nanoparticles" Current Drug Metabolism, Vol 20, No 13, 1044-1052 (9), (2019), IF: 2.1

11. **Abbasi Gharibkandi N**, Hosseinimehr SJ; "Radiotracers for imaging of Parkinson's disease" European Journal of Medicinal Chemistry, Vol 166, 75-89, (2019), IF: 6

Załącznik nr 1

Nasrin Abbasi Gharibkandi
....
imię i nazwisko kandydata
.........Dorodna 16, 03-195,
Warszawa
.... adres do
korespondencji
.........517608829
n.abbasi@ichtj.waw.pl
.... nr.
telefonu i adres email

.............................23.01.2025, Warszawa
....
miejscowość, data

Prof. Dr hab. inz. Zbiegniew Florjanczyk
....
Przewodniczący Rady Naukowej
Instytutu Chemii i Techniki Jądrowej
w Warszawie

Wniosek o wszczęcie postępowania w sprawie nadania stopnia doktora

Proszę o wszczęcie postępowania o nadanie stopnia doktora w dziedzinie nauk ścisłych i przyrodniczych, w dyscyplinie nauki chemiczne.

Temat rozprawy doktorskiej .
....

Nanoparticle radioconjugates of ^{103}Pd/^{103m}Rh and ^{109}Pd/^{109m}Ag in- vivo generators for Auger electron therapy...
....

Do wniosku dołączam:

Numer załącznika	Załączniki
	odpis dyplomu ukończenia studiów magisterskich lub równorzędnych, lub potwierdzoną przez pracownika administracyjnego IChTJ kserokopię dyplomu
	rozprawa doktorska w 5 egzemplarzach oraz w wersji elektronicznej w formacie pdf, zapisana na informatycznym nośniku danych
	streszczenie rozprawy doktorskiej w języku polskim oraz angielskim, w postaci papierowej oraz w wersji elektronicznej w formacie pdf zapisaną na informatycznym nośniku danych
	pozytywna opinia promotora, promotorów albo promotora i promotora pomocniczego, na temat rozprawy doktorskiej
	oryginały lub kserokopie dokumentów potwierdzających spełnianie kryteriów, o których mowa w §2 ust. 1 pkt 1
	wykaz dorobku naukowego
	życiorys
jeśli dotyczy	oświadczenie o przejęciu płatności za prowadzenie postępowania o nadanie stopnia doktora, w przypadku osób ubiegających się o nadanie stopnia doktora w trybie eksternistycznym nie będącymi pracownikami IChTJ
	oświadczenie o wcześniejszych przewodach doktorskich/postępowaniach o nadanie stopnia doktora kandydata
	oświadczenie kandydata o oryginalności rozprawy doktorskiej
jeśli dotyczy	oryginał lub kserokopia certyfikatu poświadczającego znajomość języka obcego na poziomie biegłości językowej co najmniej B2.

Nasrin Abbasi
.... Gharibkandi
podpis kandydata

Załącznik nr 2

Oświadczenie o przejęciu płatności za prowadzenie postępowania o nadanie stopnia doktora
*należy wypełnić część właściwą - część A albo B

część A*

..........23.01.2025, Warszawa

....

<div align="right">miejscowość, data</div>

...Nasrin Abbasi Gharibkandi

.... imię i
nazwisko kandydata

Dorodna 16, 03-195,
Warszawa

.... adres
do korespondencji

...........517608829........

.... nr. telefonu i
adres email

Oświadczenie kandydata o przejęciu płatności za postępowanie o nadanie stopnia doktora w trybie eksternistycznym

Oświadczam, że przejmuję płatność za przeprowadzenie mojego postępowania o nadanie stopnia doktora w Instytucie Chemii i Techniki Jądrowej w Warszawie. Warunki płatności zostaną określone w odrębnej umowie.

Nasrin Abbasi Gharibkandi

....
podpis kandydata

część B*

....

<div align="right">miejscowość, data</div>

....
Nazwa, adres podmiotu

....
NIP, telefon

Oświadczenie pracodawcy o przejęciu płatności za postępowanie o nadanie stopnia doktora w trybie eksternistycznym

Oświadczam, że przejmuję płatność za przeprowadzenie postępowania o nadanie stopnia doktora w Instytucie Chemii i Techniki Jądrowej w Warszawie Pani / Panu :

....

Warunki płatności zostaną określone w odrębnej umowie.

....
data i podpis osoby upoważnionej

Oświadczenie o przebiegu wcześniejszego przewodu doktorskiego / postępowania
o nadanie stopnia doktora
*należy wypełnić część właściwą - część A albo B

......23.01.2025, Warszawa....................................

miejscowość, data

...Nasrin Abbasi Gharibkandi

.... imię i
nazwisko kandydata
...Dorodna 16, 03-195,
Warszawa

.... adres do
korespondencji
517608829
n.abbasi@ichtj.waw.pl.........
.... numer
telefonu i adres email

część A*

Oświadczam, że wcześniej nie ubiegałam/em się o wszczęcie przewodu doktorskiego/postępowania o nadanie stopnia
doktora w żadnej jednostce naukowej.

Nasrin Abbasi
Gharibkandi
....

podpis kandydata

część B*

Oświadczam, że nie zostałam/-em dopuszczona/-y do obrony rozprawy doktorskiej/została mi wydana decyzja o odmowie nadania stopnia doktora*, we wcześniejszym/-ch postępowaniu/-ach* o nadanie stopnia doktora w dziedzinie ...., w dyscyplinie...

w:

....

(nazwa jednostki)

*właściwe zaznaczyć

*jeżeli postępowań było więcej niż jedno, proszę podać informacje wymagane niniejszym załącznikiem, dla każdego postępowania osobno

Tytuł rozprawy doktorskiej :

....

....

Data wszczęcia przewodu doktorskiego/postępowania o nadanie stopnia doktora :

Data i numer uchwały o niedopuszczeniu do obrony/ data i numer uchwały o odmowie nadania stopnia doktora/ data i numer decyzji o odmowie nadania stopnia doktora:

Przyczyna niedopuszczenia do obrony/odmowy nadania stopnia:

....

....

Oświadczam, że wskazana rozprawa/-y doktorska/-ie, wobec której podjęto ww. uchwałę/-y/decyzję/-e nie jest tożsama z rozprawą doktorką, która stanowi podstawę o ubieganie się o nadanie stopnia doktora w niniejszym postępowaniu.

....

podpis kandydata

Załącznik nr 3

Załącznik nr 4

...23.01.2025, Warszawa

....

miejscowość, data

............Nasrin Abbasi Gharibkandi

.... imię i
nazwisko kandydata

......Dorodna 16, 03-195, Warszawa

.... adres do
korespondencji

...517608829
n.abbasi@ichtj.waw.pl............................
.... numer telefonu i adres email

Oświadczenie kandydata o oryginalności rozprawy doktorskiej

Ja, niżej podpisana/y oświadczam, że:

a) rozprawa   doktorska   pt.:
....
...... Nanoparticle radioconjugates of ^{103}Pd/^{103m}Rh and ^{109}Pd/^{109m}Ag in- vivo generators for Auger electron therapy
....
....
....
.... jest wynikiem mojej działalności twórczej i powstała bez niedozwolonego udziału osób trzecich,

b) wszystkie wykorzystane przeze mnie materiały źródłowe i opracowania zostały w niej wymienione, a napisana przeze mnie praca nie narusza praw autorskich osób trzecich,

c) załączona wersja elektroniczna pracy jest tożsama z wydrukiem rozprawy.

Nasrin Abbasi Gharibkandi

....
podpis kandydata

Diploma Of Graduation

تاریخ ۱۳۹۹/۶/۱۵
شماره ب ۷-۷/۲۸۰۸

بسمه تعالی

جمهوری اسلامی ایران
وزارت بهداشت درمان و آموزش پزشکی

دانشنامه پایان تحصیلات

دانشکده: داروسازی

آقای/خانم: نسرین عباسی قریب کندی

فرزند: زین العابدین

صادره از: ارومیه   شماره: ۱۳۴۷   کد ملی: ۲۷۵۵۸۴۲۹۴۳

در رشته: کارشناسی ارشد ناپیوسته

به تاریخ: ۱۳۹۸/۱۱/۲۸ موفق به پایان تحصیلات شده اند.

دکتر رضا عنایتی فرد
رئیس دانشگاه

دکتر سید عباس موسوی

در مقطع تحصیلات: ۱۲۹۲۱۸۱۳۴
رشته: علوم داروهای پرتوزا

دانشگاه علوم پزشکی و خدمات بهداشتی درمانی زنجان

لیلا بندری
مترجم رسمی زبان انگلیسی قوه قضائیه- تهران
ایران، تهران، خیابان بهشتی، ضلع جنوب غربی تقاطع سهروردی، شماره ۳۹۴، طبقه اول، واحد ۸.
تلفن‌ها: ۰۹۱۲۵۴۷۷۲۰۴، ۰۹۳۸۵۵۵۱۳۵۰، ۰۹۸۲۱-۸۸۴۴۲۷۴۵

Leila Bandari, Official Translator to the Judiciary
3rd Floor, # 394, Beheshti Ave., Sohrevardi Intersection, Tehran, Iran.
Tel: +98 912 547 7204, +98 938 555 1350, +9821 88 44 2745
www.daryaa.org

شماره: ۴۱۳۳۹۸

ردیف دفتر ثبت

جمهوری اسلامی ایران

قوه قضائیه ـ اداره مترجمین رسمی

OFFICIAL TRANSLATION

In the name of God, the Almighty
Islamic Republic of Iran
Ministry of Health, Treatment and Medical Education

Mazandaran University of Medical Sciences, Health and Treatment Services
Faculty of Pharmacy

Ref. no.: P/A/2807
Date: Sep 5, 2020
Photo of the holder affixed and sealed
Hologram of the university affixed

Diploma of Graduation

Ms. Nasrin Abbasi Gharibkandi, daughter of Zeynolabedin, holder of national Id no. 275-586319-6 and

holder of Id card no. 12618, issued in Oroumieh, born in 1988, has successfully completed master's degree

program in the field of Radiopharmaceutical Sciences in this university on Feb 17, 2020.

Signed: Dean of Faculty
Signed and embossed sealed: President of the University

Overleaf:
- 10,000 Rial stamp affixed and cancelled
- Translation of this document and its approval by Ministry of Foreign Affairs is permitted. Signed and sealed: Ministry of Health, Treatment and Medical Education

---

True Translation Certified, September 19, 2020.

S. FATEMEH ATARZADEH.
LEGALIZATION OFFICER

The authenticity
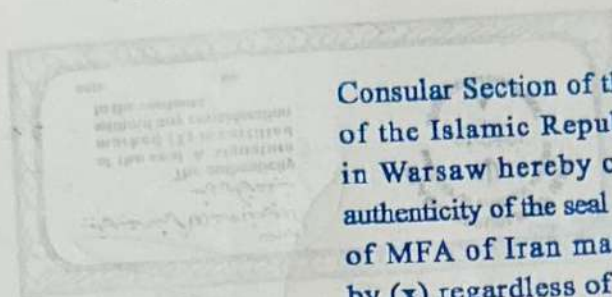of the seal & signature
marked (X) is certified
without any consideration
to the contents.
DATE: NO:

(X)

1 9 SEP 2020   804826

YUSEF ALI VEYSI
THIRD COUNSELLOR

ABSTRAKT

Mimo, braku szerokiego zastosowania terapia z wykorzystaniem emiterów elektronów Augera jest uważana za obiecującą strategię selektywnego leczenia raka, szczególnie jego przerzutów. Niskoenergetyczne elektrony Augera są emitowane przez radioizotopy, które rozpadają się poprzez wychwyt elektronów lub w wyniku konwersji wewnętrznej jądra. Liniowy transfer energii (LET) elektronów Augera jest wysoki i mieści się w zakresie od 4 do 26 keV/µm. Dzięki temu mogą one wywoływać podwójnoniciowe pęknięcia DNA. Ostatnio stwierdzono, że skuteczność terapeutyczna wewnętrznej radioterapii może zostać istotnie zwiększona poprzez jednoczesne stosowanie promieniowania o niskim i wysokim LET. Dlatego w mojej pracy zaproponowałam wykorzystanie radionuklidu ^{109}Pd ($t_{1/2}$=13,7 h) w postaci generatora *in vivo* ^{109}Pd/^{109m}Ag. ^{109}Pd ulega rozpadowi β$^-$ do ^{109m}Ag ($t_{1/2}$=39,6 s), a następnie przechodzi w stabilny ^{109}Ag, emitując kwant gamma 88 keV oraz elektrony konwersji i Augera. Pozwala to wykorzystanie zalet zarówno cząstek β$^-$ (efekt ognia krzyżowego) jak i elektronów Augera, indukując dwuniciowe pęknięcia DNA.

Ponieważ nanocząstki pozwalają na uzyskanie wysokich aktywności właściwych, w moich badaniach wykorzystałam radionuklid ^{109}Pd w postaci nanocząstek ^{109}Pd (5 nm) oraz nanocząstek typu „core shell" Au@^{109}Pd (15 nm). Aby specyficznie ukierunkować je odpowiednio na receptory Her2 i EGFR, nanocząstki Au@^{109}Pd zostały skoniugowane z przeciwciałami monoklonalnymi trastuzumabem i panitumumabem, a 5 nm nanocząstki stosowano w postaci koniugatu ^{109}Pd NPs z PEG. Najistotniejszą część rozprawy stanowią badania przeprowadzone w warunkach *in vitro* z wykorzystaniem hodowli komórek adherentnych oraz trójwymiarowych sferoidów, jako modeli guza o zdefiniowanym i ukształtowanym mikrośrodowisku. Akumulacja nanocząstek ^{109}Pd-PEG i Au@^{109}Pd w jądrach komórkowych lub na błonie jąder komórkowych doprowadziła do dwuniciowych pęknięć DNA i zmniejszenia żywotności komórek. W celu przeprowadzenia badań porównawczych, nanocząstki Pd i Au@Pd znakowano metodą chemisorpcji radionuklidami ^{125}I (emiter elektronów Augera) i ^{131}I (emiter β$^-$ i γ). Otrzymane wyniki wykazały, że nanocząstki Pd znakowane ^{109}Pd były znacznie bardziej cytotoksyczne niż znakowane ^{131}I lub ^{125}I. Badania z radiobiokonjugatami Au@^{109}Pd-trastuzumab wykazały, że pomimo braku lokalizacji jądrowej, efekt cytotoksyczny uzyskano poprzez agregację radiokoniugatów Au@^{109}Pd-trastuzumab i ich kumulację w obszarze okołojądrowym. Natomiast radiobiokoniugaty Au@^{109}Pd-panitumumab w komórkach MDA-MB-231 wykazywały obok wysokiej internalizacji, także znaczny transport do jądra komórkowego (>10%). Rozprawa doktorska składa się ze wstępu, omówienia czterech załączonych publikacji oraz podsumowania i wniosków. Praca zawiera również dodatkowy rozdział, w którym zamieściłam niepublikowane wyniki dotyczące właściwości generatorów *in vivo* opartych na również obiecującym emiterze elektronów Augera, ^{103}Pd.

ABSTRACT

Although not widely used, Auger electron emitter therapy shows promise as a selective strategy for cancer treatment. The low-energy Auger electrons are emitted by radioisotopes that decay through electron capture or internal conversion processes. Typically, 5 to more than 35 Auger electrons, with energies ranging from a few eV to approximately 1 keV, are emitted per decaying atom. The linear energy transfer (LET) of Auger electrons ranges from 4 to 26 keV/µm. This makes them capable of inducing double-stranded DNA breaks. The therapeutic efficacy of Auger electron targeted radiotherapy can be increased by the simultaneous combination of low- and high-LET radiation. Therefore, we introduce the concept of using ^{109}Pd ($T_{1/2}$= 13.7 h) in the form of a ^{109}Pd/^{109m}Ag *in vivo* generator. ^{109}Pd undergoes β$^-$ decay to ^{109m}Ag (39.6 s), thereafter transitioning to stable ^{109}Ag, comprising the emission of 88-keV photons and the cascade release of conversion and Auger electrons. Hence, we can take the advantages of both β$^-$ and Auger electrons, by inducing the cross-fire effect and DNA double-strand breaks, respectively.

Due to the unique properties of nanoparticles for cancer diagnosis and treatment, this study utilized palladium radionuclide in the form of ^{109}Pd nanoparticles (5 nm) and Au@^{109}Pd core-shell nanoparticles (15 nm). Core-shell Au@^{109}Pd nanoparticles were conjugated with the monoclonal antibodies trastuzumab and panitumumab to specifically target the Her2 and EGFR receptors, respectively, and small PEGylated Pd nanoparticles were investigated for the therapy of hepatocellular carcinoma (HCC). The most important part of the thesis consists of numerous studies carried out *in vitro* using adherent cell cultures and three-dimensional spheroids as tumor models with a defined microenvironment. The accumulation of ^{109}Pd-PEG nanoparticles and Au@^{109}Pd in the cell nuclei or cell nuclei membrane led to DNA double-strand breaks (DSBs) and cell viability reduction, even at low doses. Moreover, in order to conduct comparative studies, Pd, and Au@Pd nanoparticles were also labeled by chemisorption with radionuclides ^{125}I (Auger emitter) and ^{131}I (β$^-$ and γ-emitter). Results showed that ^{109}Pd-labeled Pd nanoparticles were significantly more cytotoxic than those labeled with either ^{131}I or ^{125}I. Studies with Au@^{109}Pd-trastuzumab radiobioconjugates showed that despite the lack of nuclear localization, a cytotoxic effect was achieved by aggregation of Au@^{109}Pd-trastuzumab conjugates in the perinuclear area. In contrast, Au@^{109}Pd-panitumumab radiobioconjugates in MDA-MB-231 cells show similar internalization but significant transport into the cell nucleus (>10%).

The doctoral thesis consists of an introduction, an evaluation of the four attached publications, and a summary and conclusions. The thesis also includes an appendix in which I have included unpublished results related to the properties of *in vivo* generators in the form of a ^{103}Pd cyclam complex and Au@^{103}Pd core-shell nanoparticles.

Prof. Aleksander Bilewicz
Institute of Nuclear Chemistry and Technology
Dorodna 16; 03-195 Warsaw; Poland
tel.: (+48.22)504 13 57
Fax: (+48.22)811 15 32
E-mail: a.bilewicz@ichtj.waw.pl

Warsaw 03.12.2024

Opinion of scientific work
for **Nasrin Abbasi Gharibkandi**

Nasrin Abbasi Gharibkandi started working at the Radiochemistry and Nuclear Chemistry Center of our Institute in June 2021, where she pursued her PhD studies. Her research focuses on the synthesis and biological studies of radiobioconjugates based on ^{103}Pd and ^{109}Pd nanoparticles and their potential application in Auger electron therapy of breast and ovarian cancers. Special effort is directed toward studies of ^{103}Pd→^{103}Rh and ^{109}Pd→^{109m}Ag recoil reaction in the metallic phase. She has made significant progress in her research, including developing a method for synthesizing core-shell nanoparticles. These nanoparticles contain gold nanoparticle cores with single or multi-layers of palladium radionuclides.

An important part of the doctoral thesis are numerous studies conducted *in vitro,* using adherent cell cultures and three-dimensional spheroids as tumor models with a defined microenvironment. Complex analyses were also performed at different molecular levels. These included cell fractionation and isolation of the cell nucleus to determine the intranuclear uptake of the obtained radioconjugates, identification of DNA damage; and the chemotoxic effects of nanomaterials on cell death type induction and cell cycle inhibition.

During the preparation of Nasrin Abbasi Gharibkandi thesis the following publications were prepared:

1. Nasrin Abbasi Gharibkandi, Agnieszka Majkowska-Pilip, Rafal Walczak, Mateusz Wierzbicki, and Aleksander Bilewicz, "Au@^{109}Pd core-shell nanoparticle conjugated to panitumumab for the combined β$^-$ - Auger electron therapy of triple-negative breast cancer" International Journal of Molecular Sciences, accepted

2. Nasrin Abbasi Gharibkandi, Kamil Wawrowicz, Agnieszka Majkowska-Pilip, Rafal Walczak, Mateusz Wierzbicki, and Aleksander Bilewicz; "^{109}Pd/^{109m}Ag in-vivo generator in the form of nanoparticles for combined β$^-$ - Auger electron therapy of hepatocellular carcinoma" EJNMMI Radiopharmacy and Chemistry, 9, 59 (2024)

3. Nasrin Abbasi Gharibkandi, Kamil Wawrowicz, Agnieszka Majkowska-Pilip, Kinga Żelechowska Matysiak, Mateusz Wierzbicki, and Aleksander Bilewicz; "Au@^{109}Pd core-shell nanoparticle conjugated to trastuzumab for the therapy of HER2+ cancers. Studies on the applicability of ^{109}Pd/^{109m}Ag

in vivo generator in combined β–Auger electron therapy" EJNMMI Radiopharmacy and Chemistry, Vol 8, No 26 (2023)

4. Nasrin Abbasi Gharibkandi, Michał Żuk, Fazilet Zumrut Biber Muftuler, Kamil Wawrowicz, Kinga Żelechowska-Matysiak, and Aleksander Bilewicz; "^{198}Au-Coated Superparamagnetic Iron Oxide Nanoparticles for Dual Magnetic Hyperthermia and Radionuclide Therapy of Hepatocellular Carcinoma" International Journal of Molecular Sciences, 24 (6), 5282, (2023)

5. Nasrin Abbasi Gharibkandi, Joanna Gierałtowska, Kamil Wawrowicz, and Aleksander Bilewicz; "Nanostructures as Radionuclide Carriers in Auger Electron Therapy" Materials, 15 (3), 1143, (2022)

The defense of Nasrin Abbasi Gharibkandi's doctoral dissertation entitled "Radiopharmaceuticals based on ^{103}Pd→^{103}Rh and ^{109}Pd→^{109m}Ag *in vivo* generators for the therapy of breast cancer (HER2+) and hepatocellular carcinoma" is planned for the first quarter of 2025.

Nasrin Abbasi Gharibkandi is a co-author of 9 papers published in renowned foreign journals (in 8 she is first author) and oral presentations at national and international conferences. She participated in research grants funded by the National Science Center, and the COST Action. Nasrin Abbasi Gharibkandi is a talented and innovative scientist. She is a good experimentalist with extensive experience in organic synthesis, various analytical methods, radioisotope techniques and radiobiological studies on cancer cells. In addition, she is a very communicative person and easily establishes scientific cooperation both in Poland and abroad.

Aleksander Bilewicz
Head of Radiopharmaceutical Chemistry Laboratory

Agnieszka Majkowska-Pilip, DSc; Prof. INCT

Institute of Nuclear Chemistry and Technology

Centre of Radiochemistry and Nuclear Chemistry

Dorodna 16, 03-195 Warsaw, Poland

Warsaw, 17th of March 2025

Opinion of scientific work

for **Nasrin Abbasi Gharibkandi**

Since June 2021, Ms. Abbasi Gharibkandi has been conducting laboratory experiments at the Institute of Nuclear Chemistry and Technology (INCT) as a PhD student from The Graduate School of Physics and Chemistry. Her research focuses on developing new radiobioconjugates based on ^{103}Pd and ^{109}Pd nanoparticles for Auger electron therapy of cancers. These studies are also carried out as part of the National Science Center - OPUS project "Bioconjugates of ^{103}Pd nanostructures for targeted Auger electron therapy", in which the PhD student is the main investigator.

During her doctoral studies she performed the synthesis of Au@^{109}Pd core-shell nanoparticles, conjugated them to trastuzumab and panitumumab antibodies and also synthesized small 5 nm ^{109}Pd nanoparticles for the treatment of hepatocellular carcinoma. The main part of the doctoral dissertation research concerned *in vitro* experiments using adherent cells and three-dimensional structures (spheroids) as tumor models. She conducted receptor affinity, internalization, cytotoxicity and DNA double-strand breaks studies of obtained radioconjugates.

Ms. Nasrin Abbasi Gharibkandi is a co-author of nine publications (including five original research articles as the first author and four reviews) in prestigious journals, and she has contributed to several conference reports. She received an award for the best poster presentation at the International Symposium on Trends in Radiopharmaceuticals (ISTR-2023) in Vienna. Her keen interest in radiopharmaceutical development is evident from her efforts to deepen her knowledge of the literature and techniques in this field.

Her PhD studies required the knowledge of many laboratory techniques, ITLC, UV-Vis, DLS, all of which Ms. Nasrin Abbasi Gharibkandi mastered effectively. She also learned the advanced biochemistry necessary to work in radiopharmacy. In addition, Ms Nasrin Abbasi Gharibkandi has a good knowledge in the synthesis of core-shell nanoparticles, radiochemistry, and radiobiology (cellular 2D and 3D studies). Ms Nasrin Abbasi Gharibkandi creatively cooperated with researchers from various fields of chemistry, which was necessary for the full characterization of the tested compounds.

In my opinion, Ms. Nasrin Abbasi Gharibkandi, is a good scientist, and her doctoral thesis is certainly inspiring and promising for the future of research in the field of radiopharmacy.

Agnieszka Majkowska-Pilip, DSc; Prof. INCT
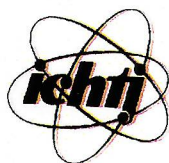
Prof. Aleksander Bilewicz
Instytut Chemii i Techniki Jądrowej
ul. Dorodna 16; 03-195 Warszawa; Poland
tel.: (+48.22)504 13 57
Fax: (+48.22)811.15.32
E-mail: a.bilewicz@ichtj.waw.pl

Warszawa 11.03.2025

Oświadczenie potwierdzające uzyskanie efektów uczenia się dla kwalifikacji na poziomie 8PRK

Oświadczam, że mgr Nasrin Abbasi Gharibkandi, kandydatka do nadania stopnia doktora uzyskała efekty uczenia się dla kwalifikacji na poziomie 8 PRK w ramach kształcenia w Szkole Doktorskiej Narodowego Centrum Badań Jądrowych i Instytutu Chemii i Techniki Jądrowej.

Z-ca Dyrektora Szkoły Doktorskiej
Narodowego Centrum Badań Jądrowych
i
Instytutu Chemii i Techniki Jądrowej
prof. dr hab. Aleksander Bilewicz

List of scientific achievements

Publications

1. **Nasrin Abbasi Gharibkandi**, Agnieszka Majkowska-Pilip, Rafal Walczak, Mateusz Wierzbicki, and Aleksander Bilewicz; "Au@^{109}Pd Core–Shell Nanoparticles Conjugated to Panitumumab for the Combined β^-- Auger Electron Therapy of Triple-Negative Breast Cancer" International Journal of Molecular Sciences, (2024), IF: 4.9

2. **Nasrin Abbasi Gharibkandi**, Kamil Wawrowicz, Agnieszka Majkowska-Pilip, Rafal Walczak, Mateusz Wierzbicki, and Aleksander Bilewicz; "^{109}Pd/^{109m}Ag in-vivo generator in the form of nanoparticles for combined β^- - Auger electron therapy of hepatocellular carcinoma" EJNMMI Radiopharmacy and Chemistry, 9, 59 (2024), IF: 4.6

3. **Nasrin Abbasi Gharibkandi**, Kamil Wawrowicz, Agnieszka Majkowska-Pilip, Kinga Żelechowska- Matysiak, Mateusz Wierzbicki, and Aleksander Bilewicz; "Au@^{109}Pd core-shell nanoparticle conjugated to trastuzumab for the therapy of HER2+ cancers. Studies on the applicability of ^{109}Pd/^{109m}Ag in vivo generator in combined $\beta-$Auger electron therapy" EJNMMI Radiopharmacy and Chemistry, Vol 8, No 26 (2023), IF: 4.6

4. **Nasrin Abbasi Gharibkandi**, Michał Żuk, Fazilet Zumrut Biber Muftuler, Kamil Wawrowicz, Kinga Żelechowska-Matysiak, and Aleksander Bilewicz; "^{198}Au-Coated Superparamagnetic Iron Oxide Nanoparticles for Dual Magnetic Hyperthermia and Radionuclide Therapy of Hepatocellular Carcinoma" International Journal of Molecular Sciences, 24 (6), 5282, (2023), IF: 4.9

5. **Nasrin Abbasi Gharibkandi**, Joanna Gierałtowska, Kamil Wawrowicz, and Aleksander Bilewicz; "Nanostructures as Radionuclide Carriers in Auger Electron Therapy" Materials, 15 (3), 1143, (2022), IF: 3.4

6. Marzena Szwed, Tina Jost, Emilia Majka, **Nasrin Abbasi Gharibkandi**, Agnieszka Majkowska - Pilip, Benjamin Frey, Aleksander Bilewicz, Rainer Fietkau, Udo Gaipl, Agnieszka Marczak, Dorota Lubgan "Pt-Au nanoparticles in combination with near-infrared-based hyperthermia increase the temperature and impact on the viability and immune phenotype of human hepatocarcinoma cells", **Accepted to be Published** in the International Journal of Molecular Sciences

7. **Gharibkandi, Nasrin A**.; Molavipordanjani, Sajjad; Mardanshahi, Alireza; Hosseinimehr, Seyed Jalal; "The Influence of Kidneys Ion Transport Inhibitors on the Pharmacokinetic and Tumor Uptake Behaviors of a HER2-targeted Small Size Radiolabeled Peptide" Current Drug Metabolism, Vol 23, No 1, 82-87 (6), (2022), IF: 2.1

8. Alireza Mardanshahi, **Nasrin Abbasi Gharibkandi**, Samaneh Vaseghi, Seyed Mohammad Abedi, and Sajjad Molavipordanjani; "The PI3K/AKT/mTOR signaling pathway inhibitors

enhance radiosensitivity in cancer cell lines" Molecular Biology Reports, Vol 48, 1-14, (2021), IF: 2.6

9. **Nasrin Abbasi Gharibkandi**, J. Michael Conlon, Seyed Jalal Hosseinimehr; "Strategies for Improving Stability and Pharmacokinetic Characteristics of Radiolabeled Peptides for Imaging and Therapy" Peptides, Vol 133, 170385, (2020), IF: 2.4

10. **Gharibkandi NA**, Molavipordanjani S, Akbari J, Hosseinimehr SJ; "Pharmacokinetic evaluation of ^{99m}Tc- radiolabeled solid lipid nanoparticles and chitosan coated solid lipid nanoparticles" Current Drug Metabolism, Vol 20, No 13, 1044-1052 (9), (2019), IF: 2.1

11. **Abbasi Gharibkandi N**, Hosseinimehr SJ; "Radiotracers for imaging of Parkinson's disease" European Journal of Medicinal Chemistry, Vol 166, 75-89, (2019), IF: 6

Conferences

1. **N. Abbasi Gharibkandi**, K. Wawrowicz, A. Majkowska-Pilip, R. Walczak, A. Bilewicz; "^{109}Pd/^{109m}Ag invivo generator in the form of nanoparticles for combined β$^-$ - Auger electron therapy of hepatocellular carcinoma" NOMATEN International Radiopharmaceutical Conference (25-27.06.**2024**), Warsaw, Poland (**Oral Presentation**)

2. **N.Abbasi Gharibkandi**, A.Majkowska-Pilip, R.Walczak, K.Wawrowicz, A.Bilewicz; "Bioconjugates of ^{103}Pd/^{103m}Rh in-vivo generator for targeted Auger electron therapy" International Symposium on Trends in Radiopharmaceuticals (**ISTR-2023**) (17-21.04.2023), Vienna, Austria (**Poster Presentation**)

3. **N.Abbasi Gharibkandi**, A.Majkowska-Pilip, R.Walczak, K.Wawrowicz, A.Bilewicz; "Bioconjugates of ^{103}Pd/^{103m}Rh in-vivo generator for targeted Auger electron therapy" International Symposium on Radiopharmaceutical Sciences (29.05-02.06.**2022**), Nantes, France (**Poster Presentation**)

4. **N.Abbasi Gharibkandi**, J.Gierałtowska, A.Majkowska, K.Wawrowicz, A.Bilewicz; "Bioconjugates of ^{103}Pd/^{103m}Rh in-vivo generator for targeted Auger electron therapy" 1st Symposium on Theranostics (9- 11.10.**2021**), Krakow, Poland (**Oral Presentation**)

Honors and Awards

Young investigator Award as a presenter at the International Symposium onTrends in -Radiopharmaceuticals (**ISTR- 2023**) (17-21.0402023), Vienna, Austria

Internal Seminar Talks for Doctoral Students

1. PhD Studies Seminar 1 (2022)
2. PhD Studies Seminar 2 (2022/2023)
3. PhD Studies Seminar 3 (2023)

4. PhD Studies Seminar 4 (2023/2024)

5. PhD Studies Seminar 5 (2024)

6. PhD Studies Seminar 6 (2024/2025)

Courses Done

1. Methods of Physical Chemistry: Principles for Novel Nature-Inspired (Nano) Technologies, 15 h, 3 ECTS, Passed, Dr. Dimitrios Giannakoudakis
2. Chemistry and Chemical Engineering in Nuclear Energy, 15 h, 2 ECTS, Grade 3.5, Prof. Andrzej Chmielewski
3. Radiobiology, 15 h, 2 ECTS, Grade 5, Dr. Slawomir Sommer
4. Radiation Chemistry, 15 h, 2 ECTS, Grade 3+, Prof. Krzysztof Bobrowski
5. Radical Process in Polymers, 15 h, 2 ECTS, Grade 5, Prof. Hanna Lewandowska
6. Research Techniques and Career Development of a Scientist, 15 h, 3 ECTS, Passed, Dr. Andrej Kupsc
7. Scientific Writting, 15 h, 1 ECTS, Passed, Dr. Andrej Kupsc
8. Astrochemistry Evolution from Stardust to Biomolecules, 15 h, 3 ECTS, Grade 5, Dr. Aron Libersten Lawzer
9. Introduction to Drug Design and Discovery, 15 h, 3 ECTS, Passed, Dr. Jan Paczesny
10. Clinical Oncology Basis, 10 h, 2 ECTS, Grade 5, Dr. Monika Dudzisz Sledz
11. Cancer Epidemiology, 10 h, 2 ECTS, Grade 5, Dr. Juanna Didkowska
12. Molecular Variety:'Isomerism', Substituent Effect Aromaticitycs, 15 h, 3 ECTS, Grade 4+, Prof. Jan cz. Dobrowolski
13. The Main Directions in Development of Inorganic Analytical Chemistry, 15 h, 2 ECTS, Grade 4+, Group of lecturers
14. Preclinical Cancer, 10 h, ECTS 2, Grade 5, Dr. Magdalena Cybulska- Lubak
15. How to Avoid Chaos? Implementation of 5S Methodology in Scientific Laboratory, 3 h, 1 ECTS, Passed, Patrycja Kuzma
16. Journal Club, 10 h, 1 ECTS, Passed, Piotr Deur
17. Methods of Physical Chemistry: Biosensing, 15 h, 3 ECTS, Grade 3+, Prof. Wlodzimierz Kutner
18. Methods of Physical Chemistry: Chemosensing, 15 h, 3 ECTS, Grade 5, Prof. Wlodzimierz Kutner

Nasrin Abbasi Gharibkandi

Warsaw, Poland, nasrinali9285@gmail.com, (0048)517608829, in/nasrin-abbasi-gharibkandi-299a82140, https://orcid.org/0000-0002-9431-9869

Education

06.2021-present	**P.h.D candidate** in chemistry, Radiopharmaceutical Chemistry
	Institute of Nuclear Chemistry and Technology of Warsaw (**ICHTJ**), Poland
	Thesis: Synthesis and biological studies of bioconjugates based on ^{103}Pd and ^{109}Pd nanoparticles and their potential application in cancer Auger electron therapy in the team of Prof. Aleksander Bilewicz
09.2016-02.2020	**Master's degree** in Radiopharmaceutical sciences (**GPA: 4**)
	Mazandaran University of Medical Sciences (**MAZUMS**), Sari, Iran
	Thesis: Pharmacokinetic Evaluation of ^{99m}Tc-labeled Solid Lipid Nanoparticles and Chitosan Coated Solid Lipid Nanoparticles
02.2009-02.2013	**Bachelor's degree** in Radiology (**GPA: 4**)
	Urmia University of Medical Sciences (**UMSU**), Iran

Publications   Link to Google Scholar

1. **Nasrin Abbasi Gharibkandi**, Kamil Wawrowicz, Agnieszka Majkowska-Pilip, Rafal Walczak, Mateusz Wierzbicki, and Aleksander Bilewicz; "^{109}Pd/^{109m}Ag in-vivo generator in the form of nanoparticles for combined β⁻ - Auger electron therapy of hepatocellular carcinoma" *EJNMMI Radiopharmacy and Chemistry*, 9, 59 (**2024**)

2. **Nasrin Abbasi Gharibkandi**, Kamil Wawrowicz, Agnieszka Majkowska-Pilip, Kinga Żelechowska-Matysiak, Mateusz Wierzbicki, and Aleksander Bilewicz; "Au@^{109}Pd core-shell nanoparticle conjugated to trastuzumab for the therapy of HER2+ cancers. Studies on the applicability of ^{109}Pd/^{109m}Ag in vivo generator in combined β−Auger electron therapy" *EJNMMI Radiopharmacy and Chemistry*, Vol 8, No 26 (**2023**)

3. **Nasrin Abbasi Gharibkandi**, Michał Żuk, Fazilet Zumrut Biber Muftuler, Kamil Wawrowicz, Kinga Żelechowska-Matysiak, and Aleksander Bilewicz; "^{198}Au-Coated Superparamagnetic Iron Oxide Nanoparticles for Dual Magnetic Hyperthermia and Radionuclide Therapy of Hepatocellular Carcinoma" *International Journal of Molecular Sciences*, 24 (6), 5282, (**2023**)

4. **Nasrin Abbasi Gharibkandi**, Joanna Gierałtowska, Kamil Wawrowicz, andAleksander Bilewicz; "Nanostructures as Radionuclide Carriers in Auger Electron Therapy" *Materials*, 15 (3), 1143, (**2022**)

5. **Gharibkandi, Nasrin A.**; Molavipordanjani, Sajjad; Mardanshahi, Alireza; Hosseinimehr, Seyed Jalal; "The Influence of Kidneys Ion Transport Inhibitors on the Pharmacokinetic and Tumor Uptake Behaviors of a HER2-targeted Small Size Radiolabeled Peptide" *Current Drug Metabolism*, Vol 23, No 1, 82-87 (6), (**2022**)

6. Alireza Mardanshahi, **Nasrin Abbasi Gharibkandi**, Samaneh Vaseghi, Seyed Mohammad Abedi, and Sajjad Molavipordanjani; "The PI3K/AKT/mTOR signaling pathway inhibitors enhance radiosensitivity in cancer cell lines" *Molecular Biology Reports*, Vol 48, 1-14, (**2021**)

7. **Nasrin Abbasi Gharibkandi**, J. Michael Conlon, Seyed Jalal Hosseinimehr; "Strategies for Improving Stability and Pharmacokinetic Characteristics of Radiolabeled Peptides for Imaging and Therapy" *Peptides*, Vol 133, 170385, (**2020**)

8. **Gharibkandi NA**, Molavipordanjani S, Akbari J, Hosseinimehr SJ; "Pharmacokinetic evaluation of ^{99m}Tc-radiolabeled solid lipid nanoparticles and chitosan coated solid lipid nanoparticles" *Current Drug Metabolism*, Vol 20, No 13, 1044-1052 (9), (**2019**)

9. **Abbasi Gharibkandi N**, Hosseinimehr SJ; "Radiotracers for imaging of Parkinson's disease" *European Journal of Medicinal Chemistry*, Vol 166, 75-89, (**2019**)

Skills

- Labeling, Immunoassay studies, Iodination, Antibody Conjugation, Nanoparticle Synthesis
- Expertise with laboratory equipment including Thin- Layer Chromatography (TLC), Gamma- spectroscopy, DLS, UV-VIS Spectroscopy
- Cancer Cell Culture 2D/3D, different cancer cell studies (MTS toxicity, Receptor binding affinity study, Cancer Cell Internalization, Cancer Cell Nucleus Isolation, Spheroids, DNA double strand break studies), Tumor cell xenotransplantation in immunocompromised mice and Biodistribution study
- Use of Microsoft Office, Image J, ChemDraw, GraphPad-Prism for data analysis

Conferences

1. **N. Abbasi Gharibkandi**, K. Wawrowicz, A. Majkowska-Pilip, R. Walczak, A. Bilewicz; "^{109}Pd/^{109m}Ag in-vivo generator in the form of nanoparticles for combined β$^-$- Auger electron therapy of hepatocellular carcinoma" *NOMATEN International Radiopharmaceutical Conference* (25-27.06.**2024**), Warsaw, Poland **(Oral Presentation)**

2. **N.Abbasi Gharibkandi**, A.Majkowska-Pilip, R.Walczak, K.Wawrowicz, A.Bilewicz; "Bioconjugates of ^{103}Pd/^{103m}Rh in-vivo generator for cancer targeted Auger electron therapy" *International Symposium on Trends in Radiopharmaceuticals (ISTR-2023)* (17-21.04.**2023**), Vienna, Austria **(Poster Presentation)**

3. **N.Abbasi Gharibkandi,** A.Majkowska-Pilip, R.Walczak, K.Wawrowicz, A.Bilewicz; "Bioconjugates of ^{103}Pd/^{103m}Rh in-vivo generator for cancer targeted Auger electron therapy" *International Symposium on Radiopharmaceutical Sciences* (29.05-02.06.**2022**), Nantes, France **(Poster Presentation)**

4. **N.Abbasi Gharibkandi,** J.Gierałtowska, A.Majkowska, K.Wawrowicz, A.Bilewicz; "Bioconjugates of ^{103}Pd/^{103m}Rh in-vivo generator for cancer targeted Auger electron therapy" *1st Symposium on Theranostics* (9- 11.10.**2021**), Krakow, Poland **(Oral Presentation)**

Honors and Awards

1. 04.2023   Young investigator Award as a presenter at the International Symposium on Trends in Radiopharmaceuticals (ISTR- 2023)
2. 2016-2020   First top student of radiopharmaceutical sciences courses in Iran
3. 2016-2020   First top student among master's students

Work Experience

1. 08.2020-04.2021   Medical Diagnostic Radiographer, Avesta Radiology Center, Sari, Iran
2. 04.2019-09.2019   SPECT Imaging Internship, Fatemeh- Zahra Reproductive Health Research Center, Sari, Iran
3. 09.2014-09.2016   Medical Diagnostic Radiographer, Dr. Leila Shahriarfar Radiology Center, Urmia, Iran
4. 03.2013-09-2016   Medical Diagnostic Radiographer, Imam Khomeini Hospital, Urmia, Iran
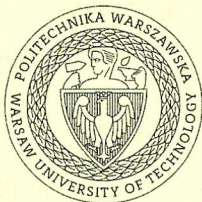
Politechnika Warszawska
Studium Języków Obcych

ŚWIADECTWO

Studium Języków Obcych Politechniki Warszawskiej

zaświadcza, że

mgr Nasrin Abbasi Gharibkandi

zdała egzamin

z języka angielskiego na poziomie B2

ustalonym według

Europejskiego Systemu Opisu Kształcenia Językowego

Ocena: 5,0

Zastępca Dyrektora
Studium Języków Obcych

mgr Joanna Kożuchowska

Warszawa dn. 21.01.2025 r.

Skala ocen:

5,0 (bardzo dobry)
4,5 (dobry plus)
4,5 (dobry)
3,5 (dostateczny plus)
3,0 (dostateczny)
2,0 (niedostateczny)

**Main topics
of research and
technological
activities:**

Radiochemistry
separation methods
and processes

radiation chemistry

analytical chemistry
activation analysis

radiobiology
radiation safety

radiation
technologies
for medicine, industry
and protection
of environment

nuclear
instrumentation

nuclear techniques
in material and
process engineering

Warsaw, 02.12.2024

MSc. Nasrin Abbasi Gharibkandi
Dorodna 16, 03-195 Warsaw, Poland
n.abbasi@ichtj.waw.pl

Prof. dr hab. inż. Zbigniew Florjańczyk
Chairman of the Scientific Council
Institute of Nuclear Chemistry and
Technology

Declaration of the Originality of Doctoral Research

I hereby affirm that my doctoral thesis, titled " **Nanostructures labeled with Pd-109 for combined β- and Auger electron targeted therapy,**" represents my original research work conducted under the guidance of Prof. dr hab. inż. Aleksander Bilewicz at the Institute of Nuclear Chemistry and Technology, Warsaw, Poland. This work has not been submitted previously for any academic evaluation or for the conferment of a doctoral degree at any institution.

Yours faithfully

Nasrin Abbasi Gharibkandi

**Main topics
of research and
technological
activities:**

Radiochemistry
separation methods
and processes

radiation chemistry

analytical chemistry
activation analysis

radiobiology
radiation safety

radiation
technologies
for medicine, industry
and protection
of environment

nuclear
instrumentation

nuclear techniques
in material and
process engineering

Warsaw, 04.12.2024

MSc. Nasrin Abbasi Gharibkandi
Dorodna 16, 03-195 Warsaw, Poland
n.abbasi@ichtj.waw.pl

Prof. dr hab. inż. Zbigniew Florjańczyk
Chairman of the Scientific Council
Institute of Nuclear Chemistry and
Technology

APPLICATION FOR PHILOSOPHY EXAMINATION

I formally seek permission to be examined in philosophy as a supplementary area

of study, adhering to the IChTJ doctoral school program requirements.

I highly appreciate your consideration and await your response with regard to my

application.

Yours faithfully

Nasrin Abbasi Gharibkandi